Cell type-specific *Runx1* enhancer-reporter mouse lines to study hemogenic endothelium



Christina Rode

St. Hugh's College
University of Oxford

A thesis submitted for the degree of
Doctor of Philosophy

Trinity 2016

This thesis is dedicated to the carrots.

Acknowledgements

First of all I would like to thank the head of my scientific family and my supervisor, Marella de Bruijn. I am extremely grateful to have been given the opportunity to learn from you, to work with you and to be continually reminded that there is only one way: forward! You have contributed massively to my growth as a scientist, colleague, and scholar. I hope that, one day I will grow enough to apply the “Marellification” technique on one of my own students, maybe even “Chrissyfying” it in the process. To me, you have been the best supervisor I could have hoped for and I have not regretted one single day of this journey (even while writing this thesis). I am also grateful to you for introducing me to Pilates, my posture is a testimony to that!

A massive thank you goes to ‘my boys’! Luke, you have been great and incredibly supportive when it really mattered! Emanuele, we’ve started at the same time in the lab, and you’ve been a great friend and postdoc in the last 4 years! Vincent, we have only known each other for a year, but I feel like we’ve been friends forever! Joe, I can’t believe how lucky I’ve been to have you around to do your ‘R magic’ on my data! Keep up the good work! Dom, you are fun and a great positive person to have in the lab! Thank you guys for being so supportive. I’d also like to thank past members of the lab: John, thank you for introducing me to the de Bruijn team so many years ago! Joey, my adopted lab brother, thank you for being such an awesome friend and postdoc. And Stella, you remain a voice of sense and reason in my ear.

The WIMM and Oxford has been my home for the last couple of years and I feel lucky to have worked in such a stimulating environment surrounded by incredible people. Additional thanks goes to my 3 ‘other mums’, Jackie, Nessy and Sue! You made me feel welcome from the start and adopted me as the ‘chick’! I am forever grateful!

A special thank you goes to Tom Milne. I am grateful for your support, your caring and the constructed criticism that have made me a better scientist and student. You have accompanied me along my PhD journey from the very start. I will always remember that mock interview 4 years ago, as well as our chats about cats and the peculiar behavior of kids! A big thank you also goes to Tatjana Sauka-Spengler, my second thesis committee advisor. I admire your energy and breadth of ideas!

I can’t thank my FACS husband, Kevin, enough! Thank you for letting me laugh, cry, rant and most importantly sort (even on weekends)! I couldn’t have wished for a better companion! Thank you to all the old and new friends that I feel privileged to have met in the last few years:
My partner in crime, Maria or Babe! I don’t know what I would have done without your ever-present support. You understand me on another level and continuously challenge me to consider another point of view! Thank

you! Jenny, my dear Liebchen, you bring out the vulnerable side of me, and although scary, I am grateful I can lean on you from time to time. Thank you! The many newer friends I have made and that have become dear friends: Erica (you beautiful Italian soul!), Gemma (you beautiful SA-NZ-AUS creature!), Jess (you beautiful awesome-haired soul! your positive outlook never ceases to amaze me) and Sorcha (the newest beautiful addition, but already part of the gang).

Thank you to The Cat Kingdom: Tiger, who has been an anchor for me over the years and continuously wants to save the world! If anyone does, it would be you! The Lioness, who even from afar, continues to spread cattish, moose-like craziness! I am forever indebted to you for entrusting me with your, now my, beloved Chitas.

A rather strange thank you goes to Ross, who suggested and encouraged me to take up horse riding again. Particularly my gorgeous Mr.P has had a soothing effect on my PhD life and my general wellbeing.

And lastly, but most importantly, I'd like to thank my parents! They have been and always will be my biggest fans and I am incredibly lucky and grateful to call them my parents. Thank you for never doubting me, for always encouraging and supporting me, for always allowing me to make my own decisions and grow, for making me a fighter and for simply loving me! Огромное спасибо!

Table of Contents

Acknowledgements 2

Table of Contents 4

List of abbreviations 8

Abstract 10

CHAPTER 1 11

INTRODUCTION 11

1.1 Hematopoietic stem cells 12

1.2 Developmental hematopoiesis 16
First wave of hematopoiesis 16
Second wave of hematopoiesis 18
Definitive wave of hematopoiesis 19

1.3 Hematopoietic sites and tissues 19
The extra-embryonic yolk sac 19
The intra-embryonic PAS/AGM region 21
The fetal liver 24
The number of HSPCs in embryonic tissues 25
The placenta as a source of HSCs 26
Additional sites of developmental hematopoiesis 27

1.4 The close relationship between endothelium and blood 29

1.5 The ontogeny of the hemtopoietic lineage 31
Hemangioblast 31
Hemogenic endothelium 32
The origin(s) of HE 34

1.6 The HSC roadmap 36
The endothelial-to-hematopoietic transition 36
HSC precursors 36

1.7 The AGM niche 40
Spatial distribution 40
Hedgehog signaling 41
Notch signaling 42
TGFβ signaling 43
BMP signaling 44
Sub-aortic mesenchyme-derived HSCs? 45
Mesenchymal stem cells or mesangioblast 46

1.8 Key intrinsic regulators of developmental hematopoiesis 48
Endothelial genes 48
Early hematopoietic genes 50
Genes of hematopoietic commitment 52

1.9 *Runx1* and developmental hematopoiesis 54
Runx1 expression during development 55
Runx1 enhancers 57

Runx1 requirement during development 62
Further dissection of Runx1 requirement during EHT 64
The role of Runx1 during hematopoiesis is conserved in fish 65

1.10 The heterogeneity of hemogenic endothelium 66

1.11 Project aims 71

CHAPTER 2 73

MATERIALS AND METHODS 73

Mice 74
2.1 Generation of transgenic mouse lines via pronuclear microinjection 74
2.2 Generation of mouse chimeras via ES cell injection 75
2.3 Mouse colony maintenance 76
2.4 Ear notching and genotyping 76
2.5 Preparation of adult mouse tissues for DNA extraction or cell sorting 78

Embryos 80
2.6 Analysis of reporter transgene expression at different developmental time points 80
2.7 Early embryo cultures 81
2.8 Embryo dye injections 81
2.9 Preparation of embryos for flow cytometry 82
2.10 Preparation and cryosectioning of embryos 82

Immunofluorescence and imaging 83
2.11 Immunofluorescence on sections 83
2.12 Wholemount immunofluorescence 85
2.13 Microscopy 86
2.14 Live embryo imaging 87

Functional assays 87
2.15 OP9 maintenance, co-culture and output analysis 87
2.16 Methylcellulose colony assays (CFU-C) 88
2.17 Long-term reconstitution analysis 89
2.18 Chondrogenic differentiation assays 89

Gene expression analysis 90
2.19 Microfluidic quantitative RT-PCR 90
2.20 Fluidigm analysis 93
2.21 Statistical analysis 94

General laboratory techniques 94
2.22 Southern blotting for 23Cherry ES cell clone analysis 94
2.23 Radioactive labeling of double-stranded DNA probes 95
2.24 DNA hybridization and autoradiography 96
2.25 ES cell culture 97
2.26 Karyotyping 97

CHAPTER 3 99

GENERATION AND PHENOTYPIC CHARACTERIZATION OF A *RUNX1* +204 ENHANCER-REPORTER TRANSGENIC MOUSE LINE 99

3.1 Generation of 204GFP founders 102

3.2 Analysis of 204GFP founder offspring: embryonic hematopoiesis 104
Hematopoietic-specific 204GFP expression at E8.5 105
Hematopoietic-specific 204GFP expression at E10.5 108
Hematopoietic-specific 204GFP expression beyond midgestation 111
Comparison to transient transgenic data 111

3.3 Analysis of 204GFP founder offspring: adult hematopoiesis 117

3.4 The 204GFP transgene is marking a subset of the embryonic endothelium 119

3.5 Quantification of 204GFP expression in different cell populations 123

3.6 The 204GFP transgene is marking a subset of the phenotypic hemogenic endothelium 128

3.7 Summary 135

CHAPTER 4 137

FUNCTIONAL CHARACTERIZATION OF THE 204GFP MOUSE LINE 137

4.1 The 204GFP+ endothelium has hemogenic potential 138

4.2 The 204GFP transgene does not label clonogenic blood progenitor cells 149

4.3 Both 204GFP+ and 204GFP- populations harbor LT-HSCs 151

4.4 Sub-aortic 204GFP+ AGM cells form cartilage in culture 155

4.5 Summary and discussion 161
Labeling distinct subsets or maturation stages of HE? 161
Are MSCs marked by 204GFP expression? 163
Concluding remarks 166

CHAPTER 5 167

MOLECULAR ANALYSIS AND FURTHER ENRICHMENT OF HEMOGENIC ENDOTHELIUM 167

5.1 Molecular profiling of 204GFP+ hemogenic endothelium 168
Expression analysis of 204GFP+ and 204GFP- endothelial subsets 169
Gene expression analysis of single 204GFP+ and 204GFP- endothelial cells 171

5.2 Generation and characterization of the 23Cherry transgenic mouse line 176
Generation of the 23Cherry mouse line 176
Phenotypic characterization of the 23Cherry mouse line 178
Functional characterization of the 23Cherry mouse line 181

5.3 Expression analysis of 204GFP::23Cherry compound transgenic embryos 186
Rare endothelial cells co-express 204GFP and 23Cherry 186
Quantification of co-expression in compound transgenic embryos 186
Single cell gene expression analysis of 204GFP and/or 23Cherry-marked endothelium 191

5.4 Summary and discussion 195

Single cell expression analysis 195
Concluding remarks 196

CHAPTER 6 198

TOWARDS TRACING THE ORIGIN OF HEMOGENIC ENDOTHELIUM IN THE GASTRULATING EMBRYO 198

6.1 Expression of the 23GFP transgene in early-stage embryos 200
Phenotypic analysis of 23GFP expression in the pre-somitic embryo 200
Live imaging of early-stage 23GFP transgenic embryos 205
Quantification of 23GFP expression at pre-somitic stages 207

6.2 Establishing and optimizing in vitro cultures of pre-somitic embryos 210

6.3 Tracing the origin of hemogenic endothelium 214
Set up of fate mapping experiments using DiI labeling 214
Distinct PS segments contribute to YS and intra-embryonic 23GFP+ HE 215

6.4 Conclusions and discussion 221
When does hemogenic endothelium become hemogenic? 222
Tracing the origin of HE 223

CHAPTER 7 225

GENERAL DISCUSSION 225

7.1 Summary of results 226

7.2 Hemogenic endothelial subsets or maturation stages? 227

7.3 Transcription factor binding and enhancer activity 229

7.4 Endoderm and developmental hematopoiesis 230
Concluding remarks 232

REFERENCES 233

List of abbreviations

AGM	aorta-gonad-mesonephros
AP	alkaline phosphatase
AVE	anterior visceral endoderm
BI	blood island
BL-CFC	blast colony-forming cell
BM	bone marrow
^{o}C	Celsius
CFU-C	colony-forming unit culture
CFU-S	colony-forming unit spleen
CMF-PBS	Calcium- and Magnesium-free PBS
CNE	conserved noncoding element
CO^{2}	carbon dioxide
DA	dorsal aorta
dHSC	definitive hematopoietic stem cell
dpc	days post coitus
DRG	dorsal root ganglia
E	embryonic day (mouse)
EB	early bud stage
EC	endothelial cell
EHF	early headfold stage
EHT	endothelial-to-hematopoietic-transition
EMP	erythromyeloid progenitor
FCS	fetal calf serum
FL	fetal liver
FMO	fluorescence-minus-one
GFP	green fluorescent protein
GLT	germline transmission
HC	hematopoietic cell
HCG	human chorionic gonadotropin
HE	hemogenic endothelium
hESC	human embryonic stem cells
HF	headfold stage
Hh	Hedgehog
HLA	human leukocyte antigen
HPC	hematopoietic progenitor cell
HSC	hematopoietic stem cell
HSCT	hematopoietic stem cell transplantation
hsp68	heat shock promoter 68
HSPC	hematopoietic stem and progenitor cell
ICM	inner cell mass
iPS cells	induced pluripotent stem cells
IVC	individually ventilated cages

LB	late bud
LHF	late headfold
LPM	lateral plate mesoderm
LT-HSC	long term HSC
MEP	megakaryocyte/erythroid progenitor
min	minute(s)
MSC	mesenchymal stem cell
NAC	no amplification control
NTC	no template control
O/N	overnight
OG	Oregon Green
PAS	para-aortic splanchnopleura
PBS	phosphate buffered saline
PCR	polymerase chain reaction
PFA	paraformaldehyde
PMS	pregnant mare serum
qRT-PCR	quantitative reverse-transcriptase PCR
RT	room temperature
SD	standard deviation
Shh	sonic hedgehog
SMA	smooth muscle actin
TF	transcription factor
UA	umbilical artery
UVA	umbilical and vitelline artery
VA	vitelline artery
VEC	vascular endothelial cadherin
VU	Vitellin and umbilical
vSMC	vascular smooth muscle cell
w/v	Weight per Volume
YS	yolk sac

Cell type-specific *Runx1* enhancer-reporter mouse lines to study hemogenic endothelium

Christina Rode (St. Hugh's College)
Doctor of Philosophy – Trinity 2016
University of Oxford

Abstract

Hematopoietic stem cells emerge from a specialized subset of endothelial cells in the midgestation mouse aorta. This subset, the so-called hemogenic endothelium (HE), undergoes a morphological and molecular change to a hematopoietic cell type, as part of the endothelial-to-hematopoietic transition (EHT). Previously, lack of specific markers prevented mechanistic studies of HE, as well as studies into its developmental origin. Runx1 is a critical regulator of developmental hematopoiesis and is expressed in all cell intermediates of EHT. Identification of the *Runx1* +23 enhancer led to the development of enhancer-reporter tools in order to isolate HE for further analysis. Here, I investigated the cell-type specific activity of another *Runx1* enhancer, located 204 kb downstream of the ATG in exon 1. I generated a novel enhancer-reporter mouse line (204GFP) and determined the expression pattern and lineage potential of 204GFP+ cells. It was established that the +204 enhancer marks all HE and part of the HSCs. Hematopoietic progenitor cells, in contrast, were not marked by the 204GFP transgene. Interestingly, the 204GFP reporter also marks part of the Runx1-expressing sub-aortic mesenchyme. To test whether the 204GFP reporter could enrich for HE when combined with a *Runx1* +23 enhancer-reporter transgene, I generated and characterized a 23Cherry transgenic mouse line. Expression analysis of aortic endothelial cells marked by both the 204GFP and 23Cherry transgenes using the Fluidigm platform indicated an enrichment of cells with a HE expression signature. This enrichment will facilitate further analysis of the molecular networks active in HE using whole genome expression profiling. The *Runx1* enhancer-reporter models are also valuable tools to track the developmental origin of HE, which remains to be established in the mouse embryo. To this end, I mapped the precise spatio-temporal expression pattern of the 23GFP transgene in pre-somitic embryos and established lineage tracing experiments. This provides the basis to revisit fate mapping of the primitive streak to determine the origin(s) of the HE lineage.

Chapter 1

Introduction

1.1 Hematopoietic stem cells

Hematopoietic stem cells (HSCs) are cells that are able to self renew as well as give rise to all lineages of the hematopoietic system. The beginning of HSC research in the 50's resulted from the observation that radiation caused an ablation of the hematopoietic system (reviewed by Eaves, 2015). Followed by the identification of the bone marrow (BM) and the spleen as organs containing cells that, after intravenous injection into irradiated animals, are able to prevent radiation-caused lethality by replenishing all blood lineages (Cole et al., 1952; Jacobson et al., 1951; Lorenz et al., 1952). During the following years analysis focused to the quantification of such cells and a mechanistic understanding of their self renewal and differentiation potentials (reviewed by Eaves, 2015). BM HSCs were found to only have a limited potential to self-renew and it was later established that 75% reside in a quiescent, inactive state (Siminovitch et al., 1964; Cheshier et al., 1999). In order to maintain steady-state hematopoiesis or to respond to challenges in the form of infection, inflammation or extensive blood loss, HSCs become active and generate the required blood types. Due to their ability to differentiate into any blood lineage, HSCs are crowning the very top of the adult hematopoietic hierarchy. They can then give rise to multipotent and later to lineage-biased blood progenitors. Over the years a plethora of studies have shown the hierarchical organization of the adult hematopoietic system, with the most recent schematic of HSC hierarchy shown in Figure 1.1 (Drissen et al., 2016).

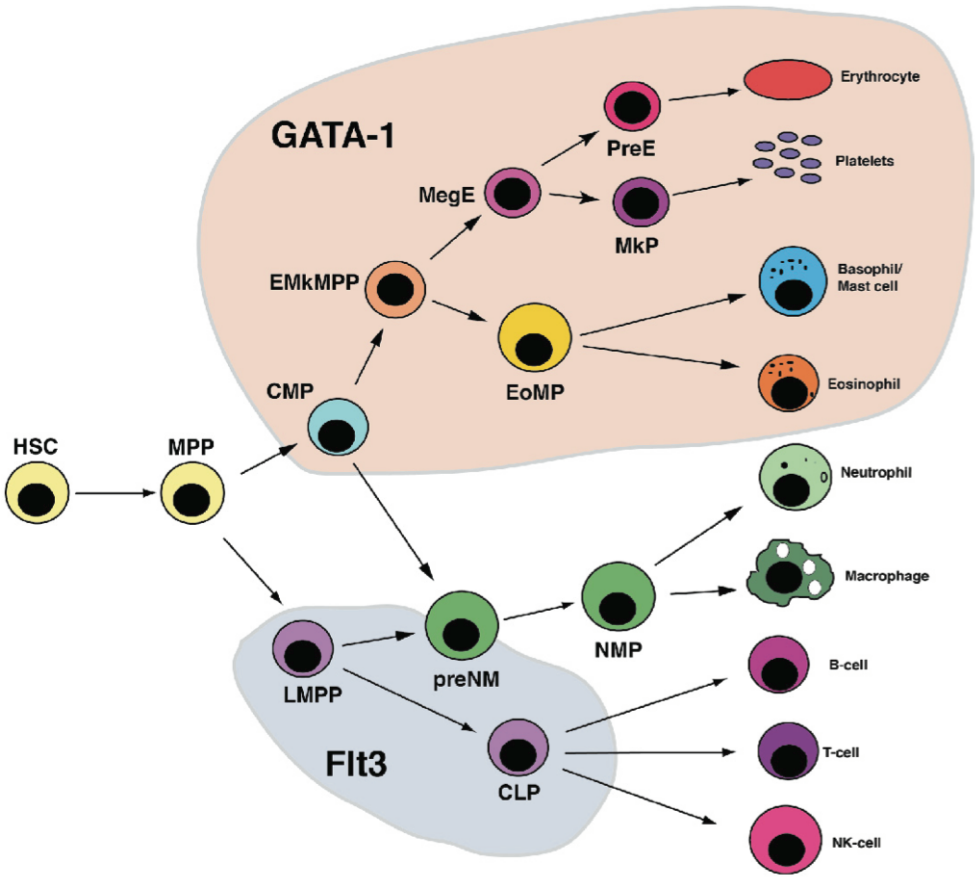


Figure 1.1: The hematopoietic hierarchy
A schematic of the adult hematopoietic hierarchy as described by Drissen *et al*., 2016. Reprinted by permission from Macmillan Publishers Ltd: Nature Immunology, Drissen *et al*, copyright 2016.

The knowledge of how the adult HSC functions and differentiates goes towards better applications in the regenerative medicine field and aids to the development of novel stem cell-based therapies. For the last 60 years treatment of several blood-related malignant diseases have benefitted from hematopietic stem cell transplantation (HSCTs) (reviewed by Müller et al., 2016). Such HSCTs were first successfully performed on leukemic patients with healthy BM cells derived from the patients' identical twins (Thomas et al., 1957, 1959). Since, HSCT is considered a 'gold-standard' (Thomas, 1957). However, such treatments rely on sufficient numbers of BM or umbilical cord donors as well as human leukocyte antigen matching to combat rejection of the donor tissue in the patient or prevent serious complications such as graft-versus-host disease (Ballen et al., 2008; Oran and Shpall, 2012; Müller et al., 2016). The ability to generate bona fide HSCs in culture would greatly circumvent the shortage of donor material, however, at present it is not possible. Research is ongoing in how best to generate or expand HSCs or specific blood cell types for use in regenerative medicine. Multiple studies have successfully differentiated embryonic stem (ES) or induced pluripotent stem (iPS) cells into primarily lymphoid cells such as B cells (Carpenter et al., 2011), T cells (Galić et al., 2006), NK cells (Knorr et al., 2013; Woll et al., 2009) and also platelets (Lu et al., 2011). However the use of ESCs has caused some controversy. Since ESCs derive from the embryo there is an ethical dilemma of using such material for research or for regenerative medicine. This is the reason why iPS cells have become increasingly more popular as they require, often easily attainable, cellular material, such as skin biopsies. These are

then reverted back to a more immature cell type by applying defined sets of transcription factors (TFs) such as Oct4, Sox2, Kfl4 and c-Myc (Hanna et al., 2007; Takahashi and Yamanaka, 2006) before subjecting the new iPS cells to differentiation cultures.

A third option has been described and involves the direct reprogramming of cells into the required cell type. For example, one study used the transcription factor Oct4 to convert human skin cell-derived fibroblasts into CD45+ blood progenitors (Szabo et al., 2010), while another group reprogrammed human hair follicle mesenchymal stem cells into red blood cells, also using Oct4 as the reprogramming factor (Liu et al., 2015). In addition, a major breakthrough recently came from the Rossi lab. Riddell et al demonstrated that committed pro- and pre-B cells and common myeloid progenitor (CMP) cells can be reprogrammed back into a multi-lineage HSC-like cell (Riddell et al., 2014). They identified that a set of 8 TFs (Run1t1, Hlf, Lmo2, Prdm5, Pbx1, Zfp37, Mycn and Meis1) co-transduced with a polycistronic virus constructs, are sufficient to impart long-term multilineage engraftment potential to committed progenitors in an transplantation setting. In addition, it was also suggested that induced HSCs are genetically similar to endogenous HSCs as demonstrated by single cell Fluidigm® analysis (Riddell et al., 2014).

Studies like this open up a whole new dimension of possibilities for the field of regenerative medicine. However, given the difficulties and challenges in generating, expanding or differentiating medical-grade transplantable HSC in culture, it is not surprising that a big part of research

still focuses on the basic understanding of HSC development with the prospect of translational applications later. The embryo has proven to be the perfect model system to study the birth of HSCs. In the following chapters, our current understanding of developmental hematopoiesis will be discussed.

1.2 Developmental hematopoiesis

Developmental hematopoieis in mammals occurs in 3 distinctive but overlapping waves. The first 2 waves generate transitory blood types such as primitive erythrocytes and some myeloid and lymphoid cells. These waves are often referred to as embryonic hematopoiesis as they do not produce adult-like blood stem cells. Instead, they support only the early stages of embryogenesis. In contrast, the third wave generates adult-like HSCs that, after birth, support the entire hematopoietic system of the organism, life-long. Therefore, the third wave is also referred to as the definitive wave of hematopoiesis. Each wave generates hematopoietic cells with varied lineage differentiation potential. These are discussed below in the developmental setting of the mouse embryo (Figure 1.2).

<u>First wave of hematopoiesis</u>

The first and primitive wave is initiated as early as the beginning of gastrulation at the mid-streak stages. Early experiments indicated that this wave exclusively generates primitive erythroid progenitors (Palis, 1999). However, later studies identified that some uni-potential megakaryocyte progenitors and bi-potential megakaryocyte/erythroid progenitors (MEPs)

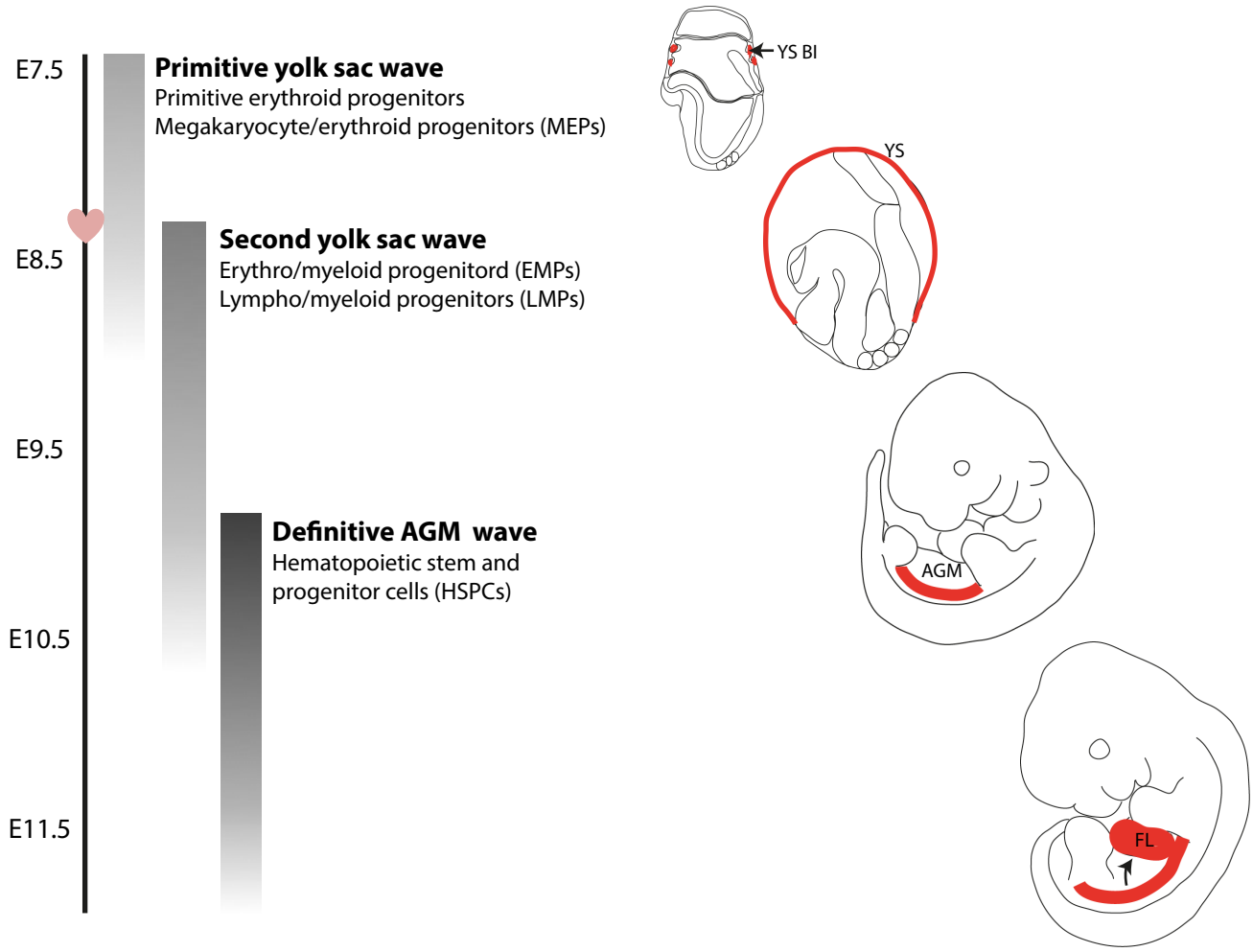


Figure 1.2: Developmental hematopoiesis
Schematic of the 3 waves of developmental hematopoiesis in relation to developmental stage of the mouse embryo. The types of blood progenitors generated in each wave are given. Embryonic sites of developmetal hematopoiesis are highlighted in red at each stage. Later sites of definitive hematopoiesis (bone marrow) are not shown. YS BI - yolk sac blood island; AGM - aorta-gonad-mesonephros region; FL - fetal liver.

were also generated during the first wave (Tober et al., 2007). Primitive erythrocytes are exceptionally large compared to the erythrocytes found in the fetal liver (3-fold larger) and in adult mice (5-6-fold larger) (Kingsley et al., 2004). Despite the cell size difference, primitive erythrocytes exhibit similar phenotypic changes associated with definitive erythrocyte maturation such as decrease in cell size over time, nuclear condensation and haemoglobin accumulation. In addition, they enucleate between E12.5 and E16.5 in circulation (Kingsley et al., 2004). Surprisingly, studying the expression pattern of embryonic βH1 globin staining, showed that mature primitive erythrocytes are found as late as 5 days postpartum in the blood stream of newborn pups (Kingsley et al., 2004). The generation of progenitors of the first wave continues till the early somite-pair stages (E8.25), after which the second wave of hematopoiesis is initiated.

Second wave of hematopoiesis

The second wave generates more erythroid progenitors, bipotential granulocyte/macrophage progenitors (Palis et al., 1999) and from E9.0 megakaryocyte progenitors (Tober et al., 2007), collectively referred to as erythro-myeloid progenitors or EMPs. In addition, tissue resident macrophages were recently found to develop from EMPs during the second wave (Gomez Perdiguero et al., 2014; Schulz et al., 2012). Further, the lymphoid lineage was previously thought to develop as part of the definitive hematopoietic wave (Douagi et al., 2002). Since, however, the origin of lympho-myeloid restricted progenitors (LMPs) has been traced back to the second wave at E9.5 (Böiers et al., 2013; Yoshimoto et

al., 2011, 2012). The initiation of the second wave coincides with the onset of blood circulation at E8.25 (McGrath et al., 2003). Around E9.5 the fetal liver rudiment starts to form and different blood progenitors colonize it by E10.5 (McGrath et al., 2011; Zorn, 2008). EMP differentiation into erythrocytes takes place in the fetal liver (McGrath et al., 2011).

Definitive wave of hematopoiesis

Around midgestation (E10.5-E11.5) the final wave of hematopoiesis establishes, generating adult-like multipotent blood progenitors but most importantly the first HSCs (Medvinsky and Dzierzak, 1996). Together with various blood progenitors from earlier waves of hematopiesis, HSCs colonise the FL and expand. Together, the generation of HSCs, their expansion within the FL and their migration to the BM just prior to birth, lead to the establishment of the future adult hematopoietic system and with it the formation of the adult blood hierarchy. The following section will discuss the significance of different hematopoietic sites associated with the three hematopoietic waves.

1.3 Hematopoietic sites and tissues

The extra-embryonic yolk sac

The site directly associated with primitive hematopoiesis is the early extra-embryonic yolk sac (YS) of the 7 days-postcoitum (dpc) embryo (Palis et

al., 1999). At this early stage of development, the extra embryonic YS comprises a band of specialized mesoderm, that is able to give rise to blood as well as endothelium and forms the YS blood islands (BI). The early YS mesoderm initially lacks vascular network or blood islands but is still able to generate primitive erythrocytes in explant cultures (Palis et al., 1995). In *in vitro* cultures of cells derived from the early YS and embryo (pre-somitic to 10dpc), Moore and Metcalfe established that the first colony-forming cells (CFCs) derive exclusively from the YS (Moore and Metcalf, 1970; Figure 1.2). Pre-somitic embryos (7dpc) cultured without their YSs were not able to acquire emergence of blood even after several days in culture with the earliest detection of hematopoietic capacity within the embryo proper occurring only from early E9 (Moore and Metcalf, 1970). In fact, at the onset of the second wave, EMPs were also shown to derive from the E9 YS (Tober et al., 2007). This is supported by the lack of CFU-Cs within the embryo proper in circulation-deficient embryos (Lux et al., 2008). Once circulation is established, CFC potential was also found within the embryo proper (Moore and Metcalf, 1970; Yoder and Hiatt, 1997; Yoder et al., 1997). In addition, midgestation (E11.5) YS-derived hematopoietic cells were able to repopulate lethally-irradiated adult recipient mice, short-term (7-30 days), and were found in all major adult hematopoietic sites such as the BM and spleen. Lymphopoietic sites (thymus and mesenteric lymph nodes) were also populated by E11.5 YS-derived progeny (Moore and Metcalf, 1970). For a while, it was widely accepted that the YS was the sole origin of the entire adult hematopoietic system, based on its repopulation ability and the lack of CFC-potential

from the embryo proper prior to circulation onset.

However, shortly after, a convincing argument for a second site of developmental hematopoiesis was proposed: In elegant chick-quail grafting experiments Dieterlen-Lievre showed that when quail embryos were grafted onto chick yolk sacs, all hematopoietic lineages were of quail origin, therefore intra-embryonic (Dieterlen-Lievre, 1975). More importantly, after 6-11 day incubation, the spleen and thymus of the grafted quail embryo contained exclusively quail cells (nuclei morphologically distinct from chick), suggesting that HSCs also originated from the quail embryo, rather than from the chick YS (Dieterlen-Lievre, 1975). This study inspired new research into the intra-embryonic origin of developmental hematopoiesis and possibly a different site of generation for adult-like HSCs. Interestingly, later studies also showed that while the E9-E10 YS-derived cells were able to engraft newborn mice, they were not able to long-term repopulate adult recipients, suggesting no adult-like HSCs are present in this population (Yoder and Hiatt, 1997; Yoder et al., 1997). In summary, although being the first site of developmental hematopoiesis, the YS seemed to only generate blood progenitors of the first two waves but not adult-like long-term HSCs.

The intra-embryonic PAS/AGM region

Since Dieterlen-Lievre reported the intra-embryonic site of hematopoiesis in the avian model system, analogous studies have been performed in the mouse embryo. It was shown that as early as 10sp (E8.5) the intra-embryonic para-aortic splanchnopleura (PAS) region contained lymphoid

potential (Godin et al., 1993, 1995). This was established by grafting PAS and YS cells under the kidney capsules in SCID mice and analyzing the engraftment potential after 2-4 months. In addition, in vitro assays on stromal cell layer established that in addition to the previously recognized YS site, the E9 PAS was also able to generate myeloid and lymphoid cells in culture (Godin et al., 1995). Of note, embryos analyzed in the above studies already exhibited blood circulation; to that end, Cumano et al separated YS from the embryo proper prior to the onset of blood flow and subjected both to a new culturing strategy that involved a whole tissue explant culture prior to expansion and clonal differentiation analysis (Cumano et al., 1996). This additional culturing step seemed to mature potential precursors so that hematopoietic progeny was detected in the embryonic portion as early as 7dpc (Cumano et al., 1996). Although yolk sacs were able to give rise to blood progenitors in this culture setup, they were, however, not able to generate lymphoid progenitors and had a reduced ability to remain in culture compared to the PAS counterpart (Cumano et al., 1996). Thus, separating the mouse embryo YS and PAS prior to circulation onset, unequivocally established the presence of an intra-embryonic hematopoietic site, containing immature blood precursors from an early stage (as early as pre somite formation) (Cumano et al., 1996). Comparable findings were also documented in human embryos, which were able to generate lymphomyeloid progeny in culture. Their YS, however, did not (Tavian et al., 2001). Additionally, the PAS, separated prior to circulation, was able to confer multi-lineage engraftment in adult mice for up to 6 months. In contrast, YS cells only provided short-term

engraftment of the myeloid lineages (Cumano et al., 2001; Tavian et al., 2001).

At later stages of embryonic development the PAS region becomes the aorta-gonad-mesonephros (AGM) region, positioned between the developing fore and hind limb buds and encompassing the dorsal aorta (DA), the genital ridges and the mesonephros. Similar to the earlier PAS region, the posteriorly located AGM region also showed hematopoietic activity, first established in colony-forming unit-spleen (CFU-S) assays from early E10 (Medvinsky et al., 1993, 1996). The most intriguing finding came soon after, when it was described that the AGM region not contained CFU-S, but was in fact the autonomous site of emergence of adult-like definitive HSCs, which were able to colonize the FL and give rise to transplantable long-term (LT-) HSCs (Medvinsky and Dzierzak, 1996; Müller et al., 1994). Starting from E10, dissected AGM regions, cultured as explants, then dissociated and the cells transplanted, were able to maintain long-term hematopoiesis in lethally irradiated recipient mice. In addition, when the AGM region was further dissected into its two anatomically most distinct components (DA and urogenital ridges), it was established that the dorsal aorta (DA) is the first and major site of definitive hematopoiesis (de Bruijn et al., 2000). The same study also discovered that, in addition to the DA, other arterial, but not venous, larger vessels of the embryo also contain high frequencies of HSCs (de Bruijn et al., 2000). These were the vitelline artery (VA) and the umbilical artery (UA), collectively termed VU. Interestingly, the VA contained fewer HSC

precursors the closer it was located to the YS (Gordon-Keylock et al., 2013). Of note, regardless of blood circulation, the YS was less efficient in generating CFU-S and, as described before, lacked long-term engraftability (Medvinsky and Dzierzak, 1996). This suggests that the AGM, and more specifically the DA with the UVA branching from it, is the exclusive site of emergence for definitive HSCs (de Bruijn et al., 2000; Medvinsky and Dzierzak, 1996; Gordon-Keylock et al., 2013). Interestingly, when the AGM and UVA were tested for EMP potential in culture, it was, once again, established that EMPs were solely found in and derived from the YS at E9.5 (McGrath et al., 2015), therefore anatomically separating the transient progenitor and definitive HSC waves.

The fetal liver

From late E11.5 the hematopoietic capacity of the AGM region decreased dramatically, while simultaneously increasing in the next hematopoietic site, the fetal liver. As described before, the FL rudiment starts to form from around E9.5 (Zorn, 2008). The first few progenitors to colonize the FL are of the single and dual megakaryocytic and erythroid lineage (Tober et al., 2007). They first expand in the YS, then via circulation seed the FL around 31sp (E10.5; Tober et al., 2007). After YS-derived progenitor cells, the AGM-derived hematopoietic stem and progenitor cells (HSPCs) contribute to FL colonization around E11. Concomitant with HSC expansion within the FL, increasing numbers of HSCs were found in the blood circulation (Kumaravelu et al., 2002). A day later the YS also becomes competent to either generate or expand HSCs (Kumaravelu et

al., 2002). It was suggested that FL colonization of definitive HSPCs occurs in 2 waves. The first HSCs are generated in the AGM and colonize the FL around E11. The second colonization wave derives from the YS. Although starting from E10.5, this second wave from the YS peaks only at E12 (Kumaravelu et al., 2002).

The number of HSPCs in embryonic tissues

Utilizing explant cultures and limiting dilution transplant assays it was possible to determine how many definitive HSCs are likely contained within the embryo at different developmental stages (E10-E13). While the E11 embryo was found to contained around 1 HSC in the AGM and FL each (3 HSCs in the whole conceptus), the E12.5 AGM harbored almost 3 HSCs and the majority (53/66) were found in the newly colonized FL (Kumaravelu et al., 2002). In parallel to the increase of HSCs within the FL, the number of HSCs within blood circulation also increased, likely due to immature HSC precursors present at earlier developmental time points which then mature into functional HSCs. The presence of immature HSC precursors was supported by the fact that at E10.5 only cells from explant-cultured, but not fresh AGMs were able to engraft (Medvinsky and Dzierzak, 1996; Rybtsov et al., 2011). Around 50,000 blood progenitors with colony-forming ability but only an estimated 30 HSPCs colonized the FL by E11.5 (Inlay et al., 2014). Such incessant increase of HSC numbers in the FL within around 24h and the possibility of immature HSC precursors colonizing the FL, suggest that, by itself, the FL is not a *de novo* source of HSC emergence but rather plays a supportive role in the

maturation of HSC precursors and expansion of other progenitor cells (Inlay et al., 2014; Johnson and Moore, 1975). Early on, it was suggested that the FL is dependent on colonization of YS-derived (and later AGM-derived) progenitors (Moore and Metcalf, 1970). Interestingly, more recent experiments have supported this statement: in E11 and E12 explant cultures, the FL was not able to maintain, let alone expand or *de novo* generate HSC (Kumaravelu et al., 2002).

The placenta as a source of HSCs

In addition to these, now considered, classical sites of developmental hematopoiesis, reports of more unusual site have also been documented. One likely site for hematopoiesis is the placenta and one of the earliest suggestions for this came from Dancis et al in 1968 (Dancis et al., 1968). Later, it was confirmed that the placenta showed hematopoietic activity starting from 20sp (E9.5) in colony-forming assays (Alvarez-Silva et al., 2003). In addition, starting from early E11 the placenta also contained definitive HSCs able to engraft adult recipients in serial transplants (Gekas et al., 2005; Ottersbach and Dzierzak, 2005). This ability peaked at E12 and frequency analysis revealed that one placenta contained around 12 HSCs at E12 (Ottersbach and Dzierzak, 2005). Interestingly, the placenta was not able to either increase the numbers of HSCs (expansion) or mature HSC precursors into functional HSCs in an explant culture step prior to transplants, compared to other known hematopoietic sites (e.g. AGM). This led to the conclusion, that while the placenta contained HSCs, it is unlikely to generate them *de novo* (Ottersbach and Dzierzak, 2005).

However, isolation and assessment of the earliest structures of the developing placenta (the allantois and chorion of the 7-8dpc embryo, which later fuse to form the chorio-allantoic placenta) revealed that these structures independently do have multi-lineage potential in culture as early as the headfold stage (7dpc; Zeigler et al., 2006). Thus, the earliest precursors of the placenta have the ability to autonomously generate hematopoietic progenitor cells. In fact, the placenta was shown to contain multi-potent progenitor cells at midgestation (Lee et al., 2010), but whether that ability extends to the generation of HSCs is still unknown.

Additional sites of developmental hematopoiesis

Several less obvious sites where hematopoietic cells or clusters were found include the head, heart and somites (Yzaguirre and Speck, 2016). Expression analysis of known markers of developmental hematopoiesis (discussed in Chapter 1.8) revealed the presence of hematopoietic progenitors within those sites. Specifically, Li *et al* functionally assessed different parts of the embryonic head for HSPC potential. They found not only that the head contains EMP and lymphoid potential but that it also harbors engraftable multi-lineage LT-HSCs when transplanted at a high dose (around 2ee at E10 and 1ee at E11). However, the efficiency of the head to generate HSCs was not as high or as frequent as the efficiency of the AGM region (Li et al., 2012, 2016). Although containing HSPCs, it is not known whether the head is a site of emergence for definitive HSCs. Recently, detailed imaging analysis of the head vasculature, cell behavior and cell markers associated with the emergence of blood contested the

notion of the embryonic head generating HSCs *de novo* (Iizuka et al., 2016; Li et al., 2016).

Similarly, the heart was shown to contribute to the pool of transient definitive progenitors with the ability to form erythro-myeloid progeny in culture (Nakano et al., 2013). In addition, phenotypic blood cells have been reported in the somites of mouse embryos before, but never functionally tested (Yzaguirre and Speck, 2016). Intriguingly, a new study in zebrafish embryos implied that the early somites are able to not only contribute to hematopoiesis but, in fact, represented an independent lineage of HSCs able to give rise to multiple blood types in serial *in vivo* transplants. Further, these somitic HSCs have a different molecular signature than conventional definitive HSCs (Qiu et al., 2016). It remains to be examined if a somitic HSC lineage is also present in the mammalian embryo.

To conclude, the major sites of developmental hematopoiesis in the mouse embryo are the YS blood islands, the PAS/AGM region and the FL. These sites correspond to but also overlap with the distinct waves of blood development. Additional embryonic and extra-embryonic blood-harboring compartments have also been discovered. They include the placenta, head, heart and somites. Identification of novel sites of hematopoietic activity is important for our understanding of developmental hematopoiesis. However, the ever-accelerating complexity makes it difficult to distinguish different progenitor and stem cell types, their individual potentials and functions and their origins and molecular

pathways in order to arrive at a comprehensive roadmap of developmental hematopoiesis. The following chapters will elucidate some of these complexities, starting with the identification of specific cell types responsible for successful blood emergence.

1.4 The close relationship between endothelium and blood

In the previous parts I have discussed that developmental hematopoiesis occurs in a short developmental timeframe and in 3 overlapping waves of hematopoiesis. In addition, the main sites that generate early blood progenitors and HSCs have been mapped to the YS and AGM region, respectively. Interestingly, in both embryonic sites, a close association of endothelial cells (ECs) with hematopoietic cells (HCs) was reported. This close link was first observed in cross-sections of the YS BIs, where from late 7dpc the primitive mesoderm differentiates into HCs surrounded by a thin layer of ECs (Murray, 1932; Palis et al., 1995). A similar EC-HC association was also observed in the AGM region where HCs were attached in clusters of cells to the endothelial lining of the dorsal aorta (DA) and other major arteries of the embryo (UVA) (Figure 1.3) (Garcia-Porrero et al., 1995; de Bruijn et al., 2000). This HC attachment to ECs was conserved in other species and was documented in the human (Tavian et al., 1996), pig (Smith and Glomski, 1982), chick (Jaffredo et al., 1998) and frog embryo (Ciau-Uitz et al., 2000). While all of these studies have identified HC clusters attached to the DA endothelium, the exact mechanism of how HCs became attached to the endothelium was not

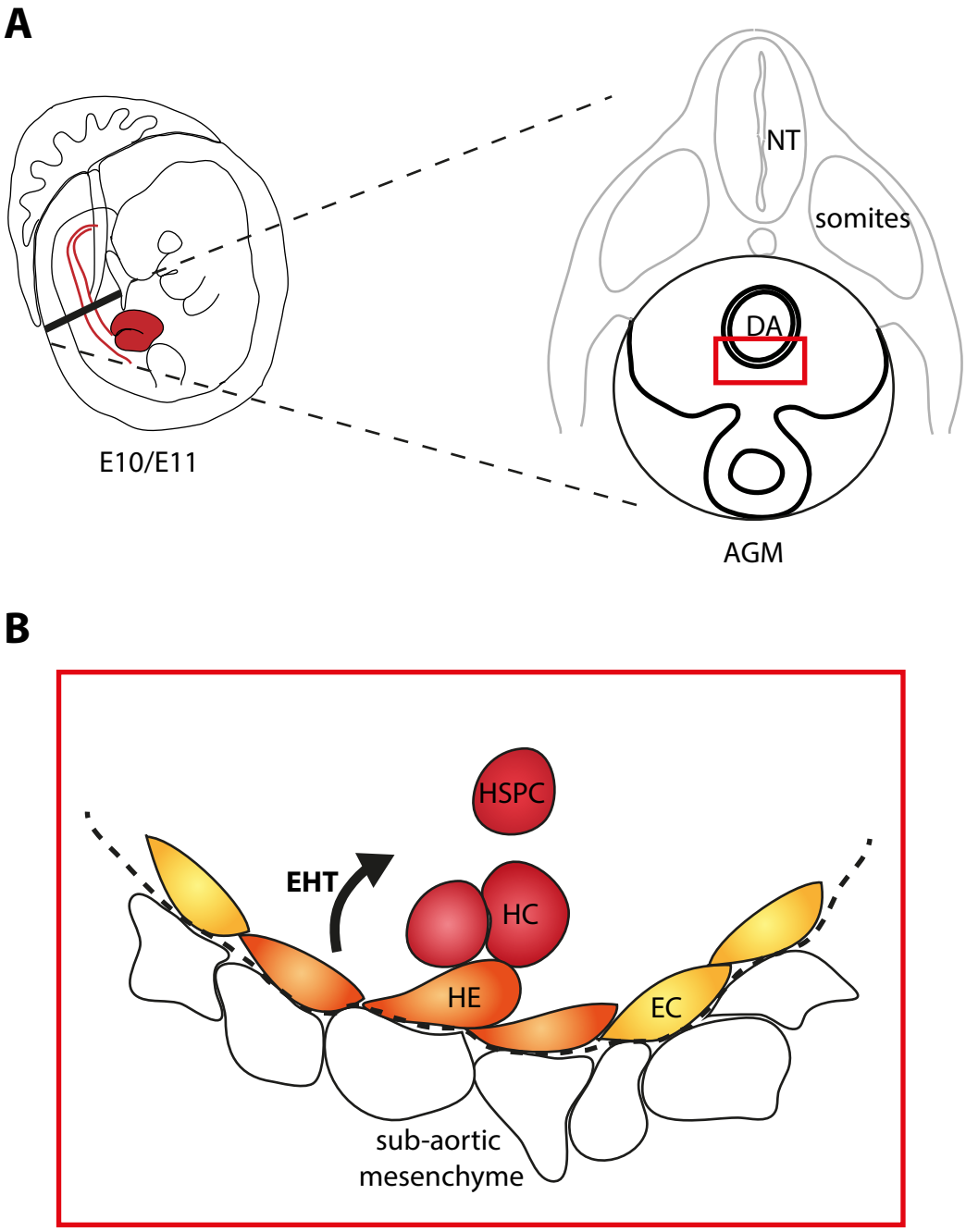


Figure 1.3: The endothelial-to-hematopoietic transition
A) Schematic of a midgestation mouse embryo and a transverse section through the AGM region. The AGM region is located below the neural tube (NT), the notochord and the somites. **B)** Zoom in on the boxed area of the AGM region, specifically focusing on the ventral aspect of the dorsal aorta (DA). A subset of the endothelium (EC, yellow), the so called hemogenic endothelium (HE, orange), buds out into the DA lumen to form intra-aortic cluster cells consisting of hematopoietic cells (HCs, red) and hematopoietic stem and progenitor cells (HSPCs), which later detach from the DA lining and migrate to the fetal liver.

known at the time. In addition, ECs and HCs in the AGM region share many markers, including the transcription factors Runx1 (North et al., 2002), Scl (Sanchez et al., 1999), and Gata2 (Minegishi et al., 1999), the cell surface proteins Sca1 (de Bruijn et al., 2002), c-kit (Bernex et al., 1996; Sánchez et al., 1996), CD31 (Baldwin et al., 1994; North et al., 2002), and CD34 (Wood et al., 1997), and the trans-membrane protein VE-Cadherin (VEC) (Alva et al., 2006; North et al., 2002; Oberlin et al., 2010; Taoudi, 2005).

1.5 The ontogeny of the hemtopoietic lineage

Hemangioblast

Anatomical proximity and immunophenotypic similarity led several early studies to conclude that endothelium and blood have a common origin, namely the hemangioblast (Murray, 1932; Sabin, 1921). The existence of a bi-potential progenitor was initially confirmed in *in vitro* ES cell differentiation cultures with the identification and characterization of a blast-colony forming cell (BL-CFC; Choi et al., 1998; Kennedy et al., 2007). The BL-CFC was found to have bi-potential properties to develop into endothelial and hematopoietic precursors and was therefore likened to the previously described hemangioblast (Choi et al., 1998; Kennedy et al., 2007). Of note, so far, the hemangioblast has been defined by its potential rather than by fate. This means, that although the potential of the hemangioblast has been defined as giving rise to both, ECs and HCs, the

fates of individual cells were not formally traced, to unambiguously provide proof of bi-potentiality on a clonal level (Ueno and Weissman, 2010). One study in the mouse embryo has identified regions of the primitive streak mesoderm to contain the potential to generate ECs, HCs and vascular smooth muscle cells (vSMC) (Huber et al., 2004). In the zebrafish embryo, a small number of cells was shown to give rise to both EC and HC, although the majority of the two cell populations had distinct origins (Vogeli et al., 2006). In brief, 1 cell-stage zebrafish embryos were injected with photo-activatable FITC compound, which was activated at the shield stage in one cell per embryo. The single cell was then traced to the 30 hpf embryo within either endothelium (Flk1-reporter), blood (Gata1-reporter) or both (potential fate map of a hemangioblast cell) (Vogeli et al., 2006). That way it was shown that the progeny of the majority of shield-stage cells have single fates for either EC or HC and only a small subset was shown to have hemangioblast-like properties. The rarity of a bi-potent precursor (hemangioblast) giving rise to both ECs and HCs and the difficulty to provide proof for the existence of such a progenitor *in vivo*, has split the opinions of scientists in this field. It led to the conclusion that while the ES cell differentiation field does observe a hemangioblast-like population, in the embryo, the evidence for such progenitor remains largely unfounded (Slukvin, 2016).

Hemogenic endothelium

An alternative origin was proposed: in the embryo, blood differentiates from the endothelium, and more specifically from the hemogenic

endothelium (HE) (Smith and Glomski, 1982). The first studies to show this differentiation potential, thus establishing the existence of HE, were performed in chick embryo dye-labeling experiments (Jaffredo et al., 1998). Briefly, prior to the emergence of HCs, ECs were labeled with fluorescent dye (AcLDL-DiI), which is readily taken up by ECs (Voyta et al., 1984). The following day, DiI was observed within HCs in clusters attached to the DA wall (Jaffredo et al., 1998). Similar experiments have been done in the E10.5 mouse endothelium and resulted in DiI presence in circulating blood cells with multilineage potential and the ability to reconstitute irradiated recipients (Sugiyama et al., 2005, 2003). Similarly, *in vitro* assays testing hemogenic potential, identified that VEC+CD45- ECs had a better efficiency to form hematopoietic progeny in culture than VEC-CD45+ HCs, supporting the endothelial origin of HCs (Nishikawa et al., 1998a, 1998b). Further, an elegant lineage tracing study in the mouse embryo determined that ECs directly contribute to the adult HSC lineage (Zovein et al., 2008). Using a tamoxifen-inducible VEC transgenic mouse line allowed the tracing of the midgestation AGM endothelium to a significant portion of FL and BM hematopoietic cells (Zovein et al., 2008). In summary, tamoxifen-mediated VEC-Cre activation was induced at E9.5 and all progeny of VEC-reporter+ cells traced to hematopoietic tissues during development as well as the adult mouse BM. In addition, using a constitutive VEC-Cre transgenic mouse line, Chen *et al.* established that approximately 85% of FL blood cells at one time in their lifespan expressed VEC (Chen et al., 2009). In addition, cells that have undergone EHT progressively lose VEC expression with advancing maturation into

HSCs (Taoudi, 2005). In the YS, a hemogenic subpopulation of the endothelium was also identified giving rise to CD41+ hematopoietic progenitor cells (Frame et al., 2016; Li et al., 2005; Ferkowicz et al., 2003). In addition, recent ES cell differentiation studies have shown the existence of HEs *in vitro* (Eilken et al., 2009). ES cell-derived ECs were plated in OP9 assays (known to support the differentiation to HCs) and their differentiation recorded over several cell generations (up to 7 days in culture). Over time ECs transitioned to a CD41+ early hematopoietic progenitors which later developed into CD41+CD45+ hematopoietic cells (Eilken et al., 2009). In order to reconcile the different hypotheses on the origin of the blood and endothelial lineages, a model was proposed, whereby the Flk1+ mesoderm (hemangioblast) differentiates into HE, which then gives rise to hematopoietic progeny (Lancrin et al., 2009). It was suggested that such *in vitro* stepwise progression is likely also a feature of YS hematopoiesis but not definitive AGM hematopoiesis (Slukvin, 2016). However, clonal analysis of primitive streak mesoderm precursors giving rise to YS BI has revealed that ECs and HCs have a polyclonal origin (Ueno and Weissman, 2006) and in fact are derived from independent epiblast mesoderm cells (Padron-Barthe et al., 2014). Such studies imply that the concept of a so-called ‘hemangioblast’ population is exclusively a feature of the *in vitro* ES cell differentiation system.

The origin(s) of HE

A question that divides opinions in the developmental hematopoiesis field is the single or dual origin of the YS HE and AGM HE and therefore the

concept between primitive and definitive hematopoietic waves. The more widely accepted model of the dual origin has been specifically shown in the frog (Ciau-Uitz et al., 2000). In the mouse embryo, primitive streak fate mapping experiments have shown that the endothelium of the YS and the AGM derive from different mesoderm compartments (Kinder et al., 1999; Lawson et al., 1991). Specifically, lineage tracing of the lateral plate mesoderm (LPM) established its contribution to the AGM endothelial and hematopoietic cells of the mouse and chick embryo (Wasteson et al., 2008; Zovein et al., 2010) and to all BM cell in the adult mouse (Zovein et al., 2010). By contrast, the YS endothelium derives from a different mesoderm subset, which was shown to ingress through the primitive streak earlier than the precursors of the LPM mesoderm (Kinder et al., 1999, 2001; Lawson et al., 1991).

In contrast, Nishikawa and colleagues have tried to establish a single origin for the mouse hematopoietic system, whereby the YS contributes to the adult BM HSC compartment and uses the AGM as an educational/maturation site of hematopoiesis (Samokhvalov et al., 2007). This study was met with controversy due to questions about the sensitivity and exact spatio-temporal activity of the inducible Cre-labeling system used. Therefore, although the majority of data support the former model, the exact origin(s) of YS HE and AGM HE are still debated (Medvinsky et al., 2011)(see Chapter 6).

1.6 The HSC roadmap

The endothelial-to-hematopoietic transition

Although it was established that the HE transitions into HCs, the exact mechanism of how this occurs was not known. However, recent advances in imaging technology and generation of reliable reporter lines have made it possible to establish the exact mechanism underlying HC generation from ECs: Several live imaging zebrafish studies have shown that aortic endothelial cells engage in a budding activity resulting in the development of hematopoietic cells which shortly after enter the blood stream (Bertrand et al., 2010; Kissa and Herbomel, 2010; Lam et al., 2010). This process required physical changes of ECs from flat, elongated to a round morphology. Imaging thick sections of the mouse AGM showed a similar budding process in the mammalian embryo (Boisset et al., 2010). This budding process or endothelial-to-hematopoietic transition (EHT) was also conserved *in vitro* on a single-cell level (Eilken et al., 2009). Interestingly, all systems that successfully showed EHT events, reported that not all but only a small subset of endothelial cells has the potential to differentiate into blood, further supporting the notion that a specialized subset of the endothelium is responsible for blood generation.

HSC precursors

Medvinsky and Dzierzak have previously suggested that in order to generate adult-like HSCs from the DA vasculature, a sequence of maturation events is required (Medvinsky and Dzierzak, 1996). It was

based on the observation that *in vitro* explant cultures of murine AGMs were able to expand the pool of clonogenic blood progenitors and more importantly adult-like HSCs. This was possible even at E10.5 (Medvinsky and Dzierzak, 1996). Previous reports showed that uncultured AGMs at E10.5 had a repopulation frequency of 3% (3 in 96 mice repopulated). This frequency increased to 73% (11 out of 19 mice repopulated) in uncultured E11.5 AGMs (Müller et al., 1994). In contrast, explant culturing E10.5 AGMs prior to transplants resulted in high-level long-term (LT)-HSC activity (Kumaravelu et al., 2002; Medvinsky and Dzierzak, 1996). More recently, a refined pre-transplant, re-aggregate culture system has been developed, in order to allow the maturation of precursor cells en route to HSC development (Sheridan et al., 2009; Taoudi et al., 2008). Such assays saw the discovery of at least 3 HSC precursors that were shown to directly link to the HSC lineage in a stage-dependent manner: the pro-HSC (E9.5), pre-HSC Type I (E10.5) and pre-HSC Type II (E11.5) (Rybtsov et al., 2011, 2014, 2016; Taoudi et al., 2008). Such HSC precursors have distinct cell-surface marker combinations, allowing their isolation and study. While all 3 precursors express VEC, CD41 expression marks pro-HSCs (Rybtsov et al., 2014), CD43 marks the pre-HSC Type I population (Rybtsov et al., 2011, 2014), and the initiation of CD45 expression labels the pre-HSC Type II subset (Taoudi et al., 2008). Of note, pre-HSC Type II and functional HSCs share the same immunophenotype and can only be distinguished by function in transplantation experiments (summarized in Figure 1.4). Interestingly, a 4-day culture is sufficient to mature HSCs from pre-HSCs Type I and II, while maturation from an earlier precursor (pro-

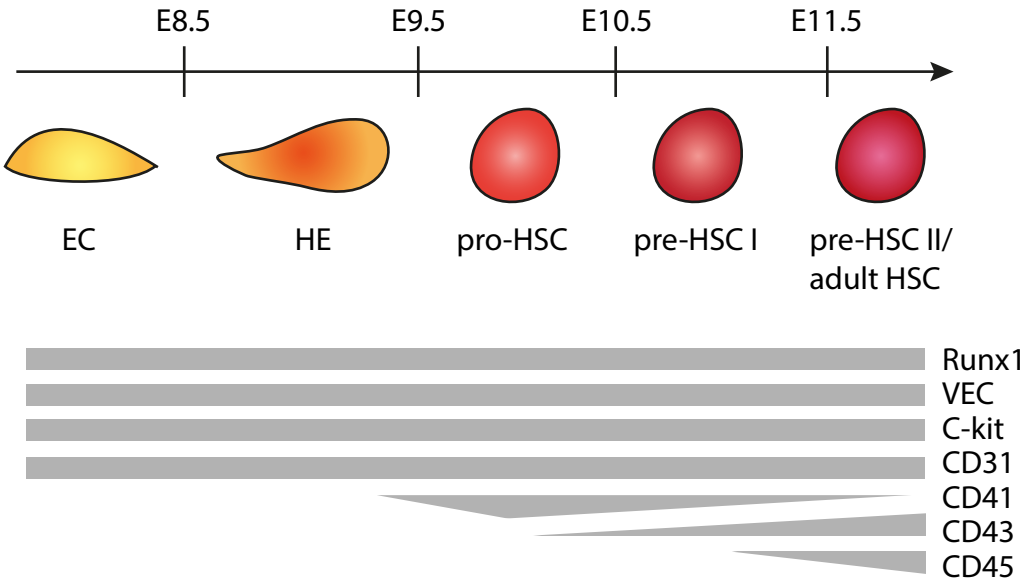


Figure 1.4: The HSC roadmap
Schematic depiction of the HSC lineage with the chracteristic immunophenotypes of individual cellular intermediates. Many cell surface markers (e.g. VEC, CD31, C-kit) and transcription factors (e.g. Runx1) are shared between the cellular intermediates of the HSC roadmap. With advancing maturation and commitment to the hematopoietic lineage other, more specific, markers are expressed and define the discreet HSC precursor stages. Adapted (with changes) from Rybtsov *et al*., 2014.

HSC) requires a 7-day culture (Rybtsov et al., 2014). This is likely due to the increasing ease of more mature cells to respond to hematopoiesis-inducing signals. Addition of specific cytokines to the reaggregate culture medium aided the expansion and differentiation potential of HSC precursors, thus mimicking the extrinsic signals from other tissues that guide HSC development *in vivo* (Rybtsov et al., 2014; Souilhol et al., 2016a)(discussed in Chapter 1.7).

More recently, the different cellular intermediates of the HSC roadmap were isolated based on phenotype and single cells analyzed by RNA-seq and functional transplantation experiments (Zhou et al., 2016). The transition from EC to pre-HSC Type I was associated with downregulation of genes involved in cell migration, development of the vasculature and blood cell morphogenesis, while genes that were upregulated were enriched for hematopoietic or lymphoid organ development and intracellular signaling cascades. Pre-HSC Type I and Type II were relatively similar to each other, but differed to HSCs in cell cycle kinetics. In short, pre-HSCs were most proliferative and showed highest chimerism in transplants. E14 FL HSCs were primarily in G1 phase, while adult BM HSCs were mostly quiescent (G0) (Zhou et al., 2016). Of note, the endothelial population analyzed in this study was the E11.5 DA endothelium, therefore not HE. Overall, such detailed transcriptome analysis of HSC roadmap cell intermediates paves the way for a better understanding of cell fate decisions.

In a recent study, our lab focused on the segregation of HE maturation stages at different developmental stages (Swiers et al., 2013). Single cell Fluidigm® and functional analysis of HEs from E8.5-E10.5 PAS and AGMs, as well as CD41+ blood progenitors and CD41+CD45+ hematopoietic cells, was able to describe EHT on a molecular level. The downregulation of endothelial genes observed in other studies (Taoudi, 2005; Zhou et al., 2016; Zovein et al., 2008) was found to be preceeded by a loss of endothelial tubule formation in OP9 co-cultures starting from E9.5, while the ability to respond to hematopoietic-inducing factors increased with developmental time (Swiers et al., 2013). Such insights illustrate the stepwise commitment to the HSC lineage and provide the tools to isolate specific cellular intermediates for further analysis.

1.7 The AGM niche

Spatial distribution

In the previous paragraphs I have described the cellular intermediates within the HSC lineage, here I focus on the role of the AGM niche for HSC generation. Of importance is the spatial distribution of the intra-aortic cluster cells within the AGM region. Several studies have reported that while both the dorsal and the ventral parts of the DA contribute to developmental hematopoiesis in the form of CFU-C activity, only the ventral portion was able to generate adult-like HSCs at midgestation (Taoudi and Medvinsky, 2007). This correlated with the observation that

the majority of both large and small intra-aortic cluster cells were detected in the ventral half of the DA at E11.5 (Taylor et al., 2010; Yokomizo and Dzierzak, 2010). Such observations would suggest that the ventral microenvironment is important for HSC generation. A number of signaling pathways are involved in developmental hematopoiesis while arguably the most critical ones are the hedgehog (Hh) and BMP pathways. This is due to their polarizing activity within the AGM region, where Hh is expressed in the notochord (Echelard et al., 1993), while BMP is localized to the sub-aortic mesenchyme (Durand et al., 2007; Marshall et al., 2000; Wilkinson et al., 2009). Such gradients along the dorso-ventral axis of the embryo are responsible for the initial stages of EHT as well as maturation stages towards the HSC (Souilhol et al., 2016a).

Hedgehog signaling

Studies in the zebrafish have identified that Hh is crucial for the definitive hematopoietic program, as Hh mutants show defects in HSC formation and Hh is thought to act at the top of the signalling cascade that regulates definitive hematopoiesis in fish (Gering and Patient, 2005). While in fish, Hh did not have a direct effect on HSC generation or maintenance (Wilkinson et al., 2009), in the mouse AGM, the sonic Hh (Shh) gradient from the notochord has an inductive effect at E10.5 but not at E11.5 (Peeters et al., 2009; Souilhol et al., 2016a). Receptors for Shh were expressed on ECs and Type I pre-HSCs and it was therefore assumed that Shh specifically acts on the pre-HSC Type I precursors, which are predominantly found in the E10.5 AGM (Souilhol et al., 2016a). *In vitro*,

addition of Indian Hh increased the number of hematopoietic progenitors derived from ES cell differentiation and E9.5 YS cultures, whereas Hh inhibition reduced progenitor generation (Kim et al., 2013). In addition, *Scl* overexpression was sufficient to rescue the phenotype caused by the blocking of Hh suggesting that Hh act upstream of *Scl* to mediate EHT (Kim et al., 2013).

Notch signaling

It has been shown that downstream of Hh, Notch signaling regulates HSC specification in zebrafish and mouse embryos (Nakagawa et al., 2006; Burns et al., 2005). Indeed, Notch activity induced the expression of *Runx1*, a critical regulator of definitive hematopoiesis (Nakagawa et al., 2006; Burns et al., 2005). In addition, different Notch ligands regulate arterial or hemogenic fates of the endothelium: High levels of Dll4 on endothelial cells maintain arterial endothelial fate. In contrast, Jagged1 induced a low level of Notch signaling thereby inhibiting the endothelial program and in turn initiating hematopoiesis in the mouse AGM (Ayllón et al., 2015; Gama-Norton et al., 2015). Moreover, Jagged1 regulates Gata2 expression, an early marker of definitive hematopoietic specification (Robert-Moreno et al., 2008, 2005). It was also established that the Notch target Hes1 is expressed in endothelial and cluster cells. There, Hes1 represses *Gata2*, thereby creating a feed-forward loop required to confine Gata2 expression in emerging HSCs (Guiu et al., 2013). Interestingly, *Hes1* deficiency results in no obvious hematopoietic abnormalities, which was attributed to the compensation with *Hes5*. Deletion of both *Hes1* and

Hes5 results in an overproduction of intra-aortic clusters with loss of functional HSPC activity (Guiu et al., 2013). Another member of the Notch pathway, membrane-bound Dlk1 which is broadly expressed in the sub-aortic mesenchyme, was also implicated in the negative regulation of HSPCs by limiting their expansion (Mirshekar-Syahkal et al., 2013). Focusing on the role of Notch activity in HSC precursors, a new study showed that Notch-dependence decreases after the transition from pre-HSCs Type I to Type II, and is dispensable in definitive HSCs in the AGM and BM (Souilhol et al., 2016b). These studies highlight the tight maturation window of Notch-dependence. Notch expression, itself, is mediated by non-canonical Wnt16 expression in the fish, whereby this effect is in turn mediated by FGF signaling (Clements et al., 2011; Lee et al., 2014).

TGFβ signaling

Like Hh, TGFβ acts upstream of Notch, and in fish, specifically regulates the expression of Jagged1 in HE, while the paracrine TGFβ3 (excreted by the notochord) regulates the initiation of EHT (Monteiro et al., 2016). This is supported by the fact that TGFβ1 is expressed in intra-aortic cluster cells in the human AGM (Marshall et al., 2000). Surprisingly, in ES cell differentiation cultures, TGFβ impairs EHT by confining cells to the arterial fate (Vargel et al., 2016). The regulation of TGFβ levels is likely of high importance for EHT, as increased TGFβ levels upregulated Sox17, which in turn repressed hematopoietic TFs Runx1 and Gata2, thereby favoring the arterial rather than hemogenic fate (Bos et al., 2015; Lizama et al.,

2015).

BMP signaling

From the ventral side of the AGM, a BMP4 gradient is also highly involved in HSPC generation and maintenance (Durand et al., 2007; Goldman et al., 2009; Wilkinson et al., 2009). BMP4 is expressed in the sub-aortic mesenchyme of the AGM region and more specifically in cells directly underneath intra-aortic cluster cells (Durand et al., 2007; Marshall et al., 2000; Souilhol et al., 2016a). Interestingly, the maturation towards HSCs seemed to be related to an increase of BMP antagonist levels in HSC precursors, suggesting an inhibitory role of BMP in this process (Souilhol et al., 2016a). However, residual BMP activity is possible, as all (pre-) HSCs showed BMP activity, as detected by a BMP-responsive reporter expression (Crisan et al., 2016). Interestingly, explant-cultured AGMs contained two types of functional HSCs: BMP-activated and non-BMP-activated HSCs. The latter was regulated by Hh signaling via the Vegf pathway (Crisan et al., 2016). Transcriptome analysis showed that the BMP-activated cells had a more hemogenic endothelial signature, while non-BMP-activated cells showed a highly hematopoietic signature. Further studies are required in order to consolidate the two publications. To add to the complexity, similar BMP-active and non BMP-active HSCs were found in the adult BM with different hematopoietic lineage outputs (Crisan et al., 2015). In order to identify the mechanistic role of BMP signaling in HSC emergence, another study established that shear stress-induced PKA-CREB activation in VEC+ endothelial cells results in the secretion of BMP

ligands to neighboring HE cells promoting hematopoiesis (Kim et al., 2015). This is further confirming a role of hemodynamic forces in the DA vasculature on developmental hematopoiesis (Adamo et al., 2009) (discussed in Chapter 1.10).

Sub-aortic mesenchyme-derived HSCs?

Over the last 2 decades, several studies have suggested that the sub-aortic mesenchyme, rather than playing a supportive and inductive role in HSC generation, could actually harbor precursors of HSCs, that would later form intra-aortic clusters (Bertrand et al., 2005; Manaia et al., 2000). The basis of such hypothesis came from imaging studies that identified a peculiar expression pattern of Gata3 in sub-aortic patches of the mouse AGM. At the time, no co-expression with CD45 was observed, although both cells were frequently found adjacent to each other (Manaia et al., 2000). A follow-up study, however, showed Gata3+Gata2+CD31+ foci in the sub-aortic mesenchyme, that also expressed CD41 and CD45 in rare, isolated cells (Bertrand et al., 2005). Of note, CD41 and CD45 expression is also a feature of HSC precursors in intra-aortic clusters (Rybtsov et al., 2011; Taoudi et al., 2008). In order to establish if such precursors localized to the sub-aortic mesenchyme, the E11.5 DA was labeled with Oregon Green (OG) dye, which would readily diffuse through cell layers creating a gradient of fluorescence in clusters (OG^{high}), endothelium (OG^{+}), first layer of sub-aortic mesenchyme (OG^{low}) and deeper layers of sub-aortic mesenchyme (OG^{-}). Direct transplantations of OG sorted cells showed that only $CD45^{+}OG^{high}$ cells reconstituted recipient mice, in line with

previous data (Rybtsov et al., 2011; Taoudi et al., 2008). However, the OG^{low} and OG^{-} subsets were able to engraft irradiated mice after *in vitro* cultures, suggesting that the sub-aortic mesenchyme harbors pre-HSCs (Rybtsov et al., 2011). In addition, a lineage tracing study suggested that the early mesenchyme may indeed contribute to definitive hematopoiesis, although it required an endothelial intermediate (Zovein et al., 2008).

The interpretation of these earlier reports were recently questioned as the concept of a sub-aortic origin of HSC emergence does not agree with our current understanding of this process. Similar to early chick labeling experiments that established the transition of ECs into HCs (Jaffredo et al., 1998), the mesenchyme of chick embryos was labeled and followed by a culture period. No labeling was observed within CD45+ hematopoietic cells in the intra-aortic clusters, therefore excluding a direct transition from mesenchyme to HC (Richard et al., 2013). A detailed study of wholemount embryos, analyzing the stepwise formation of the vitelline artery derivatives (mesenteric blood islands) had proposed an explanation for the appearance and seeming potential of sub-aortic patches (Zovein et al., 2010). It seemed that while in transverse sections these patches look like isolated islands of hematopoietic cells, analysis of wholemount embryos showed that they are, in fact, part of the larger vitelline remodeling complex and connect to the embryonic circulation (Zovein et al., 2010).

Mesenchymal stem cells or mesangioblast

Several studies have investigated the connection between the AGM niche and the emergence of mesenchymal stem cells (MSCs). These cells are

tripotent progenitors able to differentiate into cartilage, fat and bone (Wang et al., 2008; Mendes et al., 2005). A similar entity sharing these properties was described in culture as the mesangioblast (Vodyanik et al., 2010). Interestingly, two studies have suggested the embryonic endothelium as a source of mesangioblast cells. In one study, the VEC+ YS lineage was traced and their contribution observed in skeletal and smooth muscle cells. Those cells, when isolated and cultured, were able to further differentiate into smooth muscle, cartilage and bone and showed expression of some of the MSC markers (Azzoni et al., 2014). While a non-endothelial origin of such mesangioblast cells was not excluded, an earlier study found that the DA endothelium of the AGM also showed mesangioblastic properties (Minasi et al., 2002). Cells derived from quail or mouse embryonic aortae were grafted into host chick embryos and showed donor cell contribution to blood, cartilage, bone and, smooth, skeletal and cardiac muscle (Minasi et al., 2002). Interestingly, in the ES cell differentiation system the data show somewhat different results (Vodyanik et al., 2010). There, the mesangioblast was described as a bi-potent precursor able to differentiate into MSC-like cells (with tri-potential) as well as into non-hematopoietic endothelial cells (Vodyanik et al., 2010). While it is likely that the plasticity of the developing extra- and intra-embryonic tissues extend to the MSC lineage and its precursors, further studies are required to reconcile and explain the differences observed in various model systems.

1.8 Key intrinsic regulators of developmental hematopoiesis

Several genes have been described in the context of developmental hematopoiesis and its regulation. Individual expression of such genes often mark multiple cellular intermediates of the HSC roadmap (discussed in Chapter 1.4). However, specific combinations of gene expression allow the identification of distinct signatures at different stages of hematopoietic commitment (Swiers et al., 2013). A list of the most important genes and their broad association to different stages of EHT are described in the next sub-chapters.

Endothelial genes

At the top of the hierarchy that regulates developmental hematopoiesis is the Vegf receptor, Flk1. Flk1 is thought to be the first mesoderm marker that specifically marks the mesoderm that later will differentiate to hemato-endothelial fates (Nishikawa et al., 1998b). It is expressed early in mouse development (7dpc) in the proximal-lateral mesoderm and later in both extra-embryonic YS BIs and intraembryonic vasculature (Drake and Fleming, 2000; Dumont et al., 1995; Yamaguchi et al., 1993). Embryos deficient for *Flk1* die between E8.5 and E9.5 due to grossly abnormal vasculature development and defective hematopoiesis (Shalaby et al., 1995). In chimeric mice, *Flk1*-null cells do not contribute to primitive or definitive hematopoiesis and lack the ability to reach the YS BIs (Shalaby et al., 1997).

Next, Etv2, an ETS transcription factor, is downstream of Flk1 and required for the early stages of hematopoietic specification of the

mesoderm and is also expressed in a subset of Flk1+ mesoderm (Ferdous et al., 2009; Rasmussen et al., 2012). It is expressed in the YS BI at 7dpc with gradual downregulation of expression within embryonic endothelium and no expression observed by E10.5 (Eliades et al., 2016). It plays a central role in orchestrating the HC and EC programs (Liu et al., 2015). In genetic fate mapping studies it was established that only Etv2+ cells were able to give rise to endothelium and blood. Moreover the loss of *Etv2* resulted in the induction of the cardiac mesoderm, reduced Flk1 expression and early onset of vascular and hematopoietic defects, similar to *Flk1* mutant phenotypes (Ferdous et al., 2009; Lee et al., 2008; Rasmussen et al., 2011). In addition, ablation of Etv2 in the caudal-lateral mesoderm affected the vitelline plexus and DA cluster formation (Kataoka et al., 2013). Re-expression of Etv2 in *Etv2*-mutant cells, rescued the effect, while enforced expression in WT ES cells enhanced the differentiation into EC and HC (Lee et al., 2008; Wareing et al., 2012). Re-expression experiments in *Etv2*-mutant cells, established that Scl, Gata2 and Fli1 act downstream of Etv2 (Wareing et al., 2012). A more recent study confirmed that Etv2 directly interacts with *Gata2* to regulate further downstream targets, such as *Pu.1*, both *in vivo* and *in vitro* (Shi et al., 2014). Interestingly, in the adult, Etv2 has a critical role in HSC maintenance as *Etv2* deletion resulted in gene dose-dependent decrease of the number of HSCs (Lee et al., 2011).

Fli1, another ETS transcription factor, is directly regulated by Etv2 and is expressed early in development (Abedin et al., 2014). *Fli1* mutants exhibit hematomas and hemorrhage around the DA and their FLs shows reduced

CFU efficiency with subsequent embryonic lethality by E12.5 (Spyropoulos et al., 2000). In addition, it was established that Fli1 is an upstream regulator of Tie2 or Tek, which is a tyrosine kinase receptor (Abedin et al., 2014). In the early embryo, Tie2 marks the extra- and intra-embryonic mesoderm and endothelium (Dumont et al., 1995; Ema et al., 2006; Sato et al., 1993), while in the midgestation embryo, Tie2 labels all endothelium within the AGM region (Hamaguchi et al., 1999).

Early hematopoietic genes

At the onset of EHT, Gata2, a member of the Gata family of transcription factors, many of which are implicated in developmental hematopoiesis, was found to be essential for primitive and definitive hematopoiesis. It is expressed at the early stages of EHT in the YS and AGM vasculature as well as in hematopoietic cells (Kobayashi-Osaki et al., 2005; Minegishi et al., 1999, 2003). Interestingly, a Gata2-GFP reporter line, showed transgene expression in HE and all clonogenic blood progenitors (Kobayashi-Osaki et al., 2005) while in a separate Gata2-Venus reporter line, the transgene marked only a subset of hematopoietic progenitor cells (Kaimakis et al., 2016). The latter study showed that differential Gata2 expression on progenitor cells leads to differences in the molecular signature and lineage output of these cells (Kaimakis et al., 2016). In the zebrafish, the gata2b ortholog also functions within HE, while the gata2a ortholog functions in a broader fashion throughout the embryonic vasculature (Butko et al., 2015). On the other hand, *in vitro* studies have established a role for Gata2 in the generation and differentiation of the

hemangioblast, whereby *Gata2* was a direct target of BMP4 (Lugus et al., 2007). Further, when Gata2 together with either Etv2 or Scl were induced in human pluripotent stem cells (hPSC), it resulted in the generation of HE-type cells (Elcheva et al., 2014). In addition, Gata2 was also required for cluster and HSC generation during EHT (de Pater et al., 2013). *Gata2* deficiency leads to severe anemia and embryonic lethality by E10.5 concomitant with a dose-dependent block on the generation and expansion of HSCs (Kaimakis et al., 2016; Ling et al., 2004; Tsai et al., 1994). The critical element regulating *Gata2* expression is its +9.5 enhancer (Gao et al., 2013). Together*, Gata2, Fli1* and *Scl* as well as their respective enhancer elements form a triad of transcriptional regulation of developmental hematopoiesis (Pimanda et al., 2007).

Another marker of early hematopoietic commitment is *Meis1*, a homeobox gene. It exhibits a broad expression pattern within the AGM region in HE, intra-aortic cluster cells and the sub-aortic mesenchyme. In addition it is also expressed in FL HSCs (Azcoitia et al., 2005). Embryos deficient in *Meis1*, are severely underdeveloped, exhibit hemorrhage, liver hypoplasia, anemia, and gross vascular defects with reduced size of intra-aortic clusters. Loss of CFU-C potential and a complete lack of the megakaryocytic lineage eventually lead to embryonic lethality between E11 and E14 (Azcoitia et al., 2005). Similarly, Meis1 regulates hematopoiesis and vascular development in fish (Cvejic et al., 2011). In the BM, Meis1 protects HSCs from excessive proliferation by restricting oxidative stress (Kocabas et al., 2012; Miller et al., 2016; Unnisa et al., 2012).

Tal1, or Scl, belongs to the basic-loop-helix transcription factor family and is, similar to Gata2 and Meis1, expressed in the early stages of EHT. Specifically, together with Flk1, Scl is one of the earliest endothelial markers of the developing vasculature. Indeed Scl is expressed in isolated endothelial-primed mesoderm cells (angioblasts) of the early embryo, as well as in the YS BIs (Drake and Fleming, 2000). Later in development, Scl is expressed in embryonic ECs, HCs and the FL (Elefanty et al., 1999). *Scl* deficient embryos exhibit lack of primitive hematopoiesis and vascular defects in the YS, oedema, growth retardation, and embryonic lethality around E9.5 (Elefanty et al., 1999; Robb et al., 1995; Shivdasani et al., 1995). In addition, no Gata1 or Pu.1 expression was observed in mutant YSs, suggesting Scl acts upstream of these hematopoietic genes (Robb et al., 1995). Scl was also found to form a complex with Lmo2 and play a crucial and early role for the generation of ECs from mesoderm precursors (Gering et al., 1998, 2003). Similar to *Scl* deficiency in the mouse embryo, mutant fish failed to form the DA and likely HEs, resulting in a down regulation of hematopoietic and endothelial gene expression within the intermediate cell mass, the fish equivalent of the AGM region (Patterson et al., 2007, 2005). Such functional requirement of Scl was also observed *in vitro*, where *Scl*-null ES cells, although able to generate embryoid bodies (mesoderm precursor), were not able to generate myelo-erythroid progeny (Porcher et al., 1996).

Genes of hematopoietic commitment

Further along EHT several genes were identified to aid the commitment to

the hematopoietic lineage and some were direct target genes of the master regulator Runx1 (described in Chapter 1.11). *Gfi1* and *Gfi1b* were such Runx1 target genes (Lancrin et al., 2012). While Gfi1 alone is expressed in HE, together Gfi1 and Gfi1b mark CD41+ YS HCs as well as intra-aortic clusters and HSCs in the AGM region (Lancrin et al., 2012; Thambyrajah et al., 2015). In *Gfi1*/*Gfi1b*-null embryos no HSPCs are formed (Thambyrajah et al., 2015) and the endothelial signature is maintained, which suggests that both are involved in the downregulation of endothelial genes during EHT (Lancrin et al., 2012). This effect was recently attributed to the ability of *Gfi1* to recruit LSD1 (Thambyrajah et al., 2015). In the fish, Gfi1 expression is conserved, but not critical for primitive hematopoiesis (Thambyrajah et al., 2016). In the adult BM, Gfi1 is expressed in HSCs and required for HSC maintenance and proliferation (Hock et al., 2004; Zeng et al., 2004). The hematopoietic expression of *Gfi1* was mediated by its enhancer, which was bound by Runx1, Scl, Pu.1, Erg, Meis1 and Gata2, thereby implicating *Gfi1* and *Gfi1b* in the broader gene regulatory network of developmental hematopoiesis (Wilson et al., 2010).

Pu.1, another ETS transcription factor and target of Runx1, also promotes hematopoietic commitment of HE cells (Hoogenkamp et al., 2007; Huang et al., 2008). It is expressed in HE and with increasingly higher expression levels in more mature cellular intermediates of the HSC roadmap (Swiers et al., 2013; Wilkinson et al., 2014). *Pu.1* mutant embryos exhibit anemia in the last third of gestation and die just prior to birth (E18) with defective generation of the T/B lymphoid, monocytic and granulocytic lineages

(Scott et al., 1994). In the adult, Pu.1 regulates several cell-cycle genes in the BM, and therefore regulates HSC proliferation (Staber et al., 2013).

In addition, Myb marks mature HCs but not ECs during mouse and fish development (Mukouyama et al., 1999; Thompson et al., 1998). It is not required for the YS primitive wave and deletion of *Myb* has no effect on the AGM endothelium (Mucenski et al., 1991; Mukouyama et al., 1999; Thompson et al., 1998). Interestingly, the generation of mature HCs is impaired in the mutant embryos resulting in severe anemia after E13.5 (Mucenski et al., 1991; Mukouyama et al., 1999).

Overall, several critical genes have been described that contribute to the functioning and maturation of the hemato-endothelial lineage. These genes function in several cascades establishing complex gene regulatory networks. Recent studies have begun to decipher the detailed workings of such networks and investigated the involvement of gene-specific enhancer elements that drive gene expression (Goode et al., 2016; Lichtinger et al., 2012; Schütte et al., 2016a; Wilson et al., 2016). Central to such networks is the transcription factor Runx1, and its role in developmental hematopoiesis is discussed next.

1.9 *Runx1* and developmental hematopoiesis

In the mouse, *Runx1* (AML1 or Cbfa2) is located on Chromosome 16 and spans a region of 224kb. Transcription of the gene is initiated from 2 alternative promoters, the distal P1 and proximal P2 promoter, which are

128kb apart (Bee et al., 2009a). The *Runx1* locus contains 7 alternatively spliced protein-coding exons (Bee et al., 2009a). In the adult, Runx1 is highly implicated in the adult hematopoietic system and is expressed in BM HSCs (North et al., 2004). Moreover, *Runx1* is a frequent target of chromosomal translocations leading to leukemias in affected individuals (Levanon et al., 2001; Song et al., 1999). However, the role of Runx1 in adult hematopoiesis is beyond the context of this thesis and will therefore not be addressed. Instead, the importance of Runx1 for developmental hematopoiesis is discussed.

Runx1 expression during development

Runx1 expression was detected as early as 7dpc (neural plate stages) in the YS mesoderm with some reported expression also in the epiblast endoderm (Eliades et al., 2016; Lacaud et al., 2002; North et al., 1999). The early allantois and chorion also expressed Runx1 (Zeigler et al., 2006). From early E8.0 Runx1 expression was observed within the characteristic YS BI band, and specifically in primitive erythrocytes (North et al., 1999 and Figure 1.5A,D). At later stages, Runx1 expression declined in primitive erythrocytes to undetectable levels at E10.5, while exhibiting a punctate expression pattern in YS and VA ECs (North et al., 1999).

In the embryo proper, Runx1 expression was minimal at E8.0 (Figure 1.5C) and increased to around 13-30% of total AGM + VU cells at E11.5 (Eliades et al., 2016; North et al., 2002). Runx1 was expressed primarily in the ventral aspect of the AGM region, marking endothelial cells of the DA,

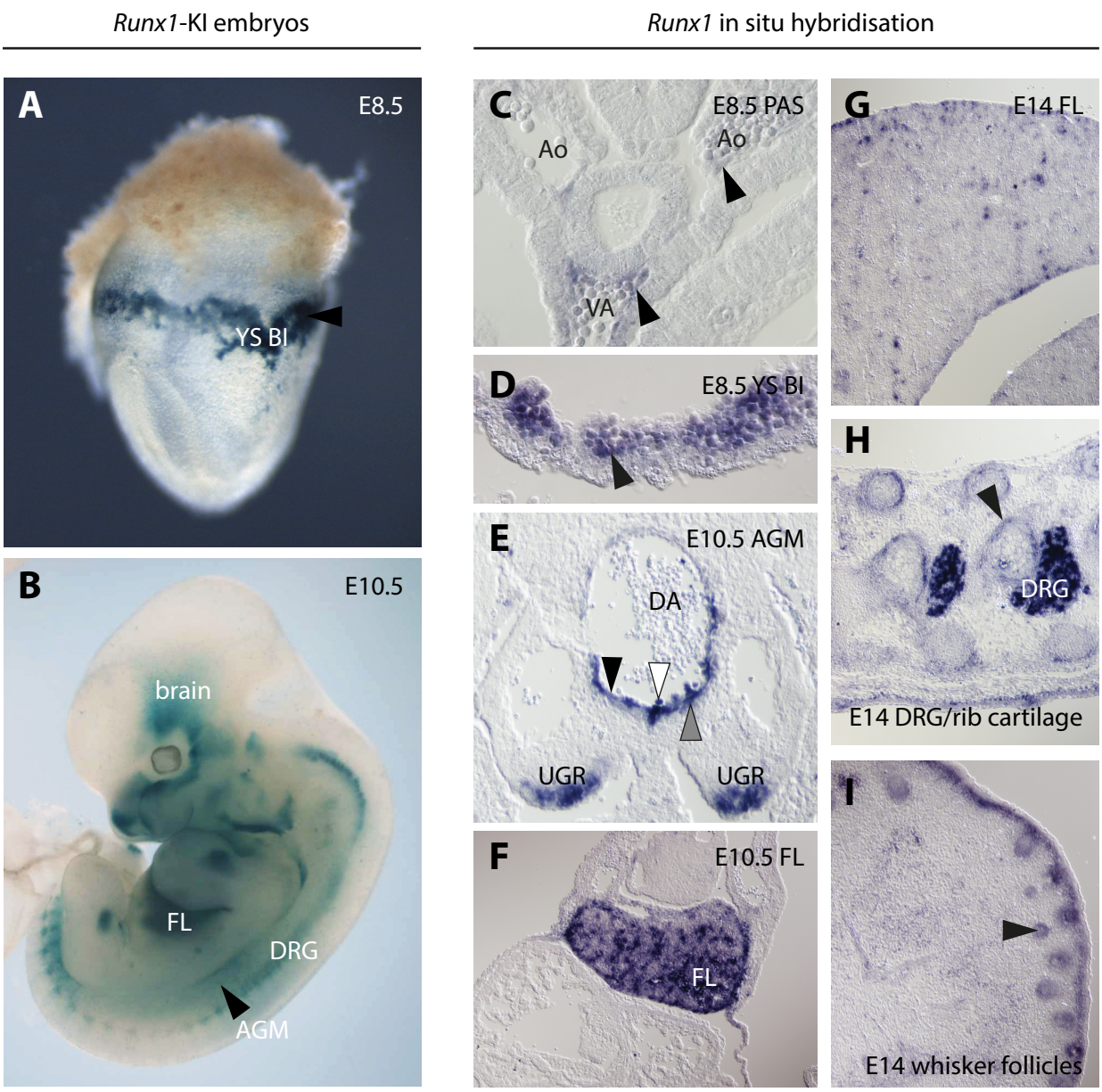


Figure 1.5 Endogenous *Runx1* expression patterns during development
A,B) Representative wholemount embryos of the *Runx1*-knock in (KI) lacZ reporter line. X-gal staining (blue) shows characteristic *Runx1* expression pattern in the yolk sac blood island band at E8.5 (arrowhead in **A**) and in the fetal liver and AGM region at E10.5 (**B**). (A is taken from Swiers et al, 2013; B is courtesy of Andrew Jarrat). **C-F)** Analysis of endogenous *Runx1* expression using in situ hybridization in embryo sections from E8.5 to E14. X-gal staining is observed in endothelial cells of the paired aortae (Ao) and vitelline artery (VA) in the E8.5 PAS region (arrow heads in **C**) as well as in blood islands of the E8.5 YS (arrowhead in **D**). At E10.5, the AGM region (**E**) shows *Runx1*-characteristic X-gal expression in the dorsal aorta (DA) endothelium (black arrowhead), intra-aortic cluster cells (white arrowhead) and in the sub-aortic mesenchyme (grey arrowhead) as well as in the urogenital ridges (UGR). The majority of the E10.5 (**B,F**) and a subset of the E14.5 (**G**) fetal liver (FL) cells express *Runx1*. Non-hematopoietic *Runx1*-specific expression is also seen in the E10.5 brain (**B**) and in the dorsal root ganglia (DRG) at E10.5 (**B**) and E14.5 (**H**). The rib cartilage is also marked by X-gal expression at E14.5 (arrowhead in **H**). The whisker follicles at E14.5 show *Runx1*-specifc X-gal expression (arrowhead in **I**). All images courtesy of Chris Vink and Andrew Jarrat.

intra-aortic cluster cells, a subset of the sub-aortic mesenchyme (North et al., 1999 and Figure 1.5E) and all AGM HSCs (North et al., 2002). Interestingly, our lab and others identified that promoter usage varied during developmental hematopoiesis: Runx1 expression in erythrocytes was driven by the P2 promoter, while more mature hematopoietic progenitors in the YS and AGM+VU regions required the activity of both promoters. Upon FL colonization, the P1 promoter gradually became the predominant hematopoiesis-driving promoter and remained so in the adult (Bee et al., 2009a; Sroczynska et al., 2009). While promoter usage varied depending on developmental stage, it was established that promoters alone are not able to confer hematopoietic specificity, and instead, relied on *Runx1* enhancer elements to mediate expression (Bee et al., 2009b).

Runx1 enhancers

In order to explore the tissue-specific activity of Runx1 regulatory elements the de Bruijn lab initiated studies to identify candidate enhancer regions. Classically, enhancers are defined as short genomic regions with contain TF binding sites (TFBS) that can attract upstream TFs, in order to drive the transcription of a particular gene (reviewed by (Pennacchio et al., 2013). A combination of multiple species sequence alignment (not shown), open chromatin conformation (DNAseI-Seq) and Chip-Seq analysis of active enhancer marks (H3K27Ac; both performed in the 416B myeloid progenitor cell line) determined putative enhancer regions within the *Runx1* locus (Figure 1.6A; (Nottingham et al., 2007; Schütte et al., 2016b; Vierstra et al., 2014)). The candidate enhancer regions were named based

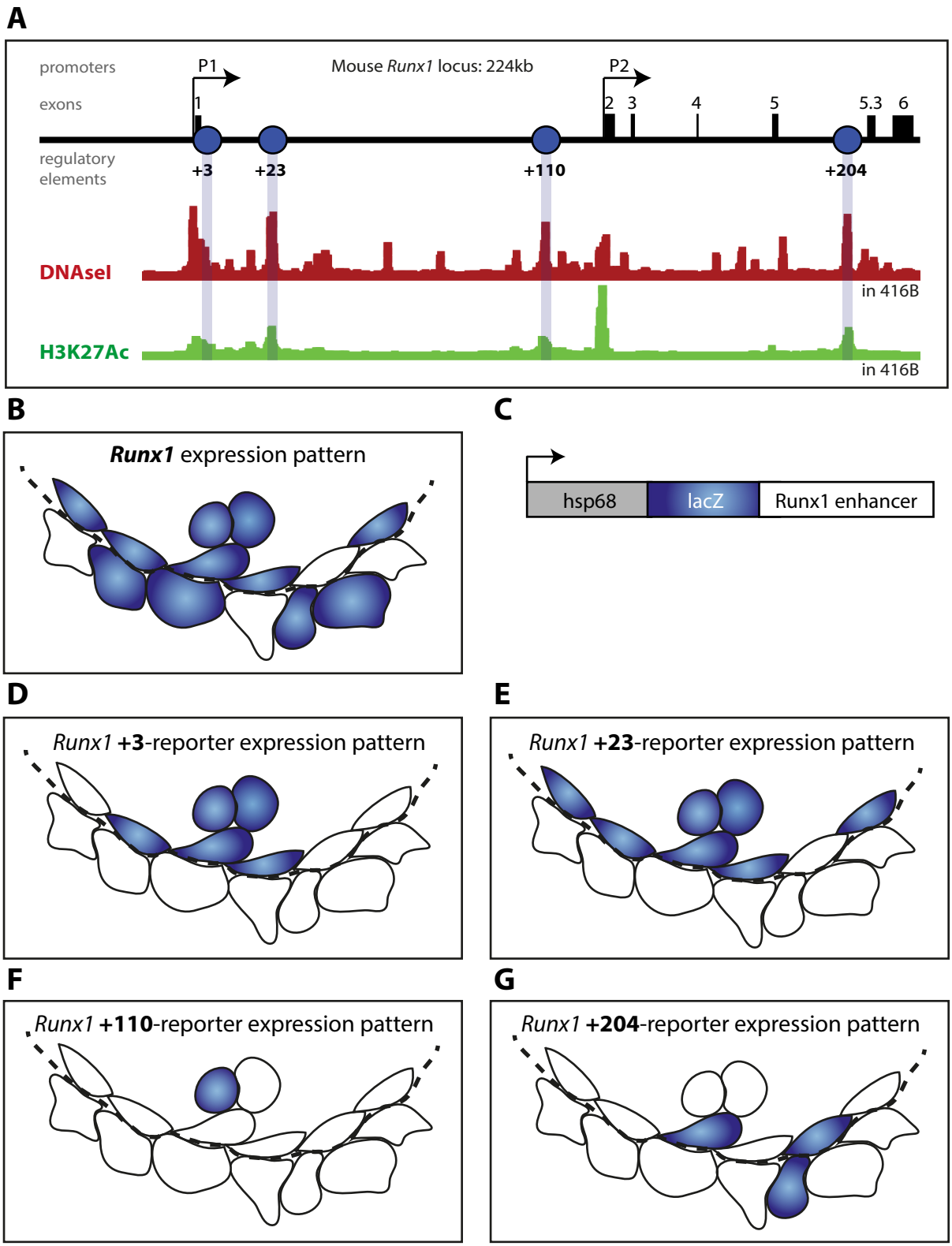


Figure 1.6 Four *Runx1* enhancers mediate reporter expression to discreet stages of EHT
A) Schematic of the mouse *Runx1* locus with the relative positions of the 2 promoters (P1 and P2), 7 exons (1-6) and 4 enhancer elements identified (+3, +23, +110 and +204). Their naming corresponds to their respective positions from the ATG codon in exon 1. Below the locus is a DNAseI-Seq track analysed in 416B myeloid progenitor cell lines (in red) and a Chip-Seq track for H3K27Ac (green), a marker for active enhancers. (DNAseI-Seq: Schuette, et al., 2016; Chip-Seq: Vierstra, et al., 2014) **B)** Schematic representation of endogenous Runx1 expression patterns in the ventral aspect of the midgestation dorsal aorta. Schematic is based on expression analysis of Runx1-lacZ KI embryos and Runx1 in situ hybridization (cf Figure 1.5). **C)** Schematic of the construct used to generate Runx1 enhancer-lacZ transient transgenic embryos. **D-G)** Schematic representations of Runx1 enhancer-reporter expression based on detailed analysis of transient transgenic embryo sections. Schematic was based on data generated and anlysed by Andrew Jarratt and Stella Antoniou.

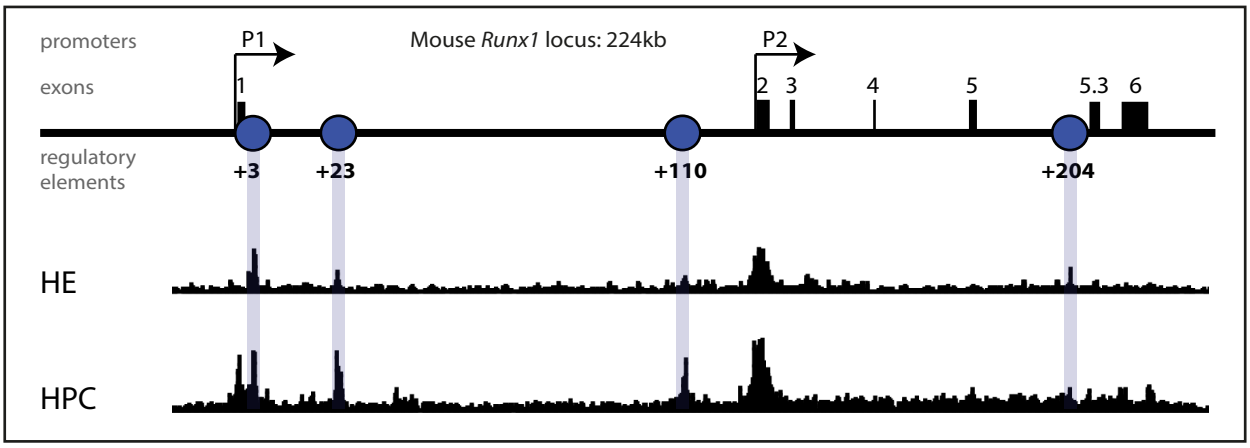
on their respective distance (in kb) from the ATG codon in exon 1. Of these candidate enhancer elements identified, our lab specifically focused on 4 that showed activity in developmental hematopoiesis. This was established based on analysis of transient transgenic mouse embryos generated with *Runx1* enhancer-reporter constructs (Figure 1.6C). Such analysis is necessary to validate the enhancer candidates and determine the cell type(s) they mediate reporter gene expression to. In addition, those transient transgenic embryos were compared to endogenous *Runx1* expression in order to distinguish between *Runx1*-specific expression and transgene insertion position-related ectopic expression (Figure 1.5 and Figure 1.6B). The *Runx1* +23 enhancer was found to be marking all aspects of EHT, including all HE, blood clusters and HSCs (Figure 1.6E; Bee et al., 2010; Nottingham et al., 2007; Swiers et al., 2013). The activity of the *Runx1* +3 enhancer followed a similar pattern as the *Runx1* +23 enhancer in transient transgenic embryos (Figure 1.6D). On the other hand, the *Runx1* +110 enhancer was found to be marking exclusively blood clusters but not endothelial subsets (Figure 1.6F). Interestingly, the *Runx1* +204 enhancer was found to mark a small subset of embryo proper and yolk sac endothelial, but not hematopoietic cells (Figure 1.6G and explained in more detail in Figure 3.1). This suggests that different *Runx1* enhancers could be used to sub-dissect *Runx1*-specific expression patterns during developmental hematopoiesis.

In addition, recent DNAseI-Seq data suggested that these *Runx1* enhancers differ in their chromatin accessibility depending on the stage of

hematopoietic commitment during EHT (Goode et al., 2016). In ES cell-derived HE and hematopoietic progenitor cells (HPCs) it was shown that the +3 and +23 enhancer were accessible at both these EHT stages, while the +110 was only accessible at the HPC stage. Interestingly, the +204 enhancer exhibited an open chromatin conformation only at the HE stage (Figure 1.7A; Goode et al., 2016). This is in agreement with the +204-reporter expression observed in ECs of transient transgenic embryos (Figure 1.6G and Figure 3.1).

To understand what upstream TFs bind to these enhancers, and subsequently regulate hematopoietic-specific *Runx1* expression, our lab and collaborators examined conserved TFBSs at each of the 4 enhancer elements (Nottingham et al., 2007; Schütte et al., 2016). Such TFBS analysis also showed differences between the 4 *Runx1* enhancers. While the +3 and +23 enhancers had motifs for the most important hematopoietic regulators analyzed, the +110 enhancer lacked Gfi, Meis and Runt binding motifs. On the other hand, the +204 enhancer had Ebox, Ets, Gfi and Runt motifs while lacking Gata and Meis binding sites (Figure 1.7B; Nottingham et al., 2007; Schütte et al., 2016). Further, *in vitro* luciferase activity analysis (in a stable 416B cell line) explored which of these binding motifs modulate enhancer activity when individual motif-families were mutated (Figure 1.7C; Schütte et al., 2016). Such TFBS mutagenesis analysis highlighted very complex and dynamic patterns: for example, although the Ebox and Ets motifs were present in all 4 enhancer regions, their mutation had different effects on luciferase activity. Adding to this complexity, TFBS mutagenesis at the +23 enhancer locus in transient transgenic +23-

A



B

+3	+23	+110	+204
Ebox	Ebox	Ebox	Ebox
Ets	Ets	Ets	Ets
Gata	Gata	Gata	✕
Gfi	✕	✕	Gfi
Meis	Meis	✕	✕
Runt	Runt	✕	Runt

C

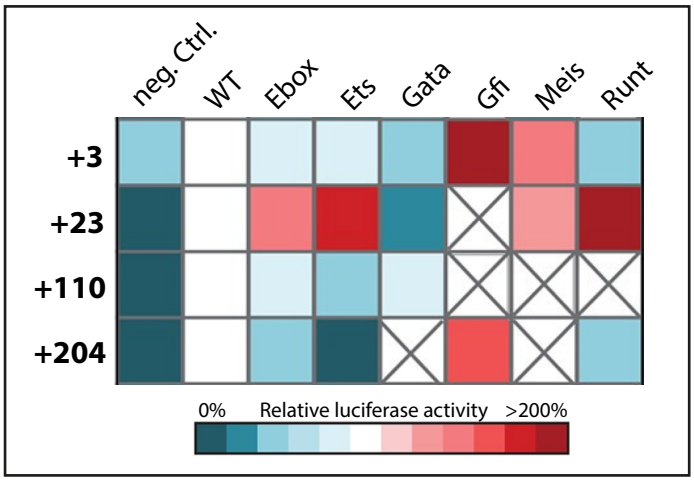


Figure 1.7 Differences in 4 *Runx1* enhancer elements
A) Schematic of the *Runx1* locus and its 4 hematopoietic-specific enhancers. Below is the open chromatin conformation analysis (DNAseI-Seq) in ES cell-derived HE and hematopoietic progenitor cells (HPC) revealing stage-dependent differences in enhancer accessibility. Data derived from Goode et al., 2015 and tracks generated by Dominic Owens. **B)** Summary table of transcription factor binding site analysis of 4 *Runx1* enhancers. Conserved binding motif families are indicated. Motifs that were not found at specific enhancer regions are indicated with a cross. Data derived from Nottingham et al., 2007 and Schutte et al., 2016. **C)** Summary of different enhancer activities (based on relative luciferase activity) when specific binding motif families were mutated. Enhancer activity was either downregulated (blue), upregulated (red) or unchanged (white), indicating which TFs are having an activating, repressive or non-functional effect on enhancer-mediated *Runx1* expression, respectively. Crossed out fileds indicate that there is either no motif for a specific TF and/or that a particular TF does not bind that enhancer region. Data adapted from Schutte et al., 2016.

reporter embryos showed differences between the *in vitro* and *in vivo* approaches (Nottingham et al., 2007). Future side-by-side comparison of different approaches should resolve any conflicting data. In summary, differences in chromatin accessibility and subsequent TF binding may explain the differential activity of the 4 Runx1 enhancers. However, in order to fully comprehend the regulatory control underlying Runx1 expression, more advanced analysis needs to be performed in primary embryonic tissues, rather than cell line models.

Runx1 requirement during development

Consistent with the hematopoietic expression of Runx1, it was also found to be required for normal progression of developmental hematopoiesis. Indeed, loss of *Runx1* had a detrimental effect on developmental hematopoiesis and overall embryogenesis. *Runx1*-null mutant embryos exhibited extensive necrosis and hemorrhaging of the central nervous system and died by E12.5 (Mukouyama et al., 2000; Okuda et al., 1996; Wang et al., 1996a). Primitive hematopoiesis was initially thought not to be affected, as YS-derived primitive erythrocytes appeared normal (Okuda et al., 1996; Wang et al., 1996a). Closer inspection, however, revealed grossly abnormal morphology and cell surface marker expression of primitive erythrocytes in *Runx1*-null embryos (Yokomizo et al., 2008). The total numbers of such erythrocytes, however, was similar to WT embryos (Lacaud et al., 2002). Interestingly, the transient definitive progenitors were dramatically reduced in *Runx1*-deficient YS (Lacaud et al., 2002). Similarly, *in vitro*, *Runx1* deficiency in ES cell differentiation cultures led to

relatively normal erythrocyte development in longer cultures, but lacked the ability to generate monocytes and macrophages. Moreover, such Runx1 deficient ES cells never contributed to hematopoietic tissues in chimeras (Okuda et al., 1996).

Another consequence of *Runx1* deletion was observed in the definitive wave of hematopoiesis. *Runx1*-deficient PAS, AGM+VU or FLs lacked CFU-C potential (North et al., 1999; Okuda et al., 1996; Wang et al., 1996a), LT-HSC potential (Cai et al., 2000) and were only able to generate endothelial, but not hematopoietic progeny in culture (Mukouyama et al., 2000; Yokomizo et al., 2001). Of note, the vasculature development in *Runx1*-deficient embryos was also affected (Takakura et al., 2000). When Runx1 expression was reintroduced in E9.5 PAS and E11.5 AGM organ cultures derived from *Runx1*-null mice, the *in vitro* production of HC was partially restored in E9.5 PAS but not E11.5 AGMs. It was therefore suggested that while the early endothelium contains a subset of cells which are able to respond to the Runx1 rescue, the later AGM endothelium has lost this ability (Mukouyama et al., 2000). This is in line with the fact that the E9.5 endothelium had the highest levels of *Runx1* transcript expression with a rapid decline at later stages (Swiers et al., 2013).

Interestingly, studies have identified that *Runx1* acts in a gene dose-dependent manner and haploinsufficiency has an effect on the spatiotemporal distribution of HSCs within the AGM region and YS (Cai et

al., 2000). When E10.5 and E11.5 *Runx1* heterozygous mutant AGM and YS cells were directly transplanted, they were able to engraft. On the other hand, when *Runx1* heterozygous AGMs were cultured as explants, dissociated and cells then transplanted, the E10.5 AGM and YS surprisingly contained HSC potential, while the E11.5 AGM did not (Cai et al., 2000). This finding deviated from the WT embryo, where HSCs are not readily found at E10.5 in the YS or AGM, while starting from E11.5 the AGM region contained a limited number of HSCs (Kumaravelu et al., 2002). This shift of definitive hematopoiesis to an earlier developmental timepoint and the decrease of HSCs within E11.5 tissues after culture, suggests that *Runx1* has a role in the maintenance of HSCs in the microenvironment of the AGM (Cai et al., 2000). In the early YS, heterozygous *Runx1* mutants developed fewer numbers of transient definitive precursors (Wang et al., 1996a; Lacaud et al., 2002). In addition, *Runx1* (*CBFα2*) has a non DNA-binding partner (*CBFβ*), which, when mutated had an embryonic phenotype similar to the one in *Runx1*-null embryos. The dosage-dependent effect observed in *Runx1*-mutants, however, was not obvious in *CBFβ* mutant embryos (Sasaki et al., 1996; Wang et al., 1996b).

Further dissection of Runx1 requirement during EHT

In order to understand the exact spatiotemporal requirement of *Runx1* during developmental hematopoiesis, *Runx1* was deleted at specific time points of development using an inducible Cre-floxed transgenic mouse system (Tober et al., 2013). The effects were evaluated at later timepoints

of development leading to the conclusion that loss of *Runx1* up to E10.5 reduced EMP formation and function (Tober et al., 2013). HSCs, on the other hand, were relying on Runx1 until E11.5, after which a switch to Runx1-independence was observed (Tober et al., 2013). Upon deletion of *Runx1* within the VEC+ ECs, it was established that Runx1 is absolutely required for normal EHT, while deletion within Vav+ HCs had no effect on CFU-C or LT-HSC potential (Chen et al., 2009). Interestingly, *Runx1* deletion within the Tie2 endothelial compartment, resulted in a *Runx1*-null phenotype (Li et al., 2006), while restoration of Runx1 within the Tie2 compartment of *Runx1*-null embryos restored definitive hematopoiesis with full CFU-C and multi-lineage LT-HSC potentials (Liakhovitskaia et al., 2009). Although such embryos showed complete recovery of the *Runx1*-null phenotype in the hematopoietic system, the effects of *Runx1* deletion on non-hematopoietic tissues was too severe and pups died shortly after birth (Liakhovitskaia et al., 2009). A similar rescue was achieved by restoring Runx1 within the CD41+ cell compartment (Liakhovitskaia et al., 2014). Interestingly, *Runx1*-deficient embryos exhibited low-level CD41 expression, a marker of early hematopoietic commitment, in the AGM region. This suggests that Runx1 was not required for the initiation of EHT but instead required for the transition from a phenotypic Type I into a Type II pre-HSC (Liakhovitskaia et al., 2014).

The role of Runx1 during hematopoiesis is conserved in fish

In the zebrafish embryo, Runx1 is first expressed in the bilateral stripes of the posterior lateral plate mesoderm (LPM), which migrate towards the

midline to form the precursor of the AGM region. In this region, Runx1 labels the ventral aspect of the DA, similar to the mouse embryo (Kalev-Zylinska et al., 2002). Interestingly, unlike in the mouse embryo, *runx1* does not label primitive erythrocytes in the fish embryo (Gering and Patient, 2005). Morpholino knock down of Runx1 expression resulted in abnormal EC and HC development. Mutant embryos exhibited vascular defects, causing lack of circulation and the accumulation of immature progenitors (Kalev-Zylinska et al., 2002). Interestingly, *Runx1*-deficient zebrafish embryos also initiate EHT, albeit with lower frequency, as evidenced by the cell shape morphology from a flat elongated EC into a rounder, budding cell (Kissa and Herbomel, 2010; Lam et al., 2010). However, further progression of EHT was halted, as such budding cells became apoptotic and fragmented (Kissa and Herbomel, 2010). In fish, the mutation of the Runx1 binding partner, *CBFβ,* results in a slight difference of phenotype. While in the *Runx1* morpholino no HSCs were formed (as evidenced by the lack of Runx1 and Myb expression in the aorta), nascent HSCs were formed in *CBFβ* knockout embryos (Bresciani et al., 2014). Interestingly, such nascent HSCs are not released from the AGM region and did not enter circulation, suggesting that *CBFβ* aids *Runx1* in releasing HSCs from the AGM region (Bresciani et al., 2014).

1.10 The heterogeneity of hemogenic endothelium

In recent years, evidence has accumulated suggesting that HE is a heterogeneous population, with differences in requirement, molecular

identity, and potential. The most obvious difference is the separation of the HE into two anatomical sites: YS and AGM. In the YS, HE contributes to either blood progenitors of the first and second wave (primitive erythroid progenitors and EMPs), while in the AGM, HE contributes to the precursors of the HSC lineage (Chapter 1.5).

Several requirements varied in YS HE and AGM HE: Blood flow was not required for EMP formation as phenotypic EMPs were present in the YS of blood flow-deficient embryos (Frame et al., 2016). In contrast, HSC formation depended on functional blood circulation in the mouse and fish embryo (Adamo et al., 2009; North et al., 2009). In short, zebrafish mutants lacking a heartbeat and therefore circulation, showed defects in HSC formation (North et al., 2009). Similarly, mouse embryos with deficient or blocked nitric oxide, an important modulator of shear stress-induced signaling, exhibited defective HSC formation (North et al., 2009) and had reduced CFU-C potential (Adamo et al., 2009). Interestingly, DA endothelium, intra-aortic clusters and AGM HSCs expressed Nos3 (nitric oxide synthase 3;(North et al., 2009)).

In addition, associations with arterial or venous fates of HE subsets have also been reported. At early developmental stages (E8.5), the YS exhibits a distinct venous-arterial distribution on the anterior-posterior axis: The vitelline artery and its capillary network reside in the posterior region, while the vitelline vein and its capillaries occupy the anterior region (Wang et al., 1998). Based on this observation, anterior and posterior YS parts were cultured on OP9 cells and it was established that both had the potential to

generate hematopoietic progeny (Frame et al., 2016). In contrast, AGM HE and consequently HSCs were previously only associated with arterial identity (de Bruijn et al., 2000). Intriguingly, in human pluripotent stem cell (hPSC) differentiation cultures it was established that the hemogenic and arterial/venous fates diverge at the mesoderm precursor stage, similar to the primitive streak in the embryo. These cell types were associated with different cell surface marker expression (Ditadi et al., 2015). Specifically, lack of CD73 expression identified the HE-fated subset, while CD73+ cells belonged to the vascular endothelial subset (Ditadi et al., 2015).

In the mouse embryo, the EMPs and HSCs share cell surface marker expression, making it difficult to segregate these lineages in the embryo, without functional assessment of their potential. Recently, however, several marker combinations unique to one or the other were identified. EMPs were found to express Gata2 (Bertrand et al., 2005) and CD16/32, while lacking *Sca1* (Ly6a) expression on the cell surface or at the transcriptional level (McGrath et al., 2015). In contrast, HSCs were positive for Gata2, Gata3, Lmo2 expression (Bertrand et al., 2005), and were exclusively contained within the Ly6A-reporter+ population (de Bruijn et al., 2002). In fact, a recent study elegantly portrayed the difference between the EMP and HSC lineages (Chen et al., 2011). In brief, GFP/CBFβ, when expressed from the *Tie2*-driven transgene, could rescue EMP formation in the FL of *CBFβ*-deficient embryos (Chen et al., 2011; Miller et al., 2002). However, the effects of *CBFβ* deficiency on HSC development were not lifted. In contrast, expression of GFP/CBFβ from *Sca1* regulatory sequences rescued HSC formation, but not EMPs. These experiments

demonstrated that Sca1 expression specifically labels HSC-fated HE (Chen et al., 2011).

Interestingly, our lab recently identified that the PAS/AGM HE itself is highly heterogeneous based on single cell molecular profiling (Swiers et al., 2013). HE differed in the molecular signature between different developmental stages. For example, at E8.5, *Etv2* expression started decreasing in a subset of HEs while expression of early markers associated with hematopoietic development, such as *Meis1,* increased (Figure 1.8). This early HE was termed the competent HE, as it was able to respond to hematopoiesis-inducing factors (Swiers et al., 2013). From E9.5 *Runx1* expression, followed by upregulation of definitive hematopoietic genes (*Gfi1*, *Pu.1*, *Myb*), indicated progressive hematopoietic commitment (Figure 1.8). Functionally, from E9.5 onwards, HE was able to respond more readily to blood-inducing signals and formed, almost exclusively, hematopoietic progeny. This later HE was termed the specifying HE, as it had initiated committment to the hematopoietic lineage. Therefore, our lab was able to establish a distinct, temporal, step-wise progression of HE maturation (therefore EHT) on a molecular and functional level. Remarkably, this process was initiated earlier than previously thought. Within each developmental time point, however, these molecular changes were only observed in a subset of HEs (Figure 1.8; Swiers et al., 2013). This suggests that further sub dissection or purification of HE is possible.

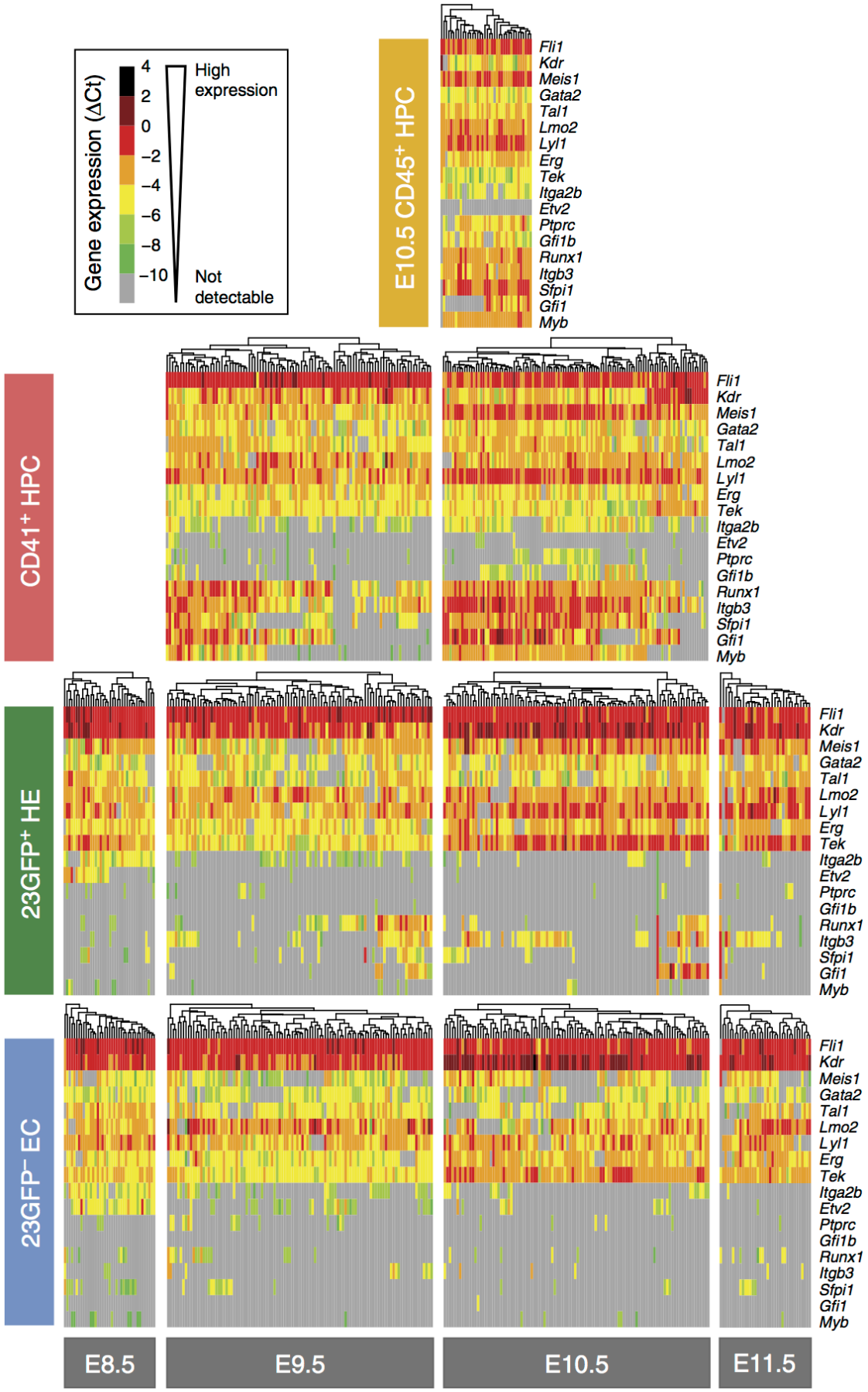


Figure 1.8 Gene expression analysis of single cells during EHT
Single cell Fluidigm analysis of 23GFP+ and 23GFP- endothelial subsets and mature hematopoietic cells. Reprinted by permission from Macmillan Publishers Ltd: Nature Communications, Swiers et al, 2013 (copyright).

1.11 Project aims

Overall, the aim of my project is to study different aspects of developmental hematopoiesis by utilizing two novel *Runx1* enhancer reporter mouse lines. Developmental hematopoiesis is a highly complex process and employs a mechanism of gradual transition from an endothelial cell type into a hematopoietic cell (EHT). To advance our understanding of developmental hematopoiesis, it is important to identify markers, which can separate discrete cellular populations of EHT. Our lab has developed such tools in the form of transgenic *Runx1* enhancer-reporter mouse lines. The +23 enhancer marks all HE, blood progenitors and long-term hematopoietic stem cells. Recently, single cell analysis of EHT populations revealed that all cellular subsets involved in this transition are heterogeneous. It is therefore of interest to identify markers which can further purify EHT populations. Being able to isolate more homogeneous cellular subsets, would allow better in-depth analysis on a molecular and functional level.

My project is focusing on another *Runx1* enhancer, the +204, and specifically whether this enhancer can be used as a tool to further sub-dissect or purify cellular subsets of EHT. I therefore generated a novel +204 enhancer reporter mouse line (204GFP) and phenotypically characterized it in **Chapter 3**. I also functionally tested the potential of cells marked by the +204 enhancer in **Chapter 4**. Next, it was of interest to identify the molecular signature of cells marked by the +204 enhancer to further establish their nature. In addition, to establish how cells marked by the 204GFP transgene relate to those marked by the +23 enhancer, I

generated and characterized a 23Cherry reporter mouse line. This line was then crossed with the 204GFP line, to isolate different endothelial subsets based on differential *Runx1* enhancer-reporter expression. To begin to examine the nature of these cell types, they were molecularly profiled as single cells in **Chapter 5**. Lastly, I have initiated studies into the cellular origin of HE, using the Runx1 reporters. This includes characterization of the *Runx1* +23 enhancer-reporter expression at the onset of gastrulation, as well as preliminary fate mapping of the lateral plate mesoderm to the +23-marked HE (**Chapter 6**).

Chapter 2

Materials and Methods

Mice

All mouse work has been performed under an ethically approved Home Office project and personal license.

2.1 Generation of transgenic mouse lines via pronuclear microinjection

One-cell stage mouse zygotes were harvested from superovulated CBAxC57BL/6 females that were set up for mating with CBAxC57BL/6 males the night before (6 females per injection session). Zygotes were visually screened and injected with ready-made DNA transgenic construct. The 204GFP construct was previously generated in the lab and comprises the heterologous hsp68 core promoter (Kothary et al., 1989), a GFP reporter and the 1.6kb +204 enhancer region. This construct was injected at a concentration of 1ng/ul into the pronucleus of zygotes using a standard microinjection set up (Leitz Labovert FS) as described in Gordon, 1980. Injections were performed in batches of 25 zygotes, and returned to a 37˚C incubator after injections. Usually around 150 embryos were injected per injection session. Embryos were allowed to develop to 2-cell stage, which served as an indication of survival post injection. Around 50% of injected cells would lyse immediately after the zona pellucida was perforated by the injection needle. Live, 2-cell stage embryos were then transplanted into the oviduct coils of pseudopregnant females. Embryos were allowed to come to full term and 3-week-old pups were genotyped for *Gfp* from ear notches. Only pups that genotyped positively for *Gfp* were further analysed for germ line transmission (GLT) and GFP expression within offspring (described in Chapter 3).

2.2 Generation of mouse chimeras via ES cell injection

Blastocyst mouse embryos were harvested at 3 days postcoitus from superovulated C57BL6 females. Embryos were visually screened and scored for developmental stage. Blastocysts with a visible blastocoel were used for injections. Batches of 5-10 blastocysts were injected with 10-15 ES cells each. Targeted ES cells derived from the 129 mouse strain were used for injection. A standard microinjection setup (Leitz Labovert FS) with wide injection needles (Eppendorf Transfer Tip ES sterile pipettes) was used to pierce through the side of the blastocyst furthest away from the inner cell mass (ICM) and ES cells were expelled into the blastocoel cavity. Injected Blastocysts were cultured for several hours to ensure their survival and confirm the integration of the ES cells inside the blastocyst. Around 50 blastocysts were injected per injection session. After brief culture, blastocysts were transplanted into the tops of the uteri, closest to the oviduct, of pseudopregnant females. Chimerism was scored based on the coat colour of the pups. High chimerism was described when pups showed mostly brown fur colouring with occasional patches of beige. Lower chimerism was scored in pups that mostly had black fur with occasional brown patches. All chimeras were set up with C57BL/6 partners to evaluate GLT. Brown pups were expected in the F1 generation, suggesting ES cell contribution to the next generation. Targeted allele contribution was subsequently confirmed via PCR genotyping of brown pups. (Longenecker and Kulkarni, 2009).

2.3 Mouse colony maintenance

Mouse colonies were housed in IVC cages with free access to food and water and enhanced environment (sizzle nest, plastic house, wood nuggets) according to local Home Office regulations. Mouse lines were kept on a mixed background (C57BL/6xCBA). Births of pups from breeding cages were recorded on the Sanger Colony Management System and pups ear notched for genotyping at 2/3 weeks and weaned at around 4 weeks (depending on litter size and individual pup size).

2.4 Ear notching and genotyping

Ear notches were recovered from 2/3-week-old pups and embryonic tissues like placental cone, part of the yolk sac or parts of embryonic heads were used for genotyping and identification purposes. Tissues were incubated in 50-100µl PBND lysis buffer (50mM KCl, 10mM Tris, 2.5mM MgCl2, 100ug/ml gelatin, 0.45% NP40, 0.45% Tween) with Protein K (250ug/ml). Incubation at 55˚C lasted for 30min (embryo tissues) to several hours overnight (ear notches). Proteinase K was then denatured at 95° C for 5 min. Samples were then centrifuged for 3 min at 13000rpm. Each DNA preparation was then used to determine the genotypes using sequence specific primers and HotStarTaq DNA Polymerase (Quiagen) (Table 2.1).

Genotyping primers	
name	primer sequence
GFP1	GACGTGAACGGCCACAAGTTCA
GFP2	GTGGCGGATCTTGAAGTTCACC
Myo1	TTACGTCCATCGTGGACAGC
Myo2	TGGGCTGGGTGTTAGTCTTA
23C_FP1	TCCCCAGCTTCACCAGTTCA
23C_RP_1	TGCACCTTGAAGGCGATGAA
23C_RP_2	TCCTTTCACGTTGTCCTCATG

Table 2.1: Sequences of genotyping primers used in this thesis

2.5 Preparation of adult mouse tissues for DNA extraction or cell sorting

Spleen, thymus and mesenteric lymph nodes were dissociated into single cell suspensions by crushing tissues through a 70um cell strainer (BD Falcon) into 10% FCS + 50U/ml penicillin and 50ug/ml streptomycin in PBS without magnesium and calcium added (from here on referred to as CMF-PBS). Femurs were flushed with a 22-gauge needle to obtain BM cells, which were further passed through a 70um cell strainer into CMF-PBS. Cells were counted using the Pentra ES 60 cell counter (Horiba). Peripheral blood (around 200ul) was collected into 1ml 0.5mM EDTA in PBS.

For DNA extraction, up to 100.000 cells were resuspended in 200ul for DNA extraction. 200ul of blood-EDTA mixture was taken for DNA extraction. DNA was extracted using the Qiagen Blood and Tissue DNA extraction kit and based on the manufacturer's manual. DNA was resuspended in 200ul of elusion buffer.

For cell sorting, BM and spleen single cell suspensions were stained for 20min and sorted on Fusion II (see Table 2.2 for FACS antibodies used).

Antibody	Conjugation	Suplier	Cat. number
B220	biotin	BD Pharmigen	553086
CD19	APC	BD Pharmigen	550992
CD3	biotin	BD Pharmigen	553060
CD31	PE	BD Pharmigen	553373
CD4	PE-Cy7	eBioscience	25-0041-81
CD41	PE	BD Pharmigen	558040
CD41	eFlour450	eBioscience	48-0411-82
CD45	APC eFlour780	eBioscience	47-0451-82
CD8	PE-Cy7	eBioscience	25-0081-81
Flk1	biotin	eBioscience	13-5821-81
Ly6C	APC	BD Pharmigen	560595
Mac1	PE	BD Pharmigen	557397
SAV	APC	Invitrogen	SA1005
SAV	PE-Cy7	Molecular probes	SA1012
Ter119	PE-Cy7	BD Pharmigen	557853
Ter119	APC-Cy7	BD Pharmigen	560509
VEC	APC	eBioscience	17-1441-82

Table 2.2: Antibodies used for flow cytometry

Embryos

2.6 Analysis of reporter transgene expression at different developmental time points

Embryos were harvested from transgenic mouse lines matings at specific developmental time points. The visual confirmation of a vaginal plug after overnight mating was assigned embryonic day E0.5. Subsequently embryos were harvested at the desired developmental time point up to and including early E14. Later embryo time points were not covered by our Home Office project licence. On the desired day of embryo harvest, pregnant females were sacrificed via a Schedule 1 method and embryos extracted from the uteri. Embryos from E8-E14 were kept in on ice during embryo dissection. Earlier embryos were kept at room temperature if they were further cultured in vitro. Embryos were stages and somite pairs counted. Embryos were either kept whole for cryosectioning or wholemount staining, or dissected for flow cytometry analysis or functional assays. All dissections were performed in 10% FCS (Gibco) + 50U/ml penicillin and 50ug/ml streptomycin in PBS with magnesium and calcium added (Gibco). Embryo dissections were performed for the desired tissues. Where necessary pieces of the embryo head or placental cone were used for genotyping by PCR. In all other cases embryos were genotyped as necessary by analysis of overall transgene expression (GFP or Cherry) with a florescent microscope.

2.7 Early embryo cultures

Pre-somitic embryos were dissected at RT and placental cones and the Reichert's membranes carefully dissected away. Embryos were cultured in un-coated 24-well culture plates (Falcon) in a 37˚C incubator with 5% CO2. The culture media was made up of CMRL (Gibco, add 1:100 glutamine prior to use) and KO serum (Gibco, Cat. No. 10828101) at a ratio of 1:1. The same culture media was used for live imaging studies.

2.8 Embryo dye injections

Pre-somitic embryos were injected at specific locations of the primitive streak with CM-DiI (Life technologies). A 20% (w/v) DiI stock was made in 100% EtOH and kept at -20˚C. For injections, different dilution series from the DiI stock solution were trialed (1:3 - 1:200). I noticed the 1:100 or 1:200 dilutions gave the best results. Injection needles were made from filamented glass capillaries (Clark Electromedical Instruments) and pulled using the microforge pipette puller (Sutter Instrument Co.). Dye was loaded by placing the wide opening of the glass needle into the DiI dilution and allowed to fill the tip of the needle via capillary action (20-30min). Injection needles were then loaded into a mouth pipette and the dye injected in the required primitive streak locations via gentle expulsion using a mouth pipette. Embryos were immediately checked for DiI fluorescence and images taken to record the injection site and the stage of embryo development. Individual embryos were then placed into separate culture wells (24-well plate) and cultured in CMRL media.

2.9 Preparation of embryos for flow cytometry

Dissected embryos were washed in CMF-PBS and treated with 0.12% w/v Type I collagenase (Sigma) at 37˚C for 20min. Tissues were then mechanically separated into single-cell suspension by pipetting. Next, the cells were washed and centrifuged at 1000rpm for 3-5min. Cell pellets were resuspended in a desired volume of CMF-PBS and cells counted using single-use Neubauer hemocytometers and trypan blue (Invitrogen) to exclude dead cells. Cells were then stained with conjugated or biotinylated antibodies for FACS for 20min on ice according to the experimental set up (see Table 2.2 for antibodies used). After staining, cells were washed in CMF-PBS and centrifuged again. Cell pellets were resuspended in 150ul CMF-PBS with added Hoechst 33258 (diluted 1:1000 from the stock solution) to select for live cells. The cells were passed through FACS filters into 5ml tubes (BD) before analysis. Cells were either analyzed on the flow cytometers CYAN or Fortessa or Fusion II. Sorted cells were either collected into tubes containing 100% 0.45um-filtered FCS (Gibco) or directly sorted into wells containing pre-amplification buffer for Fluidigm® (see section 2.19).

2.10 Preparation and cryosectioning of embryos

Whole embryos were fixed in 4% PFA in PBS. Embryos up to E9.5 were fixed for 20-30min at room temperature (RT). Embryos from E10.5 to E13.5 were fixed for 30-45min at RT and E14.5 embryos were halved and fixed for 1h at RT. All embryos were then washed 3 times with PBS and transferred to a 15% sucrose solution at RT. Once embryos sunk to the

bottom of the well, they were placed in plastic molds according to their size, all excess sucrose pipetted away and molds topped with Tissue-Tek OCT compound (Sakura, Siemens Medical Solutions Diagnostic, Newbury, UK). Embryos were oriented as desired and the plastic molds placed on a mixture of dry ice and 100% EtOH. Once frozen, blocks were removed, and stored at -80˚C until further use. For cryosectioning, frozen embryo blocks were transferred to the cryostat (Leitz) and set up as per manufacturers instruction. Usually 10um-thick sections were transferred on Superfrost slides. After sectioning, slides were frozen at -20˚C until further use.

Immunofluorescence and imaging

2.11 Immunofluorescence on sections

Embryo or tissue sections were incubated in a PBS bath to wash off OCT. Sections were incubated with 0.4% TritonX, 2-5% FCS in PBS for 30min. Primary antibodies were then added to the same buffer and slides incubated with 100ul of the mixture for 30min-1h at RT. Slides were washed in PBS and then incubated with secondary antibodies for 30min. After washing in PBS, the excess of PBS was wiped off and the slides were mounted with Vectashield containing DAPI. See Table 2.3 for primary and secondary antibodies used.

1° antibody	raised in	company	cat number	dilution used
alpha-SMA-Cy3	mouse	sigma	c6198-2ml	1:200
anti-GFP	chicken	Abcam	ab13970	1:200
anti-RFP	rabbit	Rockland	600-401-379	1:400
beta-gal	rabbit	MP Biomedicals	55976	1:4000
CD31	goat	R&D Systems	AF3628	1:200
CD31	rat	BD Pharmingen	557355	1:1000
CD45	rat	BD Pharmigen	550539	1:100
Col1A1	goat	Santa Cruz	sc-8784	1:30
Runt (Runx1)	rabbit	abcam	ab92336	1:200

fluorophore	against	raised in	company	cat number	dilution used
AlexaFluor488	chicken	donkey	jackson immuno research	703-545-155	1:100-1:400
AlexaFluor488	goat	donkey	Invitrogen	A11055	1:100-1:400
AlexaFluor555	rabbit	donkey	Invitrogen	A31572	1:100-1:400
AlexaFluor594	rat	donkey	Invitrogen	A21209	1:100-1:400
AlexaFluor647	goat	donkey	Invitrogen	A21447	1:100-1:400
IgG H&L specific AP conjugate	rat	goat	Southern Biotech	3050-04	1:250

Table 2.3: Primary and secondary antibodies used for immunofluorescence staining of tissue sections and embryo wholemounts

2.12 Wholemount immunofluorescence

Whole embryos were fixed in 4% PFA in PBS. Embryos up to E9.5 were fixed for 20-30min at room temperature (RT). Embryos from E10.5 to E13.5 were fixed for 30-45min at RT and E14.5 embryos were halved and fixed for 1h at RT. All embryos were then washed 3 times with PBS. For long-term storage of the embryos prior staining, 50% and 100% MeOH washes were performed and embryos stored in 100% MeOH at -20˚C. The heads and one set of fore and hind limbs of E10.5 embryos or older were dissected away. Embryos were incubated in individual Eppendorf tubes in 0.4% TritonX, 5-10% FCS in PBS for up to 3h at RT on a shaking rack. Primary antibodies were diluted in the same buffer and 100-200ul used for each embryo. Incubation lasted overnight at 4˚C. The next day, embryos were washed in 0.4% TritonX, 5-10% FCS in PBS for up to 5-8h at RT on a shaking rack. Wholemounts were then incubated with the secondary antibody solution overnight at 4˚C and subsequently washed again for several hours or up to 24h with several changes of the buffer. Embryos were then dehydrated in 50% and 100% MeOH and then cleared in 50% and 100% BABB (one part benzyl alcohol with two parts benzyl benzoate). Embryos were then mounted into Fastwells (1.5cmx1.5cm, 1mm hight) that were pre-attached to a microscope slide with a coverslip and clear nail polish. Fastwells were sealed with another coverslip (1.5cmx1.5cm) and nail polish.

2.13 Microscopy

Cultured cells (e.g. OP9 co-cultures or functional MSC assays) were imaged on the EVOS XL Core imaging system. Unfixed whole embryos were imaged on Leica MZFLIII brightfield microscope equipped with an Argon lamp. Immunofluorescence in sections was imaged using the Zeiss 510 and Zeiss 780 Inverted confocal microscopes. 25x (LD LCI PA 25x/0.8 DIC), 40x (LD C-Apochromat 40x/1.1) and 63x (Plan Apochromat 63x/1.4) objectives were used with oil immersion. Immunofluorescence of the wholemounts was imaged overnight using the Zeiss LSM 780 Upright confocal microscope and a 25x oil immersion objective (LD LCI PA 25x/0.8 DIC). The Zeiss 780 microscopes were both equipped with 7 lasers/lamps and the following were used throughout this thesis: Diode (405nm – nuclear stain e.g. DAPI/Hoechst); Argon multiline (458/488/514nm – GFP and AlexaFluor488); HeNe (543nm – AlexaFluor555 and DiI); HeNe (594nm – AlexaFluor594); HeNe (633nm – AlexaFluor647). To image wholemount embryos the appropriate number of tiles was set to cover the imaging area with a tile overlap of 8%. The average range of z-stacks was 300um, depending on the thickness of the embryo. Z-stack slices were set to 5um apart. All Zeiss confocal microscopes use the ZEN 2011 LSM (black) software to acquire images. The program imaged each slice/tile twice and took the average to compile imaging data. Z-stacks and tiles of wholemount images were then 3D reconstructed in the IMARIS software. Images were stored and analysed in OMERO. Adobe Photoshop was used for final image processing and Adobe Illustrator to generate figures.

2.14 Live embryo imaging

Live imaging of early embryos was performed on the DeltaVision® Elite Olympus IX71 Inverted wide-field microscope with a C-Plan 10X air (0.3 NA) objective. Embryos were imaged every 19-20min for 3-6h. At each time point, one midplane bright field image was taken and a z-stack of the FITC (23GFP) channel. Z-stacks were then deconvoluted, 3-D projected and time points stacked to generate a movie file using the Huygens Professional Remote Analysis software.

Functional assays

2.15 OP9 maintenance, co-culture and output analysis

OP9 cells (kindly provided by M. Yoder, Indianapolis) were maintained in alpha-MEM media (Gibco) supplemented with 20% FCS (Hyclone) and 0.22% sodium bicarbonate (Gibco). Cells were passaged every 3 days. For co-cultures, OP9 cells were pre-plated 24h in advance at a density of 23x10^3 cells per cm^2. If the cells of interest were directly sorted into OP9 pre-plated wells, the differentiation media (detailed below) was added 2-3h before sorting. If cells were sorted in bulk, they were resuspended in differentiation media and plated onto OP9 cells. Differentiation media consisted of alpha-MEM (Gibco), supplemented with 10% FCS (Hyclone), 1x10^-4 M 2-mercaptoethanol (Sigma), 10ng/ml IL7, 10ng/ml SCF and 10ng/ml Flt3-ligand (all cytokines from Peprotech, Table 2.4). OP9 co-cultures were kept at 37˚C for up to 7-8 days, no media changes were

performed during that time. The formation of visible blood colonies was recorded from day 4 in culture. After 7-8 days, the supernatant was collected and wells washed in PBS (which was also collected). Non-adherent cells collected were processed for flow cytometry analysis (see section 2.9). Cells that stayed attached to the OP9 stromal layer were fixed in 4% PFA and stained with a rat anti-mouse CD31 antibody (Table 2.3). The secondary antibody anti-rat IgG coupled with a Alkaline Phosphatase (Table 2.3) was applied and the staining was revealed using a Vector Blue AP substrate kit (Vector).

Cytokine	suplier	working concentration	cat number
Flt3-ligand	Peprotech	10ng/ml	250-31L
IL7	Peprotech	10ng/ml	217-17
SCF	Peprotech	10ng/ml	250-03
TGFbeta	Peprotech	20ng/ml	100-21c

Table 2.4: List of cytokines used in this thesis

2.16 Methylcellulose colony assays (CFU-C)

CFU-Cs were performed using embryonic tissues dissected from 7dpc to E10.5. Cells were resuspended into Methocult GF 3434 semi-solid methylcellulose-based media (Stem Cell Technologies) and plated into 35x10mm Cellstar tissue culture dish (Greiner Bio-One). Depending how many cells were recovered from cell sorting, around 1400 to 47000 cells were plated per dish. For control dishes, 30000 cells were plated. Plates were cultured in a humidified chamber at 37˚C for up to 14 days. Hematopoietic colonies were counted at 4, 7, 10 and 14 days.

2.17 Long-term reconstitution analysis

Male mice (C57BL/6xCBA), no older than 3 months old were sub-lethally irradiated with a split dose of 9Gy from a 137Cs source. 204GFP+ and 204GFP- cells were sorted from E11.5 AGM+VUs as outlined in section 2.9. 1ee of each population together with 200.000 spleen cells (carrier cells) were injected into the tail veins of irradiated recipient males. Recipients were checked daily for the first 2 weeks post-treatment and weekly thereafter. Tail bleeds were performed at 4 weeks and 4 months post treatment. 2-3 drops of blood were harvested into 200ul 0.5mM EDTA in PBS and genomic DNA extracted as described in section 2.5. At 4 months post-transplantation, recipient mice were sacrificed and tissues (spleen, thymus, mesenteric lymph nodes (MLN), and BM) harvested for genomic DNA extraction and cell sorting (Table 2.2). The level of donor reconstitution in all tissues was determined by *Gfp*-specific PCR and subsequent analysis in ImageLab software (see Table 2.1 for PCR primers).

2.18 Chondrogenic differentiation assays

Mesenchymal cells (VEC-Ter119-CD41-CD45-) were sorted from AGM+VUs of 204GFP transgenic and WT embryos and plated into chondrogenic differentiation media. This media consisted of DMEM (Gibco) supplemented with 50U/ml penicillin, 50ug/ml streptomycin, 0.1mM L-ascorbic acid 2-phosphate (Sigma), 0.001mM Dexamethasone (Sigma), 20ng/ml human TGFbeta1 (Peprotech) and 1x ITS+ (Sigma). Media was made up fresh for each experiment. Cells were resuspended in

200ul of complete media after sort and plated into wells of ultra non-adhesive 96-well plates (Corning Costar). Cells were cultured in 37˚C incubator for up to 2 weeks. Media changes were performed weekly whereby around 2/3 of the media was changed without disturbing cell aggregates. Chondrogenic foci were harvested after 2 weeks and processed for cryosectioning and staining as described (section 2.10 and 2.11).

Gene expression analysis

2.19 Microfluidic quantitative RT-PCR

The Fluidigm® platform (Biomark^{TM}) was used to analyse gene expression levels in sorted pools of 20-25 or single cells. For the multiplex qRT-PCR, TaqMan assays (Applied Biosystems, Table 2.5) were pooled to a final concentration of 0.2x. A pre-amplification master mix was prepared immediately before cell sorting and consisted of 5ul CellsDirect 2x Reaction mix (Invitrogen), 2.5ul of 0.2x TaqMan assay mix, 1.2ul RT/Taq enzyme (CellsDirect qRT-PCR kit, Invitrogen), 1.2ul TE buffer (Invitrogen) and 0.1ul SUPERase-In (Ambion). 10ul of this mix was pipetted into individual wells of a 96-well micro-well plate (Invitrogen). Cells were directly sorted into these 96-well plates, covered with adhesive film, vortexed and briefly centrifuged. RNA was reverse transcribed at 50˚C for 15min and inactivated at 95˚C for 5min; the resultant cDNA was amplified by 22 cycles (15 sec at 95˚C followed by 4min at 60˚C). After this program

was complete, samples were immediately frozen at -20˚C until further analysis. For the Fluidigm® analysis samples were diluted 5-fold (in some instances 6-fold, to derive at 'cleaner' Ct curves) and analysed on 48.48 Dynamic Arrays according to manufacturers' instructions. The following PCR conditions were used: 95˚C for 10min, then 40 cycles of 95˚C for 15sec and 60˚C for 1min (Fluidigm®, Biomark^{TM}). After amplification, curves were manually checked at a threshold of <0.65. BioMark^{TM} Real-Time PCR analysis software calculated raw Ct values and data were exported to Excel as a .csv file for further analysis.

Gene Symbol	Gene	Assay Id	notes
Atp5a1	Atp5a1	Mm00431960_m1	housekeeping gene
Atp5a1	Atp5a1	Mm01257366_m1	housekeeping gene
Cadh5	VE-Cadherin	Mm00486938_m1	not used for analysis
Cbfb	CBFbeta	Mm00491551_m1	not used for analysis
Erg	Erg	Mm01214246_m1	
Etsrp71	EtsRP	Mm00468389_m1	
Fli1	Fli1	Mm00484409_m1	
Gata2	Gata2	Mm00492300_m1	
Gfi1	GFi1	Mm00515855_m1	
Gfi1b	Gfi1b	Mm00492318_m1	
Hrpt1	Hprt1	Mm01545399_m1	housekeeping gene
Itga2b	CD41	Mm00439768_m1	
Itgb3	CD61	Mm00443980_m1	
Kdr	Flk1	Mm01222421_m1	
Lmo2	Lmo2	Mm01281680_m1	
Lyl1	Lyl1	Mm00493219_m1	
Meis1	Meis1	Mm00487664_m1	
Myb	Myb	Mm00501741_m1	
Ptprc	CD45	Mm00448490_m1	
Runx1	Runx1	Mm01213404_m1	
Sfpi1	Pu.1	Mm00488142_m1	
Tal1	SCL	Mm01187033_m1	
Tek	Tie2	Mm00443243_m1	
Ubc	Ubc	Mm01201237_m1	housekeeping gene

Table 2.5: List of TaqMan assays used for Fluidigm® analysis

2.20 Fluidigm analysis

Exported raw Ct tables were further processed in Excel. Before any analysis, cells that have failed the assays in 3 (or more) of the 4 housekeeping genes were excluded from analysis. Similarly, assays that showed Ct values in more than 30% of NTCs (no template controls) were excluded where necessary. Each assay was run in duplicate, therefore, prior to further analysis, all duplicate values were averaged. The exception was in assays where one replicate failed across the entire chip, then only single values for that assay were further analyzed. Data was filtered according to NTC and NAC (no amplification control). For bulk cell analysis, each time point was analyzed in 3 experimental replicates and data for E9.0 and E9.5 were pooled. Data was analyzed by the deltaCt method (Livak, 2001) and normalized to the average of the housekeeping genes *Atp5a1* and *Ubc* (Table 2.5). Relative mRNA expression values were calculated and used to generate graphs in Prism7. Significance was established based on Two-way ANOVA with Tukey correction. For single cell analysis, genes that were not expressed were set to Ct=27 and all Ct values subtracted from the NTC background of 27 (logEx Ct -sample). The average *Atp5a1* and *Ubc* housekeeping gene values within each individual cell was calculated and subtracted from the NTC background of 27 (logEx Ct -HK). logEx deltaCt values were calculated by subtracting logExCtHK from logExCtsample to derive at 2^-deltadeltaCT. Hierarchical clustering, Pearson's correlation and principal component analysis were performed in R (http://www.r-project.org). Batch comparison was performed with Scater (https://bioconductor.org/packages/release/bioc/html/scater.html)

2.21 Statistical analysis

Results are presented as average ± SD. Unpaired, two-tailed Student's t-test with Welch's correction was used to determine the level of significance. The following p-values were considered statistically significant and were highlighted by asterisks: * $p<0.05$; ** $p<0.005$; *** $p<0.0005$; **** $p<0.0001$.

General laboratory techniques

2.22 Southern blotting for 23Cherry ES cell clone analysis

23Cherry-targeted ES cell clones were expanded to confluency in a T25 flask (Falcon). After confluency was reached, ES cell media was replaced with 1ml lysis buffer consisting of 50mM Tris-Hcl (pH 8.0), 0.5% Triton-X-100 and 1mg/ml Proteinase K. Flasks were incubated at 37˚C for 2 days. The resultant lysate was then used for genotyping or Southern blotting. DNA was then digested with either NcoI or NheI (New England Biolabs) in a 40ul reaction (10ug DNA, 1x NEB buffer, 40U of restriction enzyme, rest H2O). Digestion took place overnight (O/N) at 37˚C. The next day, genomic DNA digests were run on 0.8% agarose gel at 35-40 volts for the entire day. Undigested genomic DNA was run as a control. A 1kb DNA size ladder (New England Biolabs) as well as a lambda-ladder that was labeled with radioactive CTP were run in separate wells for band size estimation. Gels were stained with 400ng/ml ethidium bromide in TBE and DNA visualized under long-wave UV light. Long smears of DNA should be

visible on the gel in all lanes apart from the undigested control and ladder lanes. Gels were subsequently washed in first denaturing solution (1M NaOH) for 30min-1h and then in neutralizing solution (3M NaCl, 1M Tris pH7.5) for 30min-1h. The Gels were finally rinsed in water and DNA molecules were transferred from the gel to a nylon transfer membrane (GE Healthcare) by blotting in 6x SSC O/N. DNA was fixed to the membrane by UV cross-linking with UV Stratalinker 2400 (120,000 microjioules for 30sec) followed by baking in an 65˚C oven for 2h.

2.23 Radioactive labeling of double-stranded DNA probes

Two probes (at 5' and 3' homology arms of the 23Cherry construct) were radioactively labeled (see Table 2.6 for primer sequences). Briefly, 50-100ng of probe DNA was labeled with 32P-dCTP using the Megaprime labeling kit (Amersham Biosciences) following the manufacturer's instructions. Probes were then denatured at 95˚C , annealed to random primers and labeled with 2ul (0.0925MBq) alpha32P dCTP (Perkin Elmer) by incubation with Klenow enzyme at 37˚C for 30min. Labeled probes were separated from un-incorporated nucleotides using Sephadex Nick columns following the manufacturer's instructions (Amersham Biosciences).

5' probe	FW	ccaggtggtggtggtgaaca
	RV	ggtcaccctgggaacagagg
3' probe	FW	ctgtaggaagccatcctgattac
	RV	gacagaggctggcagggtggg

Table 2.6: Primer sequences for the 23Cherry probes

2.24 DNA hybridization and autoradiography

Cross-linked and baked membranes were wetted in 2x SSC and placed in hybridization bottles (Thermo-Fisher Scientific). No overlap of the membranes was allowed it was ensured that membranes were evenly sticking to the inside of the bottles. Membranes were pre-hybridized at 42˚C for 1h in 10ml of hybridization solution containing 50% formamide, 1x SSC, 1x Deharts, 20ug/ml ssDNA (salmon sperm DNA), 6% dextran and 1/20th volume 10% SDS (added just before hybridization). The denatured labeled probes were added to the hybridization buffer and membranes incubated in bottles O/N at 42˚C. After 10min incubation, bottles were checked with Geiger counter for potential leaks. The following day, membranes were washed in 2x SSC at RT for 20min and then in a 65˚C pre-heated solution of 0.1x SSC and 0.1% SDS. The last wash lasted for around 10min, with frequent checks for decreasing Geiger activity from the membrane. When the Geiger counts reach 5-50 counts, membranes were considered sufficiently washed and were allowed to dry on M3 paper. Dried membranes were sealed in cling film pockets and exposed to 2 (one on each side of labeled membrane) autoradiography Hyperfilms (GE Healthcare) in radiographic cassettes (Biorad) at -80˚C. One of the Hyperfilms was checked after 3-4 days for sufficient exposure, the 2nd film was left to expose longer (up to 2 weeks). Films were developed using a Kodac processor (Xograph Imaging Systems).

2.25 ES cell culture

E14 ES cells (129 background) were cultured in GMEM Glasgow BHK 21 media supplemented with 10% FSC, 1x glutamine, 1x sodium pyruvate, 1x non-essential amino acids, 1mM mercaptoethanol (all purchased from Gibco) and 1x Lif (house made). ES cells were passaged or split every 3-4 days and cell maintained around 60% confluency. Cells were grown in 0.1% gelatin-treated plates or dishes. Incubation of cells with 0.05% Trypsin (Gibco) for 2minutes and subsequent gentle mechanical dissociation generated single cell suspensions. Cells were frozen in 90% FCS (Gibco) and 10% DMSO (Sigma).

2.26 Karyotyping

Cells were expanded to a T75 flask (Falcon) and allowed to reach 80-90% confluency. 0.1ug/ml of Colcemid (Gibco) was added to the culture media in the flask and incubated for 2-2.5h at 37˚C. Colcemid arrested cell division in metaphase. Cells were washed with PBS and single cell suspensions were generated (as described in section 2.25). Cells were washed in PBS and centrifuged for 5min at 800-1000rpm. The supernatant was discarded and as much PBS removed from the cell pellet as possible. Cell pellets were resuspended in 5ml of 0.075M KCl, which was pre-warmed at 37˚C, and left at RT for 10min. After centrifugation, pellets were gently resuspended in 1ml of ice-cold fixative (3 parts Methanol, 1 part glacial acetic acid) and left on ice for 10min. Cells were centrifuged at 600rpm for 5min and the supernatant discarded. Using a glass dropper pipette, around 400ul of the ice-cold fixative was added drop-by-drop to

the cells, while continuously flicking the tube, to prevent cell cluster formation and retain cells in a single cell suspension. The solution should be opaque in appearance. Individual drops of this cell suspension were transferred onto poly-L-lysine slides from a height of around 20-50cm off the bench. This is important aspect as the impact of the drop on the slide will cause the burst of the cell membrane and induce the release and spreading of the chromosomes. Not enough impact would result in cells not bursting sufficiently, and too much impact (too high) would spread the chromosomes of one cell too far apart, so the height from which cells are dropped is crucial. It is suggested that several slides are prepared and cells dropped at different heights. Slides were then stained with Giemsa stain and chromosomes counted manually under bright field microscope at 100x magnification with oil immersion.

Chapter 3

Generation and phenotypic characterization of a *Runx1* +204 enhancer-reporter transgenic mouse line

The study of HE and EHT had been previously hindered by a lack of positive markers for the identification and isolation of these cells in the embryo. Since, the development of HE-specific tools by the de Bruijn lab has been fundamental in our understanding of EHT and specifically HE (Chapter 1.10 and Swiers et al., 2013). Utilizing the hematopoietic TF Runx1 and determining which of its enhancer regions mediated hematopoietic-specific Runx1 expression, it was possible to generate transient Runx1 enhancer-reporter mouse lines which, in turn, allowed the labeling of specific aspects of EHT (described in Chapter 1.9). Further, the generation of a stable +23 enhancer-GFP (23GFP) mouse line and its ability to isolate and study HEs on a molecular and functional level, had led to new, previously unrecognized, insights into hematopoietic commitment during EHT (Chapter 1.11; Swiers et al., 2013). Unfortunately, although all HE potential resided in the 23GFP+ endothelial fraction, on a single cell level, only a subset of these cells showed molecular profiles associated with hematopoietic commitment. This suggested that further purification of HE is possible and necessary for more in-depth RNA-Seq analysis.

Here, I focus on another Runx1 enhancer, the +204. In transient transgenic +204-reporter (204lacZ) expression analysis, previously performed in the lab, it was established that the +204 enhancer predominantly marked the developing endothelium but no hematopoietic cells. At E8.5 +204-reporter expression was seen in rare ECs of the YS and paired aortae (Figure 3.1B,C); At E10.5, some expression was seen in the AGM region but mainly in the sub-aortic layers of the DA (Figure 3.1E).

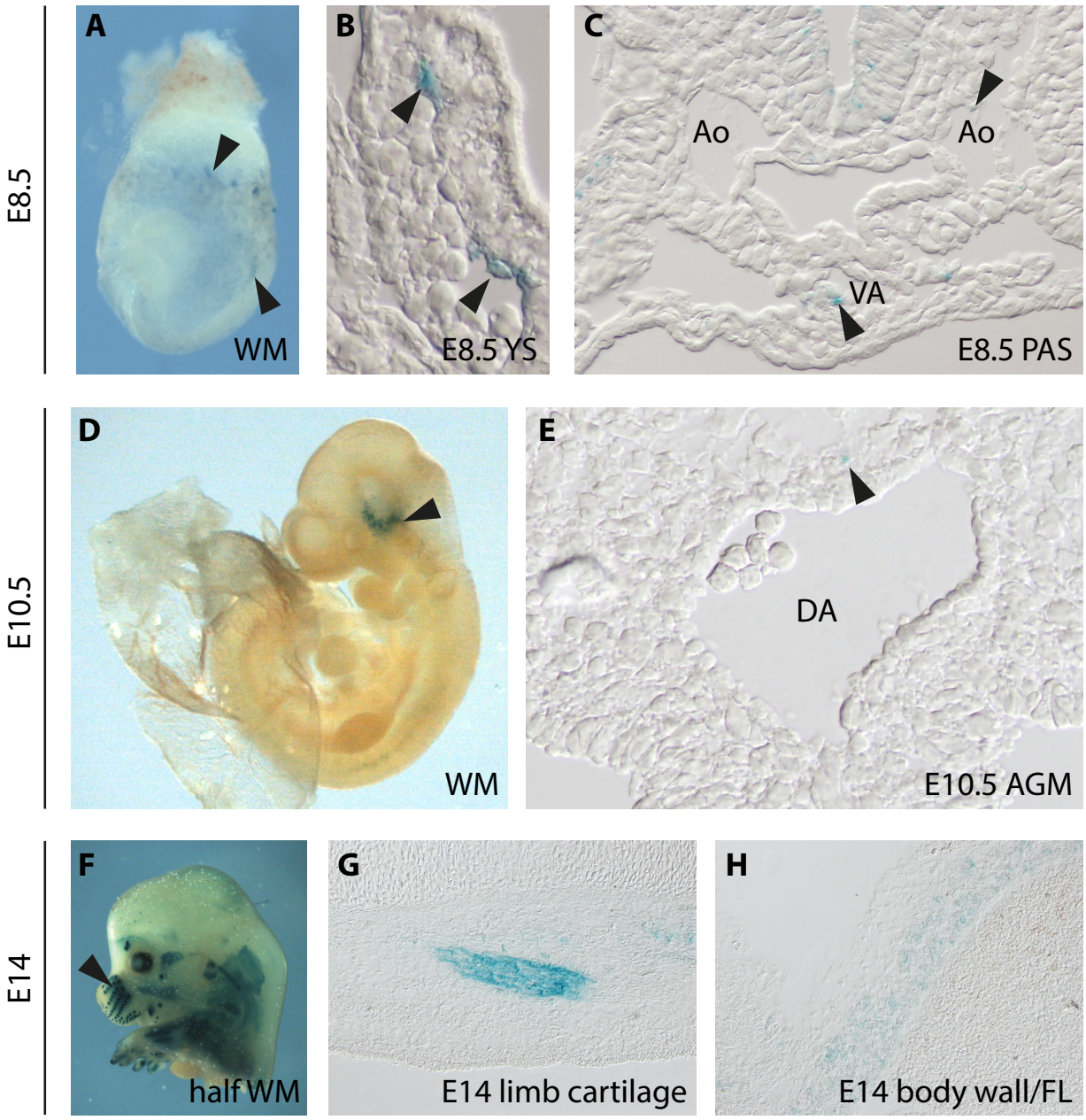


Figure 3.1 Analysis of expression pattern in *Runx1* +204 enhancer reporter transient transgenic embryos

Expression patterns of *Runx1*+204 enhancer-lacZ transient transgenic embryos at E8.5 (**A-C**), E10.5 (**D-E**) and E14.5 (**F-H**) are shown. Weak X-gal staining (blue) was observed in the YS and the posterior embryonic parts of E8.5 embryos (arrowheads in **A**) and sections through those regions confirmed the expression in the YS vasculature (arrowheads in **B**) and in the vasculature of the paired aortae (Ao) and vitelline artery (VA) of the E8.5 PAS region (**C**). At E10.5 few X-gal+ cells were observed in the AGM region (arrowhead in **E**). No expression was observed in the E14 fetal liver (FL, **H**). In addition, non-hematopoietic expression in the E10.5 brain (arrowhead in **D**) as well as in the limb cartilage at E14 (**F,G**) and in the E14 whisker follicles (arrowhead in **F**) was observed. Such expression is reminiscent of endogenous Runx1 expression (cf Figure 1.5). All images are courtesy of Andrew Jarrat.

Interestingly, even at later developmental stages, no expression was observed in hematopoietic cells of the E14 FL (Figure 3.1H). These data hinted at the endothelial-specific activity of the Runx1 +204 enhancer and provided the basis to generate a stable +204-reporter mouse line, with the intention to utilize it as a tool to further dissect or purify HE. In this chapter I describe the generation of this novel mouse line and its detailed phenotypic expression analysis during developmental hematopoiesis.

3.1 Generation of 204GFP founders

A stable reporter mouse line was needed for the comprehensive analysis of *Runx1* +204 enhancer-reporter marked cells. The +204 enhancer GFP reporter construct was generated previously in the lab (Andrew Jarratt). It comprises the heterologous hsp68 core promoter (Kothary et al., 1989), GFP and the 1.6 kb +204 enhancer (Figure 3.2A), and will from here on be referred to as 204GFP. To generate transgenic founder mice, I injected this construct into the pronucleus of mouse zygotes. Injected embryos were allowed to develop for several hours in a 37°C incubator until they reached the 2-cell stage, indicative of zygote survival, as usually around 50% of injected zygotes lyse or die post injection. I then transplanted healthy-looking 2-cell stage embryos into the oviduct coils of pseudopregnant female mice and embryos were allowed to develop to full term. Six injection sessions resulted in a total of 9 founder mice carrying the transgene. Out of the 9 founders, 7 successfully showed germ line transmission of the transgene to the next generation. Of those 7, the

A



B

line	Wholemount expression at E8.5		Expression in sections at E8.5			
	embryo	YS	Ao	VA	YS	other
Line 1	✗	✗	✗	✗	✗	✗
Line 2	✓	✓	✓	✓	✓	✓
Line 3	✗	✓(weak)	✓	✓	✓	✓
Line 4	✗	✗	✗	✗	✗	✗
Line 5	✓(weak)	✓(weak)	ND	ND	ND	ND
Line 6	✓	✓	✓	✓	✓	✓
Line 9	✓(weak)	✓(weak)	ND	ND	ND	ND
Total	**4/7**	**5/7**	**3/5**	**3/5**	**3/5**	**3/5**

C

line	Wholemount expression at E10.5				Expression in sections at E10.5				
	AGM	FL	YS	Other	DA	VA	FL	YS	Other
Line 1	ND	ND	ND	ND	ND	ND	ND	ND	ND
Line 2	✓	✗	✗	✓	✓	✓	✓	ND	✓
Line 3	✗	✗	✗	✓	✓	✓	✓	ND	✓
Line 4	ND	ND	ND	ND	ND	ND	ND	ND	ND
Line 5	ND	ND	ND	ND	ND	ND	ND	ND	ND
Line 6	✗	✗	✓	✓	ND	ND	ND	ND	ND
Line 9	ND	ND	ND	ND	ND	ND	ND	ND	ND
Total	**1/3**	**0/3**	**1/3**	**3/3**	**2/2**	**2/2**	**2/2**	**ND**	**2/2**

D

line	WM	Expression in sections at E14					
	any	FL	Limb buds	Whisker follicles	Skin follicles	neurons	Somite/DRG?
Line 1	✗	✓ (weak)	✓ (weak)	✗	✗	✗	✓ (weak)
Line 2	✓	✓ (weak)	✓	✓	✓	✓	✓
Line 3	✓	✓	✓ (weak)	✓ (weak)	✗	✗	✓ (weak)
Line 4	✓ (weak)	✓	✓	✓ (weak)	✗	✗	✗
Line 5	ND	ND	ND	ND	ND	ND	ND
Line 6	ND	ND	ND	ND	ND	ND	ND
Line 9	ND	ND	ND	ND	ND	ND	ND
Total	**3/4**	**4/4**	**4/4**	**3/4**	**1/4**	**1/4**	**3/4**

Figure 3.2 Assessment of 204GFP founder lines

A) Schematic of the Runx1 +204 enhancer reporter construct used to generate the 204GFP mouse line via pronuclear microinjections. **B-D)**Seven founder lines that showed germline transmission to their offspring were scored for 204GFP expression at E8.5 **(B)**, E10.5 **(C)** and E14 **(D)**. Initial analysis in wholemounts and more detailed analysis in embryo sections was performed. 204GFP expression in different hematopoietic and non-hematopoeitic tissues was scored for the founder lines analyzed. Dark green highlights three 204GFP lines that showed the most reproducible expression at E8.5 and E10.5. Light green highlights weaker and less consistent expression at E8.5 and E14.5. The number of founders in which expression per tissue was observed per the number of total founders analyzed is shown. YS – yolk sac, Ao – aorta, VA – vitelline artery, AGM – aorta-gonad-mesonephros, FL – fetal liver, DA – dorsal aorta, DRG – dorsal root ganglia, ND – not determined.

embryo offspring was analyzed for 204GFP expression at 3 developmental timepoints in overall wholemount analysis as well as in sections (Figure 3.2B,C,D). Analysis of multiple founder lines is necessary to validate the expression pattern in multiple lines in order to exclude possible ectopic expression caused by random transgene insertion and often seen in lines generated via transgenesis (Martin and Whitelaw, 1996). If a particular 204GFP expression pattern is observed in multiple lines and the pattern is comparable with that of the endogenous Runx1 expression, it is considered 'reproducible' and a true representation of enhancer-specific activity. In total, 5/7, 3/3 and 4/4 founders showed transgene expression in their offspring at E8.5, E10.5 and E14.5 respectively (green highlight in Figure 3.2B,C,D). Overall wholemount analysis identified several lines with varying degree of 204GFP expression, while more detailed confocal microscopy analysis of transgenic embryo sections established a 204GFP-specific expression pattern in lines 2, 3 and 6 at E8.5, in lines 2 and 3 at E10.5 and in lines 1, 2, 3 and 4 at E14.5 (Figure 3.2B,C,D). Next, the 204GFP-specific expression pattern in these founder mouse lines was analyzed for *Runx1*-related expression patterns in hematopoietic tissues during development and in the adult.

3.2 Analysis of 204GFP founder offspring: embryonic hematopoiesis

Freshly-harvested transgenic embryos were examined for 204GFP expression at E8.5, E10.5 and E14.5. Expression was compared with the staining pattern of endogenous *Runx1* expression; a *Runx1*-lacZ knock in

(KI) reporter line and Runx1 *in situ* hybridization (ISH) staining was used for that (cf. Figure 1.5). This was necessary in order to assess what aspect(s) of the endogenous *Runx1* expression pattern were mediated by the enhancer.

Hematopoietic-specific 204GFP expression at E8.5

At E8.5, 204GFP expression was marking a subset of yolk sac cells (arrowheads in Figure 3.3). The 204GFP expression pattern was punctuate in 2 of the lines, where 204GFP was not expressed in the blood island band – a pattern characteristic for *Runx1* (cf. arrowhead in Figure 1.5A) – but was more dispersed throughout the YS, reminiscent of *Runx1* expression in the YS vasculature. This was validated in 10um-thick cross-sections through the E8.5 concepti, where indeed 204GFP expression was observed in YS cells with a more elongated shape that appeared to surround clusters of round cells (Figure 3.4 YS). Such distinctive feature suggests the 204GFP+ YS cells are ECs rather than HCs. In addition to the 204GFP expression in the YS, sections revealed that the 204GFP transgene was also expressed in the PAS region, which was not obvious from the wholemount analysis (Figure 3.3). Specifically, 204GFP expression was observed in the paired dorsal aortae and vitelline artery (Figure 3.4), similar to what is seen in endogenous *Runx1* expression (Figure 1.5C,D). At E8.5, the three 204GFP transgenic lines analyzed exhibited similar expression patterns in the PAS and YS, although the number of cells marked and/or intensity of 204GFP expression differed between the lines (Figure 3.4).

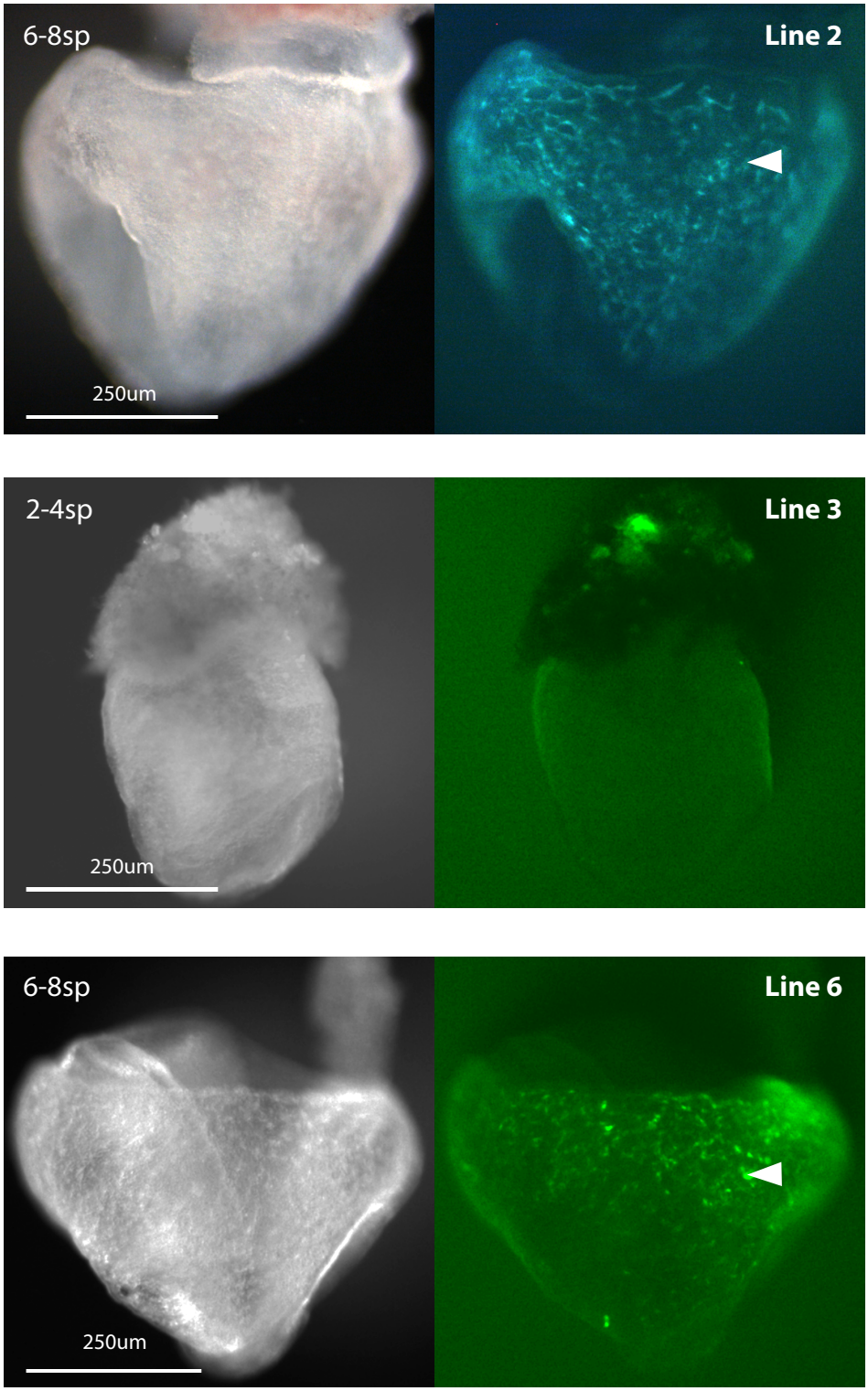


Figure 3.3 204GFP expression in E8.5 wholemount embryos
Representative images of 204GFP expression in Line 2, 3 and 6 at E8.5 are shown. Left panels – brightfield image, right panels – 204GFP expression. Arrowheads point to 204GFP expression in the yolk sac vasculature. Embryos were staged between 4-13sp. Images were taken on the Leica MZFLIII brightfield microscope with a 1X planapo objective. Anterior – left, proximal – up.

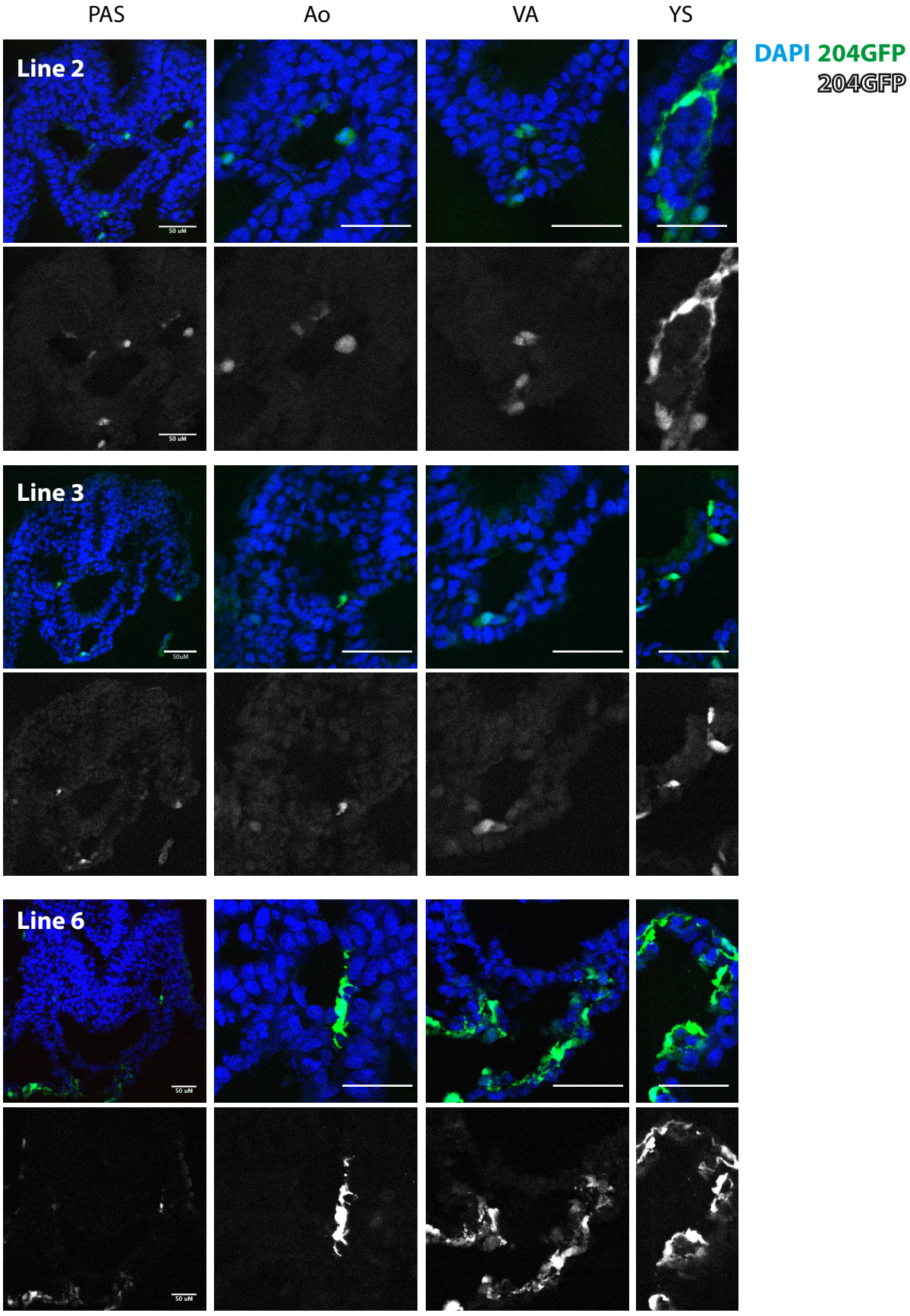


Figure 3.4 204GFP is expressed in hematopoietic tissues at E8.5
Representative images of transverse sections through the E8.5 PAS and YS of 204GFP embryos in Line 2, 3 and 6 are shown. Zoomed images of 204GFP expression in the aorta (Ao), vitelline artery (VA) and yolk sac (YS) are shown. Nuclear stain (DAPI, blue) and 204GFP (green) are shown in the top panels and 204GFP only (white) in the bottom panels. Images were taken on the Zeiss 510 confocal microscope with a 40X and 63X oil-immersion objective. Scale bars = 50μm. PAS - para-aortic-splanchnopleura.

Hematopoietic-specific 204GFP expression at E10.5

At midgestation (E10.5), I observed faint 204GFP expression in the AGM region in wholemount embryos of Line 2 (closed arrowhead in Figure 3.5), similar to what is seen in the *Runx1*-LacZ KI embryos (arrowhead in Figure 1.5B). Lines 2 and 3 were also analyzed in embryo sections at E10.5, where 204GFP expression was seen in the AGM region, corroborating the wholemount expression analysis in Line 2 (Figure 3.6). Interestingly, even though no transgene expression was detected in wholemounts of Line 3, analysis of sections, however, revealed weak 204GFP expression within the AGM region (Figure 3.6). Within the AGM region, 204GFP expression was observed in what appears to be the first aortic layer and several cell layers surrounding the dorsal aorta (DA) lumen (Figure 3.6), a pattern reminiscent of *Runx1* expression (Figure 1.5E). Thus, it is likely that 204GFP is labeling the endothelium, and possibly HE, and (part of) the sub-aortic smooth muscle cells that express *Runx1* (Mirshekar-Syahkal et al., 2013). A few rare 204GFP+ cells were also seen within the lumen of the aorta, which could either represent circulating progenitors, or cells part of a larger cluster outside the plane of the section. Interestingly, while no obvious FL expression was observed in the E10.5 wholemounts (Figure 3.5), sections through the midgestation fetal liver primordium identified very few (line 2) to some cells (line 3) that express the 204GFP transgene (Figure 3.6 FL), which is in contrast to endogenous *Runx1* expression observed throughout the entire E10.5 FL (Figure 1.5F).

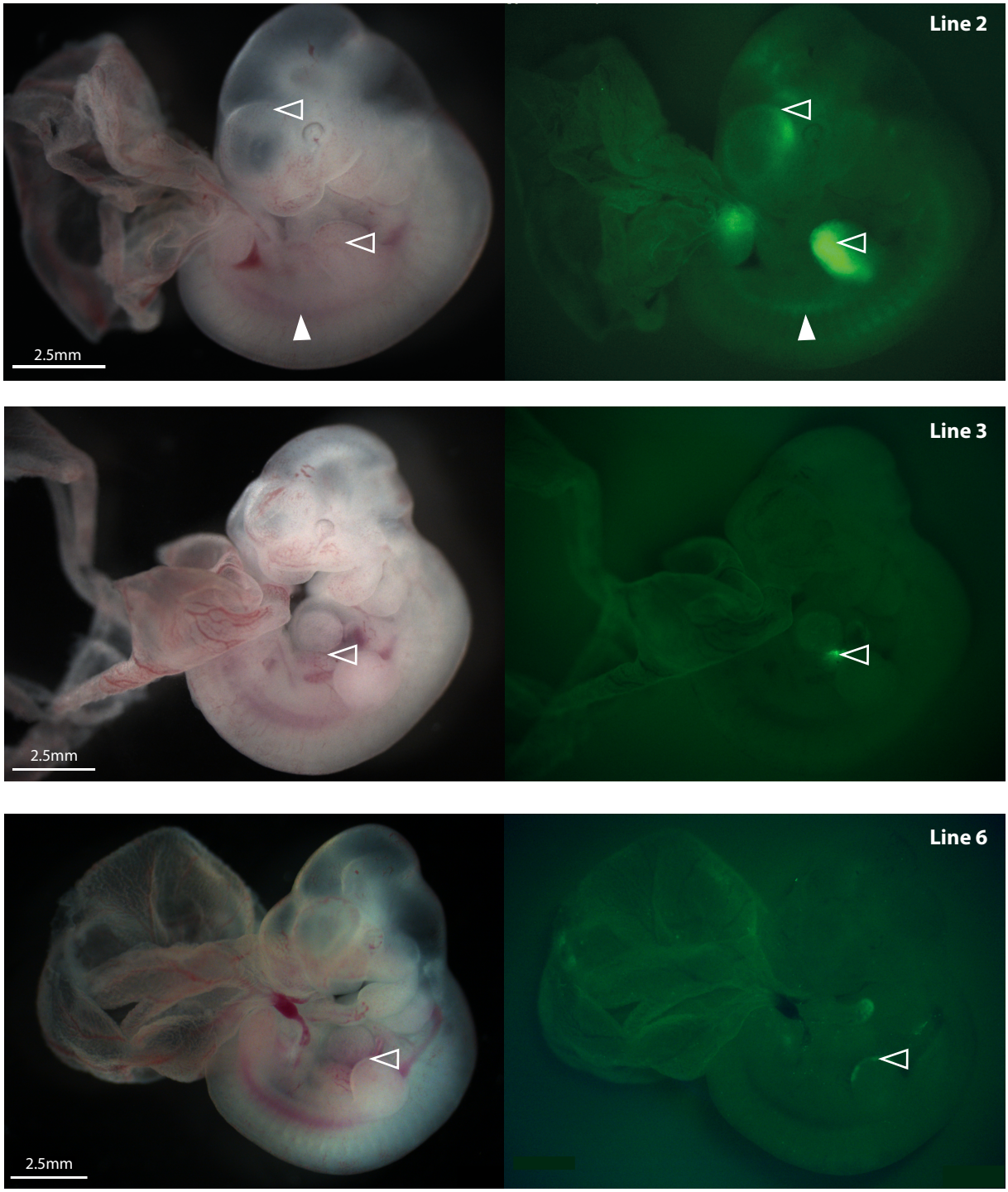


Figure 3.5 204GFP expression in E10.5 wholemount embryos
Representative images of 204GFP expression in Line 2, 3 and 6 at E10.5 are shown. Left panels – brightfield image, right panels – 204GFP expression. Closed arrowheads point to faint 204GFP expression in the AGM region in Line 2. Ectopic GFP expression in limb buds, head and heart region are marked with open arrowhead. Embryos were staged between 28-37sp. Images were taken on the Leica MZFLIII brightfield microscope with a 1X planapo objective.

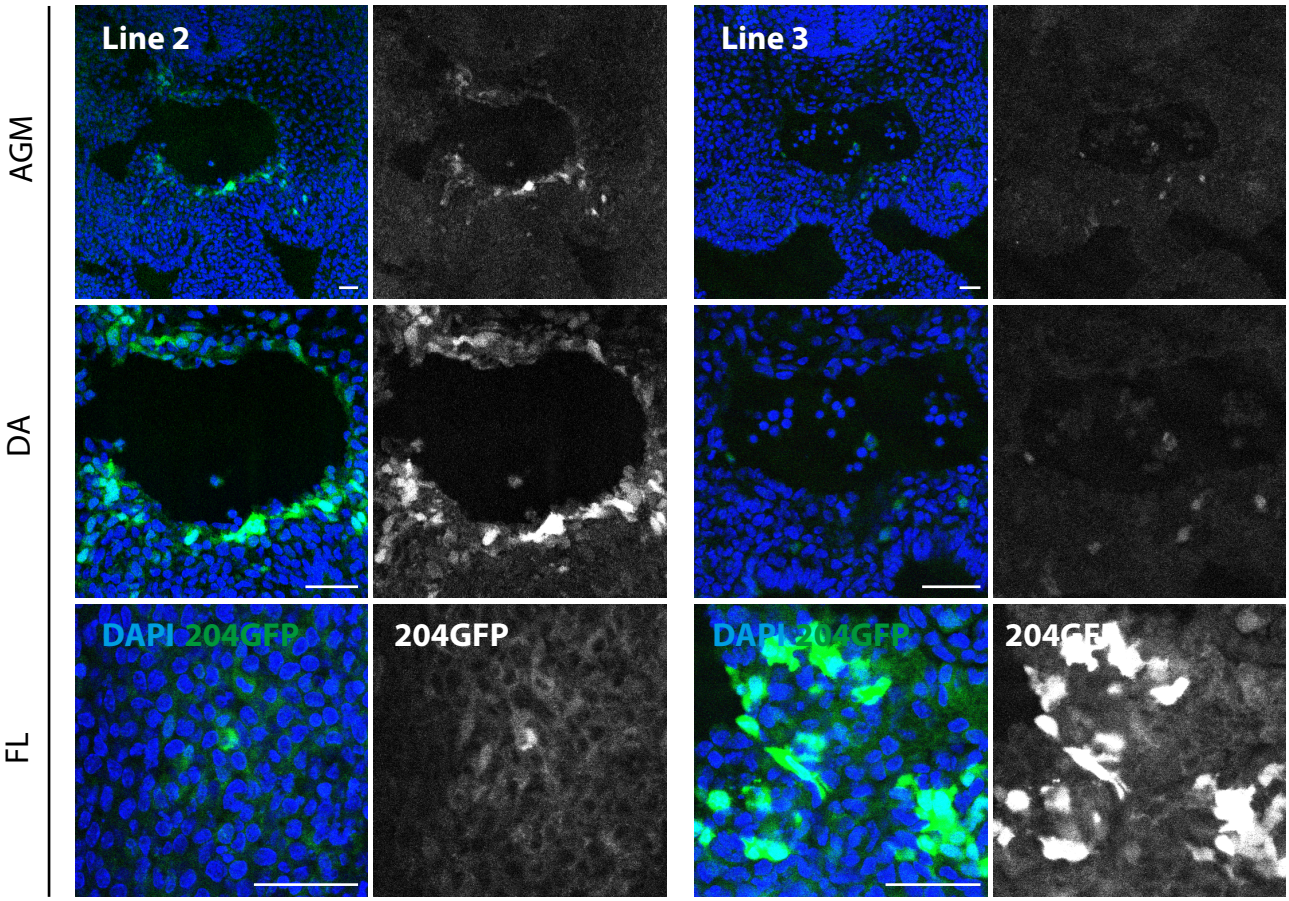


Figure 3.6 204GFP is expressed in hematopoietic tissues at E10.5
Representative images of transverse sections through the E10.5 AGM region and FL of 204GFP embryos in Line 2 and 3 are shown. Middle panel – zoomed images of the dorsal aorta (DA). Bottom panel – images of the fetal liver (FL). Nuclear stain (DAPI, blue) and 204GFP (green) are shown on the left of each line panel and 204GFP only (white) is shown on the right of each line panel. Images were taken on the Zeiss 510 confocal microscope with a 40X and 63X oil-immersion objective. Scale bars = 50µm. AGM - aorta-gonad-mesonephros.

Hematopoietic-specific 204GFP expression beyond midgestation

When 204GFP expression (line 2) was analyzed a day later (E11.5), the number of cells that expressed 204GFP in the FL remained small (not formally counted; Figure 3.7A,B). Interestingly, when FL sections were stained with CD45 and Runx1, no co-expression with the 204GFP transgene was observed (arrow heads in Figure 3.7A,C,D). In addition, no obvious 204GFP expression was detected in the FL of E14.5 wholemount embryos (Figure 3.7E,F). This suggests that the 204GFP transgene is not marking hematopoietic cells.

Comparison to transient transgenic data

In order to fully validate the +204 enhancer-specific activity during developmental hematopoiesis, I compared the 204GFP expression pattern observed here to Xgal staining patterns observed in transient transgenic 204LacZ embryos generated previously in our lab (Andrew Jarratt). Both, the 204GFP and the 204lacZ, transgenes were expressed in the same embryonic regions at all time points analyzed (cf. Figure 3.1). The difference was the extent of the expression pattern. Whereas the 204lacZ transgene also marked cells with predominantly endothelial morphology in the E8 YS, the 204GFP transgene marked overall a higher proportion of these cells (compare Figure 3.1A,B and Figure 3.3). Likewise, at E10.5, only rare cells were detected in the AGMs of transient transgenic embryos, but the pattern was comparable to that observed in the 204GFP transgenic embryos, with Xgal+ cells present in the endothelial (not shown) and sub-mesenchymal areas of the AGM (compare Figure 3.1E and Figure 3.6).

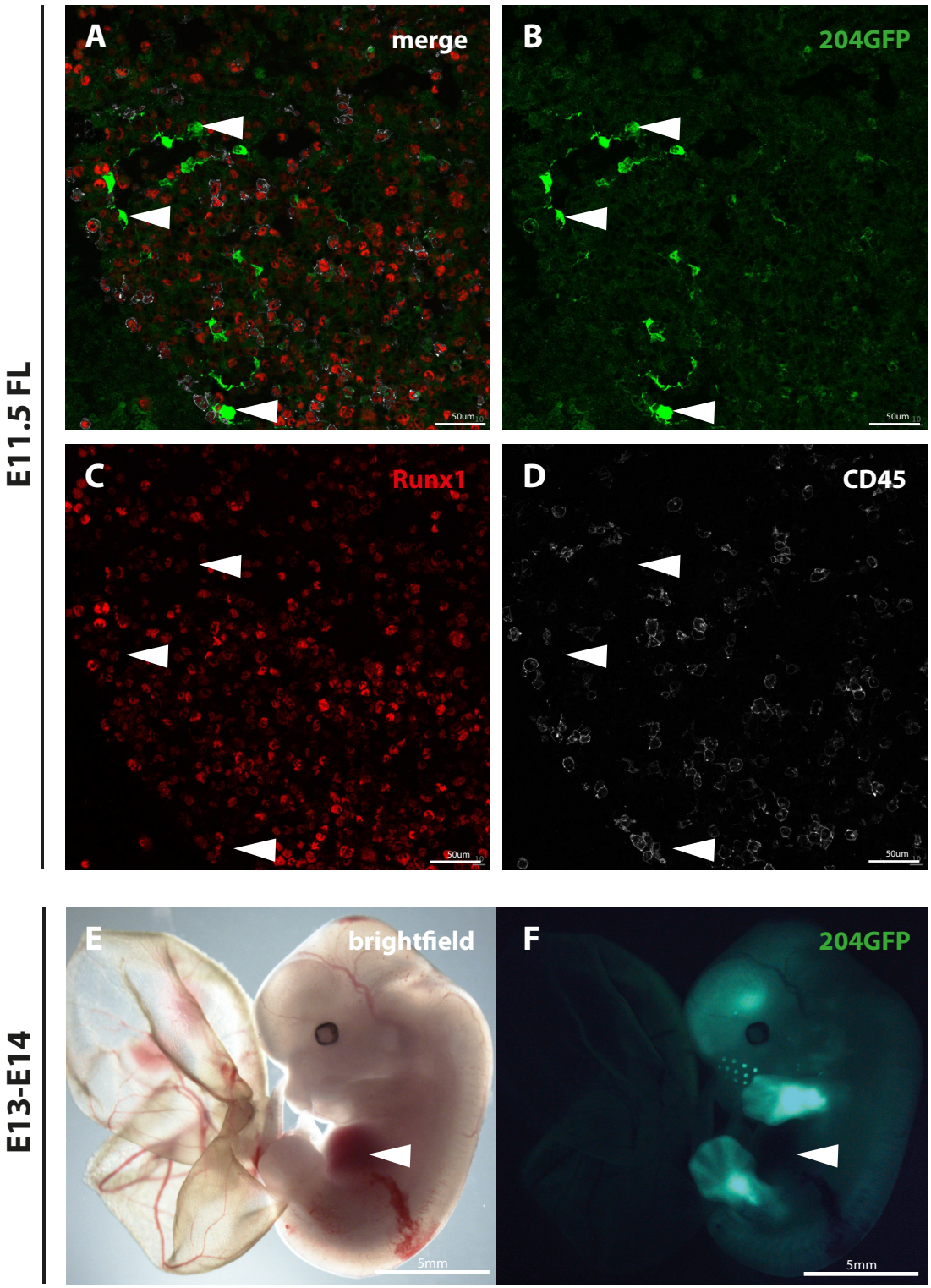


Figure 3.7 The 204GFP transgene is not marking hematopoietic cells in the fetal liver
A-D) Transverse section through the E11.5 fetal liver is shown. 204GFP (green, B), Runx1 (red, C) and CD45 (white, D) staining is shown. 204GFP was minimally expressed in fetal liver (FL) cells and did not co-express with Runx1+ or CD45+ hematopoietic cells (arrowheads). Images were taken on the Zeiss 780 confocal microscope with a 40X oil-immersion objective. **E,F)** Brightfield and GFP image of a wholemount E13-E14 transgenic mouse embryo. No obvious 204GFP expression was observed in the FL (arrowheads). Images were taken on the Leica MZFLIII brightfield microscope with a 1X planapo objective. Scale bars as shown.

Interestingly, at E10.5 additional 204GFP expression was detected in non-hematopoietic tissues such as the limb buds, parts of the head region, and faint expression in the somites and in the tissue close to the heart (empty arrowheads in Figure 3.5). Further, some Xgal staining was observed in the head and somite region of 204lacZ embryos and, more importantly, recapitulated endogenous Runx1 expression (compare Figure 1.5B and 3.1D). This suggests that apart from marking hematopoietic tissues, the 204GFP also showed a non-hematopoietic, but Runx1- and +204 enhancer-specific expression pattern at midgestation.

At the later embryonic stages (E14.5), virtually no X-gal staining was detected in the FLs of 204lacZ transient transgenic embryos analyzed, similar to the 204GFP transgene (compare Figure 3.1H and 3.7F), and only very few non-hematopoietic cells were detected in the E10.5 and E11.5 FLs (Figure 3.6 and 3.7A-D). This is different from endogenous *Runx1* expression, where the majority of FL cells are labeled (cf. Figure 1.5F,G and 3.7C). Although lacking (strong) expression in the FL, the 204GFP transgene showed expression in limb buds, brain, whisker follicles and in the area of dorsal root ganglia (DRG) at E14 (Figure 3.7F). Similarly, such non-hematopoietic expression was also observed in the 204lacZ transient transgenic embryos (Figure 3.1F,G). More importantly, such expression is also in line with endogenous *Runx1* expression (Figure 1.5H,I). However, closer expression analysis of the E14.5 whisker follicles and DRG revealed that although the 204GFP transgene was expressed in these tissues, on a cellular level, the exact expression pattern rarely overlapped with Runx1 expression (Figure 3.8). Of note, the Runx1

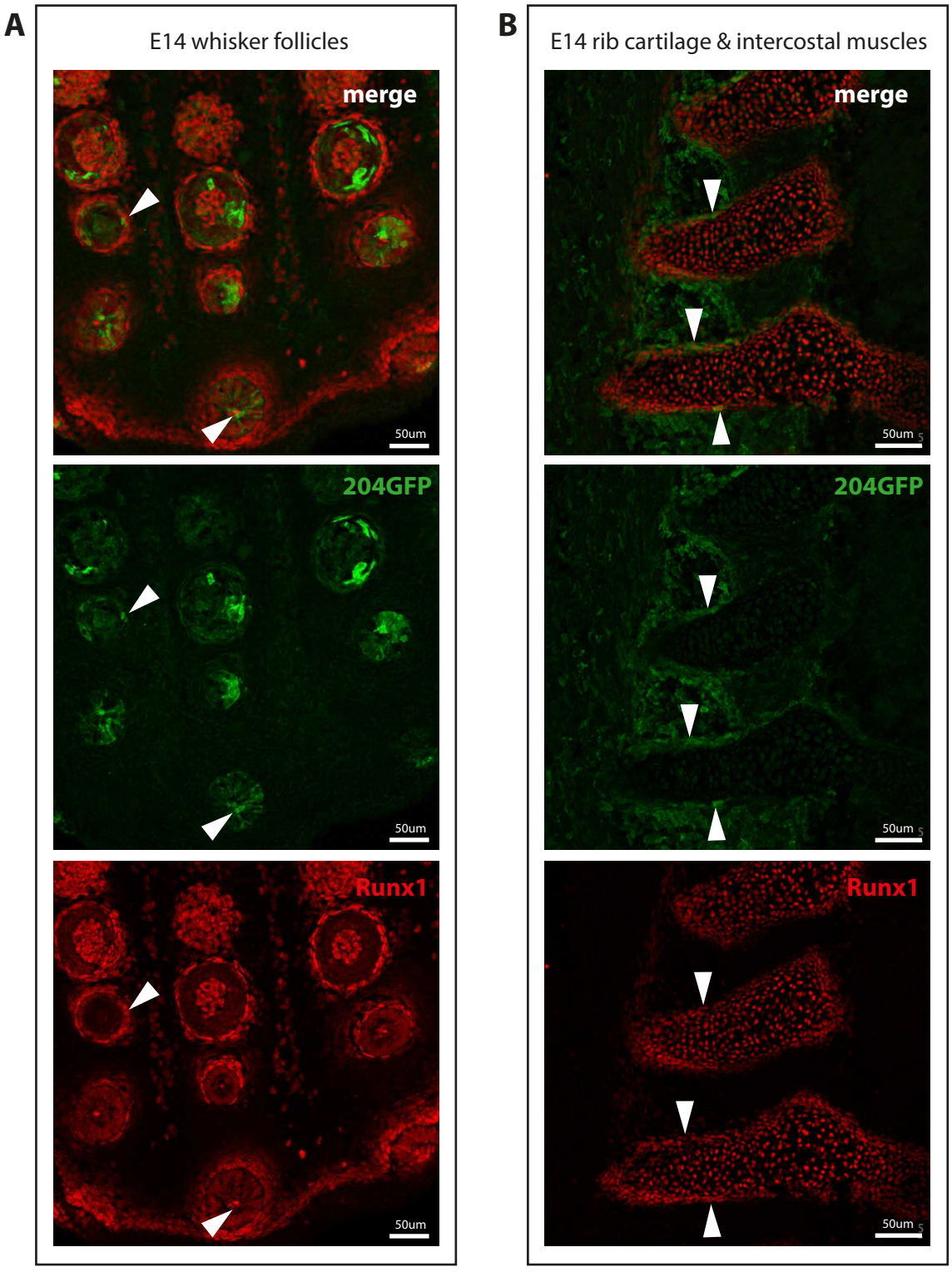


Figure 3.8 The 204GFP transgene recapitulates overall Runx1 expression in non-hematopoietic tissues but not an a cellular level

A) Transverse section through the E14 whisker follicles of 204GFP line 2 trangenic embryos. 204GFP (green) expression is observed in the same areas as Runx1 antibody (red) expression but only few cells are co-expressing 204GFP and Runx1 (arrowheads). **B)** Transverese section through the E14 rib cartilage and intercostal muscle tissues. 204GFP (green) expression is observed predominantly in the intercostal muscle tissue, while Runx1 antibody (red) expression is marking the rib cartilage. At the boundary of these tissues, 204GFP co-expresses in a small subset Runx1+ cells (arrowheads). Scale bars = 50um. Sections were stained by and images taken by Joe Harman. Images were taken on the Zeiss 780 confocal microscope with a 40X oil-immersion objective.

antibody used in this experiment detected the Runt domain, and therefore was not specific for Runx1, but could also label Runx2 and Runx3. The latter two are also expressed in the developing limb bud and DRG cartilage (Liakhovitskaia et al., 2010; Wang et al., 2005; Yamashiro et al., 2004). Therefore, the non-hematopoietic expression pattern of the 204GFP transgenic mouse lines at E14.5 was +204 enhancer-specific and probably Runx1-specific.

Interestingly, when I analyzed 204GFP expression in pre-somitic 7dpc embryos, very few cells were expressing 204GFP and, in wholemounts, none were observed at known hematopoietic sites (Figure 3.9). Instead, parts of the endoderm and specifically cells in the anterior visceral endoderm (AVE) were labeled with the 204GFP transgene, similar to the 204lacZ expression in the endoderm layer (Figure 3.9A,B). Further, endogenous *Runx1* expression was also reported but not shown in the 7dpc endoderm (North et al., 1999). This suggests that the earliest 204GFP transgene expression at early bud stage is also *Runx1*- and +204 enhancer-specific but not hematopoietic.

Combined, these data suggest that the YS, AGM and FL expression patterns seen with 204-reporter transgenes is highly reproducible and representative of the tissue-specificity of the enhancer. In addition, the expression I observed compares to endogenous *Runx1* expression in hematopoietic sites. Thus, the 204GFP expression seen in hematopoietic tissues throughout development is likely intrinsic to this *Runx1* enhancer. Since the 204GFP Line 2 showed the strongest and most consistent

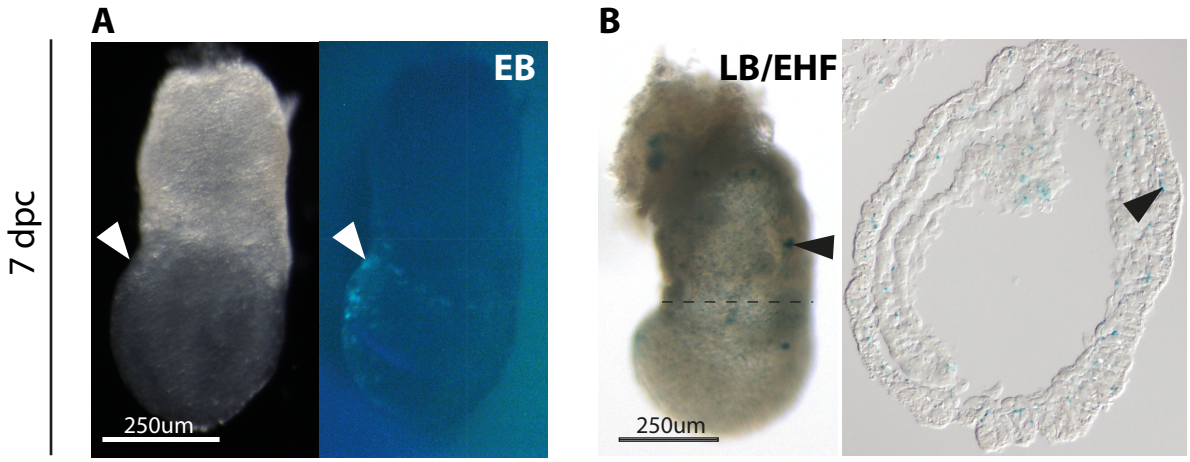


Figure 3.9 No hematopoietic-specific 204GFP expression in 7dpc embryos
A) Representative images of wholemount 204GFP (line 2) expression at the early bud stage (EB). Brightfield – left, GFP – right. 204GFP expression is observed in the anterior visceral endoderm (AVE, arrow heads). AVE has been linked to the development of the anterior mesodermal structures and the foregut, but not to developmental hematopoiesis (Tam, 2007). Images were taken on the Leica MZFLIII brightfield microscope with a 1X planapo objective. **B)** Representative image of wholemount and transverse section through a 204lacZ transient transgenic embryo at the late bud/early headfold stage (LB/EHF). X-gal staining (blue) is dispersed throughout the entire endoderm layer of the epiblast and some speckled cells were observed in the mesoderm layer (arrow head in section) (Image courtesy of Andrew Jarrat).

expression pattern over all embryonic stages analyzed, it was selected for all further experiments.

3.3 Analysis of 204GFP founder offspring: adult hematopoiesis

To complete the overall expression analysis I also looked at 204GFP expression in the BM of line 2 and compared it to BM of line 6 and WT mice. Adult mice were sacrificed and their BM cells harvested. Stem and progenitor cell populations were segregated on the basis of CD31/Ly6C expression (de Bruijn et al., 1996, 1998) (Figure 3.10A,B), and the contribution of 204GFP+ cells to the individual lineages was determined. The two founder lines showed different expression of 204GFP within the different blood lineages, with Line 2 showing overall lower levels of 204GFP expression in adult bone marrow (Figure 3.5C). Line 2 had the highest proportion of GFP-expressing cells in blast-like and myeloid progenitor cell populations (11.4% and 14.8% respectively), with very little 204GFP expression persisting to the granulocyte and monocyte stages. Limited expression was seen in the lymphoid lineage, and no erythroid cells expressed the transgene (Figure 3.10C). For Line 6, the relative distribution of 204GFP expression was broadly similar to that seen in Line 2, but a larger proportion of cells within the individual lineages expressed the transgene. This was particularly true for the granulocyte population, which seemed elevated in this line (n=1). Endogenous *Runx1* expression on adult BM cells has been reported before. North *et al*. observed *Runx1* expression in 73±4% of myeloid progenitors, 88±2% of granulocytes and

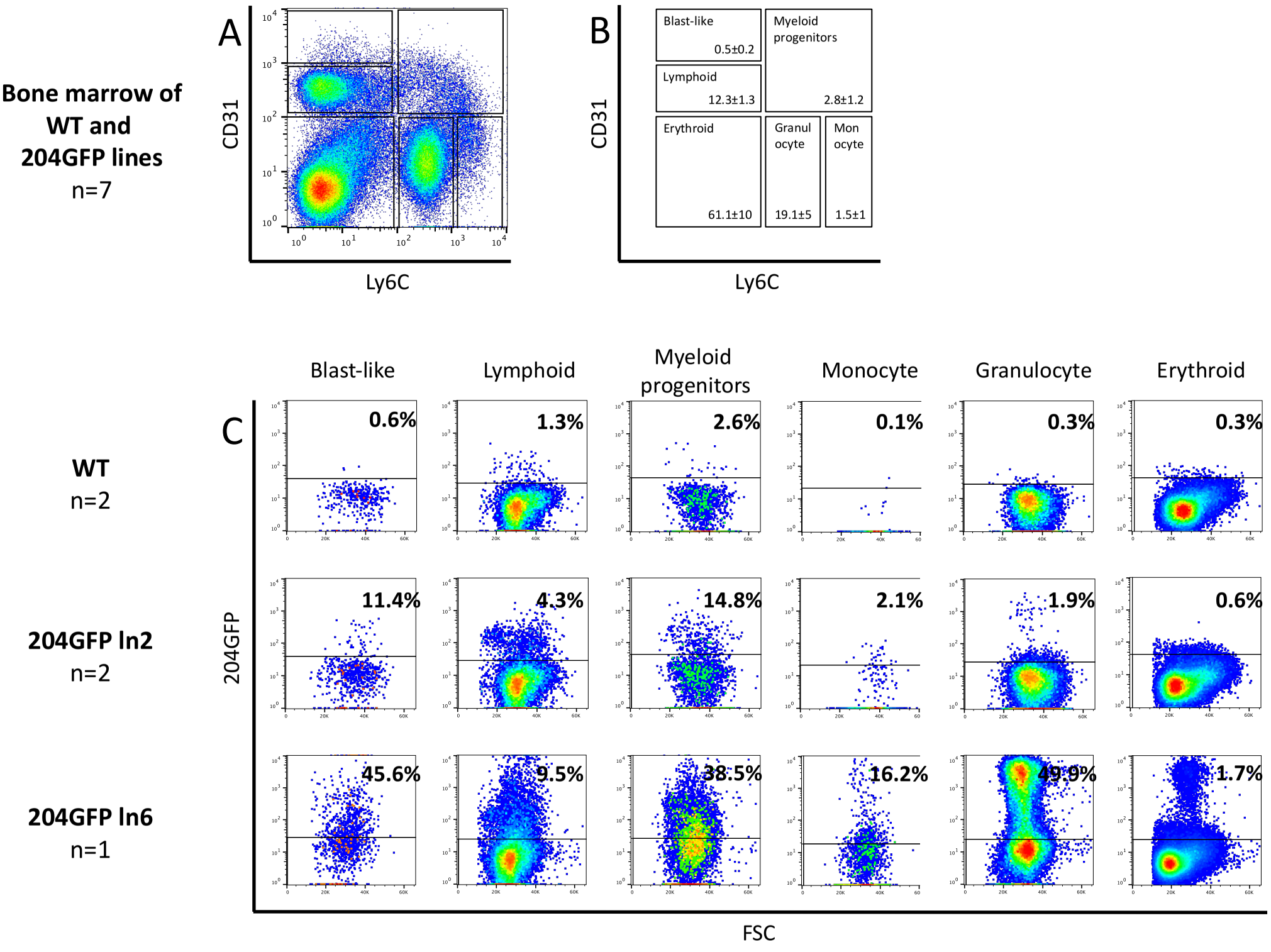


Figure 3.10 Flow cytometry analysis of 204GFP expression in the bone marrow of adult mice
A-B) Gating strategy and blood lineage breakdown based on CD31/Ly6C expression in the adult bone marrow (de Bruijn, et al., 1996, 1998). Single, live bone marrow cells were gated for CD31/Ly6C and differential expression was indicative of 6 broad blood cell lineages as shown in A and percentages ± SD in separate blood lineages is shown in B (n=7). **C)** Each blood lineage population was analyzed for GFP expression and the bone marrow of the WT mice (top panel) compared to the bone marrow of the 204GFP Line 2 (middle panel) and 204GFP Line 6 (bottom panel) mice. CD31/Ly6C gates were set based on fluorescence-minus-one (FMOs; not shown) and GFP gates based on WT controls. Where n=2, average GFP percentages in each blood population are shown.

89±7% of monocytes (North et al., 2004). *Runx1* expression in the erythroid lineage started off at 64±17% at the pro-erythroblast stage and decreased to 16±4% at the normoblast stage (all of these fall within the CD31-Ly-6C- population in our analysis), and is absent from mature erythroid cells (North et al., 2004; Lorsbach et al., 2004). Bone marrow B cells (main cell type in the $CD31^{lo}$ $Ly6C^{-}$ population) ranged from 61±9% (early B cells) to 46±13% (late B cells) (North et al., 2004). Thus, in adult BM, the 204GFP transgene does marks a subset of the populations in which *Runx1* is normally expressed. This is in line with its limited activity in the FL. In summary, the reproducible 204GFP expression observed during developmental hematopoiesis in several founder lines as well as similar expression patterns in the adult BM, emphasizes the +204 enhancer-specific activity of this novel *Runx1* enhancer reporter-mouse line. In the following sections I describe which specific cell types the 204GFP transgene marks.

3.4 The 204GFP transgene is marking a subset of the embryonic endothelium

Based on overall expression we have identified that the 204GFP is expressed in the tissues and time points that are associated with developmental hematopoiesis. Here we wanted to identify which cellular subsets are marked by the new reporter line. And in particular, assess whether the 204GFP transgene is indeed labeling the embryonic endothelium. Although the expression in the 7dpc 204GFP transgenic wholemount embryos did not mark hematopoietic tissues (e.g. YS BI), but

instead labeled a subset of the endoderm (cf. Figure 3.9), flow cytometric analysis of pre-somitic embryos was able to detect that a subset of the developing endothelium is indeed labeled by the 204GFP transgene (n=1, Appendix 3.1). This suggests that while the earliest 204GFP transgene expression at early bud stage is *Runx1*-specific but non-hematopoietic, 204GFP expression in the developing endothelium starts around the late headfold stage of development, although only detectable by flow cytometry. Next, I sectioned transgenic embryos at E8.5 and E10.5 and stained them with CD31 and an antibody directed against GFP. In the E8.5 PAS region, CD31 marks the endothelial layer of the paired dorsal aortae and a subset of this layer was co-expressing the 204GFP transgene (arrow heads in Figure 3.11B,C). Similarly, at E10.5, a subset of the CD31+ endothelium of the dorsal aorta expressed 204GFP (arrowhead in Figure 3.12B,C). In addition, intra-aortic cluster cells or budding cells only occasionally exhibited 204GFP expression (asterisk in Figure 3.12B,C). The strongest and broadest 204GFP expression was observed in several cell layers of the sub-aortic mesenchyme and a subset stained positive for the stromal cell marker alpha smooth muscle actin (α-SMA)(arrow heads in Figure 3.12D,E). α-SMA expression was previously reported in the sub-aortic mesenchyme of the human AGM, marking the ventral part of the AGM, associated with the generation of HSPCs (Marshall, 2006). It was also shown to overlap with Runx1+ cell in the sub-aortic mesenchyme of the midgestation AGM region (Mirshekar-Syahkal et al., 2013). In conclusion, we showed that the *Runx1* +204 enhancer mediates reporter gene expression to a subset the endothelium, rare hematopoietic cells,

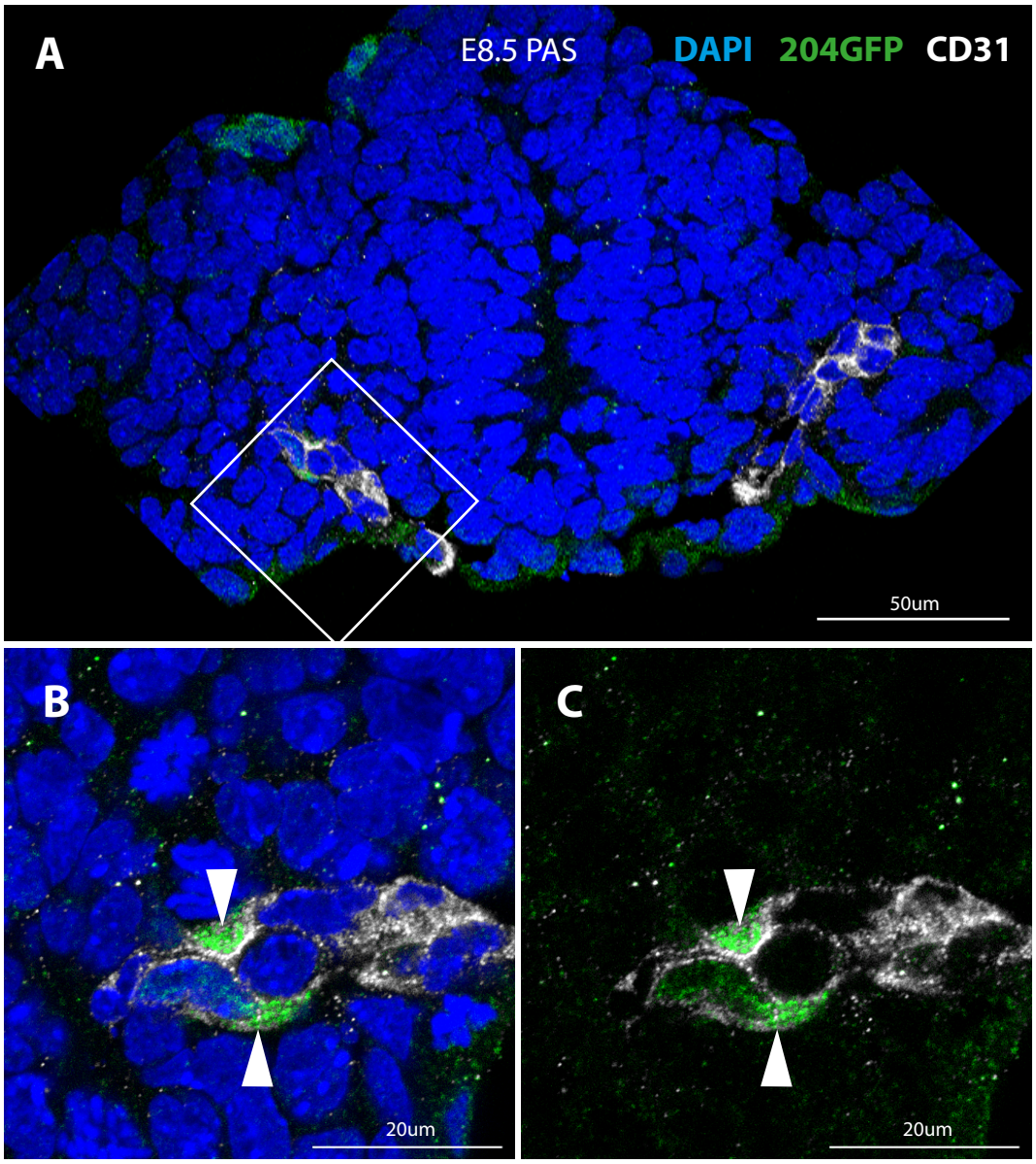


Figure 3.11 The 204GFP transgene labels a subset of the E8.5 endothelium
A) Transverse section (10um thick) through the E8.5 PAS region is shown. White box highlights the zoom in B and C. **B,C)** Zoomed in image on one of the paired aortae. DAPI (blue), 204GFP (green) and CD31 (white) staining is shown. 204GFP is expressed in a subset of the E8.5 endothelium (arrowheads). Scale bars as shown. Images were taken on the Zeiss 510 confocal microscope with a 40X and 63X oil-immersion objective. PAS - para-aortic-splanchnopleura.

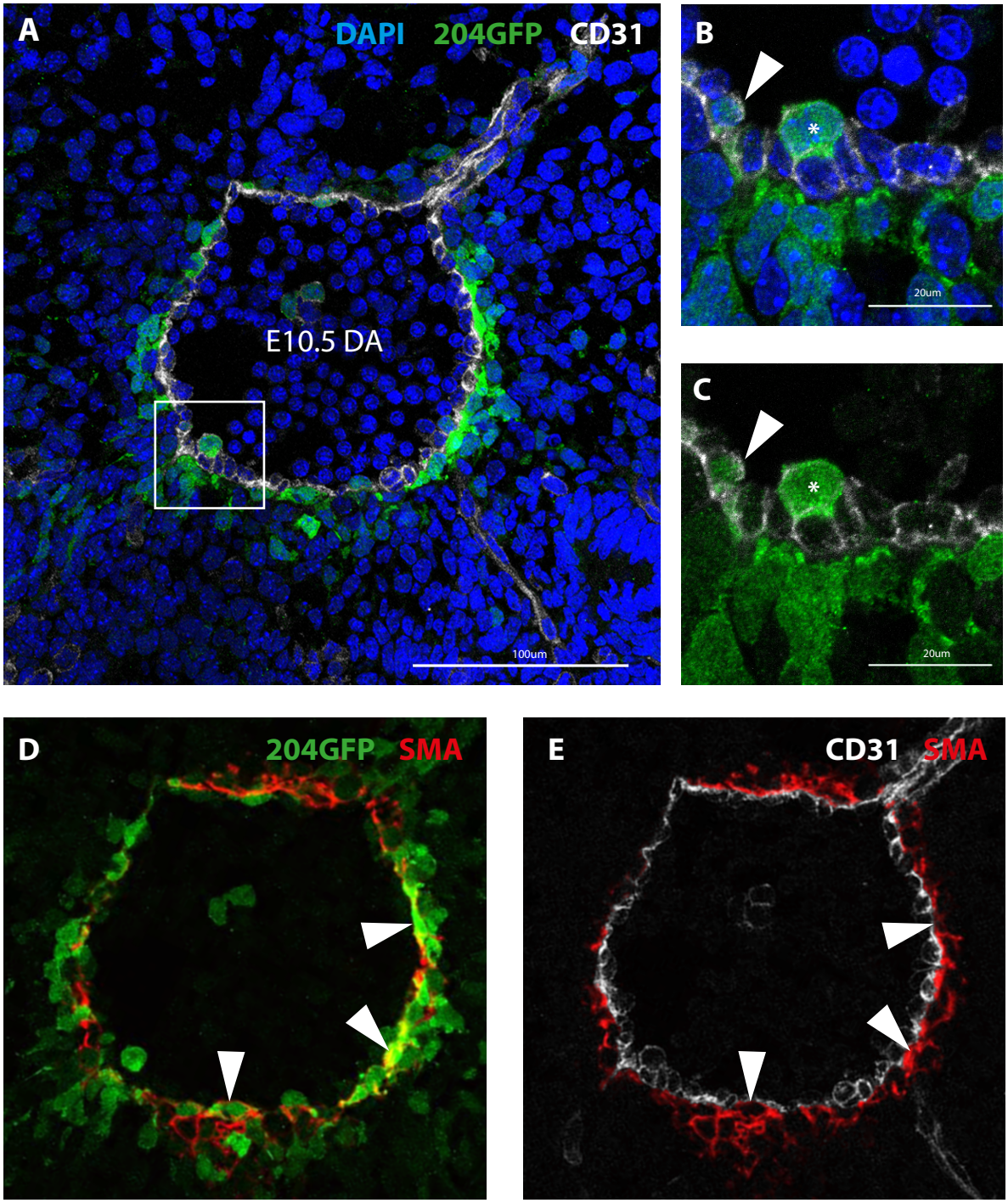


Figure 3.12 The 204GFP transgene labels a subsets of the E10.5 endothelium, rare blood cluster cells and a subset of cell in the sub-aortic mesenchyme

A) Transverse section of a E10.5 AGM region is shown. **B,C)** Zoomed in images on the ventral part of the dorsal aorta (DA) highlighted in A (white box). DAPI (blue), 204GFP (green) and CD31 (white) staining is shown. 204GFP is expressed within a subset of the E10.5 endothelium (arrowheads) and in rare blood cluster cells (asterisk). **D,E)** 204GFP expression is widespread in the sub-aortic mesenchyme and co-expressed in a subset of α-SMA (arrow heads). A clear boundary between endothelium (white) and smooth muscle actin (red) is shown in E. Images were taken on the Zeiss 780 confocal microscope with a 40X and 63X oil-immersion objective. AGM - aorta-gonad-mesonephros; DA - dorsal aorta. Scale bars as shown.

and (part of) the sub-aortic mesenchyme at E10.5.

3.5 Quantification of 204GFP expression in different cell populations

Next, I quantified 204GFP expression by flow cytometry throughout development. Embryos from E8.5 to E11.5 were harvested, dissected as required, dissociated into single cell suspensions and stained with various conjugated antibodies for flow analysis. To quantify 204GFP expression in E8.5-E11.5 embryos the following gating strategy was used (Figure 3.13). Live, single cells were sequentially gated on the basis of 1) VEC and Ter119 expression and 2) CD41 and CD45 expression. 204GFP expression was then measured in the endothelium (VEC+Ter119-CD41-CD45-), blood clusters (VEC+Ter119-CD41+CD45+/-) and more mature blood cells (VEC+Ter119-CD41-CD45+). In addition, erythroid cells (VEC+/-Ter119+) and the mesenchyme (VEC-Ter119-CD41-CD45-) were also analyzed for 204GFP expression (Figure 3.13).

At E8.5, one fifth of all endothelium expressed 204GFP (20.1±1.3%). At E9.5 and E10.5 approximately 8% of the endothelium was 204GFP+ (8.4±0.6% and 8.2±3.2%, respectively). This decreased to 4% by E11.5 (4.3±2.1, Figure 3.14). Of note, at E8.5 the whole concepti were analyzed (YS and embryo proper), while from E9.5 onwards, only the PAS/AGM and VU regions were analyzed. This likely explains the drop in the percentage of 204GFP+ endothelial cell between E8.5 and E9.5, as more endothelial cells in the yolk sac express this transgene than in the (paired) dorsal

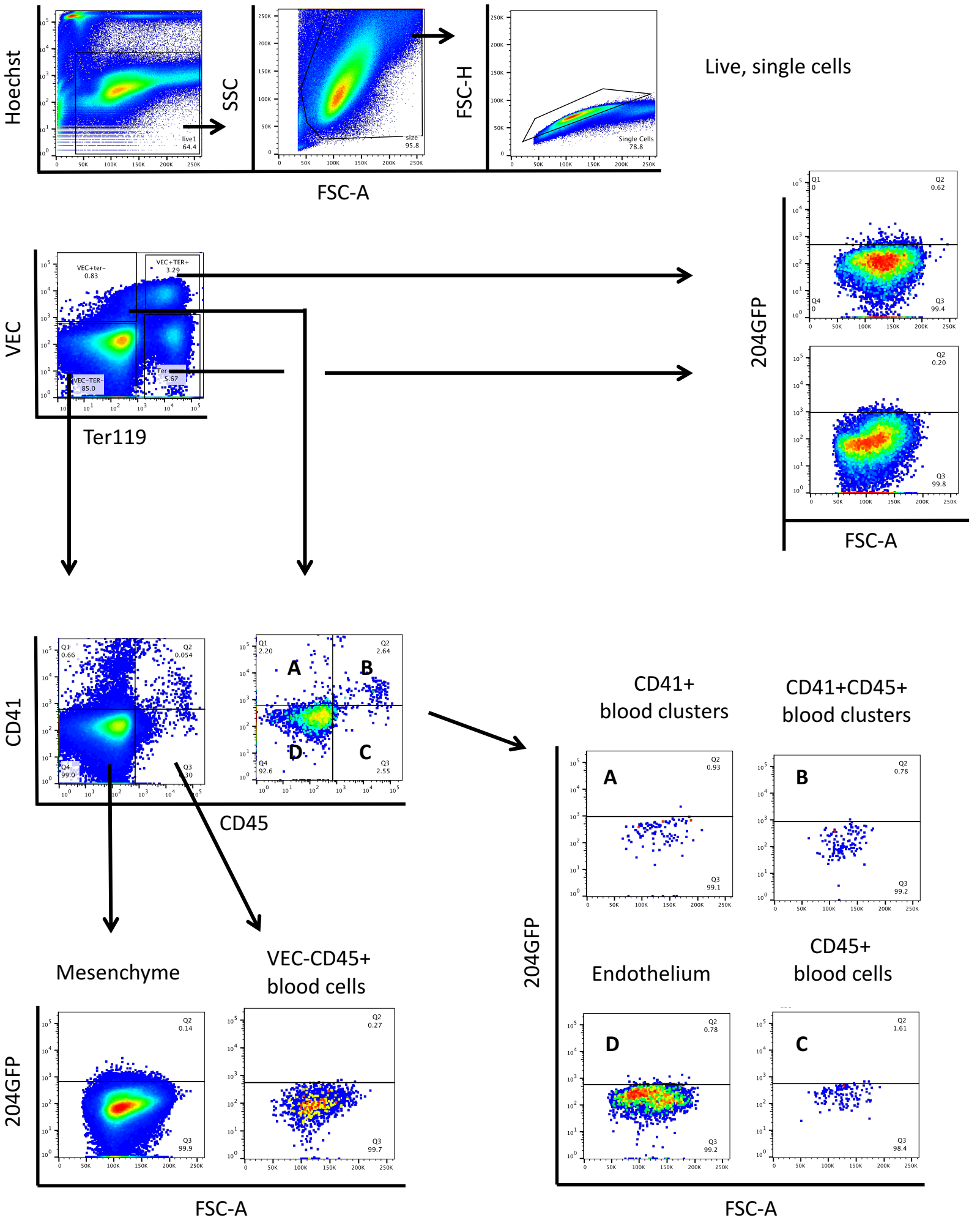


Figure 3.13 Gating strategy for flow cytometry experiments

Representative plots for flow cytometry gating strategy used for phenotypic characterisation of 204GFP transgenic embryos. Live (Hoechst^{-}), single cells of E8.5 concepti and E9.5 to E11.5 AGM+VU were sequentially gated for first VEC and Ter119 expression and then for CD41 and CD45 expression. 204GFP expression was evaluated in endothelial (**D**: VEC^{+}Ter119^{-}CD41^{-}CD45^{-}), CD45^{+}CD41^{-} blood cells (**C**), and CD41^{+}CD45$^{+/-}$ blood clusters (**A/B**), in the mesenchyme (VEC^{-}Ter119^{-}CD41^{-}CD45^{-}), mature blood cells (VEC^{-}Ter119^{-}CD41^{-}CD45^{+}) as well as in erythrocyte populations (VEC$^{+/-}$Ter119^{+}).

aorta (data not shown).

Phenotypic analysis showed rare 204GFP-expressing intra-aortic cluster cells (Figure 3.12). Quantification of 204GFP expression within blood clusters showed that 5-12% of these cells were marked by the 204GFP transgene between E8.5 and E9.5 (Figure 3.14). At later time points, it is possible to distinguish HSC precursors based on CD41/CD45 expression (Rybtsov et al., 2011). Interestingly, 204GFP marked 13.5±8.1% of phenotypic pre-HSC Type I at E10.5 and only around 5.1±1.3% of pre-HSC Type II at E11.5 (Figure 3.14). Of note, the phenotypic pre-HSC Type II population also contains functional LT-HSCs (Taoudi et al., 2008).

In embryo sections, 204GFP expression extended beyond the DA into the sub-aortic mesenchyme at E10.5 (cf. Figure 3.12). Here, the earliest mesenchymal GFP expression (VEC-Ter119-CD41-CD45-204GFP+) was observed from E8.5 and gradually increased from 1.2±0.7% to 12.6±2.3% at E11.5 (Figure, 3.14). We also analyzed more mature CD45+ hematopoietic and Ter119+ erythroid cells. Interestingly, Ter119 single-positive cells did not express 204GFP at any developmental stage analyzed, in line with the lack of erythroid expression in adult BM (Figure 3.15 and Figure 3.10). In contrast, 204GFP was expressed in 30-40% of more mature VEC+CD41-CD45+ hematopoietic cluster cells and VEC+Ter119+ cells at E8.5 and gradually decreased to nearly undetectable levels at E11.5 (Figure 3.15). The flow expression gates for different markers and their fluorescence-minus-one (FMOs) controls for each time point are provided in the appendix (Appendix 3.2 - 3.5).

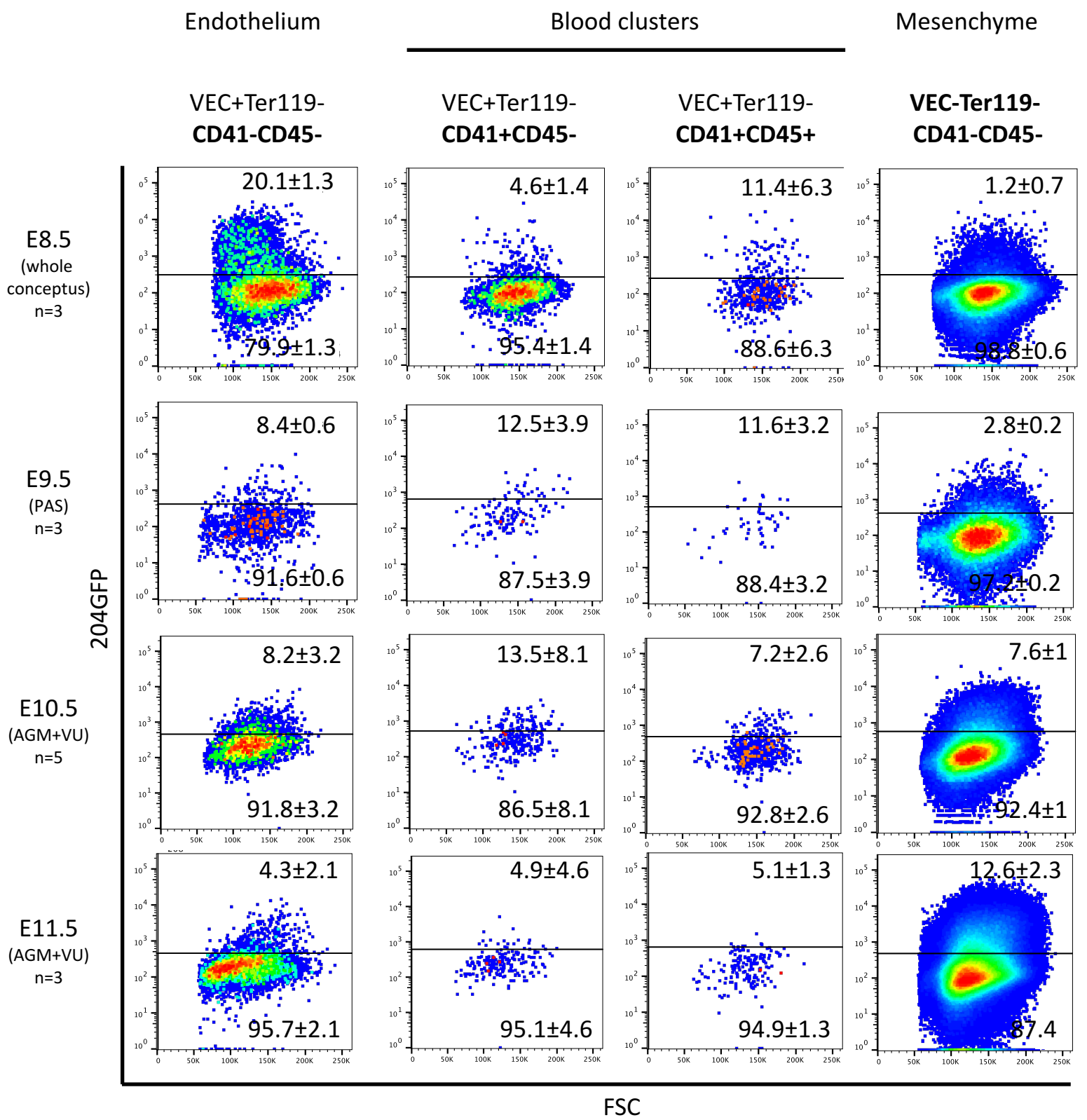


Figure 3.14 204GFP expression in the AGM region

Representative plots for 204GFP expression in endothelium (VEC^{+}Ter119^{-}CD41^{-}CD45^{-}), two types of blood clusters (VEC^{+}Ter119^{-}CD41^{+}CD45$^{-/+}$) and mesenchyme (VEC^{-}Ter119^{-}CD41^{-}CD45^{-}) from E8.5 to E11.5. Tissues analyzed are indicated. Percentages represent the average ± SD. Number of experimental replicates performed for each time point is given.

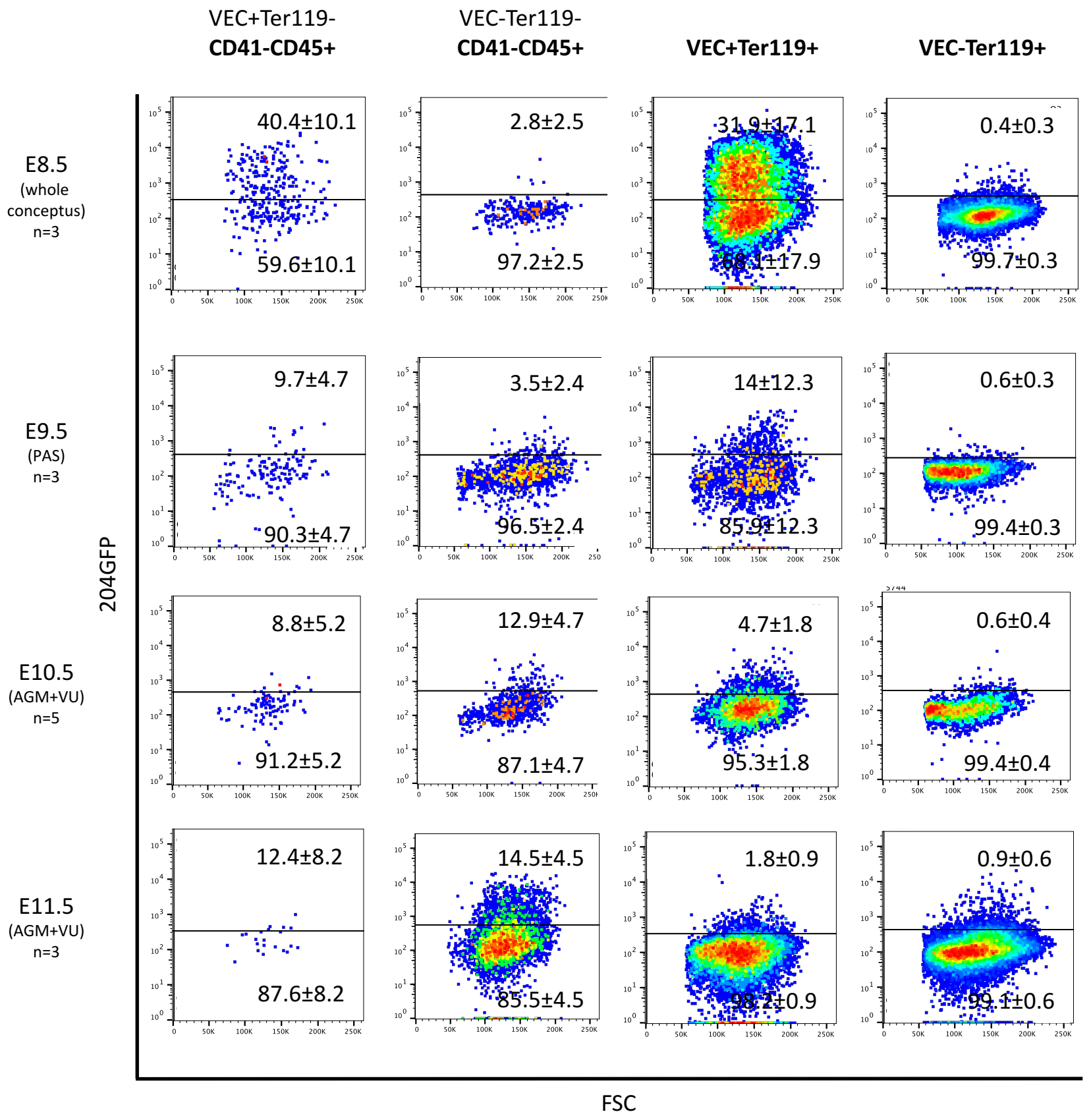


Figure 3.15 204GFP expression in more mature blood cell types
Representative plots for 204GFP expression in mature blood cluster cells ($VEC^{+}Ter119^{-}CD41^{-}CD45^{+}$) and two different stages of erythrocyte maturation ($VEC^{+/-}Ter119^{+}$) from E8.5 to E11.5. Tissues analyzed are indicated. Percentages represent the average ± SD. Number of experimental replicates performed for each time point is given.

Overall, flow cytometry analysis established that 204GFP was clearly expressed in all cellular intermediates involved in EHT, but that the fractions of 204GFP+ cells within each intermediate varied. The dynamic nature of the expression pattern suggests that this enhancer may be marking specific functional subsets or maturation stages of EHT (Figure 3.16). In addition to labeling a sub-population of the endothelium, which might include all or subsets of HE, the 204GFP transgene seems to label preferentially progenitors such as cluster cells, pre-HSC Type I and erythroid progenitors (VEC+Ter119+) rather than more differentiated cell types such as Ter119+ erythrocytes or phenotypic HSCs. This could suggest that the +204 enhancer is specifically active in the earlier stages of EHT.

3.6 The 204GFP transgene is marking a subset of the phenotypic hemogenic endothelium

To address whether the 204GFP transgene marks (part of) the phenotypic HE of the dorsal aorta, I assessed overlap between 204GFP and 1) endogenous *Runx1* expression and 2) expression of a *Runx1* +23 enhancer-reporter transgene. Both Runx1 and the Runx1 +23 enhancer are known to mark HE (Chen et al., 2009; North et al., 1999; Swiers et al., 2013). For analysis of co-expression of Runx1 and 204GFP, I stained whole E10.5 embryos with antibodies directed against Runx1, CD31, and GFP for confocal microscopy. Imaging analysis revealed that a small subset of the E10.5 *Runx1*+ HE co-expressed the 204GFP transgene

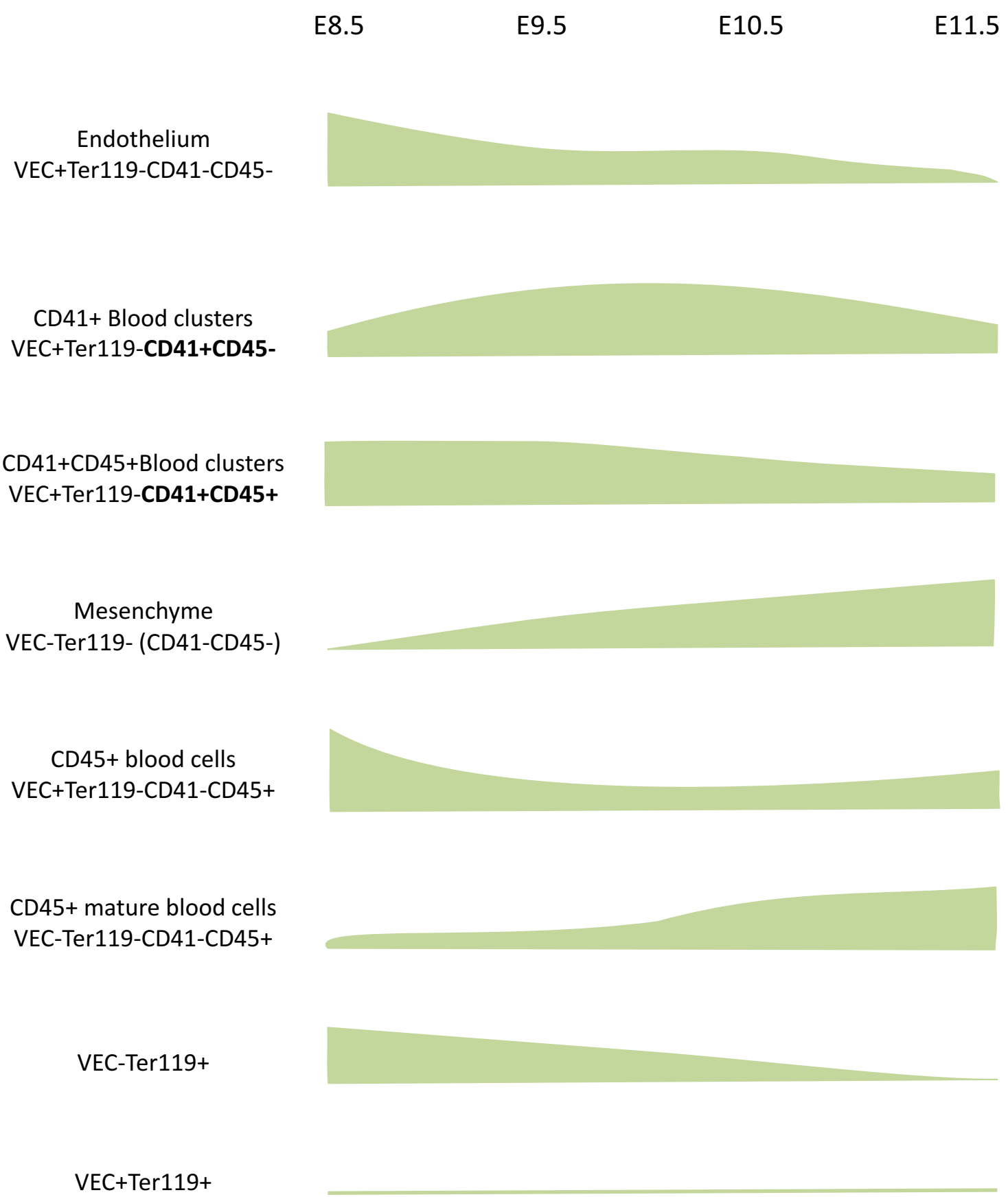


Figure 3.16 Summary of dynamic 204GFP expression through development
Schematic representation of the dynamics of 204GFP expression through development (E8.5 - E11.5) in different cellular subsets is shown. Dynamic expression is roughly based on percentages from Figure 3.14 and 3.15.

(arrowheads in Figure 3.17, see Appendix 3.6 for FMOs). In order to quantify these results, 3 wholemount embryos were analyzed and images processed with the IMARIS software. After identifying individual *Runx1*+ and 204GFP+ cells in separate channels, CD31+ cells located within the aortic lumen and co-expressing 204GFP and *Runx1* were quantified (see Figure 3.18 for the workflow). Quantifying Runx1/204GFP co-expression in this manner established that 6.3±5.5% of the *Runx1*+ HE also expressed 204GFP. Within the 204GFP+ endothelial population, 8.7±3.1% of cells co-expressed *Runx1*+ (Figure 3.19). These data indicate that the 204GFP transgene marks at least a subset of phenotypic HE in the midgestation dorsal aorta.

To assess overlap between the *Runx1* +204 and +23 enhancers, I used a Runx1 +23 *LacZ*-reporter line previously generated in the lab, which similar to the 23GFP was shown to mark blood stem and progenitor cells and a subset of the dorsal aorta endothelium, but not the sub-aortic mesenchyme (23LFLacZln7, A. Santos and M. de Bruijn, unpublished; here referred to as 23LacZ). The 23LacZ line was crossed with the 204GFP line, embryos were harvested at E8.5 and E10.5, and after fixation and cryosectioning, reporter gene expression was visualized in sections of the DA with anti-beta-galactosidase (23LacZ) and anti-GFP (204GFP) antibody staining. The two transgenes were co-expressed in a subset of the E8.5 endothelial cells of the paired aortae (identified as cells lining the lumen of the aortae; asterisks in Figure 3.20A), with approximately 1/3 of 23lacZ-marked cells co-expressing 204GFP. In the

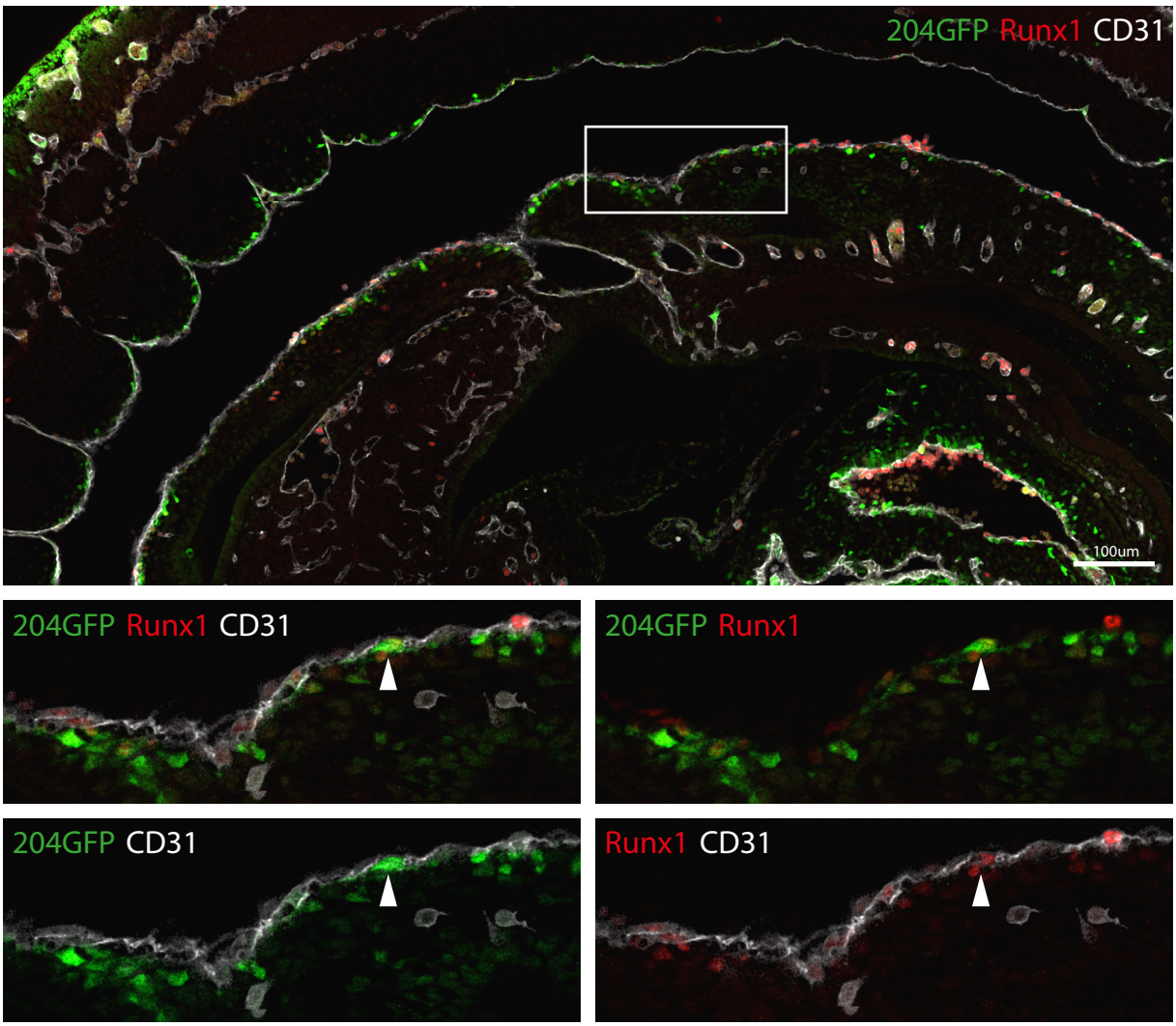


Figure 3.17 Co-expression analysis of 204GFP and Runx1 in E10.5 wholemount embryos
Top: A longitudinal optical slice through a E10.5 wholemount 204GFP transgenic embryo is shown. The dorsal aorta vasculature (CD31 - white) is shown with expressions of the 204GFP transgene (green) and Runx1 antibody (red). Zoomed in images of the dorsal aorta floor (white box) are shown in the bottom panels. 204GFP is co-expressed in a small subset of Runx1+ hemogenic endothelium (arrowheads). Images were taken on the Zeiss 780 upright confocal microscope with a 25X oil-immersion objective. The entire AGM projection was reconstructed from tiled images and 5um optical slices. Optical zooms were generated in the IMARIS software. Scale bars as shown.

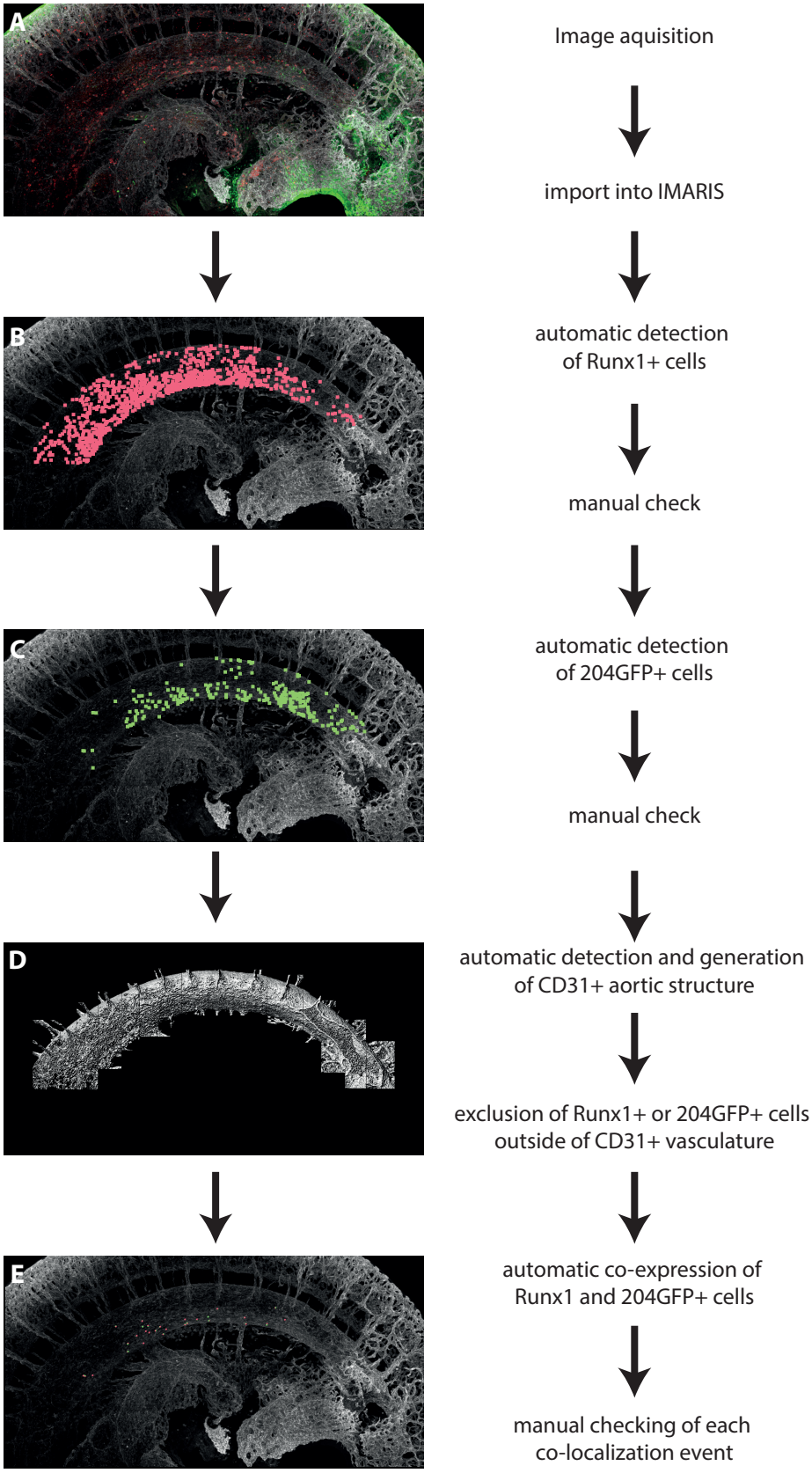


Figure 3.18 Co-expression analysis workflow of E10.5 wholemount embryos
A) Image acquisition on the upright Zeiss 780 confocal microscope and import to IMARIS software. **B)** Automatic detection and dot-labelling of Runx1+ cells in the red channel and detailed manual check. **C)** Automatic detection and dot-labelling of 204GFP+ cells in the green channel and detailed manual check. **D)** Automatic detection and generation of the CD31+ aortic structure (surface). All Runx1+ and 204GFP+ 'dots' outside the CD31+ surface were manually detected and deleted. **E)** Automatic detection of Runx1+ and 204GFP+ co-expressing 'dots' and manual check of each individual co-expression event with comparison to raw imaging data.

Embryo, sp	No. of colocalized /204GFP+ cells analyzed	% of colocalized cells out of 204GFP+	No. of colocalized/Runx1+ cells analyzed	% of colocalized cells out of Runx1+
Imm095-D, 33sp	30/245	12	30/1101	2.7
Imm095-E, 31sp	26/430	6	26/742	3.5
Imm095-F, 34sp	174/2137	8	174/1379	12.6
Average percentage and SD		**8.7±3.1**		**6.3±5.5**

Figure 3.19 Summary of Runx1 and 204GFP co-expression analysis in E10.5 wholemount embryos

Data of three individual embryos with corresponding somite pairs are shown. Individual numbers of cells that co-localised out of the total number of cells analysed are shown for both 204GFP and Runx1 channels. Percentages calculated and average percentages ± SD are given.

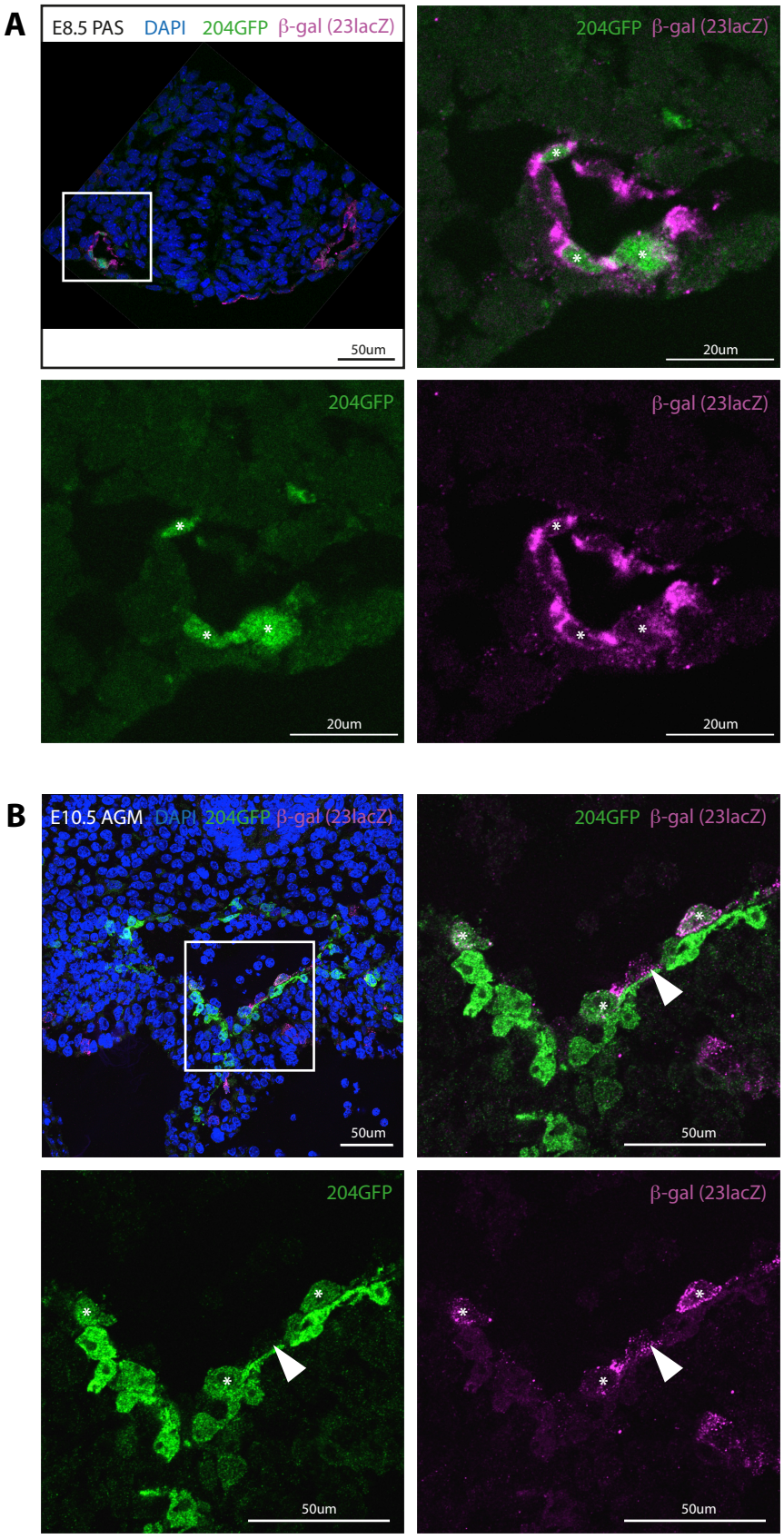


Figure 3.20 Co-expression analysis of 204GFP::23lacZ compound embryos
Transverse sections (10um thick) through a E8.5 PAS region (A) and a E10.5 AGM region (B) with zoomed images focusing on the aorta (white boxes). A subset of the endothelium co-expresses the (asterisks) 204GFP (green) and 23lacZ (magenta) transgenes. 23lacZ+204GFP- cells are also shown (arrowhead). Images were taken on the Zeiss 780 confocal microscope with a 40X and 63X oil-immersion objective.Scale bars as shown.

few sections and embryos (n=2) analyzed, no 204GFP+23lacZ- endothelial cells were observed. At E10.5 a small subset of endothelium co-expressed both reporter transgenes (asterisks in Figure, 3.20B). In addition, single-positive 23lacZ cells in the endothelial lining were present at E10.5 (arrow head in Figure 3.20B). It can therefore be inferred that based on phenotypic co-expression analysis, at least a subset of HE is marked by the novel 204GFP transgene. Thus, it will be interesting to test whether the 204GFP transgene marks (part of) functional HE (Chapter 4).

3.7 Summary

In this chapter I have described the generation of a new 204GFP mouse line to enable more detailed analysis of EHT. Detailed analysis of 3 out of 7 germline-transmitting 204GFP founder mouse lines as well as comparison to endogenous *Runx1* expression established a reproducible *Runx1*-specific expression pattern of the 204GFP transgene in embryonic and adult hematopoietic sites. Additional 204GFP expression in non-hematopoietic tissues was shown to be also largely *Runx1*-specific. Comparison of 204GFP transgenic and 204lacZ transient transgenic embryos showed reproducible and comparable expression patterns, although the novel 204GFP mouse line exhibited a broader expression pattern. A combination of imaging and flow cytometry analysis determined that the 204GFP transgene labels a small subset of the developing endothelium, and an even smaller sub-population of intra-aortic cluster cells. In addition, co-expression analysis with *Runx1* and 23lacZ showed

that the 204GFP transgene marks a subset of the phenotypic HE. In Chapter 4, in vitro and in vivo assays testing the various potential of cells marked by 204GFP will shed light on whether this novel *Runx1*-enhancer reporter mouse line is labeling functional aspects of EHT.

Chapter 4

Functional characterization of the 204GFP mouse line

In the previous chapter I have described the expression pattern of the 204GFP transgene within embryonic and adult hematopoietic tissues. In the AGM region, 204GFP labels subsets of the developing endothelium, rare intra-aortic cluster cells and sub-aortic mesenchyme. Here I set out to functionally test the AGM cells marked by the 204GFP transgene in a range of *in vitro* and *in vivo* assays for hemogenic, blood progenitor, LT-HSC and mesenchymal stem cell (MSC) potential.

4.1 The 204GFP+ endothelium has hemogenic potential

Since 204GFP expression was observed within a subset of the E10.5 Runx1+ HE, I speculated that the 204GFP transgene may mark a subset of the HE only. To test this, I assessed the hemogenic potential of 204GFP+ and 204GFP- endothelium in OP9 co-culture assays. The OP9 co-culture system is known to support the generation of blood and endothelium from HE (Swiers et al., 2013). Transgenic embryos were harvested at E10.5, the AGM region dissected and single cell suspension generated. Cells were gated for an endothelial phenotype (VEC+Ter119-CD41-CD45-) and sorted into the 204GFP+ and 204GFP- endothelial populations by flow cytometry (see Figure 4.1A,B for gating strategy and FMO controls). Sort purity was assessed on sorted WT endothelial cells and typically ranged between 96.5% and 100% (Figure 4.1C). Sorted cells were immediately plated onto an OP9 stromal layer and cultured in the presence of blood-promoting cytokines. Whole endothelium (from the WT littermate pool) and CD41+ blood progenitor cells (VEC+Ter119-CD41+

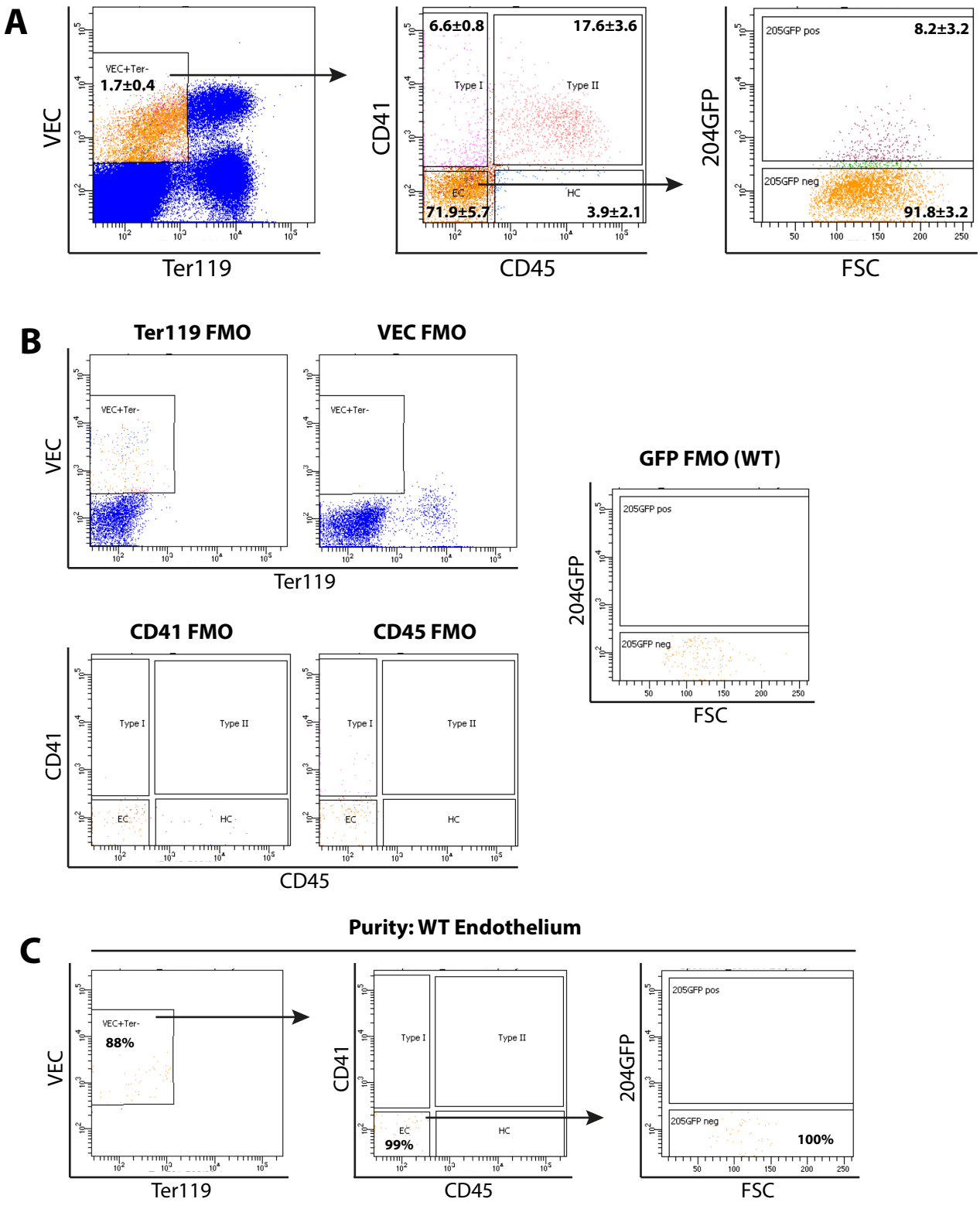


Figure 4.1 Gating strategy for E10.5 FACS
A) Representative plots for all E10.5 sorts (FACS088/OP9018 shown). The E10.5 AGM + VU was sorted (31-39sp). Endothelium was defined as VEC+Ter119-CD41-CD45- and the 204GFP+ and 204GFP- endothelial cells sorted for OP9 co-culture experiments. Average percentages ± SD are given (n=3). **B)** Representative plots of FMO controls for all five fluorochromes are given. **C)** Purities of WT endothelium were performed post sort.

CD45-) were plated as controls. A 'no cell control' (OP9-only) was also included in these cultures (not shown). 40-500 cells for each endothelial population was plated per well, and 40-100 cells were plated for the CD41+ control (see Appendix 4.1).

After 7-8 days of OP9 co-culture, only the 204GFP+ ECs, but not the 204GFP- ECs, was able to generate hematopoietic progeny (Figure 4.2A vs. C). In culture, blood cells appeared as round, bright, semi-adherent cells (compare to CD41+ progenitor control well, Figure 4.2G). They are not to be confused with the adipocytes seen in all bright field images (Figure 4.2A,C,E,G). Such adipocytes are the result of spontaneous OP9 stromal cell differentiation with the characteristic appearance of a 'foamy' large cytoplasm. Supernatant, containing the semi-adherent cells, was collected for flow cytometric analysis. Staining for CD45 determined that virtually all semi-adherent round cells in the 204GFP+ EC cultures were hematopoietic (Figure 4.3A). I also analyzed those cells for blood lineage markers and showed that the CD45+ cells contain subsets of myeloid Mac1+ cells (Figure 4.3B) and a small percentage of erythroid Ter119+ (Figure 4.3C) and B/T-lymphoid B220+/CD3+ cells (Figure 4.3D). Of note, no visible bright semi-adherent cells were detected in the E10.5 whole endothelium (Figure 4.2). It is likely that the frequency of HE cells within the whole endothelium is very low and therefore very difficult to detect them within the entire endothelial population in these functional assays.

Next, I assessed the hemogenic potential of E8.5 204GFP endothelium, following the same sorting strategy as for the E10.5 AGM endothelium. Here the entire E8.5 conceptus was used, with the exception of the

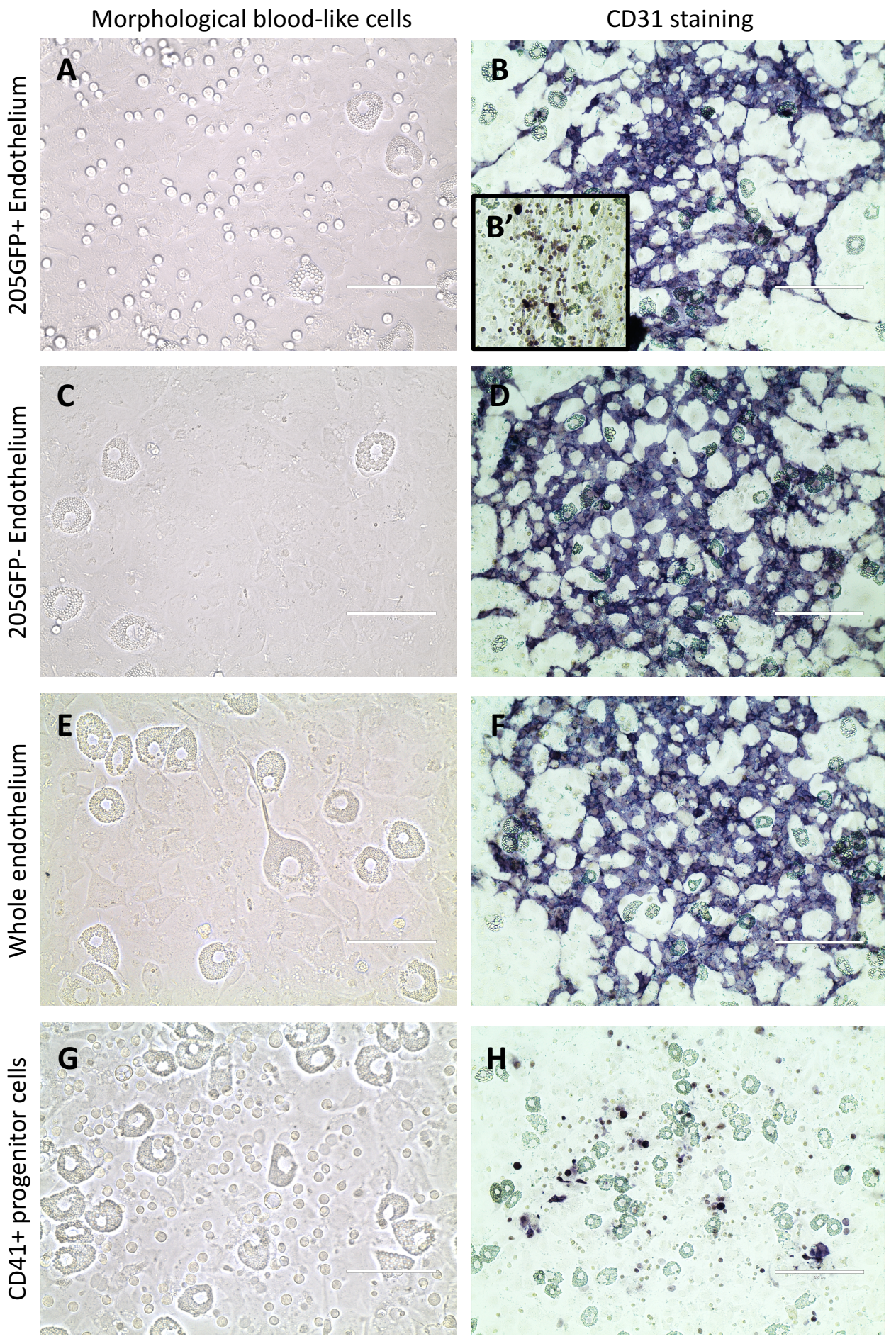


Figure 4.2 Blood and endothelial output from the E10.5 OP9 co-cultures
Representative images of hematopoietic and endothelial output of E10.5 endothelial subsets after OP9 co-cultures (n=4). **A,C,E,G)** Blood like cells generated in OP9 co-cultures from 204GFP+ endothelium and from CD41+ control cells (**A,G**). Blood cells are bright, round and semi-adherent to the stromal layer. The stomal layer often contains cells that have differentiated into adipocytes and show a characteristic 'foamy' morphology (**C,E**). **B,D,F,H)** CD31+ staining (blue) of endothelial networks generated in OP9 co-cultures from sorted endothelial cells (**B,D,F**). CD31 also stains a subset of hematopoeitic cells in these cultures (**B'** and **H**). Images were taken on EVOS XL Core imaging system with 20X and 40X objectives. Scale bars at 100um (left panels) and 200um (right panels).

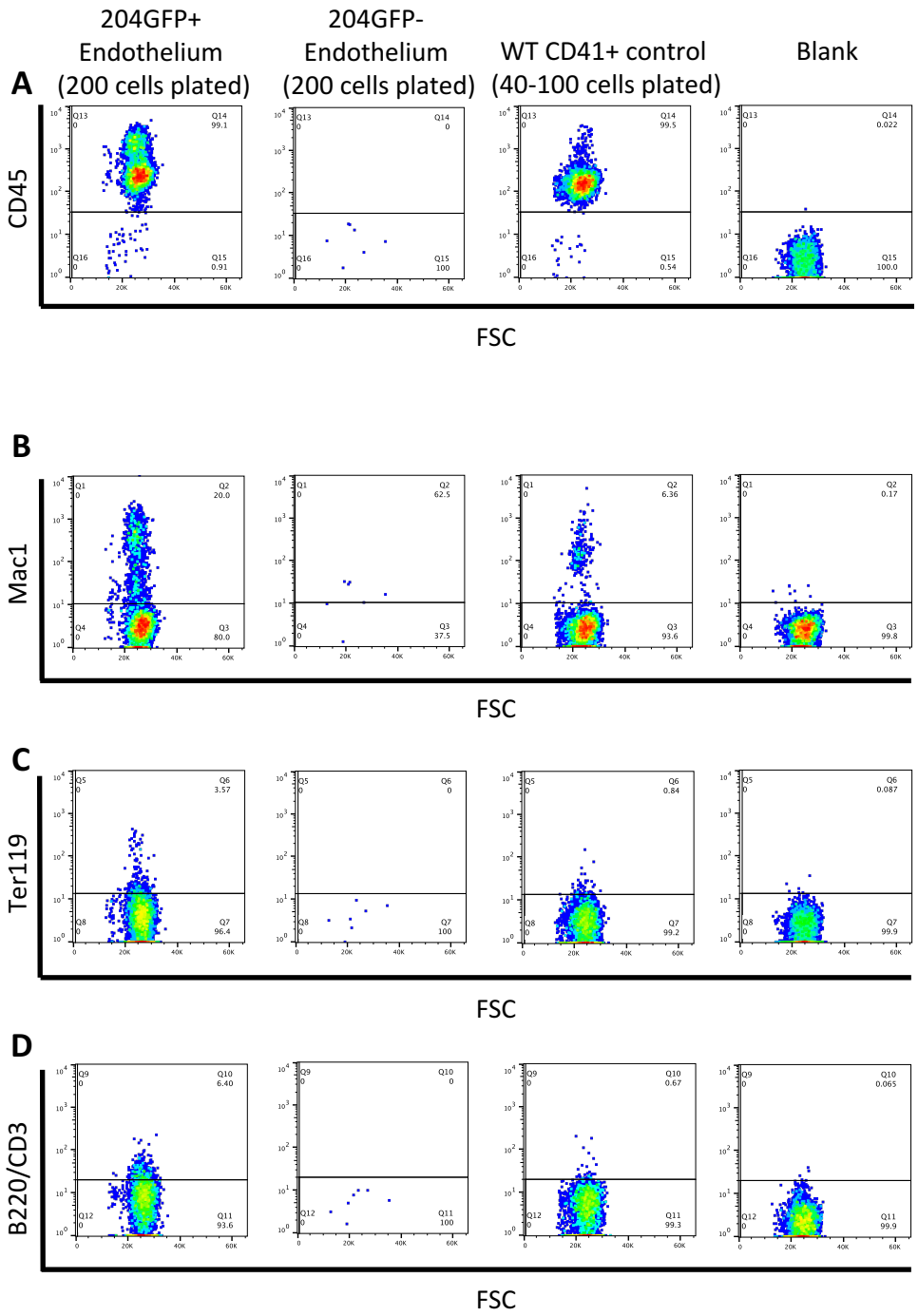


Figure 4.3 Semi-adherent cells from E10.5 OP9 co-cultures are multi-lineage hematopoietic cells

A) CD45 cell surface expression of cells collected in the supernatant of E10.5 OP9 co-culture experiments. The 204GFP+ endothelium and the CD41+ assay control generated CD45+ mature blood cells (n=3). Blank control is the unstained population collected from CD41+ assay control well. **B-D)** Hematopoietic cells were also analyzed for myeloid (Mac1), erythroid (Ter119) and B-lymphoid (B220/CD3) expression (n=1).

ectoplacental cone or a part of the head, which was used for genotyping. Endothelium was sorted into 204GFP+ and 204GFP- populations (see Figure 4.4 for gating, controls and purities). Sorted WT endothelium and CD41+ blood progenitor cells were included as assay controls. Between 500 and 3000 cells were plated for each endothelial population (Appendix 4.2). In these cultures, however, neither the 204GFP endothelial fractions nor the WT endothelial control generated blood progeny (Figure 4.5A,C,E), and also the control CD41+ hematopoietic progenitors produced limited offspring with a blood-like morphology (Figure 4.5G). Our lab has found the E8.5 OP9 co-cultures less robust than cultures from later developmental time points, which might explain the lack or reduced efficiency of blood generated in the present cultures. Additional experiments, including co-cultures on new OP9 cells, would need to be done to formally confirm HE potential among E8.5 204GFP+ endothelium.

Swiers *et al* previously established that with the increasingly more hematopoietic signature of the E10.5 HE, the potential of HE to form endothelial networks in culture decreases (Swiers et al., 2013). I therefore also tested endothelial network-forming ability in the E8.5 and E10.5 OP9 co-cultures by fixing the remaining adherent cell layers and staining them for the endothelial marker CD31. Endothelial networks varied in sizes from a cluster of endothelial cells to entire large interconnecting networks. Both types were counted as one network each if a clear colony boundary was observed. If two colonies looked like they had merged, it was still considered one network. Sporadic single ECs were also observed and

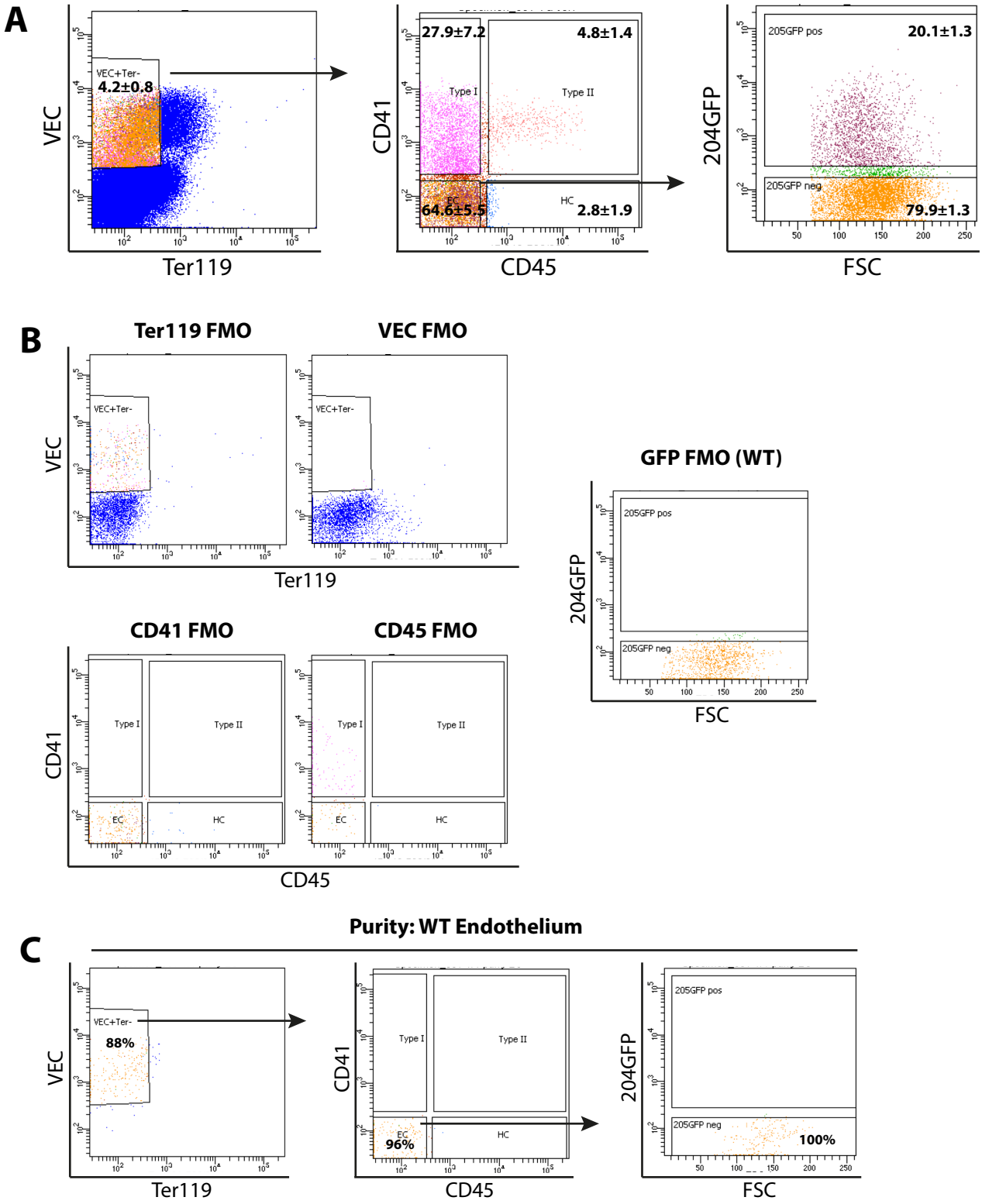


Figure 4.4 Gating strategy for E8.5 FACS

A) Representative plots for all E8.5 sorts (FACS089/OP9019 shown). The whole E8.5 conceptus was sorted (3-13sp). Endothelium was defined as VEC+Ter119-CD41-CD45- and the 204GFP+ and 204GFP- endothelial cells sorted for OP9 co-culture experiments. Average percentages ± SD are given (n=3). **B)** Representative plots of FMO controls for all five fluorochromes are given. **C)** Purities of WT endothelium were performed post sort.

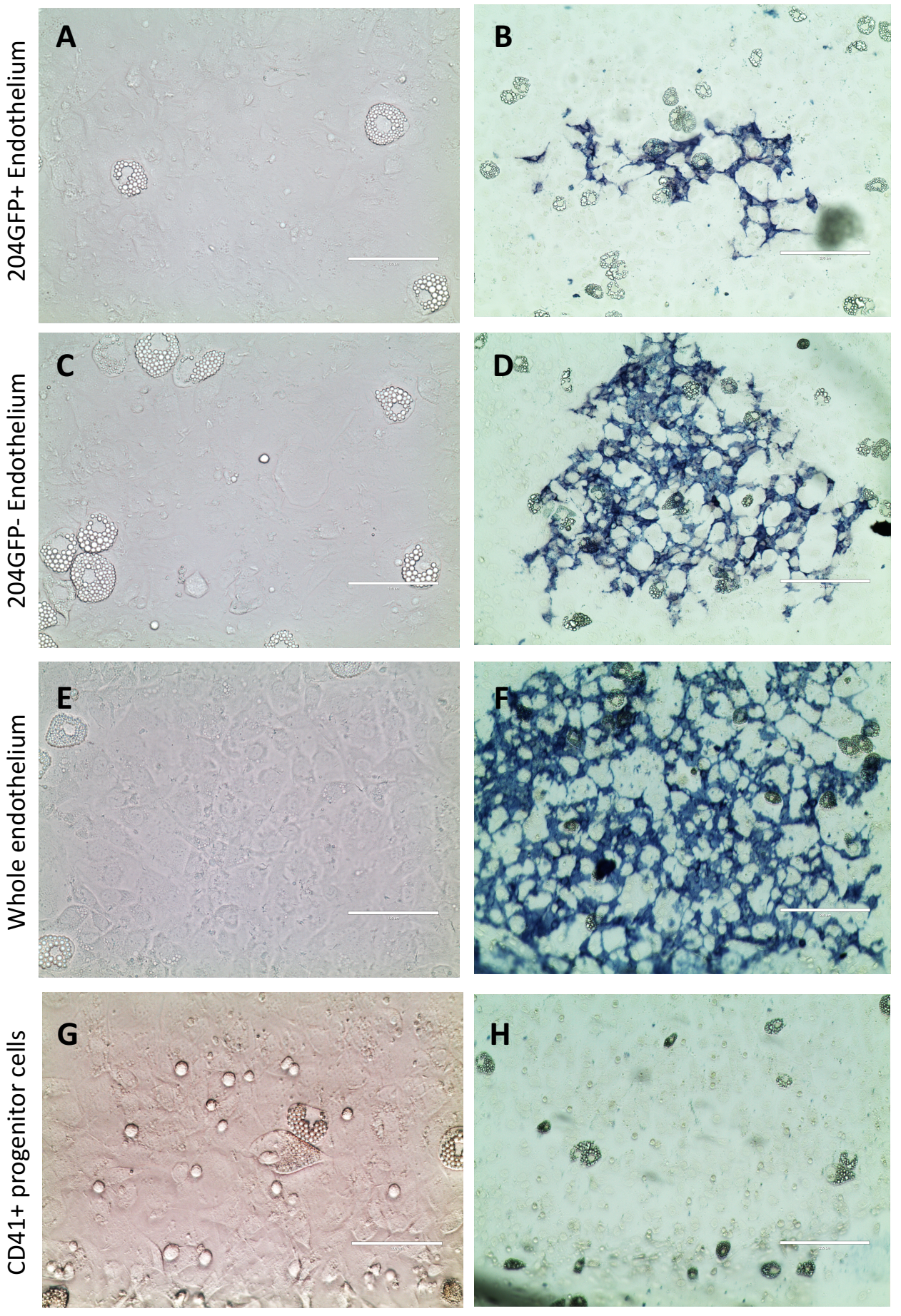
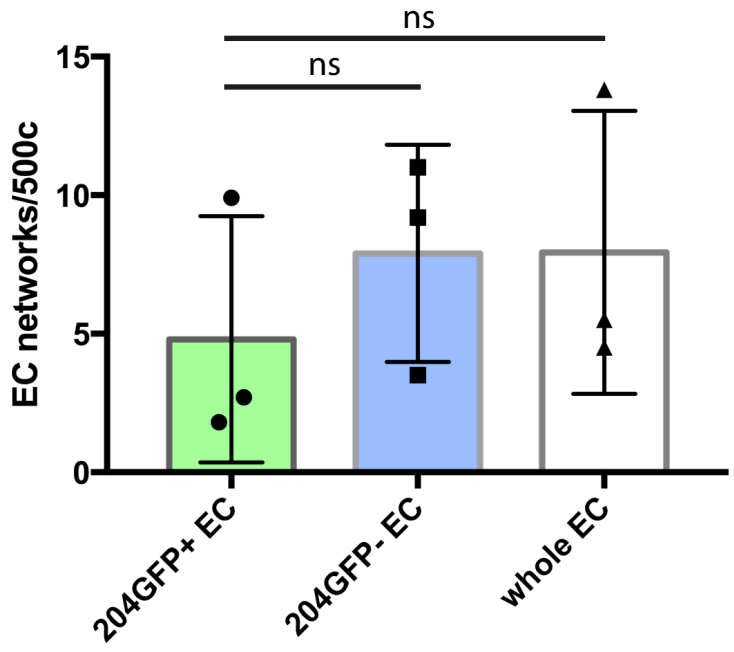


Figure 4.5 Blood and endothelial output from the E8.5 OP9 co-cultures
Representative images of hematopoietic and endothelial output of E8.5 endothelial subsets after OP9 co-cultures (n=3). **A,C,E,G)** Blood like cells generated in OP9 co-cultures from the CD41+ control cells (**G**) only; no blood was generated from either endothelial subsets or whole endothelium (**A,C,F**). Blood cells are bright, round and semi-adherent to the stromal layer. The stomal layer often contains cells that have differentiated into adipocytes and show a characteristic 'foamy' morphology (**A & C**). **B,D,F,H)** CD31+ staining (blue) of endothelial networks generated in OP9 co-cultures from sorted endothelial cells (**B,D,F**). Images were taken on EVOS XL Core imaging system with 20X and 40X objectives. Scale bars at 100um (left panels) and 200um (right panels).

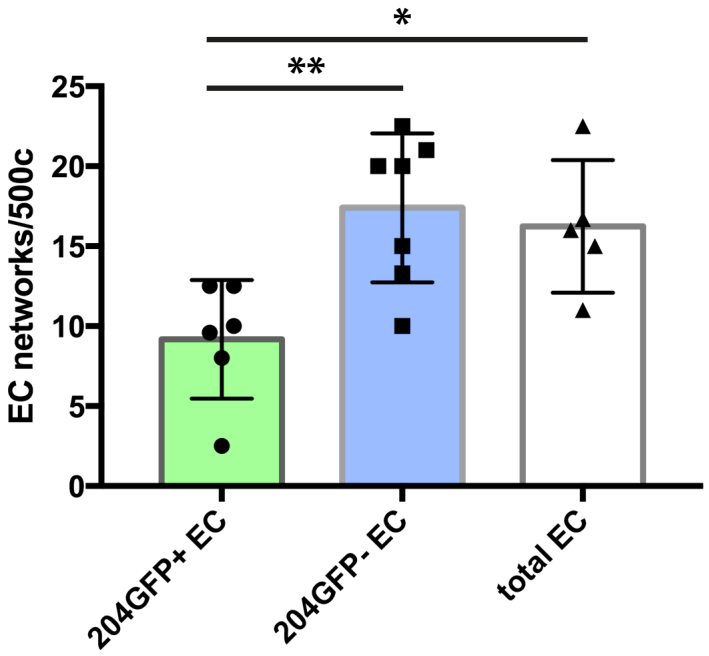
counted but not included in the EC network analysis. At E8.5, both 204GFP+ and 204 GFP- ECs generated endothelial networks in culture (Figure 4.5B,D,F), with a comparable frequency (Figure 4.6): 4.8±2.6 versus 7.9±2.3 per 500 204GFP+ and 204GFP- cells plated, respectively. The WT EC population gave rise to 7.9±2.9 endothelial colonies per 500 cells plated. In contrast, at E10.5 the number of EC networks formed per 500 cells plated was significantly lower in the 204GFP+ EC population (9.2±1.5) compared to either 204GFP- EC (17.4±1.8) or whole EC (16.2±1.9) populations (Figure 4.7 and Figure 4.2B,D,F), in line with the hemogenic nature of the E10.5 204GFP+ endothelium. Of note, CD31 expression is not restricted to endothelial cells, but is also expressed by early blood progenitors. Accordingly, the round, bright semi-adherent cells that remained attached to the 204GFP+ endothelium, and the remaining semi-adherent cells in the CD41+ control wells were also stained with CD31 (Figure 4.2B' and H, respectively).

In summary, I have shown that the novel Runx1 +204 enhancer mediates reporter gene expression to all functional HE at E10.5 (the specified HE, Chapter 1.10). I was unable to establish if it is similarly marking the competent HE at E8.5 due to a lack of blood progeny development in those cultures, including in the controls. The overall frequency of competent HE cells might be a lot lower at the earlier time point and more cells need to be plated to reach a conclusive result. However, the whole endothelium control was not able to generate hematopoietic progeny either, in contrast to previous reports (Swiers et al., 2013). It is possible



Embryo stage	Experiment no.	population	Cells plated	No. of EC networks	EC networks/ 500 cells
E8.5 5-13sp	OP90019	204GFP+ EC	863	17	9.8
		204GFP- EC	1200	22	9.2
		Whole EC	1200	33	13.8
E8.5 6-12sp	OP90020	204GFP+ EC	569	2	1.8
		204GFP- EC	2000	14	3.5
		Whole EC	2000	22	5.5
E8.5 3-13sp	OP90021	204GFP+ EC	2941	16	2.7
		204GFP- EC	500	11	11.0
		Whole EC	2000	18	4.5

Figure 4.6 Analysis of endothelial network formation in E8.5 OP9 co-cultures
Graph representation of the number of endothelial networks generated in OP9 co-culture assays from 500 endothelial cells plated. Average bars ± SD for 204GFP+ (green), 204GFP- (blue) and whole (white) endothelium are shown. Individual network counts from separate wells/experiments are shown as dots, squares and triangles, respectively (n=3). Table represents raw counts from 3 independent experiments with the somite pairs of embryos, the number of endothelial cells per subset plated and the number of networks counted after co-culture. ns - not significant (Welch's t test).



Embryo stage	Experiment no.	population	Cells plated	No. of EC networks	EC networks/ 500 cells
E10.5 31-34sp	OP90018	204GFP+ EC	200	5	12.5
		204GFP- EC	200	9	22.5
		204GFP- EC	500	20	20.0
		Whole EC	200	9	22.5
E10.5 32-39sp	OP90022	204GFP+ EC	200	1	2.5
		204GFP+ EC	209	4	9.6
		204GFP- EC	200	8	20.0
		204GFP- EC	300	8	13.3
		Whole EC	200	6	15.0
		Whole EC	300	10	16.7
E10.5 31-36sp	OP90024	204GFP+ EC	100	2	10.0
		204GFP+ EC	200	5	12.5
		204GFP+ EC	500	8	8.0
		204GFP- EC	100	3	15.0
		204GFP- EC	200	4	10.0
		204GFP- EC	500	21	21.0
		Whole EC	500	16	16.0
		Whole EC	1000	22	11.0

Figure 4.7 Analysis of endothelial network formation in E10.5 OP9 co-cultures
Graph representation of the number of endothelial networks generated in OP9 co-culture assays from 500 endothelial cells plated. Average bars ± SD for 204GFP+ (green), 204GFP- (blue) and whole (white) endothelium are shown. Individual network counts from separate wells are shown as dots, squares and triangles, respectively (n=3). Table represents raw counts from 3 independent experiments with the somite pairs of embryos, the number of endothelial cells per subset plated and the number of networks counted after co-culture. *P < 0.05; **P < 0.005 (Welch's t test).

that the supportive potential of the OP9 cells used here decreased over time, which is a common issue with OP9 cells. Reverting to an early passage of OP9 cells may be required for the E8.5 cultures.

4.2 The 204GFP transgene does not label clonogenic blood progenitor cells

Previously, it was shown that at E10.5 intra-aortic cluster cells contain primarily blood progenitors, HSC precursors and from E11.5 rare HSCs which soon after seed the fetal liver and expand the HSC pool (Rybtsov, 2016). Here, I aimed to assess if the rare 204GFP+ cells observed in the intra-aortic clusters represent clonogenic blood progenitors. For this, E10.5 AGMs of 204GFP transgenic embryos were sorted into 204GFP+ and 204GFP- subsets, which comprised 3.4±1.9% and 89.4±4.1% of the gates, respectively (Figure 4.8A). Both populations were then plated in methylcellulose cultures (Appendix 4.3B). As the YS contains most of the clonogenic blood progenitors in the embryo, I also analyzed E8.5 concepti which were sorted for 204GFP+ and 204GFP- populations at 3.4±0.9% and 87.5±5.6%, respectively (Figure 4.8A). Hematopoietic colonies generated by these progenitors (CFU-C) were counted at day 7 of culture. At both time points, CFU-C were found in both, the 204GFP+ and 204GFP- populations, as shown in Figure 4.8B. However, due to the low percentage of 204GFP+ cells within the AGM and conceptus (Appendix 4.3), the large majority, if not all, of CFU-C within the E8.5 conceptus and E10.5 AGM were 204GFP- (Figure 4.8C,D). In the 204GFP+ subset not all

A

	204GFP+	204GFP-
E8.5	3.4±0.9%	87.5±5.6%
E10.5	3.4±1.9%	89.4±4.1%

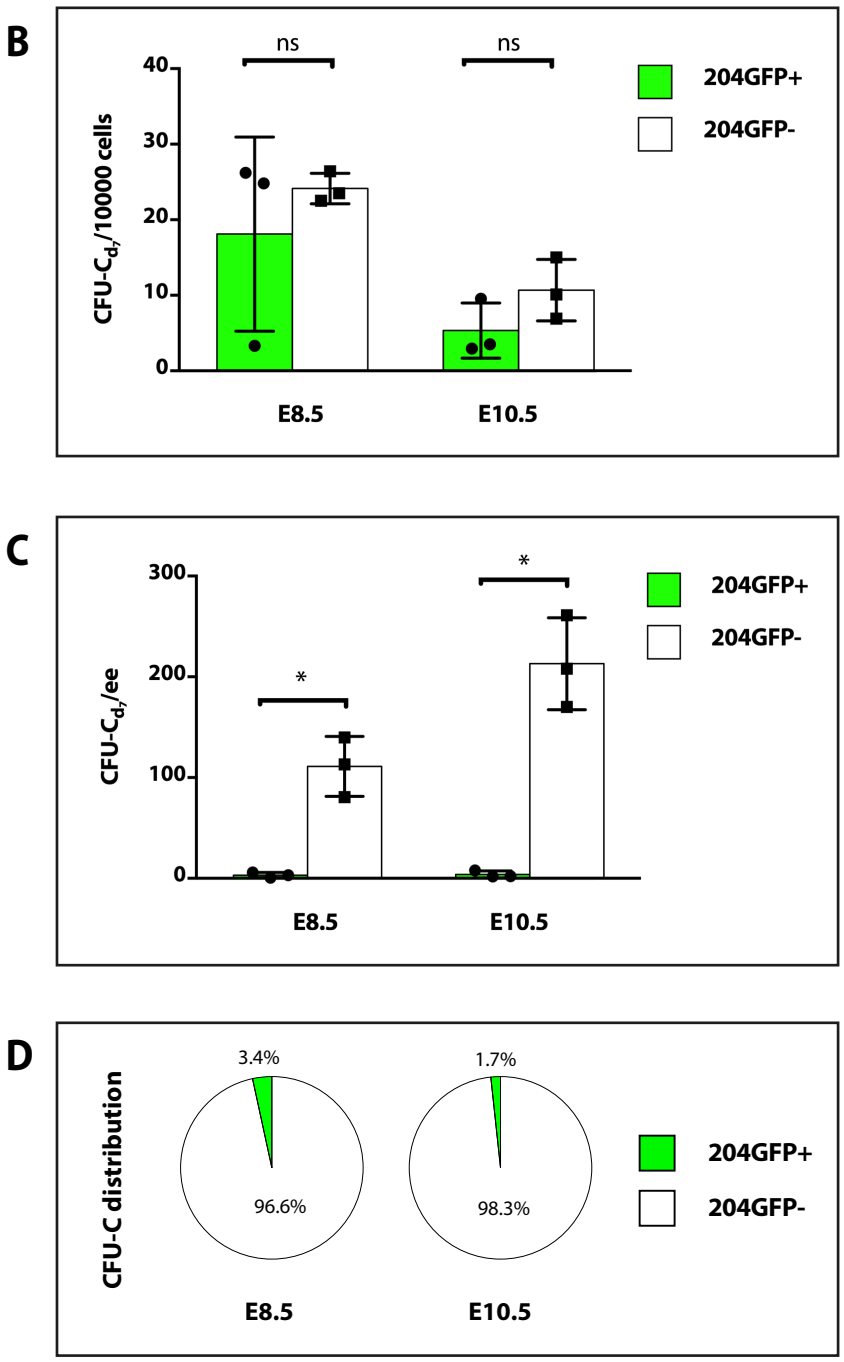


Figure 4.8 Blood progenitor potential of 204GFP+/- subsets
A) Average percentage ± SD of 204GFP+ and 204GFP- cell sorted for CFU-C experiments (n=3). **B-)** The 204GFP+ (green) and 204GFP- (white) fractions of whole E8.5 concepti and E10.5 AGM+VUs were tested for blood progenitor potential. Colonies were counted on day 7 of culture. Graphs depict CFU-C colonies counted per 10000 cells plated (**B**) and CFU-C colonies counted per ee (**C**). CFU-C distribution between 204GFP+ (green) and 204GFP- (white) fractions is shown (**D**). ns - not significant; *P < 0.05 (Welch's t test).

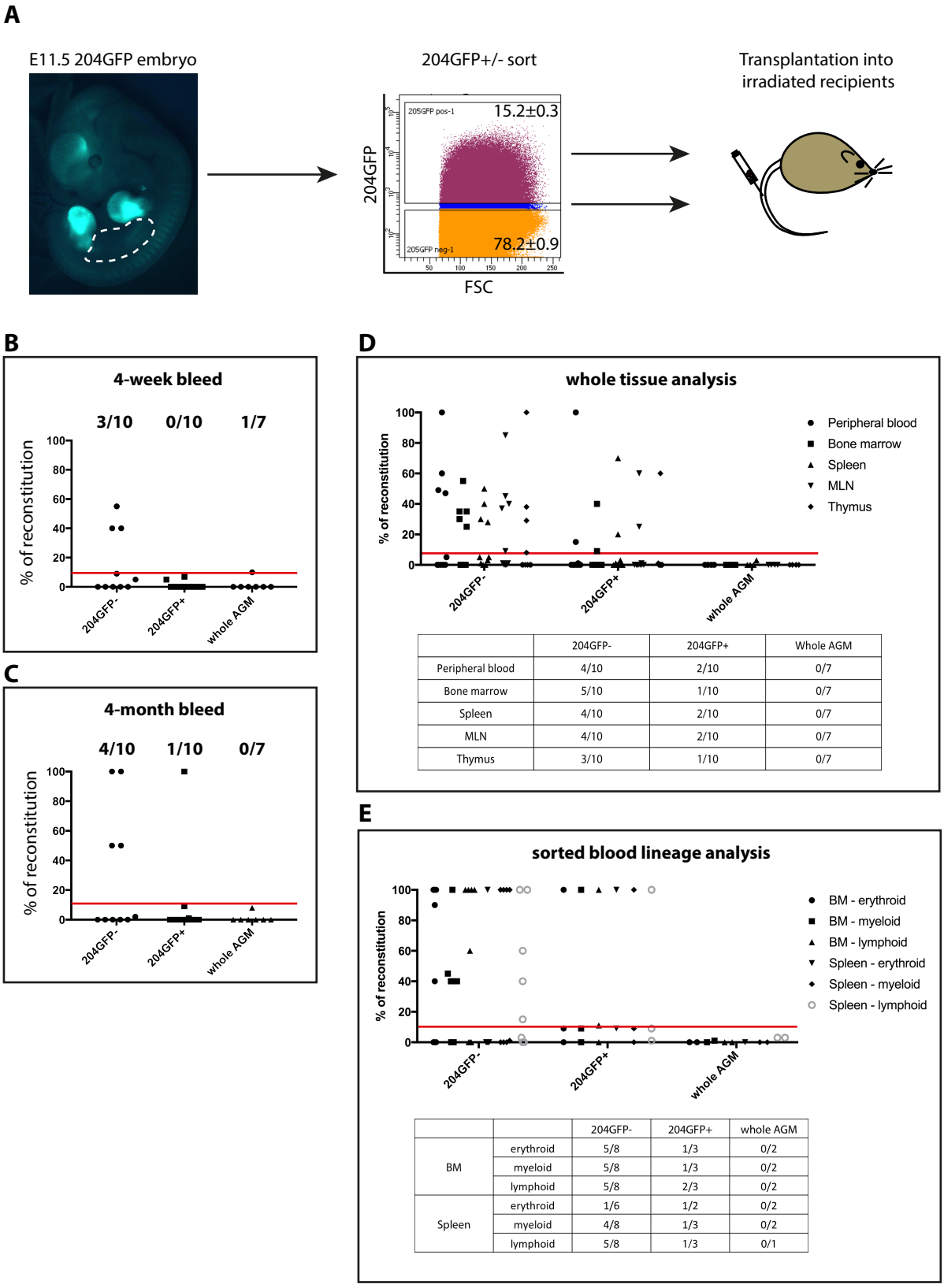
progenitor types were present, though given the small number of CFU-Cs counted, this could be random (Appendix 4.4). Purity checks were performed after each sort, which ranged between 96%-100% purity for the 204GFP- gate. The purities for the 204GFP+ gate averaged 87% but included 2 outliers at 50% and 63% (FACS027 and FACS021, respectively; Appendix 4.3). In those two sorts, the number of CFU-C/10000cells and subsequently the number of CFU-C/ee increased somewhat. This may have resulted in the calculation of a seemingly larger percentage distribution of hematopoietic progenitors within the 204GFP+ fraction. It is therefore likely that the few CFU-Cs generated in the 204GFP+ population are in fact due to contamination with 204GFP- cells. In summary, the 204GFP transgene marks no or very few clonogenic blood progenitors, which is in line with my previous observations that only very rare intra-aortic cluster cells are labeled with the 204GFP transgene.

4.3 Both 204GFP+ and 204GFP- populations harbor LT-HSCs

I previously observed 204GFP expression in the phenotypic pre-HSC/HSC populations (Fig. 3.14) and therefore set out to test whether the 204GFP transgene labels functional long-term HSCs in transplantation assays. AGM+VUs from E11.5 204GFP transgenic embryos were dissected, single cell suspensions made and cells sorted into 204GFP+ and 204GFP- cell populations. These populations were injected at a dose of 1ee per recipient into sub-lethally irradiated mice, together with carrier spleen cells to support recipients for the first few weeks after transplantation (Figure

4.9A). Mice injected with 1ee of unsorted AGM cells or only spleen cells served as positive and negative controls, respectively. Peripheral blood was analyzed at 4 weeks and 4 months post transplantation, by genomic PCR for donor-derived *Gfp.* The percentage of reconstitution was established by comparison to a dilution series with known donor (*Gfp*) to WT ratios, using ImageLab software. A threshold for reconstitution of 10% was applied. Interestingly, at 4 weeks post-transplantation only the 204GFP- population resulted in high-level donor-derived reconstitution in peripheral blood, with 3 out of 10 recipients showing 40-55% donor-derived cells (Figure 4.9B). Out of 10 mice injected with the 204GFP+ cells, not one reconstituted at or above the 10% threshold. At 4 months post transplantation, the number of mice showing engraftment with 204GFP- cells rose to 4. However, at this later time point 1 out of 10 recipients showed 100% engraftment of the 204GFP+ cells (Figure 4.9C and Appendix 4.5 and 4.6).

Shortly after the 4-month bleeds, recipient mice were sacrificed and their peripheral blood, bone marrow (BM), spleen, mesenteric lymph nodes (MLN) and the thymus analyzed for donor-derived multilineage hematopoietic reconstitution. This analysis revealed that 204GFP- cells successfully engrafted the BM of 5/10 transplanted mice (Figure 4.9D and Appendix 4.7A,B). In addition, I analyzed specific blood lineages in BM and spleen of successfully reconstituted mice. BM cells were sorted into erythroid, myeloid and lymphoid lineages based on differential CD31/Ly6C expression (cf. Figure 3.10A,B), while spleen cells were sorted for CD19 (B-lymphoid), CD19-Mac1+Ter119- (myeloid) and CD19-Mac1-Ter119+



	204GFP-	204GFP+	Whole AGM
Peripheral blood	4/10	2/10	0/7
Bone marrow	5/10	1/10	0/7
Spleen	4/10	2/10	0/7
MLN	4/10	2/10	0/7
Thymus	3/10	1/10	0/7

		204GFP-	204GFP+	whole AGM
BM	erythroid	5/8	1/3	0/2
	myeloid	5/8	1/3	0/2
	lymphoid	5/8	2/3	0/2
Spleen	erythroid	1/6	1/2	0/2
	myeloid	4/8	1/3	0/2
	lymphoid	5/8	1/3	0/1

Figure 4.9 Long-term HSC potential of 204GFP+/- subsets

A) Schematic of the experimental set up to test the LT-HSC potential of 204GFP+ and 204GFP- populations. AGM+VUs from E11.5 204GFP transgenic embryos were sorted for 204GFP+/- (percentage ± SD, n=3) and 1ee transplanted into irradiated recipients. **B)** Percentage of reconstitution in blood samples at 4 weeks post-transplantation. The total number of reconstituted mice out of total transplanted is shown for each population. **C)** Percentage of reconstitution in blood samples at 4 months post-transplantation. The total number of reconstituted mice out of total transplanted shown for each population. (continued)

Figure 4.9 (continued)
D) Percentage of reconstitution in different tissues at 4 months post-transplantation. Table view summary of the total number of reconstituted mice out of total transplanted in individual tissues is shown. **E)** Percentage of reconstitution in sorted erythroid, myeloid and lymphoid cells from BM and spleens of recipient mice analysed. Table view summary of the total number of reconstituted mice out of the number of recipient mice analysed in detail. Not all mice were analysed - only tissues of recipients that showed reconstitution at 4 months were sorted and analysed. In parallel, tissues of 1-2 non-reconstituted mice per experiment were also sorted and served as controls. The overall reconstitution threshold was set at 10% (red line).

(erythroid) populations. At least 10.000 cells were sorted for each population and the DNA extracted to assess donor-derived *Gfp* contribution by PCR. Analysis of BM from 204GFP- transplants confirmed that 5 mice showed reconstitution in all 3 blood lineages. While within the spleen, the percentage of engraftment was more varied between blood lineages (Figure 4.9E and Appendix 4.8).

At the time of the final analysis, 2/10 mice transplanted with 204GFP+ cells showed donor-derived engraftment of peripheral blood, spleen and MLN above 10%. In fact, one of the recipient mice showed 100% reconstitution in all 3 blood lineages of BM and spleen cells. The second 204GFP+ recipient however, although engrafting to around 20% in the peripheral blood, spleen and MLN, only showed sub-threshold reconstitution in erythroid and myeloid lineages of the BM and spleen. In addition, the lymphoid lineages in the BM and spleen showed just-above (11%) and just-below (9%) threshold reconstitution, respectively (Figure 4.9E and Appendix 4.8). Mice transplanted with 1 ee of separated AGM cells showed only short-term, low level reconstitution (1/7 at 4-weeks bleed) but not long-term multilineage reconstitution. This was unexpected, and likely to be due to a technical issue, for example that a higher number of dead cells were transplanted than in the experimental populations, since the AGM control sample was not sorted for Hoechst- live cells prior to transplants. It would be reasonable to speculate that the overall conditions of these experiments were sub-optimal for full reconstitution of the AGM control population, leading to the question whether the data for the test populations (204GFP+/-) are an underestimation of true LT-HSC potential.

Future experiments will need to include a sorted AGM control population, to exclude any data variation due to technical differences.

To conclude, while LT-HSC potential was present in both 204GFP+ and 204GFP- populations of the E11.5 AGM, engraftment appeared more robust after transplantation of 204GFP- cells. Although there did not seem to be an obvious lineage bias in 204GFP- or 204GFP+ HSCs, more transplants would need to be performed to assess this.

4.4 Sub-aortic 204GFP+ AGM cells form cartilage in culture

In Chapter 3 I documented that the 204GFP transgene is not only expressed in aortic endothelium and rare hematopoietic cluster cells, but also in part of the sub-aortic mesenchyme. Thus, in order to fully characterize the 204GFP mouse line, I aimed to identify whether the sub-aortic 204GFP+ cells could harbor mesenchymal stem cells (MSCs), in addition to the smooth muscle cells that were identified (cf. Figure 3.10D,E) The E11.5 AGM was previously shown to contain multi-lineage MSCs able to generate chondrocytes, osteocytes and adipocytes in culture, similar to MSCs in the adult bone marrow (Mendes et al., 2005). Therefore, E11.5 AGM+VUs from 204GFP transgenic embryos were dissected and mesenchymal cells (VEC-Ter119-CD41-CD45-, see Figure 3.10 for gating strategy) sorted into 204GFP+ and 204GFP- populations. Both populations were then assayed for their potential to form cartilage in chondrogenic differentiation assays. Cells were immediately plated into ultra-low adhesive 96-well-plates in chondrogenic differentiation media and

allowed to form chondrogenic foci over two weeks of culture. WT total mesenchymal cells and unsorted AGM cells served as positive controls. Negative controls were YS or FL cells, previously shown not to contain MSCs (Mendes et al., 2005). Strikingly, only the 204GFP+ mesenchyme aggregated into clusters of cells, and did so within the first few days of culture (Figure 4.10 d0, d1, d4). No cell clusters were formed in cultures of 204GFP- mesenchymal cells. At 2 weeks of culture the clusters of cells developed into large aggregates in the 204GFP+ and the WT mesenchyme and whole AGM controls. Of note, as little as 65.000 204GFP+ mesenchymal cells were sufficient to form these aggregates. In comparison, the positive control wells formed aggregates slower and required large numbers of cells (240.000 cells) to form compact foci. Lower cell numbers (120.000 cells) in the positive controls resulted in small, fragmented foci (Figure 4.10 d14). In order to assess whether the aggregates that formed during these cultures were truly chondrogenic, I harvested, sectioned and stained them with commonly-used markers for chondrogenic tissues. Toluidine Blue stains proteoglycans in cartilage tissues (Geyer and Linss, 1978) and antibody labeling of collagens is commonly used to identify cartilage foci. In cross sections of such foci, collagen type I and II exhibit juxtaposing expression patterns: while collagen type I is mainly present the outer layers of the foci, collagen type II is present more uniformly throughout (Craft et al., 2015; Nakayama et al., 2003). Finally, the Runx transcription factor family plays an important role in cartilage development, with Runx2 and Runx1 marking different aspects of cartilage development (Liakhovitskaia et al., 2010; Wang et al.,

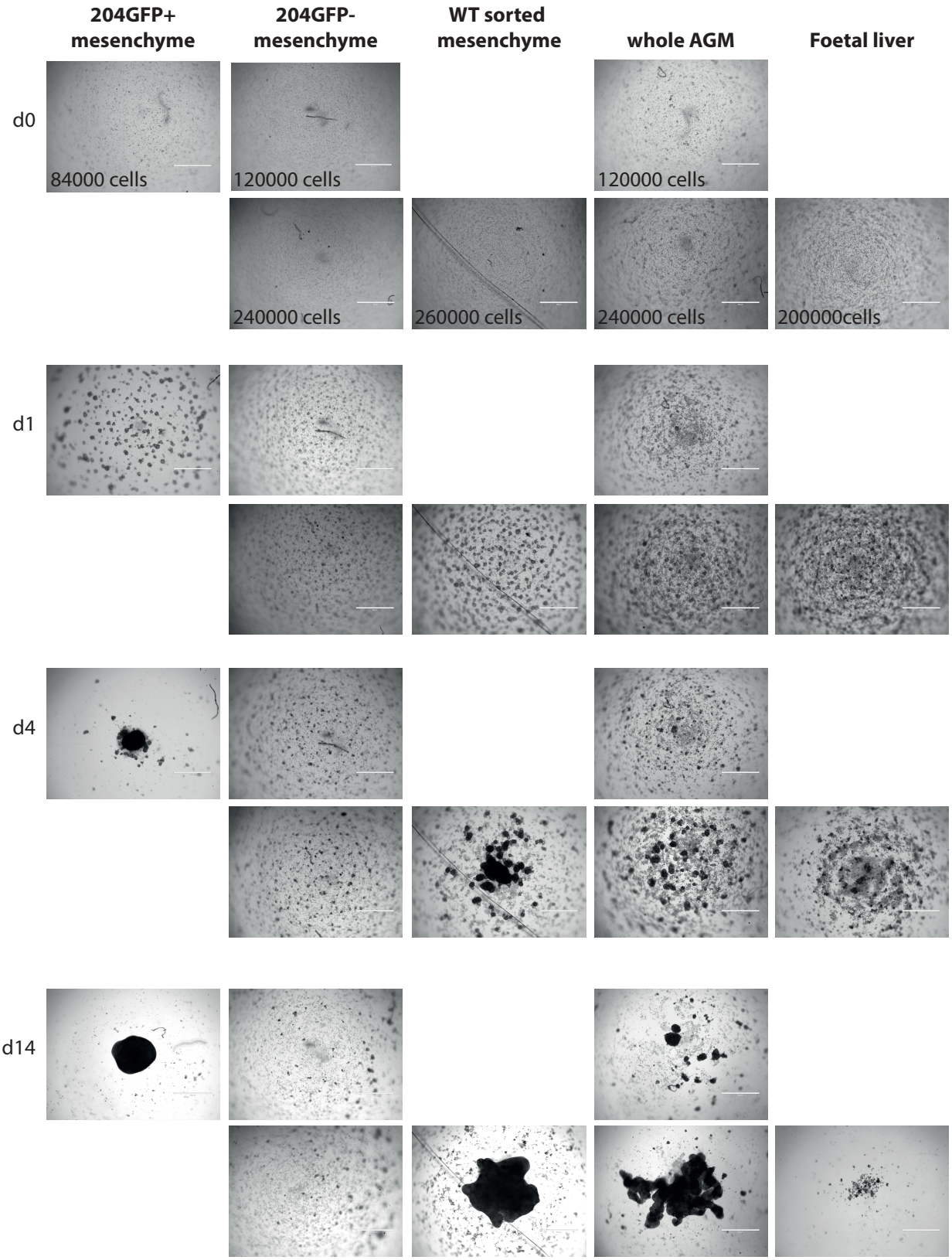


Figure 4.10 Cartilage-forming potential of 204GFP+ cells
Cartilage differentiation progress of 204GFP+/- mesenchyme (VEC-Ter119-CD41-CD45-), WT sorted mesenchyme (sort control), unsorted AGM cells (positive assay control) and fetal liver cells (negative assay control). Images were taken immediately after plating cells into 96-well plates (d0) and at one day (d1), four days (d4) and two weeks (d14) in culture with chondrogenic differentiation media. The number of cells plated per well is indicated. Only 204GFP+ mesenchymal and control WT sorted and unsorted cells aggregated and formed cartilage foci at 2 weeks (dark shapes/spheres). Images taken on the EVOS XL core imaging system with 2X and 4X objectives. Scale bars at 1mm (n=3).

2005; Yamashiro et al., 2004). I therefore stained the fully formed aggregates with Toluidine Blue, Collagen type I and a Runt antibody (which can detect all Runx family members), to confirm the cartilage nature of these foci. All aggregates generated from the 204GFP+ mesenchyme as well as aggregates from the total mesenchyme and whole AGM controls stained positive for Toluidine Blue, Collagen Type I (in the characteristic pattern) and Runx family members (Figure 4.11).

In addition to the chondrogenic potential, I also aimed to establish the adipogenic and osteogenic potential of 204GFP+ and 204GFP- mesenchymal cells. To that end, differentiation assays were performed on whole AGM controls to optimize culture conditions. Whole AGM controls were able to generate both adipocytes and osteocytes in 1 out of 3 and in 2 out of 5 experiments, respectively (Figure 4.12). However, I also observed alkaline phosphatase+ cells (AP+; osteocytes) in the YS controls, that was meant to serve as a negative control for the assay (Mendes et al., 2005). However, it is important to note that the overall morphologies of AP+ cells in the YS control and whole AGM culture were different (Figure 4.12 B). Based on these inconsistencies with published work, the low success rate of both differentiation cultures, and the known difficulty of performing these types of cultures on low cell numbers, I decided not to continue with these assays. In summary, my data showed that 204GFP+ mesenchymal cells can form cartilage in culture, indicating that the 204GFP transgene marks chondrogenic progenitors/stem cells. Whether the 204GFP also marks more broadly the MSCs remains to be established.

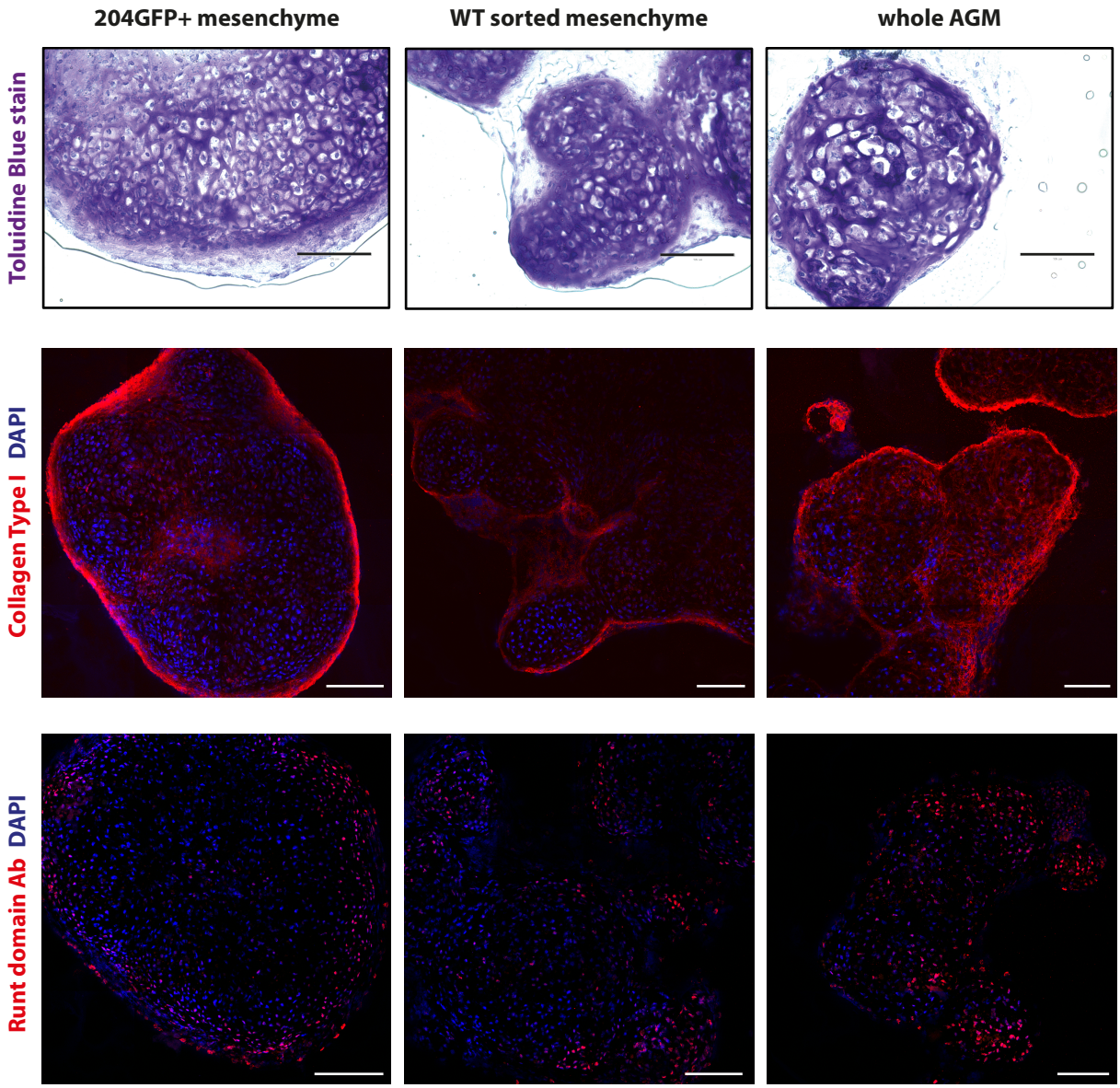


Figure 4.11 Expression analysis of cartilage foci
Sections of cartilage foci formed during differentiation cultures were stained with Toluidine Blue (purple, **top row**), Collagen Type I (red, **middle row**) and an antibody against the Runt domain, recognizing all Runx family members (red, **bottom row**). Nuclei were stained with DAPI (blue). Toluidine images were taken on the EVOS XL core imaging system with 20X and 40X objectives. Fluorescent images were taken on the Zeiss 780 confocal microscope with a 25X and 40X oil-immersion objective. Scale bars at 100um.

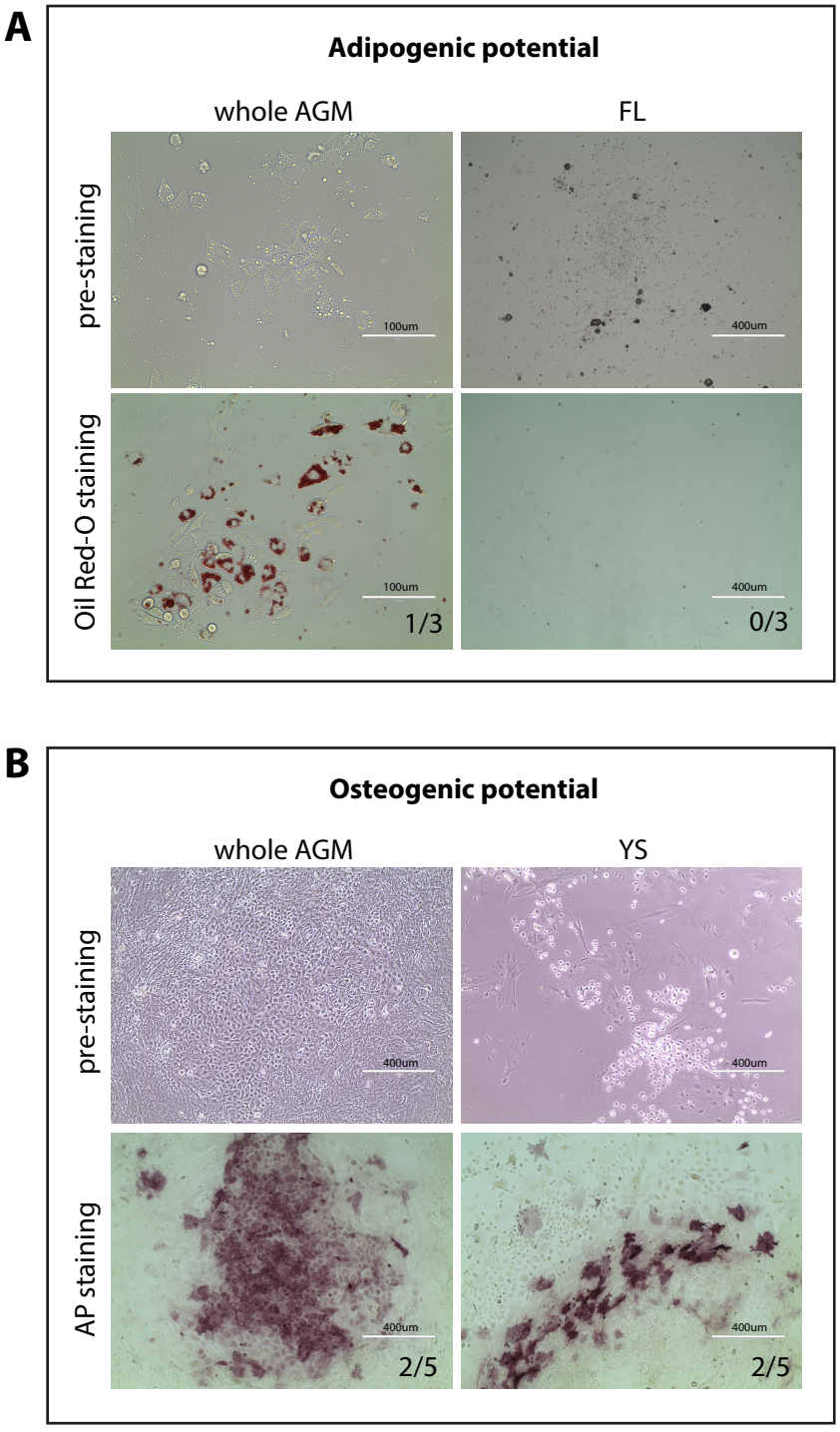


Figure 4.12 Adipogenic and Osteogenic differentiation cultures
A) Adipogenic cultures were performed on whole AGM cells and FL cells (negative control). Top row shows brightfield images of cells in culture prior to staining. The characteristic foamy appearance of adipocytes is already visible here. Bottom row shows Oil Red O staining (red) of adipocytes generated in these cultures. The number of experiments that generated adipocytes per total number of experiments performed is shown. **B)** Osteogenic cultures were performed on whole AGM cells and YS cells (negative control). Top row shows brightfield images of cells in culture prior to staining. Dense, overlapping cell colonies formed in whole AGM wells. Bottom row shows alkaline phosphatase staining (AP,purple) of osteocytes generated in these cultures. The number of experiments that generated AP+ osteocytes per total number of experiments performed is shown. Images were taken on the EVOS XL core imaging system with 20X and 40X objectives. Scale bars as shown.

4.5 Summary and discussion

This chapter described the different functional properties of cells labeled with the 204GFP transgene. In brief, I have established that the 204GFP+ ECs possess hemogenic properties while the potential to form CFU-Cs was mainly restricted to the 204GFP- fraction. Interestingly, both 204GFP+ and 204GFP- AGM fractions showed LT-HSC engraftment. Taken together, this mouse line provides a tool to study HE in more detail and thereby enriching our understanding of EHT.

Labeling distinct subsets or maturation stages of HE?

Due to the more restricted expression pattern of the +204 enhancer reporter transgene, compared to the +23 enhancer, it was initially postulated that the +204 enhancer could be labeling a specific subset of HE. Here, the functional assessment of hemogenic potential within the +204-marked ECs, suggested that a sub-dissection was not likely: My data indicated that at E10.5 all hemogenic potential is within the 204GFP+ ECs only. It is also known that the 23GFP transgene labels all HE. It would therefore suggest that a combination of both enhancer reporter transgenes would enrich the HE population. This is analyzed in more detail in Chapter 5.

In addition, the early expression pattern of 204lacZ transient transgenic embryos, led to the speculation that the +204 enhancer is marking the early stages of EHT. In the current study, the 204GFP transgene was expressed in a broader pattern than its 204lacZ counterpart (Chapter 3). However, even in the 204GFP mouse line I saw evidence that the

transgene is labeling the earlier stages of hematopoiesis and recedes towards more mature cell types. For example, the decreased levels of 204GFP expression with increasing maturation from pre-HSC Type I to pre-HSC Type II (Figure 3.14). Similarly, while the 204GFP transgene is expressed in phenotypic erythroid progenitors (VEC+Ter119+), 204GFP levels are virtually undetectable in Ter119+ erythrocytes (Figure 3.15). Functional data in this chapter established that the 204GFP transgene is marking HE and LT-HSCs. However, while all hemogenic potential was restricted to the 204GFP+ population, the potential to generate LT-HSCs was split between 204GFP+ and 204GFP- subsets. This suggests that the Runx1 +204 activity declines as HE transitions to more mature pre-HSCs and finally HSCs.

Furthermore, not only does HE transition to hematopoietic cell intermediates on its way to a functional HSC, but HE itself exhibits subtle maturation changes depending on developmental stage (Swiers et al., 2013). It would be therefore interesting to assess whether the 204GFP transgene is preferentially marking the earlier HE. Unfortunately, due to technical issues, I was not able to determine hemogenic potential of 204GFP-marked ECs at E8.5. Further co-cultures using low passage OP9s may address this question. Alternatively, lineage tracing experiments using an inducible 204CRE line might establish whether E8.5 204GFP+ ECs contribute to the HSC lineage. Inducible Cre-systems have been widely used to trace cell progenies and require crossing to a floxed-reporter line followed by tamoxifen induction. However, tamoxifen dosage and specific timing of induction need to be well controlled to exclude

unspecific labeling due to leakiness (Kretzschmar and Watt, 2012) and the risk of unwanted labeling of later +204-marked endothelium due to prolonged presence of the tamoxifen.

Are MSCs marked by 204GFP expression?

In addition to the 204GFP mouse line analysis within the context of developmental hematopoiesis, I have also examined the Runx1-specific expression of the 204GFP transgene in a subset of the sub-aortic mesenchyme. While a subset of these cells is co-expressing α-SMA, in line with previous findings (Marshall et al., 2000; Mirshekar-Syahkal et al., 2013), I also assessed functional properties of 204GFP+ mesenchymal cells in differentiation assays. Chondrogenic differentiation cultures established the cartilage-forming potential of 204GFP+ mesenchymal cells (Figure 4.10 and 4.11). It is tempting to speculate that this potential is due to functional MSC cells within the 204GFP+ mesenchyme subset.

Interestingly, Runx1 marks both aortic endothelium and sub-aortic mesenchyme (North et al., 1999), and recent studies have suggested a common origin of (hemogenic) endothelium and (part of the) mesenchyme, which may hint at a closer association between these two lineages than previously thought (Azzoni et al., 2014; Vodyanik et al., 2010, discussed in Chapter 1.7). Whether this is the case for 204GFP+ mesenchyme and endothelium remains to be established.

In connection with this, a recent study determined that Runx1 expression within ECs (HE) and the emergence of intra-aortic cluster cells is tightly regulated by the sub-aortic mesenchyme and showed that important

signaling pathways (e.g. Notch or BMP signaling) are involved (Richard et al., 2013; Wilkinson et al., 2009). Further, in *Runx1* ablation and rescue experiments it was suggested that Runx1 itself may play a role within the sub-aortic mesenchyme compartment (Bee et al., 2010; Liakhovitskaia et al., 2009). Interestingly, I have frequently observed (but not formally quantified) that at E10.5 the 204GFP+ mesenchyme is in direct contact with HE cells (Figure 4.13; HE defined as 23Cherry+ ECs as reported in Chapter 5). This suggests that the sub-aortic mesenchymal cells that are labeled by the 204GFP transgene, aside from containing potential MSCs, may play a supporting role for EHT and thus blood generation. Previously, numerous studies have reported on the blood-supporting activity of AGM mesenchymal cells (Durand et al., 2006, 2007; Oostendorp et al., 2002). Interestingly, deriving stromal cells lines from various parts of the AGM, led to the conclusion that specifically the aorta and the associated mesenchyme as well as the urogenital ridges provided the strongest support for blood formation (Oostendorp et al., 2002). Incidentally, strong BMP4 expression was identified underneath HSC-primed HE within the sub-aortic mesenchyme (Ly6a-GFP, (Durand et al., 2007; de Bruijn et al., 2002; Marshall et al., 2000). It would be interesting to establish whether the +204-marked mesenchyme expresses BMP signaling components and how it compares to the mesenchymal subsets described in the above studies. To that end, molecular profiling of genes expressed in the 204GFP+ sub-aortic cells as well as co-expression analysis of different BMP or Notch ligands/target genes could go towards a better understanding of processes involved in the AGM niche during EHT.

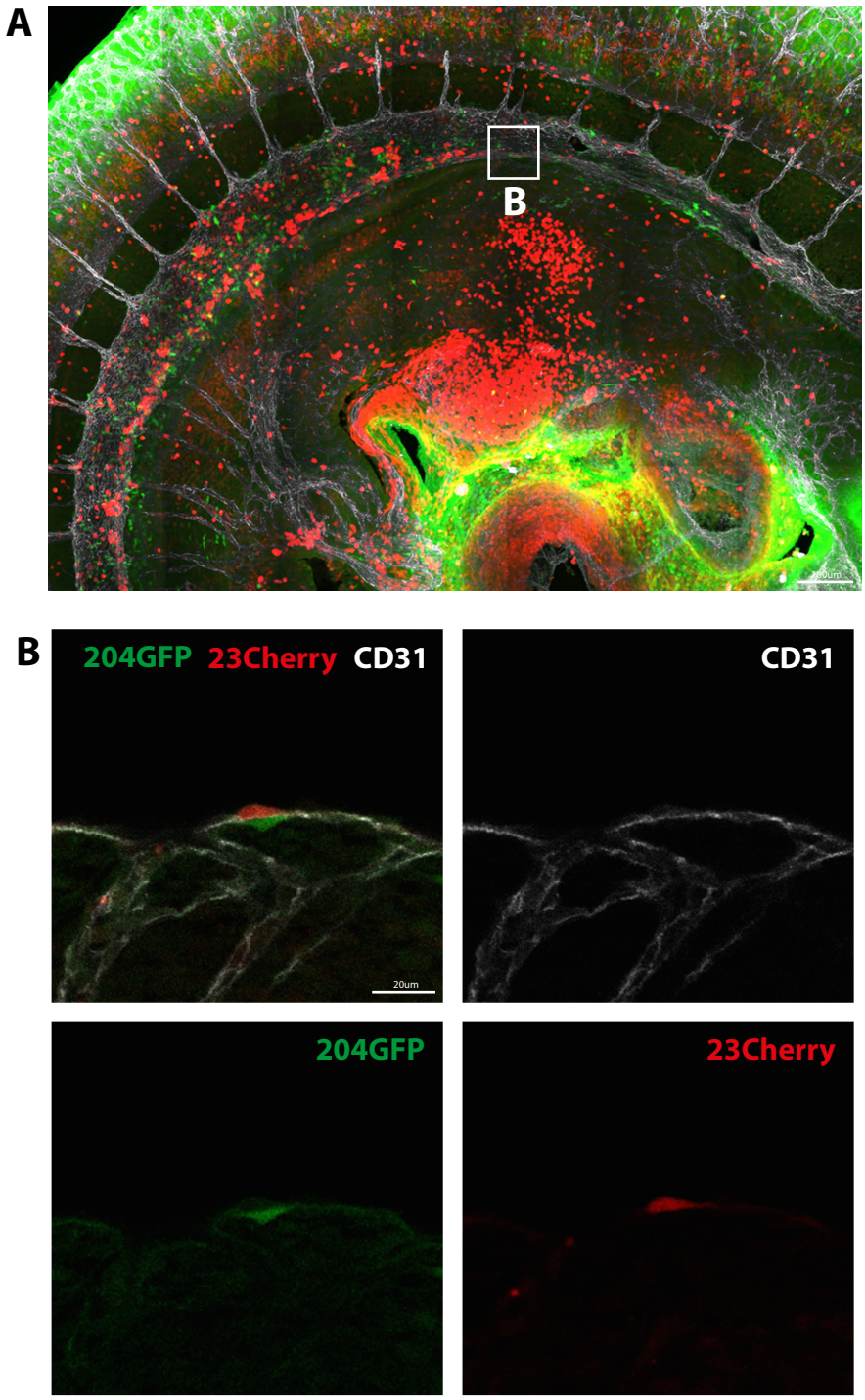


Figure 4.13 Close association of HE and mesenchyme
A) Wholemount z-stack projection of a 204GFP::23Cherry compound embryo (described in Chapter 5). **B)** Zoom in on box in A. The close association of 23Cherry+ HE with the 204GFP+ mesenchyme is shown. Images were taken on the Zeiss 780 upright confocal microscope with a 25X oil-immersion objective. The entire AGM projection was reconstructed from tiled images and 5um optical slices. Optical zooms were generated in the IMARIS software. Scale bars as shown.

Concluding remarks

Taken together, I have established the functional output and spatiotemporal expression pattern of the 204GFP transgene. This novel *Runx1* +204 enhancer reporter mouse line has the potential to enrich for HE, providing a valuable tool for further studies.

Chapter 5

Molecular analysis and further enrichment of hemogenic endothelium

In the previous chapter I established that all functional HE is marked by the 204GFP transgene. Here I wanted to further support this finding on a molecular level. I therefore analyzed 204GFP+ and 204GFP- ECs for expression of endothelial and hematopoietic genes associated with the establishment of the hematopoietic lineage using the Fluidigm® platform. In addition, I wanted to decipher whether HE can be further enriched using a combination of +204 and +23 enhancer-reporter transgenes. For this I generated and characterized a new 23Cherry transgenic mouse reporter line, crossed it with the 204GFP mouse line and profiled the resulting endothelial fractions for blood and endothelial gene expression.

5.1 Molecular profiling of 204GFP+ hemogenic endothelium

To assess the molecular signature of 204GFP+ HE and 204GFP- ECs, quantitative RT-PCR (qRT-PCR) was performed. I analyzed expression of 18 genes that have been associated with the hematopoietic and endothelial program. Included in the 18 genes were 10 core transcription factors of hematopoiesis. This set of genes was previously used in a similar experiment to profile 23GFP+ HEs (Swiers et al., 2013). The goal was to 1) establish endothelial and hematopoietic gene expression in populations of 204GFP+ HE and 204GFP- ECs, and 2) analyze gene expression at the single-cell level.

Expression analysis of 204GFP+ and 204GFP- endothelial subsets

204GFP transgenic embryos were harvested at three developmental timepoints and the whole conceptus (E8.5) or AGM+VUs (E9.5-E10.5) dissected for cell sorting. Endothelial cells were split into 204GFP+ HE and the remaining 204GFP- ECs and pools of 20-25 cells were processed for Fluidigm®-based qRT-PCR. Pools of CD41+ hematopoietic progenitor cells were also sorted and processed – they served as a control for hematopoietic gene expression. Relative mRNA expression levels were calculated based on Ct values. As expected, the most obvious differences in gene expression were observed between CD41+ hematopoietic and endothelial cell populations (Figure 5.1). Some differences were observed between 204GFP+ and 204GFP- ECs (e.g. Gata2 and Meis1), but these were not significant. This is surprising as the 204GFP+ endothelial population, like the 23GFP+ one, contains the functional HE. One explanation could be that non-HE cells are contaminating the populations analyzed. This is suggested by the relatively high expression of e.g. *Tal1* and *Myb* in the 204GFP- non-hemogenic population, which could be due to contamination of the EC by primitive erythroid and/or other hematopoietic cells. This could also explain the slightly increased levels of *Runx1* expression in the 204GFP- ECs at E8.5. Hematopoietic genes such as *Runx1* and its target genes *Sfpi1* (PU.1), *Gfi1* and *Itgb3* (CD61) are usually associated with differentiation towards the hematopoietic lineage. To conclude, gene expression analysis of populations of 204GFP+ and 204GFP- endothelial cells showed very subtle differences, in contrast to what was reported for the 23GFP+ and 23GFP- ECs, where the 23GFP+

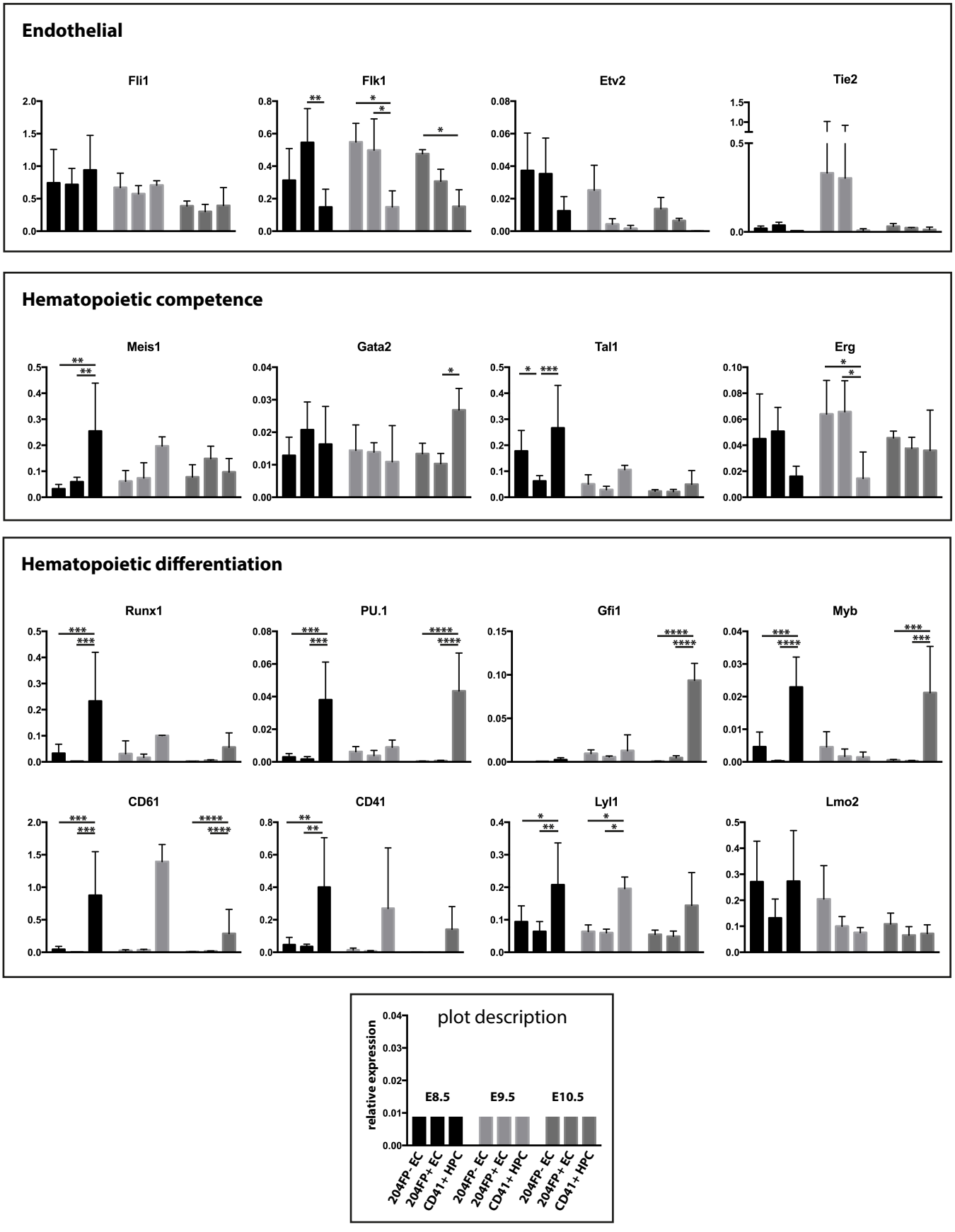


Figure 5.1 Gene expression analysis in 204GFP+/- endothelial populations
Relative mRNA expression levels of endothelial genes and genes associated with hematopoietic competence and differentiation in 204GFP+/- endothelial populations and WT CD41+ progenitor popualtions. Populations were sorted from E8.5 (7-12sp) whole concepti, E9.5 (17-29sp) and E10.5 (31-37sp) AGM+VUs. Expression levels were normalised to average expression of *Atp5a1* and *Ubc* (housekeeping genes).* p<0.05; ** p<0.005; *** p<0.0005; **** p<0.0001 (Two-way ANOVA with Tukey correction).

HE population was characterized by increased expression of genes associated with hematopoietic competence and differentiation (Swiers et al., 2013).

Gene expression analysis of single 204GFP+ and 204GFP- endothelial cells

Given that gene expression analysis of 204GFP+ and 204GFP- EC populations did not show any obvious differences, I tested whether single cell analysis would reveal more dynamic differences in gene expression within these endothelial cells. Using the Fluidigm®-based platform the expression levels of the same 18 genes were measured. Previously, our lab has shown the dynamic expression changes of these genes during EHT, starting from non-hemogenic endothelium, over the transitioning HE and recently emerged CD41+ cells to mature CD45+ cells. Such analysis clearly demonstrated a gradual transitioning of EHT with subsequent loss of endothelial potential and increasing commitment to blood emergence over developmental time (Swiers et al., 2013). Here I only focused on endothelial cells, which were separated into 2 subsets based on 204GFP expression. I sorted and analyzed a total of 113 204GFP+ and 103 204GFP- single endothelial cells at 4 timepoints: E8.5 (7-12sp), E9.0 (17-24sp), E9.5 (26-29sp) and E10.5 (31-37sp) (Appendix 5.1)

First, I analyzed the overall hierarchical clustering of gene expression profiles in all my data (Appendix 5.2). In addition to endothelial and hematopoietic signatures (according to Swiers, 2013), I observed gene

signatures suggestive of contaminating erythroid and mesenchymal cells among the single cells analyzed. At E8.5, the 204GFP- population isolated from the conceptus contained a cluster of cells characterized by lack of *Kdr,* no or low *Fli1, Tek*, and *Etv2* expression, absence of *Gata2* and *Meis1* and strong expression of *Gfi1b, Runx1, Itgb3* and *Myb*, indicative of erythroid cells (van der Meer et al., 2010) (Appendix 5.3). Putative AGM mesenchymal cells, characterized by expression of Meis1 (Azcoitia et al., 2005), but lack of other hematopoiesis-associated genes and low/no expression of endothelial genes appeared among both 204GFP+ and 204GFP- cells starting from E9.5. These contaminating cells are likely to have slipped into the analysis through the lower end of the VE-Cadherin gate (clustered in the large left arm in Appendix 5.2). More advanced flow cytometry methods may circumvent such technical setbacks in the future. For example, index sorting records the exact cell surface marker expression and intensity of each individual single cell sorted and therefore allows to pre-select cells for further gene expression analysis (Osborne, 2011).

I filtered out any cells that showed an erythroid or mesenchymal signature. Therefore, analysis was performed on a total of 84 204GFP+ and 77 204GFP- single cells (Appendix 5.1). Analysis of filtered data, resulted in the identification of a clear hemogenic signature among the E9.5 204GFP+ cells (Figure 5.2): expression of endothelial markers, *Runx1* and its downstream transcriptional targets (Swiers et al., 2013). Similar cells were not apparent in the E9.5 204GFP- population, in line with the functional HE

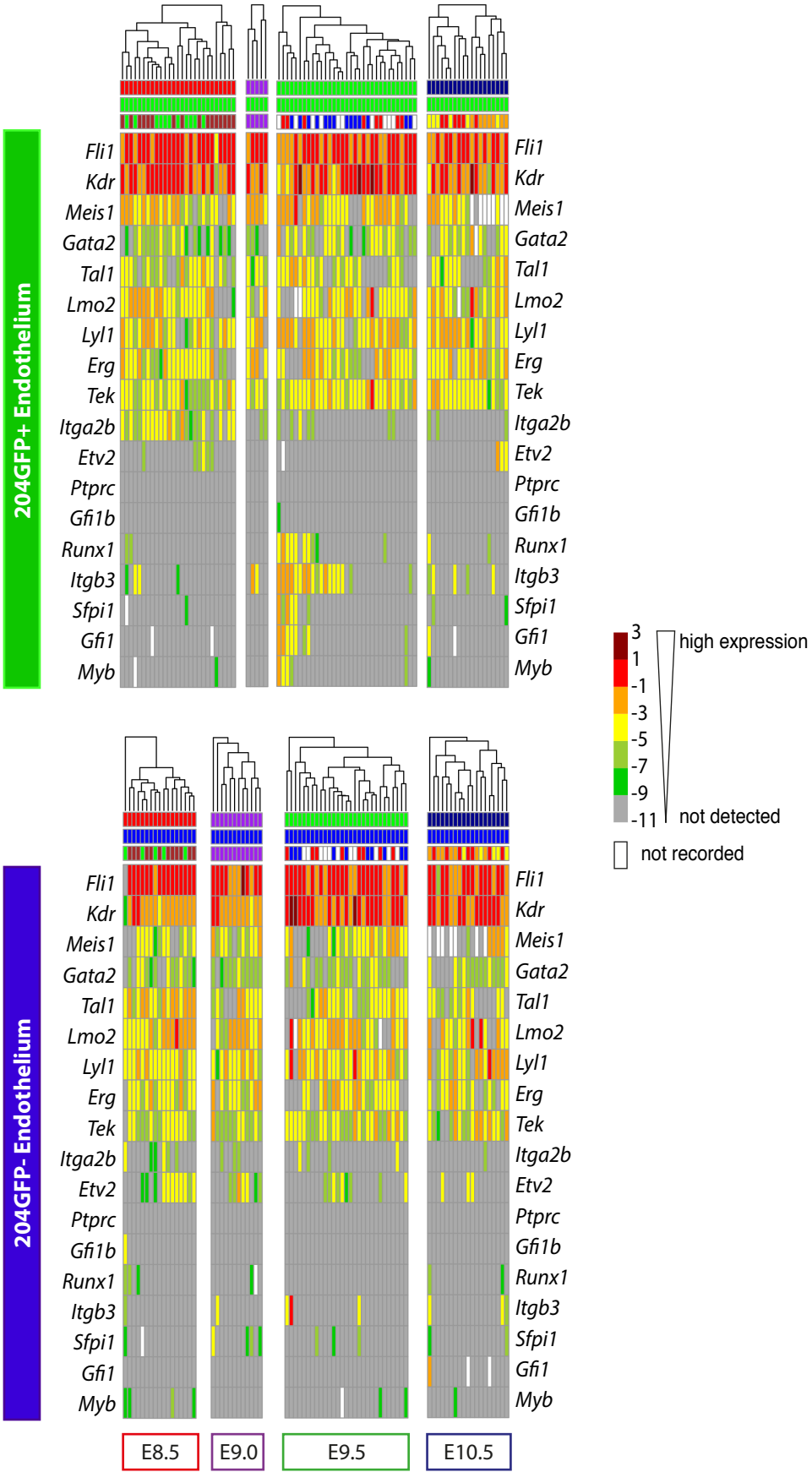


Figure 5.2 Single cell gene expression analysis of the 204GFP+/- endothelium
Heatmaps showing the expression of 18 genes involved during developmental hematopoiesis. Single cells of 204GFP+ and 204GFP- endothelium were analysed at 4 developmental timepoints: E8.5 (7-12sp), E9.0 (17-24sp), E9.5 (26-29sp) and E10.5 (31-37sp). Data are deltaCt values to the mean of *Atp5a1* and *Ubc* housekeeping genes. Expression levels from 3 to -11 ranged from high to undetectable. (continued)

Figure 5.2 (continued)
White indicates not recorded values. Columns represent individual cells, hierarchically clustered for similar expression profiles. Rows represent individual genes. Data was filtered based on lack of *Kdr* and *Fli1* (with a simultaneous strong expression of *Gfi1b, Runx1, Itgb3* and *Myb*, indicative of erythroid cells). In addition, cells that expressed high *Meis1* (above -4) but no expression of *Gata2* and *Tal1* were considered mesenchyme and also filtered out. The raw, unfiltered expression heatmap is provided in Appendix 5.2 and 5.3.

being restricted to the 204GFP+ population (Chapter 4). The absence of a clear hemogenic signature among E10.5 cells is likely due to the relatively low number of cells analyzed so far at this time point (previously the highest proportion of cells with a hemogenic signature was found at E9.5; (Swiers et al., 2013)) and more cells will need to be analyzed at E10.5 to detect those unambiguously. No hemogenic signature was detected among E8.5 cells, in line with what was reported before for 23GFP+ cells ((Swiers et al., 2013). However, I did observe an increased *Meis1* and decreased *Etv2* expression among 204GFP+ endothelial cells (Figure 5.3), in line with what was reported for 23GFP+ competent HE cells (Swiers et al., 2013).

In summary, expression analysis of the 204GFP- and 204GFP+ endothelial populations isolated from the E8.5 conceptus and E9.5 and E10.5 AGM+VU further supports the hemogenic nature of the 204GFP+ endothelium. Analysis of more single cells, using index sorting and more stringent sort gates, is expected to corroborate this result. This identifies the 204GFP transgene as a new tool to isolate HE from the embryo. As not all 204GFP+ ECs showed a HE signature, similar to what was seen with 23GFP+ ECs, I next set out to examine whether combination of both *Runx1* enhancer-reporter transgenes would further purify the HE from the embryo. For this I first generated and characterized a new 23Cherry transgenic mouse line.

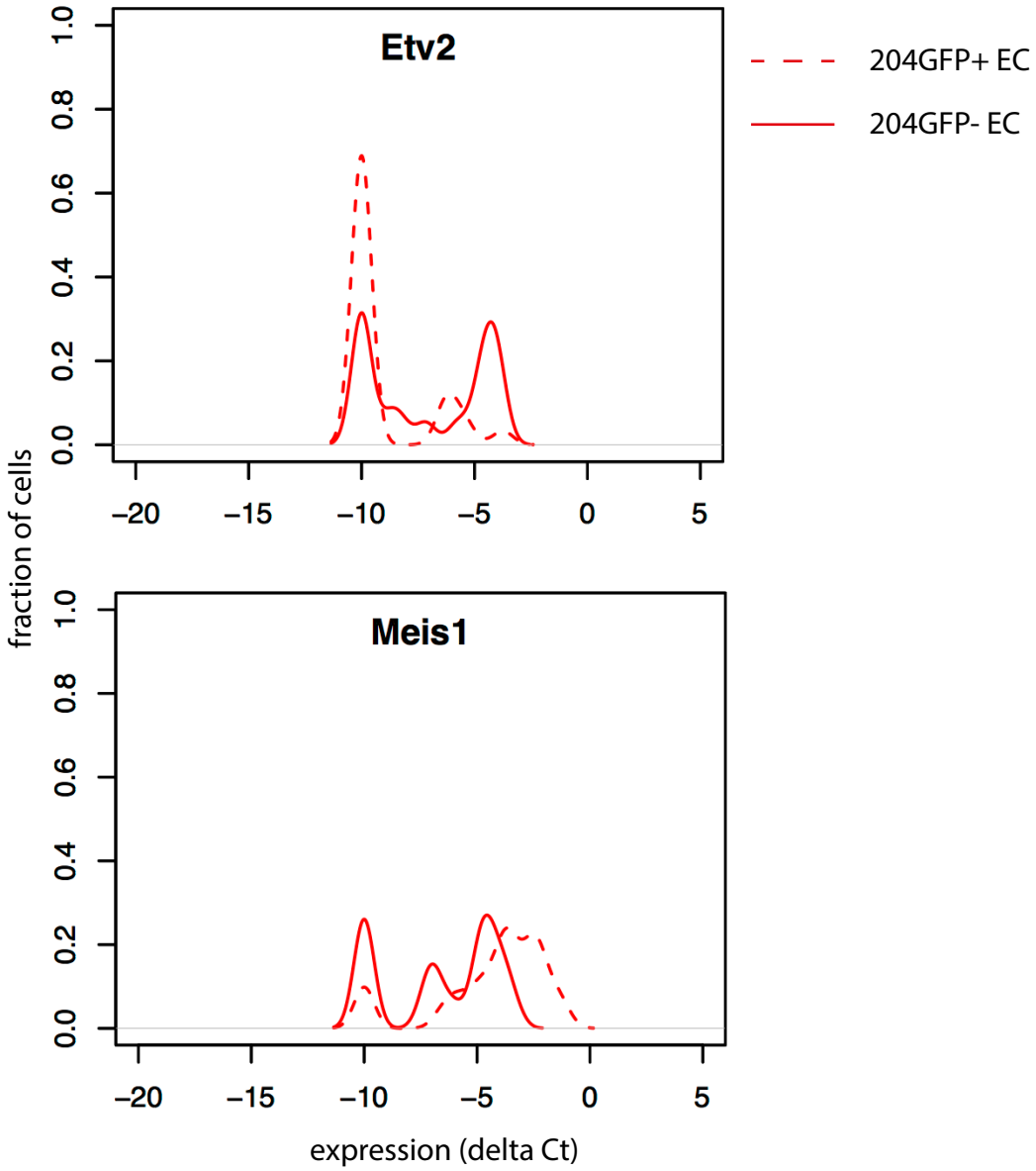


Figure 5.3 *Etv2* and *Meis1* expression at E8.5
Kernel density plots of the filtered single cell data at E8.5. Endothelial cells that express 204GFP exhibit higher *Meis1* expression, compared to 204GFP- ECs. Reversely, ECs that do not express 204GFP had higher *Etv2* expression.

5.2 Generation and characterization of the 23Cherry transgenic mouse line

Generation of the 23Cherry mouse line

The transgenic construct for generating a *Runx1* +23 enhancer-Cherry reporter mouse line (23Cherry) was designed and cloned by the WIMM Genome Engineering facility (Philip Hublitz). A targeting cassette containing the 23Cherry transgene (Figure 5.4A) was targeted to the *Col1A1* locus in E14 ES cells, using CRISPR/Cas9-mediated homology mediated repair. The 23Cherry construct contained a mCherry reporter transcribed from the heterologous hsp68 core promoter under the regulatory control of the 531bp *Runx1* +23 enhancer region (Figure 5.4A). ES cells were transfected and positive clones picked and grown into ES cell colonies (Lucas Greder). I then screened the ES cell colonies generated by PCR and Southern blots to confirm successful and correct integration of the construct. This resulted in the identification of 2 ES cell clones. One of the clones showed bi-allelic targeting success (cl.9), while the other clone had only one allele targeted (cl.10; Figure 5.4B). I then expanded and karyotyped both clones. Euploidy of 75% and over is considered sufficient for chimera generation and germ line transmission (Longo et al., 1997). In both clones, 75% of cells and over had the right karyotype (Figure 5.4C). Both clones were then passed on to the Wellcome Trust Centre for Human Genetics (Oxford) Transgenic Unit for blastocyst injections (Ben Davies and lab). A total of 9 strong chimeras were generated from cl.10 and 6 chimeras from cl.9; all were male (Figure

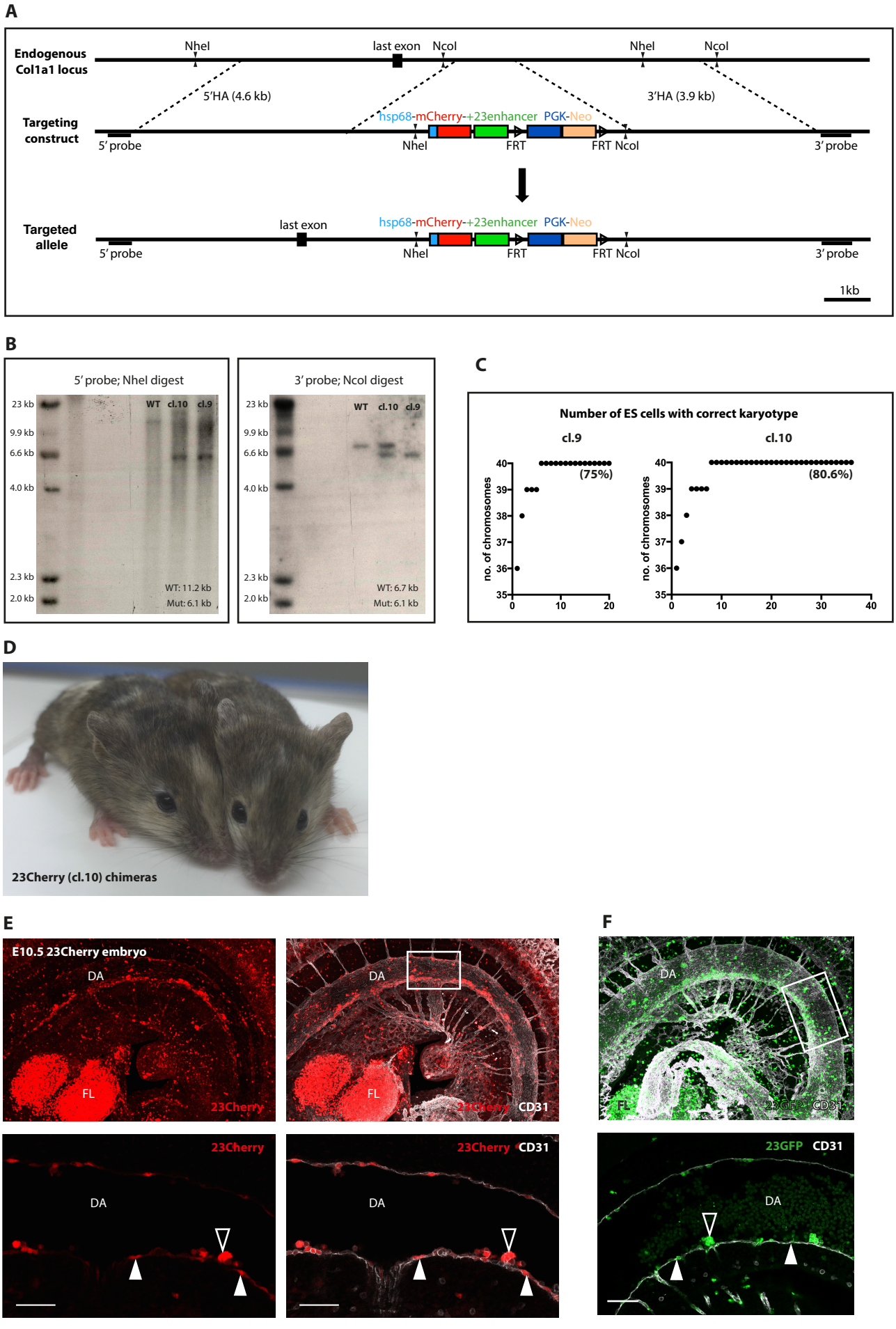


Figure 5.4 Generation of the 23Cherry mouse line (continued)

Figure 5.4 (continued)
A) ES cell targeting strategy in the *Col1A1* locus. **B)** Southern blot analysis of correct construct integration. Two correctly targeted ES cell clones were then karyotyped **(C)**, prior to blastocyst injection. **D)** Example of highly chimeric mice generated. **E)** Wholemount z-stack projection of a E10.5 23Cherry embryo, showing transgene expression in the dorsal aorta (DA) and fetal liver (FL). Zoom in on boxed area shows 23Cherry+ cells within the CD31+ endothelium (solid arrow-heads) as well as 23Cherry+ intra-aortic cluster cells (empty arrowhead). **F)** As comparison a wholemount z-stack projection of a E10.5 23GFP embryo, also showing transgene expression in the DA , FL, endothelum and cluster cells (23GFP image courtesy of Emanuele Azzoni). Images were taken on the Zeiss 780 Upright confocal microscope with a 25X oil-immersion objective. The entire AGM projection was reconstructed from tiled images and 5um optical slices. Optical zooms were generated in the IMARIS software.

5.4D). Since the targeted E14 ES cells derived from an agouti mouse strain (129 A^W/A^W) and were injected into C57BL/6 blastocysts (black), chimeras were back-crossed onto the C57BL/6 background in order to detect germline transmission. After several litters, the chimera pairings resulted in the birth of brown pups (agouti), indicative of ES cell-derived germline and thus the transmission of the targeted allele. This was confirmed by genotyping, which was done by genomic PCR for the 23Cherry allele.

Phenotypic characterization of the 23Cherry mouse line

Once the 23Cherry mouse line was established, I assessed the expression pattern of 23Cherry in E10.5 embryos and compared this to the known 23GFP and endogenous Runx1 expression patterns. As expected, 23Cherry was expressed in the AGM region and more specifically in a subset of the DA ECs and intra-aortic cluster cells (Figure 5.4E). In addition, the E10.5 FL showed strong 23Cherry expression. Both the AGM and FL expression patterns are comparable to previous observations in 23GFP and Runx1-LacZ embryos (Figure 5.4F and (Bee et al., 2010; North et al., 1999; Swiers et al., 2013).

23Cherry expression was also determined at E8.5. Here, compound transgenic 23GFP::23Cherry embryos were analyzed, to allow direct comparison of 23Cherry and 23GFP expression. Overall, both reporter transgene expression patterns broadly overlapped at E8.5 (Figure 5.5). Clear co-expression in the YS as well as the PAS region was observed. In the YS, the 23Cherry and 23GFP both labeled the blood island band

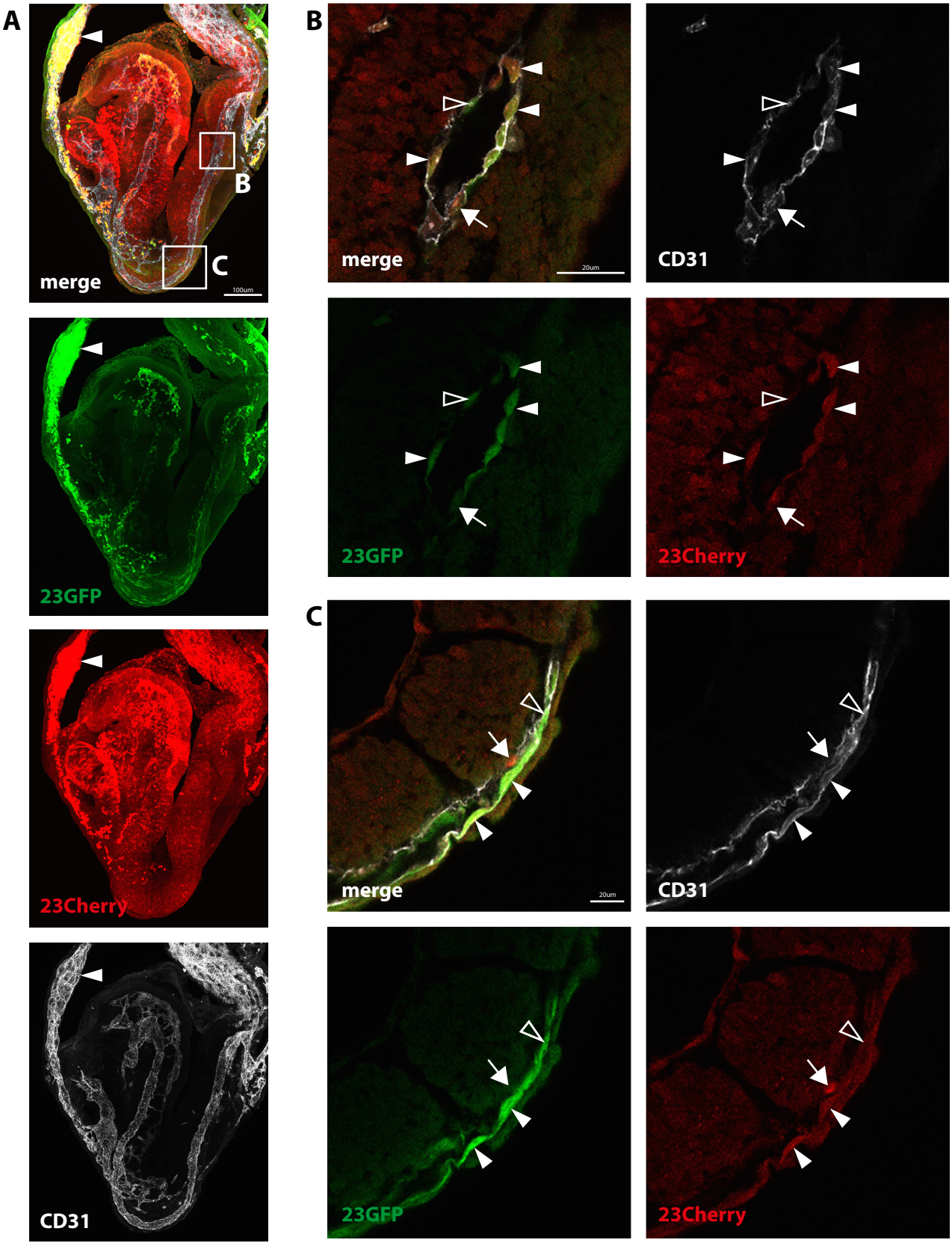


Figure 5.5 Co-expression analysis of 23Cherry and 23GFP
A) Wholemount z-stack projection of a 23Cherry::23GFP compound transgenic embryo at E8.5. Co-expression in the YS blood island is shown (block arrowhead). **B,C)** Zoom-in on a slice through (**B**) and along (**C**) one of the aortae showing co-expression in the endothelium (block arrowhead). Some 23Cherry (arrow) and 23GFP (open arrowhead) single-expressing cells were also observed. Images were taken on the Zeiss 780 Upright confocal microscope with a 25X oil-immersion objective. The entire embryo projection was reconstructed from tiled images and 5um optical slices. Optical zooms were generated in the IMARIS software.

(arrowhead in Figure 5.5A). In the PAS, the majority of the endothelium of the paired dorsal aortae co-expressed both transgenes (solid arrowheads in Figure 5.5B,C). Occasionally, 23GFP single positive cells (open arrowhead) and single positive 23Cherry cells (arrow) were also observed. While I did not quantify co-expression, the number of single positive cells seemed small.

I observed that the level of 23Cherry expression was overall weaker than the level of 23GFP expression. Post-imaging enhancement of the 23Cherry channel was generally required to clearly visualize the expression (although expression was readily detectable by flow cytometry, see Figure 5.8). Several possible explanations exist for the lower 23Cherry expression. Firstly, it could be due to the nature and strength of the two fluorescent proteins, as eGFP is known to be twice as bright as mCherry (Tatjana Sauka-Spengler, personal communication). Secondly, different enhancer lengths were incorporated into the targeting constructs. While the 23GFP construct contained a 1.1kb +23 enhancer fragment (Bee et al., 2010), the 23Cherry construct contained a 531bp +23 enhancer fragment (Nottingham et al., 2007). In transient transgenic embryos and stable transgenic lines generated in the lab, the 1.1 kb fragment was found to be less sensitive to position effects at the site of transgene integration (Marella de Bruijn, personal communication). However, as the *Col1A1* locus is a 'safe harbour' locus (Beard et al., 2006), the effect of enhancer fragment size on transgene expression may be limited. Finally, the 23Cherry allele still contains the PGK-Neo cassette (Figure 5.4A), which may interfere with mCherry expression. It is possible that the strong pgk

promoter is sequestering the transcription machinery away from the enhancer cassette, therefore causing a reduction in mCherry production. Future excision of this cassette will reveal whether this indeed negatively affects transgene expression. In addition to differences in expression levels, the 23Cherry transgene showed ectopic (i.e. non-Runx1 related) expression in the head, neural tube, and the heart, distinct from the 23GFP line (Figure 5.5A). Head and neural tube expression was also frequently seen with the hsp68 promoter alone (Nottingham et al., 2007), and may be more prominent in the *Col1A1* locus than at the 23GFP site of integration (chromosome 1, not shown). The heart expression could be *Col1A1* locus-specific (Peacock et al., 2008).

Overall, I have successfully generated a novel 23Cherry reporter mouse line that exhibits an expression pattern similar to that observed in previous +23 enhancer-reporter transgenic mouse lines. The phenotypic expression confirmation prompted me to continue with functional characterization of the 23Cherry line.

Functional characterization of the 23Cherry mouse line

In order to establish whether the 23Cherry line functionally behaves in the same manner as the other +23 reporter lines, I tested the CFU-C potential of 23Cherry+ and 23Cherry- cell fractions. E8.5 whole concepti and E10.5 AGM+VU regions were dissected, processed for FACS, and separated into 23Cherry positive and negative cell populations. Sorted cells were immediately plated into methylcellulose cultures and cultured for up to 10 days. Blood progenitor colonies were counted on day 7 and 10 of culture.

As expected, the 23Cherry positive cell populations were highly enriched for CFU-C, and virtually all CFU-C resided in the 23Cherry positive cell populations of the E8.5 conceptus and E10.5 AGM+VU (Figure 5.6). Although some clonogenic progenitors were detected in cultures of the 23Cherry negative fraction, especially at E8.5, this could be due to contamination with 23Cherry+ cells. At E8.5 (but not E10.5), 1.4% of 23Cherry- cells was found in the 23Cherry+ fraction in the post-sort purity check (n=1, data not shown). Comparison of the distribution of CFU-C over 23Cherry+/- (Figure 5.6C) and 23GFP+/- populations (Bee et al., 2010), showed that CFU-C were labeled similarly by the 23Cherry and 23GFP transgenes, with 99% and 98% of CFU-C in the E10.5/E11 AGM+VU labeled by the 23Cherry and 23GFP transgenes, respectively.

Next, in order to establish in which endothelial fraction the hemogenic potential resides, I also performed two OP9 co-culture experiments. 23Cherry+ and 23Cherry- ECs were sorted and plated onto OP9 stromal cells (Figure 5.7A). Following a 7-day culture period the supernatant, which contained round, bright, semi-adherent cells (not shown), was collected and cells analyzed for CD45 expression by flow. Surprisingly, I detected CD45+ cells in the supernatant derived from both endothelial fractions, in contrast to previous data (Figure 5.7 B and Swiers et al., 2013). Interestingly, the endothelial network output, although somewhat lower in the 23Cherry+ ECs, also suggested a split in hemogenic potential (Figure 5.7 C). This was unexpected and may be due to the largely different number of ECs plated in these assays (Figure 5.7A). In addition,

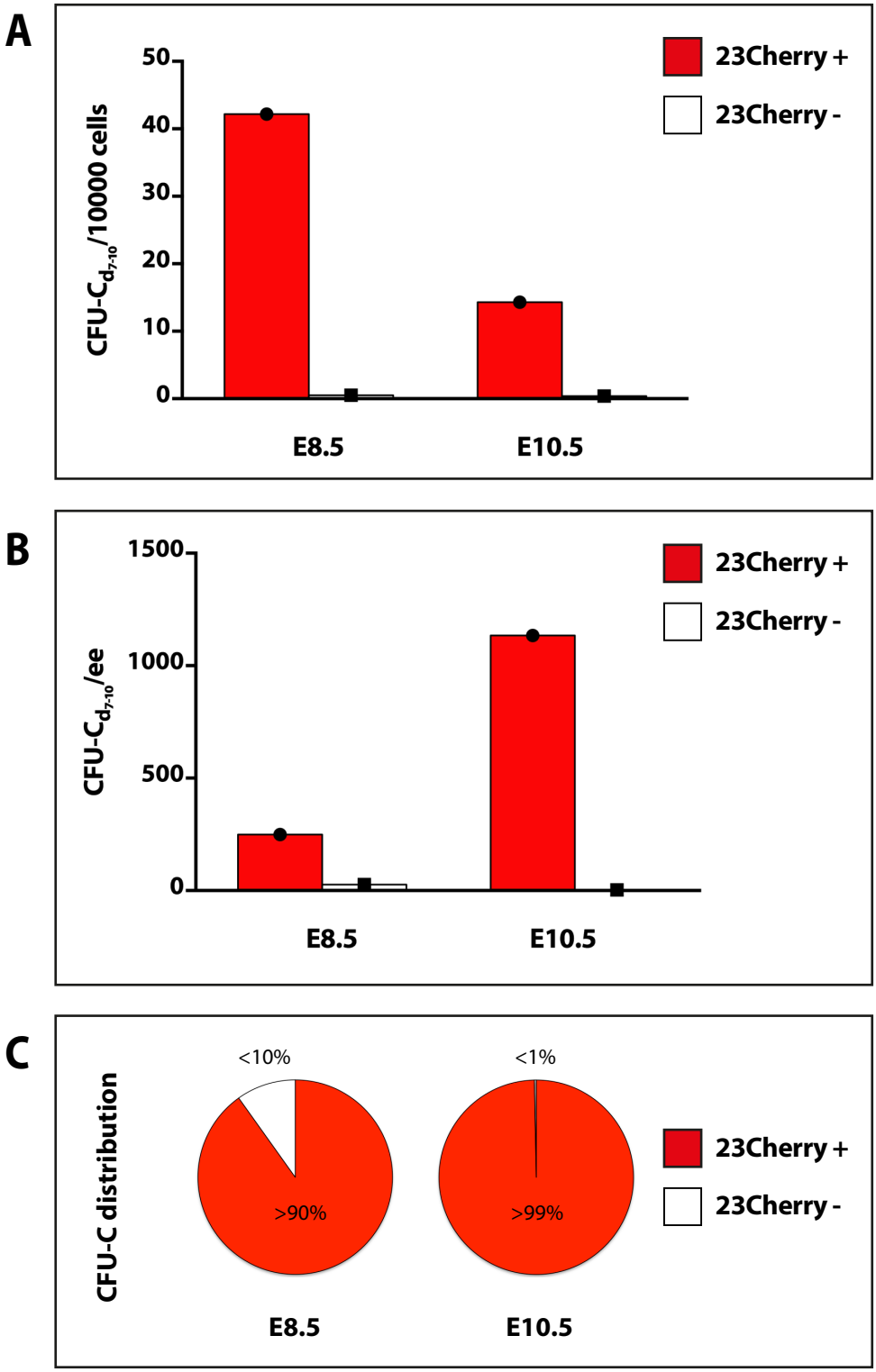
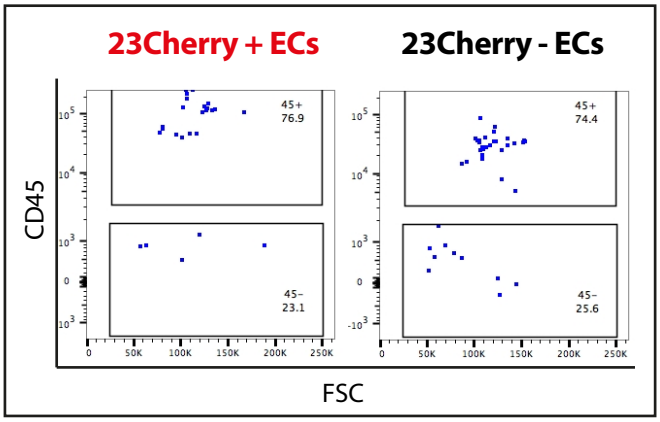


Figure 5.6 Blood progenitor potential of 23Cherry+/- subsets
The 23Cherry+ (red) and 23Cherry- (white) fractions of whole E8.5 concepti and E10.5 AGM+VUs were tested for blood progenitor potential. Colonies were counted on day 7 (for E8.5) and day 10 (for E10.5) of culture. Graphs depict CFU-C colonies counted per 10000 cells plated (**A**) and CFU-C colonies counted per ee (**B**). CFU-C distribution between 23Cherry+ (red) and 23Cherry- (white) fractions is shown (**C**). n=1.

A

	23Cherry+ ECs	23Cherry- ECs
Exp. 1	80 cells	1500 cells
Exp. 2	250 cells	2500 cells

B



C

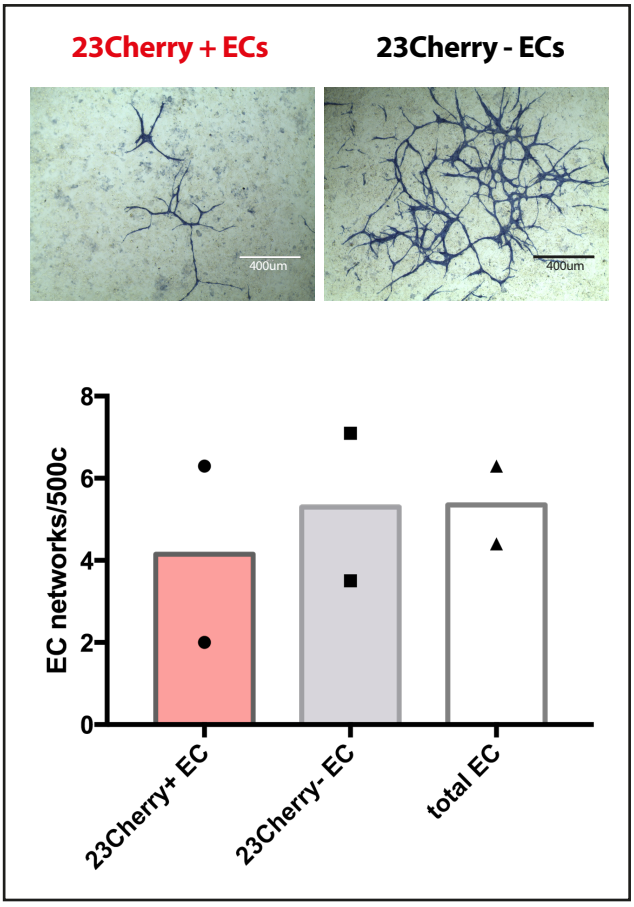


Figure 5.7 OP9 co-culture analysis of 23Cherry+/- endothelial cells at E10.5
A) Table depicting the number of 23Cherry+/- endothelial cells plated into OP9 co-cultures in 2 separate experiments**. B)** Hematopoietic output: CD45 cell surface expression of cells collected in the supernatant of E10.5 OP9 co-culture experiments. **C)** Endothelial output: CD31+ staining (blue) of endothelial networks generated in OP9 co-cultures. Graph representation of the number of endothelial networks generated in OP9 co-culture assays from 500 endothelial cells plated. Average bars for 23Cherry+ (pink), 23Cherry- (grey) and total (white) endothelium are shown. Images were taken on the EVOS XL core imaging system with a 10X and 20X objective. Scale bars as shown.

as mentioned above, the Cherry protein has about half the brightness of a GFP protein (Tatjana Sauka-Spengler, personal communications). Interestingly, in my flow analysis the 23Cherry+ population was about a log lower (not shown) than what is observed with 23GFP+ cells. Of note, due to cell number limitations, only WT EC purity checks were performed (96% in both experiments). It is therefore possible that some low-expressing 23Cherry+ cells were missed during the sort and ended up in the 23Cherry- gate, leading to this unexpected result. Nevertheless, the 23Cherry+ endothelial subset likely contains a high proportion of HEs and can be used to isolate this EHT intermediate for further analysis.

In summary, we successfully generated the 23Cherry mouse line via ES cell targeting into the *Col1A1* locus, blastocyst injection and chimera production. Analysis of transgenic embryos during development established a 23Cherry expression pattern highly comparable to that of the 23GFP transgenic mouse line. In addition, similar to the 23GFP transgenic line, virtually all clonogenic blood progenitors were marked by transgene expression in the 23Cherry mouse line. In addition, the majority of HEs reside within the 23Cherry+ EC fraction. This means that this new mouse line is a faithful reporter of *Runx1* +23 enhancer activity, and in the remainder of this chapter 23Cherry+ ECs will be referred to as HE. Together, the new 23Cherry and 204GFP mouse lines now allow for the identification, isolation and study of distinct subsets of AGM endothelium to further elucidate the early dynamic changes in these cells during hematopoietic specification and commitment.

5.3 Expression analysis of 204GFP::23Cherry compound transgenic embryos

Rare endothelial cells co-express 204GFP and 23Cherry

In Chapter 3 I established that a small subset of the developing endothelium is marked by expression of two *Runx1* enhancer-reporter transgenes, 204GFP and 23LacZ (Figure 3.20). Here, I extended this analysis to 204GFP::23Cherry compound transgenic embryos. Embryos were harvested at different developmental stages and genotyped for both transgenes. Double-transgenic embryos were used for all co-expression and molecular profiling analysis, while single-transgenic and WT embryo littermates served as controls. Phenotypic analysis by confocal microscopy of wholemount E10.5 embryos showed rare co-expressing cells within the CD31+ endothelial layer of the DA (solid arrowheads in Figure 5.8B,C). Single positive 23Cherry and 204GFP HE cells were also observed (arrows and empty arrowheads, respectively in Figure 5.8B,C). The intensity of 23Cherry expression in the HE was usually lower than in the blood cells (solid arrowheads in Figure 5.8B; this is similar to what is seen for the 23GFP transgene (Swiers et al., 2013).

`

Quantification of co-expression in compound transgenic embryos

In addition, I quantified co-expression of 204GFP and 23Cherry in E8.5 to E10.5 endothelium by flow cytometry. At all three developmental stages, the endothelium was divided into 4 fractions based on the expression profiles of the 2 reporter lines. Interestingly only 1-3% of the endothelium

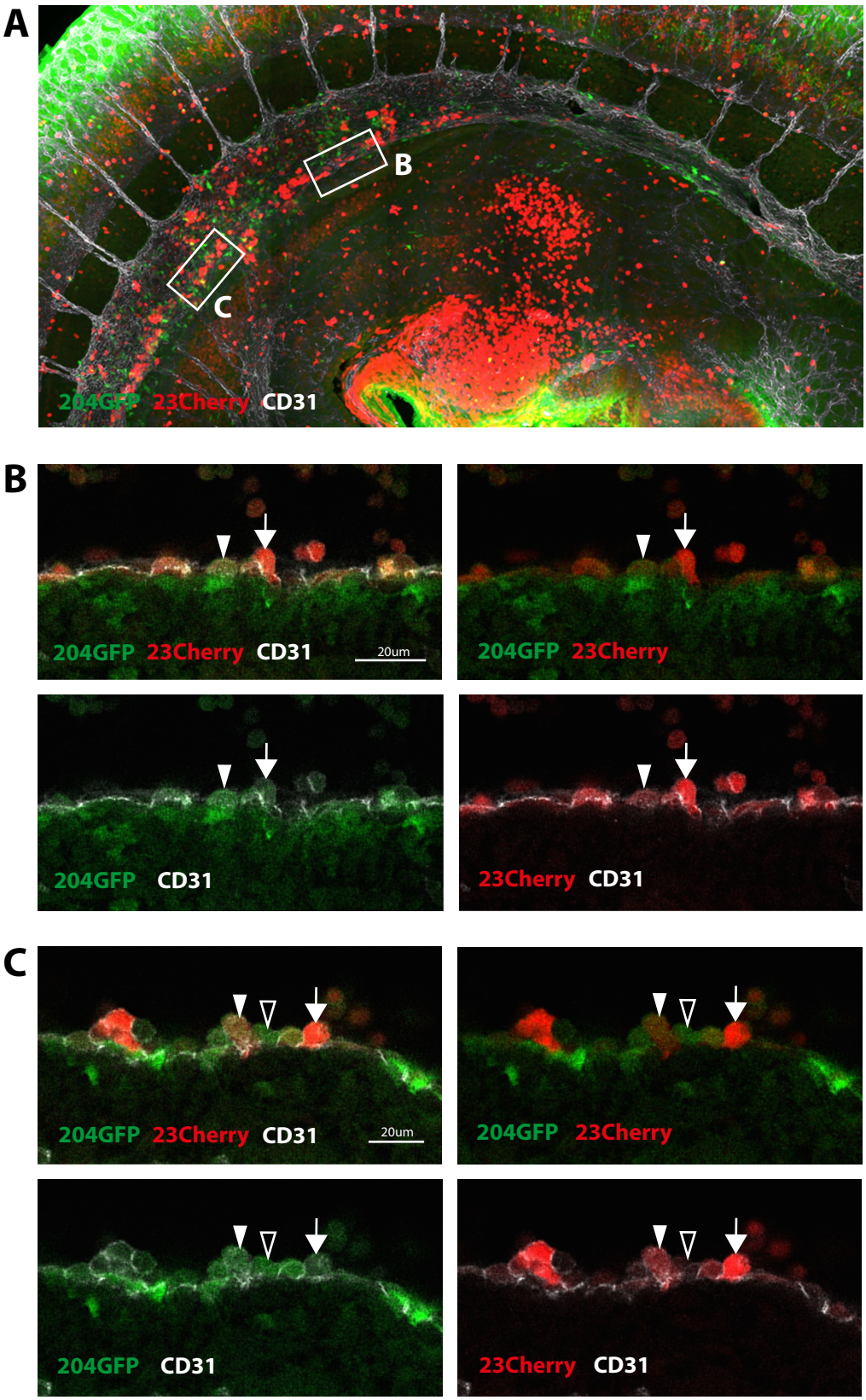


Figure 5.8 Co-expression analysis of 204GFP and 23Cherry
A) Wholemount z-stack projection of a 204GFP::23Cherry compound transgenic embryo at E10.5. **B,C)** Examples of co-expression within the CD31+ DA. Co-expression of 204GFP and 23Cherry was observed in a subset of the endothelium (solid arrowhead). Some 204GFP (empty arrowhead) and 23Cherry (arrow) single-expressing cells were also observed. Images were taken on the Zeiss 780 upright confocal microscope with a 25X oil-immersion objective. The entire AGM projection was reconstructed from tiled images and 5um optical slices. Optical zooms were generated in the OMERO software. Scale bars are given.

was marked by both transgenes, with the percentages of 204GFP+23Cherry+ ECs being relatively constant at all three developmental timepoints (Figure 5.9, 5.10 and Appendix 5.4 - 5.6). In addition, around half (at E8.5) and a quarter (at E9.5 and E10.5) of all endothelial cells were labeled by either one of these transgenes. Among the transgene-positive endothelial cells, 23Cherry single-positive cells made up the largest population at E8.5 (approximately 40%), while the percentages for 23Cherry-single positive cells at E9.5 and E10.5 and 204GFP single-positive cells at all timepoints comprised around 6-10% of total endothelium, similar to previous reports (Figure 5.9, Figure 3.14 and Swiers et al., 2013). These data corroborate my observations in wholemount E10.5 204GFP::23GFP compound transgenic embryos (Figure 5.8) and in sections of E8.5 and E10.5 204GFP::23LacZ embryos (Figure 3.20).

Overall, I have confirmed my previous imaging observations of rare endothelial cells that show combined activity of both *Runx1* +204 and +23 enhancers. Functional experiments established that, at least at E10.5, all hemogenic capacity resides within the 204GFP+ endothelium (Chapter 4). Similarly, the +23 enhancer has been shown to mark all HE potential (Ng et al., 2010; Swiers et al., 2013). Thus, in the 204GFP::23Cherry compound transgenic embryos all HE should reside in the 204GFP+23Cherry+ population, allowing for its purification. To begin to examine whether this is indeed the case on a molecular level, I sorted 204GFP+23Cherry+ endothelial cells along with single positive

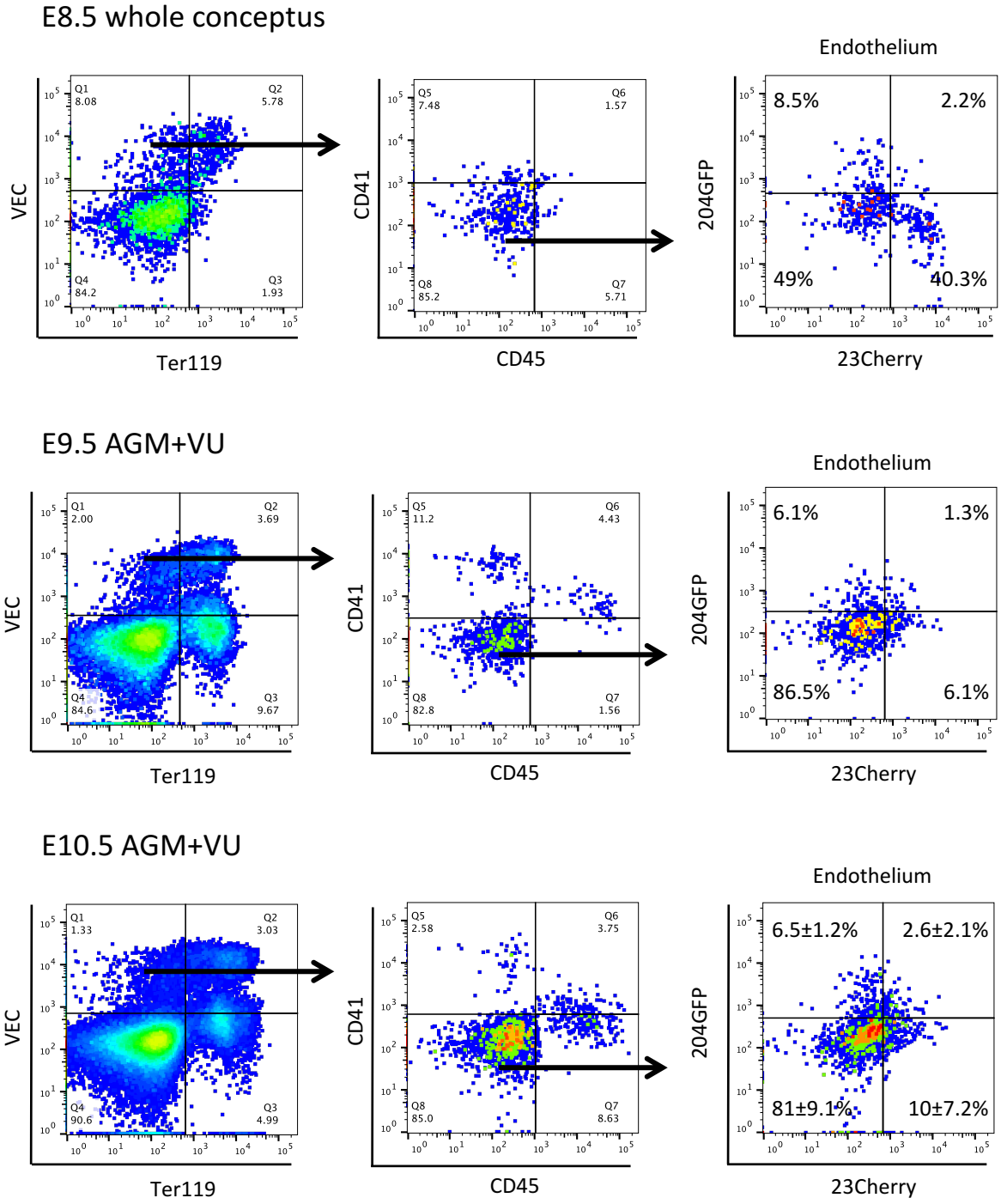


Figure 5.9 Flow cytometr analysis of 204GFP::23Cherry compound transgenic embryos (continued)

Figure 5.9 (continued)
Flow cytometry analysis of 204GFP::23Cherry compound transgenic embryos at E8.5 to E10.5. The endothelium (VEC+Ter119-CD41-CD45-) was analyzed for differential expression of 204GFP and 23Cherry. n=1

endothelium to determine whether there is enrichment for a hemogenic expression signature among the double positive endothelial cells.

Single cell gene expression analysis of 204GFP and/or 23Cherry-marked endothelium

Utilizing the novel 204GFP and 23Cherry mouse lines I isolated and analyzed single endothelial cells divided into 4 fractions based on transgene expression profiles (Figure 5.11). Analysis was performed on 3 developmental timepoints (E8.5 conceptus and E9.5 and E10.5 AGM+VU) and gene expression in individual single cells was visualized in heatmaps using hierarchical clustering (Figure 5.12). Due to some contamination from primitive erythroid and mesenchymal cells (discussed above in Chapter section 5.1) filtering of data was necessary (raw, unfiltered data is provided in Appendix 5.7). In addition, index sorting was applied to a subset of experiments at E10.5. After filtering, a total of 35 204GFP-23Cherry- (G-C-), 40 204GFP+23Cherry- (G+C-), 36 204GFP-23Cherry+ (G-C+) and 58 204GFP+23Cherry+ (G+C+) single cells were analyzed (Appendix 5.1). In addition, 21 hematopoietic single cells (CD41+ and CD41+CD45+) were analyzed as assay controls for hematopoietic genes.

Interestingly, in spite of the low cell numbers analyzed so far, an enrichment of cells with a hemogenic expression signature among the 204GFP+23Cherry+ cells was observed. Previously, a hemogenic signature was defined as expression of endothelial markers, as well as *Runx1* and its downstream transcriptional targets (Swiers et al., 2013).

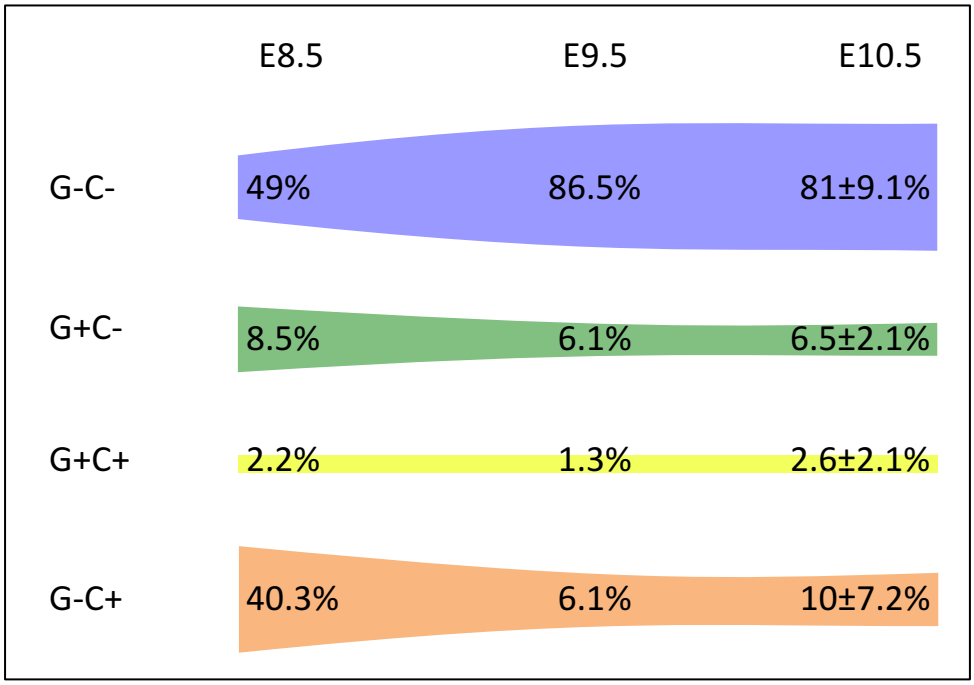


Figure 5.10 Dynamic 204GFP and 23Cherry expression patterns during endothelial development
Schematic overview of what percentage of the endothelium is marked by different combinations of 204GFP (G) and 23Cherry (C) transgene expressions. Percentages taken from Figure 5.9.

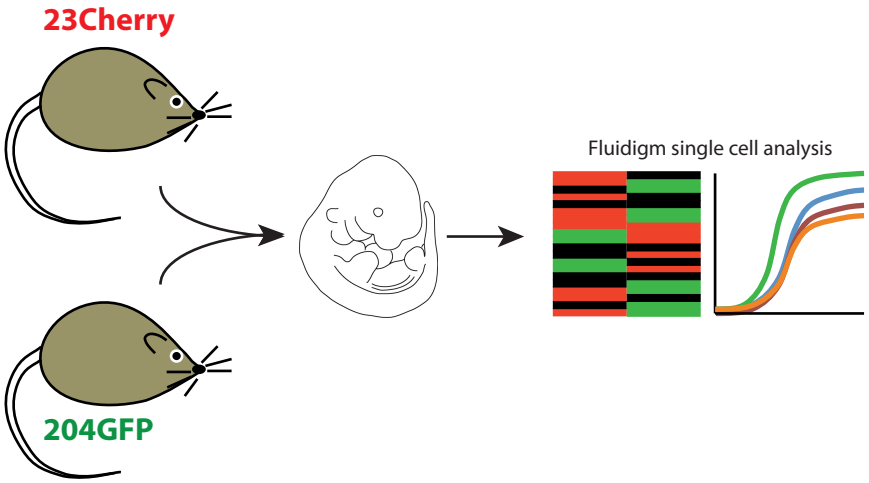


Figure 5.11 Schematic of the experimental set-up for expression profiling
23Cherry and 204GFP transgenic mice were crossed and compound transgenic embryos harvested for Fluidgm single cell expression analysis

This observation was particularly remarkable for the E10.5 timepoint, as only a small subset (2/20 cells) of the 204GFP+ EC fraction at E10.5 exhibited such hemogenic signature (cf. Figure 5.2), while around a quarter (11/43 cells) of 204GFP+23Cherry+ cells showed such a signature. In the E10.5 204GFP transgenic AGM, approximately 8% of endothelium was 204GFP+ (Figure 3.14), while in the 204GFP::23Cherry compound transgenic AGM, only around 3% of endothelium expressed both transgenes (Figure 5.9), resulting in an almost 3-fold enrichment of the putative HE.

At earlier developmental timepoints the number of cells analyzed was even smaller, making it difficult to draw finite conclusions. However, even at E8.5 it seemed a further purification with the compound transgenic embryos was possible: In the 204GFP transgenic conceptus, around 20% of endothelium expressed the 204GFP transgene (Figure 3.14). When utilizing the 204GFP::23Cherry compound transgenic embryos, only approximately 2% of endothelium expressed both transgenes (Figure 5.9). This suggests a 10-fold enrichment of the putative HE. This is also reflected in the number of single ECs that exhibited a hemogenic signature: 3 in 18 204GFP+ cells (17%), but as many as 3 in 8 204GFP+23Cherry+ cells (38%; Figure 5.12). Thus, this preliminary data suggests that using two novel *Runx1* enhancer-reporter lines, the 204GFP and 23Cherry lines, the HE can be enriched, at least on a molecular level. Future experiments will reveal whether this corresponds with enrichment for functional HE.

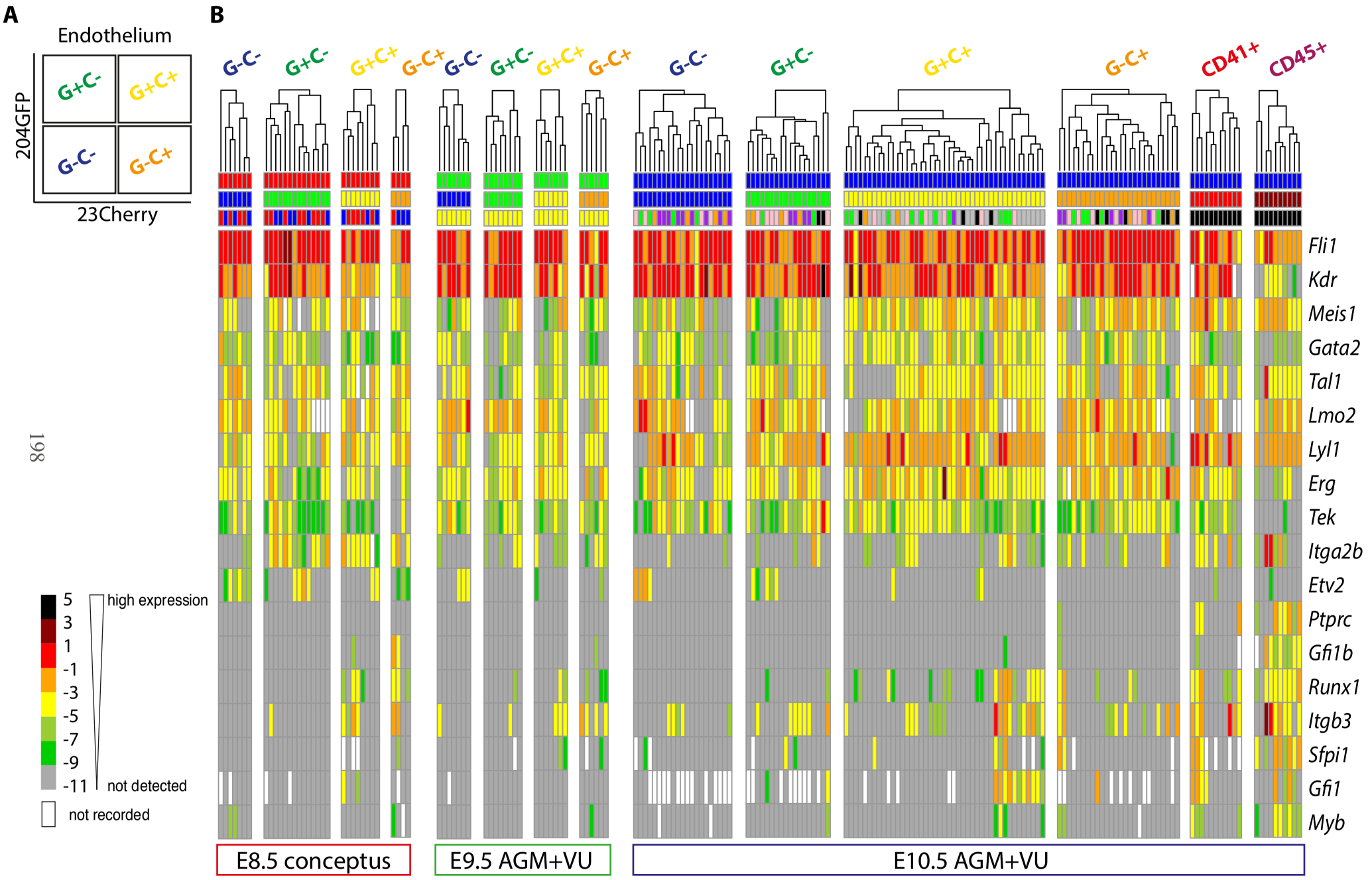


Figure 5.12 Single cell gene expression analysis of 4 endothelial subsets (continued)

Figure 5.12 (continued)
A) Schematic of a FACS plot where the endothelium was subdivided into 4 fractions based on 204GFP (G) and 23Cherry (C) expression. **B)** Heatmaps showing the expression of 18 genes involved during developmental hematopoiesis. Single endothelial cells of 4 different subsets were analyzed. The subsets were segregated based on differential expression of the 204GFP (G) and 23Cherry (C) transgenes. Three developemtal timepoint were analysed: E8.5 (6-7sp), E9.5 (19-26sp) and E10.5 (30-36sp). Data are deltaCt values to the mean of *Atp5a1* and *Ubc* housekeeping genes. Expression levels from 5 to -11 ranged from high to undetectable. White indicates not recorded values. Columns represent individual cells, hierarchically clustered for similar expression profiles. Rows represent individual genes. Data was filtered based on lack of *Kdr* and *Fli1* (with a simultaneous strong expression of *Gfi1b, Runx1, Itgb3* and *Myb*, indicative of erythroid cells). In addition, cells that expressed high *Meis1* (above -4) but no expression of *Gata2* and *Tal1* were considered mesenchyme and also filtered out. No filtering for endothelial cells was performed for CD41+ and CD45+ HPC control single cells. The raw, unfiltered expression heatmap is provided in Appendix **5.7.**

5.4 Summary and discussion

This chapter described the molecular profiling and enrichment of HE. In order to do so, I utilized the distinct expression patterns mediated by two *Runx1* enhancer reporter transgenes: the 204GFP and 23Cherry. The latter was generated via ES cell targeting and chimera generation and was shown to express 23Cherry in the same embryonic tissues and cells as the 23GFP transgene. In addition, functional assessment of the blood progenitor-forming potential of 23Cherry+ cells, confirmed that this novel reporter line behaves in comparable ways to the 23GFP mouse line. Next, 204GFP::23Cherry compound transgenic embryos were generated and the endothelium separated into four distinct populations based on combinations of marker expression. This allowed the identification of distinct endothelial subsets.

Single cell expression analysis

Combining the functional data from Chapter 4 with the preliminary molecular analysis in this chapter, it appears that the novel 204GFP transgenic mouse line labels HE. In addition, I have established that the E10.5 204GFP+ HE is able to generate blood progeny in culture. On a molecular level, such 204GFP+ HE exhibits a molecular signature comparable to the gene expression profiles of 23GFP+ HE, at least in the E9.5 AGM where the specifying HE was described (Swiers et al., 2013). When the endothelium was divided into 4 fractions based on 204GFP and 23Cherry expression, it was possible to further purify HE. The double-positive ECs had a higher frequency of cells with a specific hemogenic

gene expression signature at all timepoints analysed. Of note, although I was not able to functionally validate the 204GFP+ EC fraction at E8.5 (Figure 4.5), the molecular analysis in this chapter establishes that cells with a strong hemogenic signature are present within the 204GFP+ EC fraction (Figure 5.12). Inclusion of CD41+CD45- and CD41+CD45+ single cells in the E10.5 analyses allowed a better separation of gene expression signatures. Such hematopoietic cells will need to be included in the analysis of earlier timepoints, in order to get a clearer separation between the different cellular intermediates of the EHT.

In addition, it would be of interest to examine what the 204GFP and 23Cherry single-positive ECs are and how they differ from the 204GFP+23Cherry+ fraction. To that end, functional (single cell) assays and expression profiling would need to be performed to explore the nature of and lineage relationships between these cells.

Concluding remarks

The generation and combined use of novel *Runx1* enhancer-reporter mouse lines has allowed the separation of the developing endothelium into four distinct subsets. More importantly I have shown that the novel 204GFP mouse line is able to enrich for the HE population, thereby providing a valuable tool for future analysis. Molecular profiling has established subtle but consistently characteristic differences in the expression signature of HE and EC populations marked by differential *Runx1* enhancer reporter transgene expression. How the endothelial

subsets (which show a largely differential molecular signature) behave on a functional level remains to be established.

Chapter 6

Towards tracing the origin of hemogenic endothelium in the gastrulating embryo

One of the most disputed questions in the field of developmental hematopoiesis is whether embryonic and adult hematopoiesis share a common origin or emerge independently. Although it is well established that definitive HSCs emerge autonomously in the AGM region of the amniote embryo (Dieterlen-Lievre, 1975; Medvinsky and Dzierzak, 1996), the origin of its precursor, the HE is not clear. In other words, do the YS HE and AGM HE have a single or dual origin in the gastrulating embryo. Interestingly, in the frog embryo, the equivalent YS and intra-embryonic blood compartments have been traced back to distinct blastomeres (Ciau-Uitz et al., 2000). However, the origin of YS and AGM HE in the mouse embryo is less clear. Previously, the origin of the adult hematopoietic system, including all endothelial compartments associated with blood cells (HE), has been traced to the LPM ((Zovein et al., 2010), discussed in the introduction). The LPM, in turn, originates from specific segments of the primitive streak. This was determined in detailed fate mapping experiments where different subsets of the mesoderm were traced from labeled or grafted cells (Kinder et al., 1999; Lawson et al., 1991). It was shown that the primitive streak sequentially produces progenitors for, first, the YS mesoderm at the early streak stages, followed by progenitors for the intra-embryonic LPM at late-streak/bud stages (summarized in (Kinder et al., 2001)). However, the developmental window that generates LPM is relatively large and overlaps with other mesoderm progenitor subsets. Combined with the lack of suitable markers to identify HE specifically, it was therefore not possible to determine the exact origin(s) of HE in these previous studies. With the aim to revisit those fate mapping studies and

specifically address the primitive streak origin of HE, I utilized our 23GFP reporter line to mark the HE. In this chapter I first set out to report the early expression pattern of the 23GFP transgene in E6.5-E8.0 embryos. Specific knowledge of the expression pattern is necessary for future experiments on the origin of HE. In addition, I set up an *in vitro* culture system of post-implantation embryos, required for the primitive streak fate mapping experiments, and performed preliminary lineage tracing of the HE using dye labeling.

6.1 Expression of the 23GFP transgene in early-stage embryos

Phenotypic analysis of 23GFP expression in the pre-somitic embryo

Our lab has previously shown that the 23GFP marks all HE. In addition, at 7dpc only the 23GFP+ mesoderm (Flk1+VEC-/loCD41-) was able to give rise to endothelium, blood or a mixture of both from single cells (Swiers et al., 2013). Here I characterized the transgene expression at pre-somitic embryo stages, carefully staged according to Downs and Davies (Downs and Davies, 1993). Age heterogeneity within the same litter is very common in mouse development and especially at the earlier timepoints. This allowed me to acquire embryos, which ranged in developmental progress from the primitive streak (PS) to head fold stages (HF) when harvested at 6-7 days post-coitus (see schematic of pre-somitic and early-somite embryo stages in Figure 6.1).

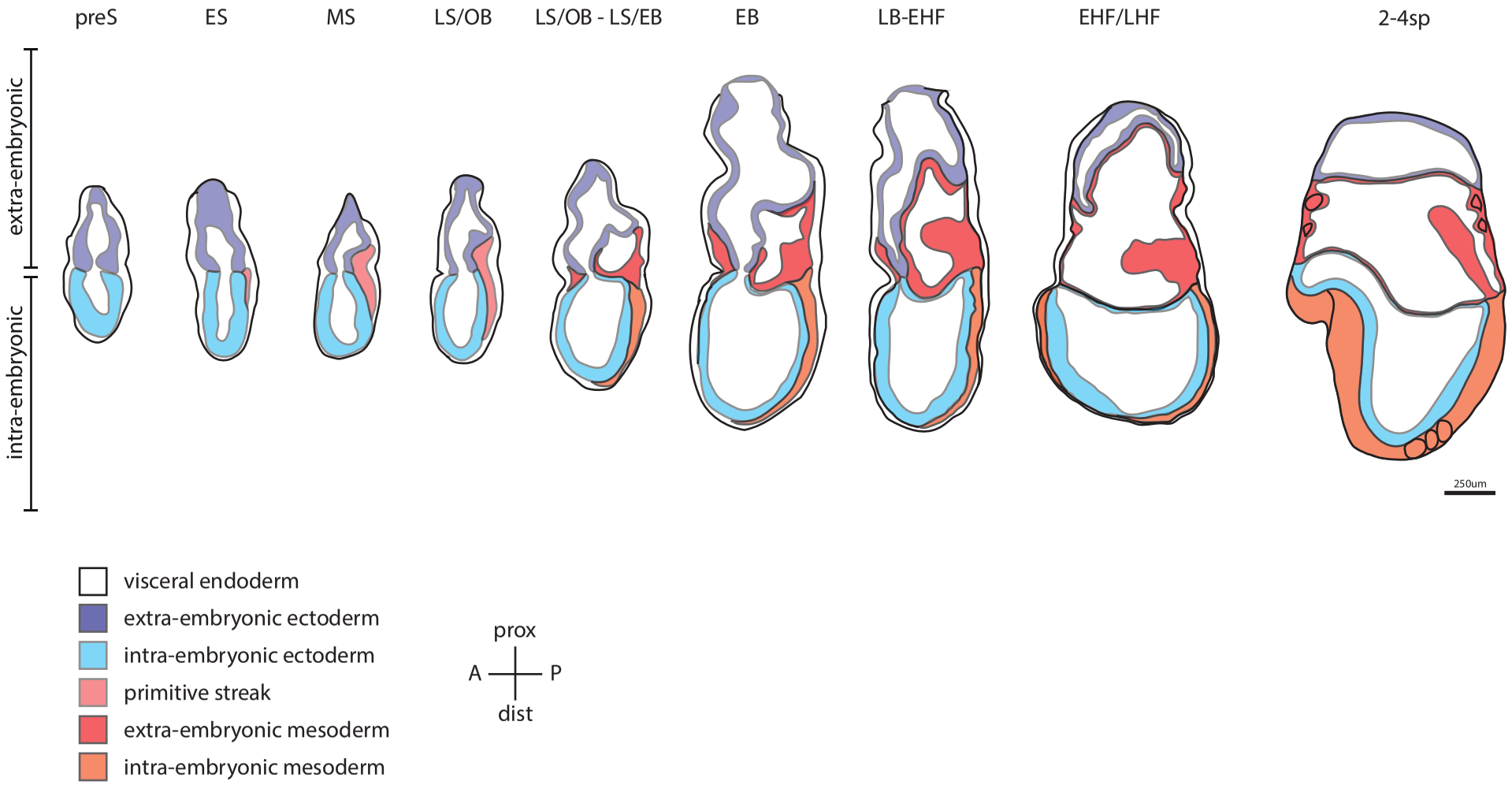


Figure 6.1 Schematic of pre-somitic and early somite pair mouse embryo morphology
Mouse embryo morphology from pre-streak (preS) to 2-4sp stages. Visceral endoderm as well as intra and extra-embryonic ectoderm and mesoderm are highlighted. Embryo orientation as shown. ES — early strew; MS — mid streak; LS/OB — late streak/zero bud; LS/EB — late streak/early bud; EB — early bud; LB-EHF —late but to early headfold; EHF/LHF — early headfold/late headfold; sp — somite pairs. Scale bar at 250um. Adapted from Pereira et al, 2011.

23GFP expression of unfixed concepti was initially observed as early as zero bud/early bud (OB/EB) stage in the extra-embryonic portion of the epiblast (not shown). When embryos were fixed and subjected to immunofluorescence staining and wholemount imaging, GFP was in fact present in the extra-embryonic portion as early as the late primitive streak stages (LS) and increased in intensity during development (Figure 6.2). From early bud stages a clear strip of 23GFP expression was present which encompassed the early blood island band of the extra embryonic mesoderm (Figure 6.2 D). Co-expression of CD31 and Runx1 confirmed this (solid bars in Figure 6.2, (Ema et al., 2006)). Slightly later, at the headfold stages, 23GFP expression started extending distally from the lateral parts of the blood island band to around the half-way mark of the embryonic portion (dashed bars in Figure 6.2 B, E, H, K). Such extension is a characteristic feature of the step-wise establishment of extra-embryonic vasculature and has been documented before (Chong et al., 2011; Drake and Fleming, 2000). Interestingly, detailed confocal analysis revealed that from early headfold stage (EHF) 23GFP expression is also initiated in the embryonic portion of the epiblast (arrow heads in Figure 6.2 E). To add, it coincided with CD31 expression, which at this time point labels the angioblast cells — precursors of the intra-embryonic vasculature (Figure 6.2 B, K). Further, Runx1 expression at the HF stage was still confined to the blood island band and no protein expression was observed in the intra-embryonic portion at this stage (solid arrow heads in Figure 6.2 H, K). This is in line with previous reports of Runx1 expression in the pre-somitic embryo, although low-level mRNA expression cannot be excluded

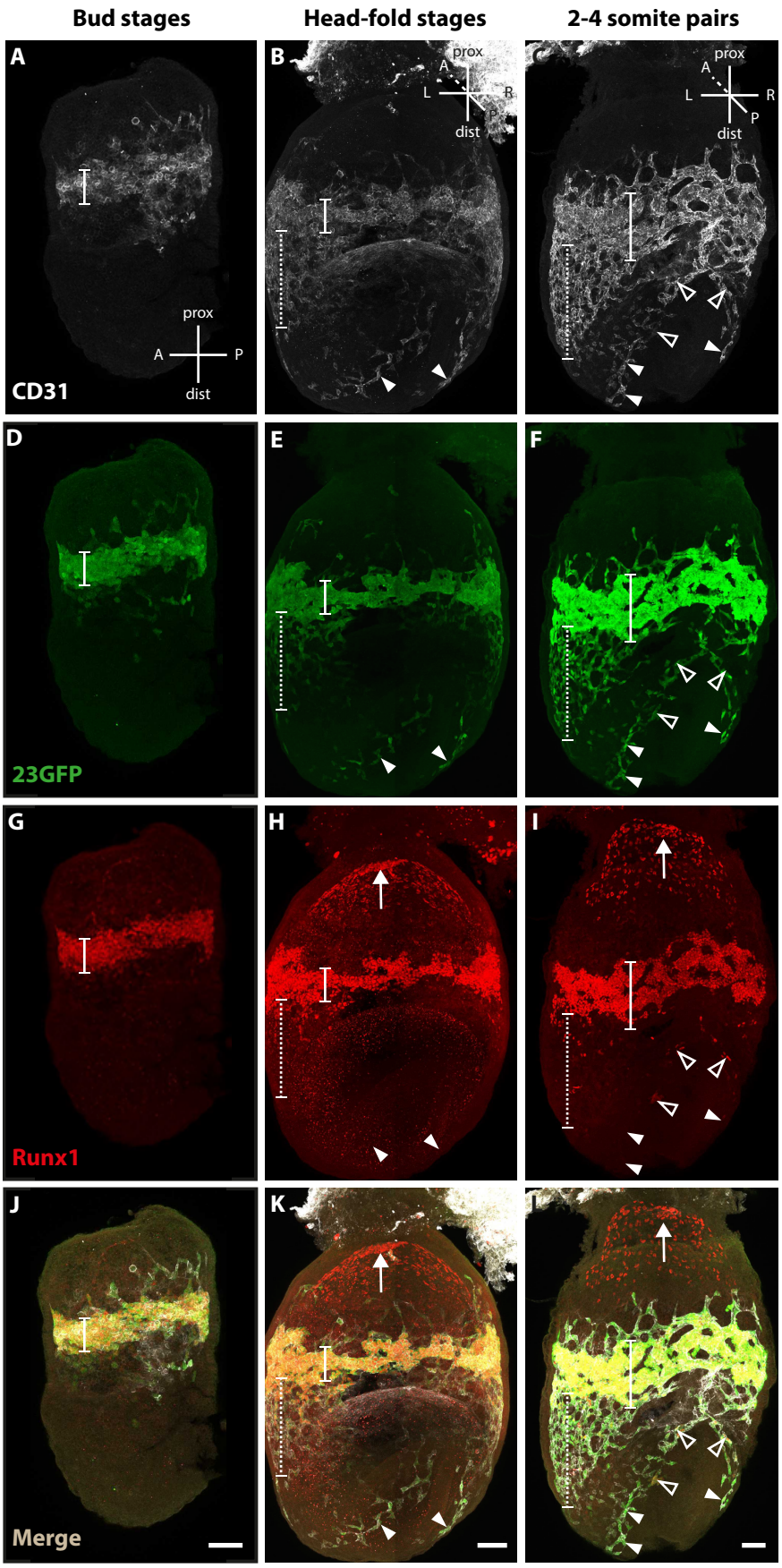


Figure 6.2 Expression patterns of CD31, 23GFP and Runx1 in the early embryo
A-C) CD31 (white) expression through the early mouse developmental stages. **D-F)** 23GFP (green) expression through the early mouse developmental stages. **G-I)** Runx1 (red) expression through the early mouse developmental stages. (continued)

Figure 6.2 (continued)
J-L) Merged images of CD31, 23GFP and Runx1 expression. Expression is shown at bud stages (**A**,**D**,**G**,**J**), the headfold stages (**B**,**E**,**H**,**K**) and 2-4sp stages (**C**,**F**,**I**,**L**). Block bars indicate the width of the extra-embryonic blood island band. Dashed bars indicate the lateral vasculature extensions from the blood island band. Solid arrowheads indicate 23GFP+ angioblast cells. Open arrowheads indicate Runx1+ expression within 23GFP+ angiogenic cord cells. Arrows indicate Runx1 expression within the chorion. Images were taken on the Zeiss 780 upright confocal microscope with a 25X oil-immersion objective. Embryo projections was reconstructed from tiled images and 5um optical slices. Orientation of embryos is indicated: A-P — anterior-posterior axis; prox-dist — proximal-distal axis; L-R — left-right axis. Scale bar at 50um.

(Daane and Downs, 2011; North et al., 1999; Zeigler et al., 2006; Lacaud et al., 2002).

Drake and Fleming previously reported a bi-directional development of the intra-embryonic vasculature, starting at the anterior and posterior ends of the embryo and joining intermedially (Drake and Fleming, 2000). In addition, CD31 expression in angioblasts was shown to increase in intensity with advancing maturation of the vasculature (angiogenic cords), with the stage of luminization of the fully formed vessels (paired aortae) coinciding with the strongest CD31 expression (Drake and Fleming, 2000). Similarly a gradual increase of CD31 expression levels in the developing angiogenic cords was observed. This increase was accompanied by rising levels of 23GFP expression in the majority of intra-embryonic CD31+ angiogenic cord cells (solid arrow heads in Figure 6.2 C, F, L). Interestingly, from the late headfold stage (LHF, not shown), and specifically in the early somite pair stages, I observed the first Runx1 expression in intra-embryonic angioblast cells which co-expressed with CD31 and 23GFP (open arrow heads in Figure 6.2 I, L).

In addition to the progressive maturation of the intra-embryonic vasculature, the extra-embryonic vascular network forming laterally in the 2-4sp embryo became more pronounced (E8.0). The distally moving extension covered around 2/3 of the lateral embryonic halves at this stage (dashed bars in Figure 6.2 C & L). A small subset of cells that seemed to move proximally from the blood island band was also observed, although these cells were only marked by CD31+23GFP+ and none expressed Runx1. Of note is the striking Runx1 expression in the chorion (Figure 6.2

H, I), which has been previously reported elsewhere (Zeigler et al., 2006; Lacaud et al., 2002).

Live imaging of early-stage 23GFP transgenic embryos

To follow the dynamic 23GFP expression pattern of pre-somitic embryos, I imaged HF embryos overnight. One brightfield (mid plane) and a whole z-stack of GFP images was taken every 20 minutes over the duration of 6-7h. When viewed as a movie, I observed the dynamic intra-embryonic expression of the 23GFP transgene (Movie 1 and 2). Similar to the wholemount analysis in Figure 6.2, a gradual upregulation of 23GFP in the sites of paired angiogenic cords was observed. Since I lacked a reporter transgene for the early endothelium, this observation was based on morphology and anatomical hallmarks of the embryo. Movie 1 shows a clear increase of 23GFP expression in terms of the number of cells expressing as well as the level of expression (compare 145min to 290min time point in Figure 6.3 B). In the last part of Movie 2, I also observed an example of luminization of the paired aortas (dashed circle at 308min in Figure 6.3 C). The gradual initiation of 23GFP expression appeared to follow an anterior to posterior direction (yellow arrows in Figure 6.3 B and Movie 1). In addition, the 6h 20min-long movies stopped before 23GFP was observed in the most posterior part of the two angiogenic cords (converging around the vessel of confluence (VoC;) (Daane and Downs, 2011), suggesting embryogenesis had not reached the early somite pairs yet (compare to Figure 6.2 C,F).

When analyzing 23GFP expression at the extra-embryonic blood island

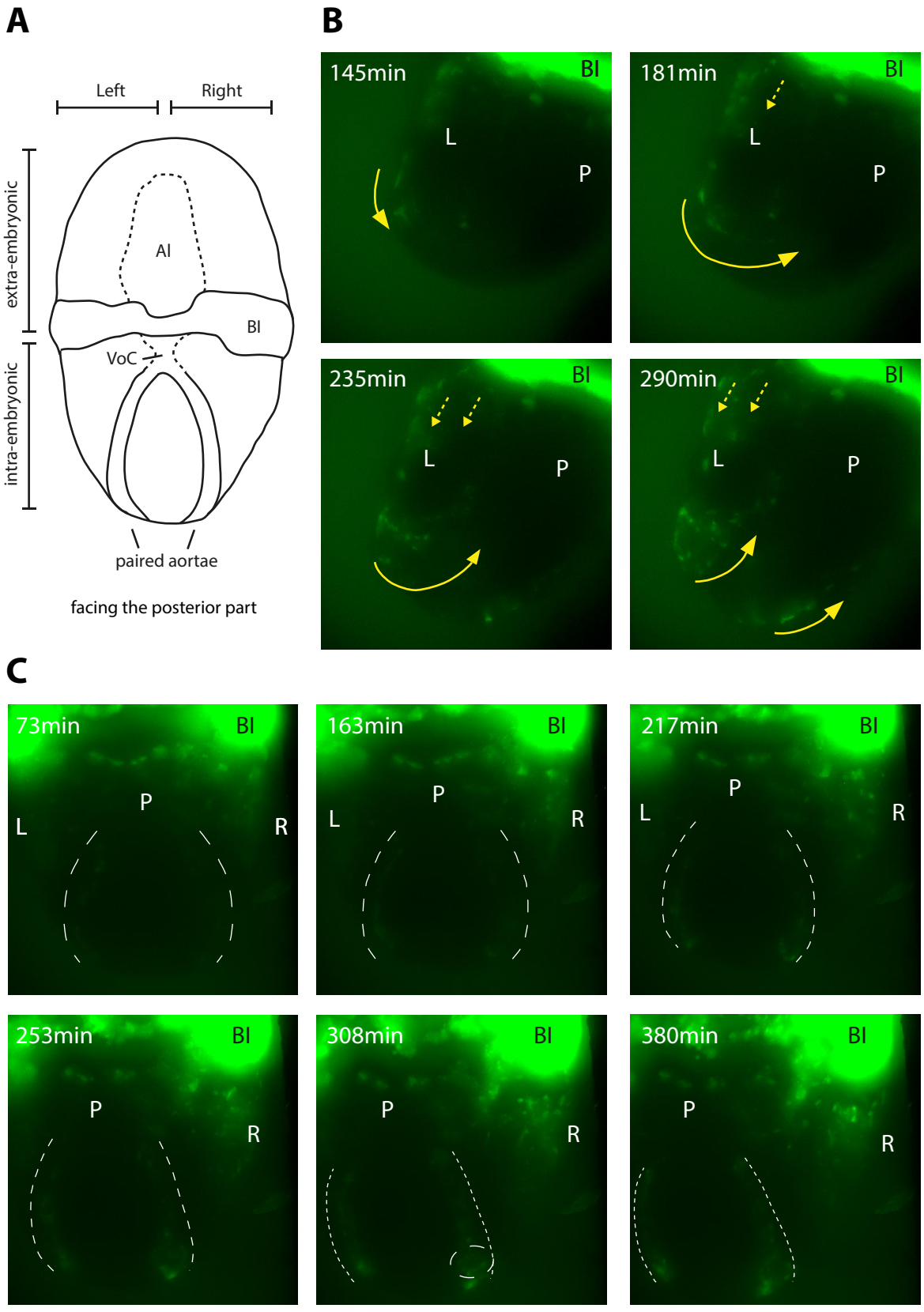


Figure 6.3 Dynamic upregulation of 23GFP expression in the developing intra-aortic vasculature at 7dpc
Still images of live videos. Images are the projection of Z-stacks at the timepoints of imaging indicated. Headfold stage embryos were cultured for 6h 20min and imaged every 20min. (continued)

boundary, I again observed bi-lateral (left and right) expansion of 23GFP expression towards the distal part of the epiblast (dashed yellow arrows in Figure 6.3 B). Analyzing the expression in real-time, revealed that although some movement of 23GFP+ cells in those lateral areas exist, these cells did not move far. Instead, the growth and the 3-dimensional expansion of the embryos contribute to the illusion of cell migration (Movie 2). In addition, no migration of such lateral cells into the proximity of intra-embryonic angiogenic cords was witnessed. Additionally, the characteristic gap between the YS vasculature and the paired aortas was also evident in the transgenic embryos (n=10).

Quantification of 23GFP expression at pre-somitic stages

Next I quantified 23GFP expression in the intra- and extra-embryonic portions of concepti at 3 developmental stages, to determine the percentage of 23GFP expression within the mesoderm (Flk1+VEC-CD41-CD45-) and endothelium (Flk1+VEC+CD41-CD45-) (Figure 6.4, gating and FMO controls in Appendix Figure 6.1). Both mesoderm and endothelium was present in the extra embryonic part starting from the primitive streak stages onwards. In the embryo proper, endothelial cells were not detected until later, at the headfold stage, while mesoderm was seen from the primitive streak stage. The onset of endothelial expression intra-embryonically nicely corroborates the imaging data (Figure 6.2). Similar to the imaging data, 23GFP was marking all extra-embryonic endothelium and a large proportion of the mesoderm (Figure 6.5). Also, the intra-embryonic endothelium of the HF stage embryo was almost exclusively

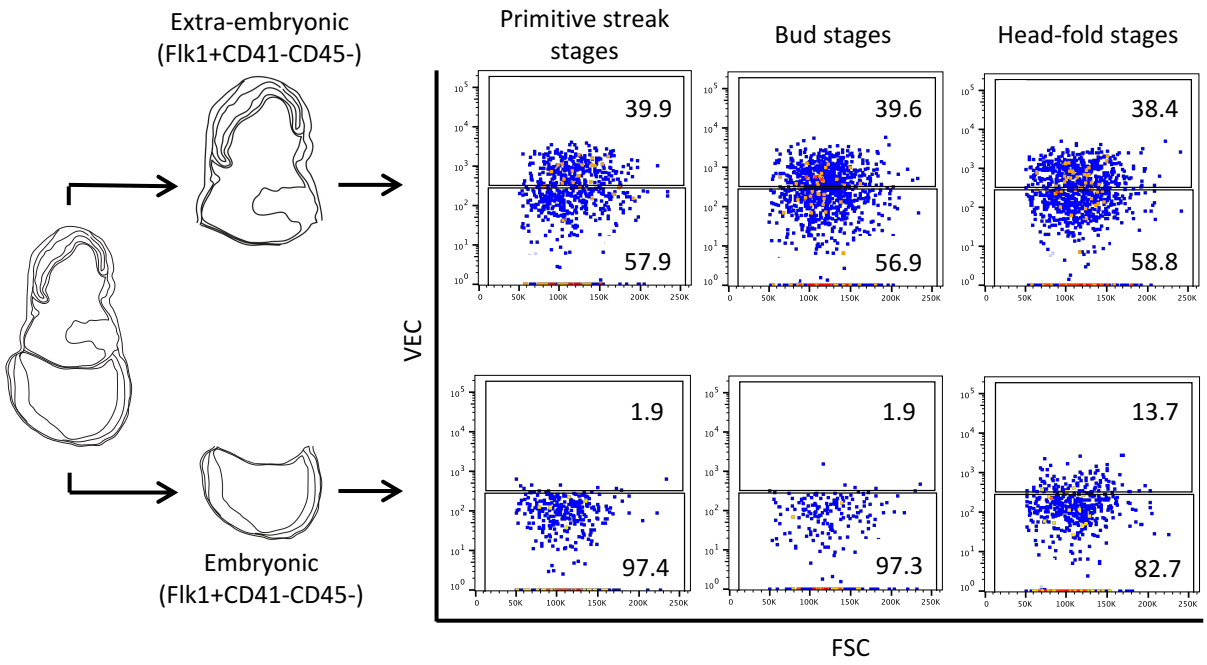


Figure 6.4 VEC+ endothelium in extra- and intra-embryonic portions of pre-somitic embryos

Schematic representation of split 7dpc embryos that were gated for Flk1+CD41-CD45-VEC+/-. Three separate pre-somitic stages are indicated. n=1

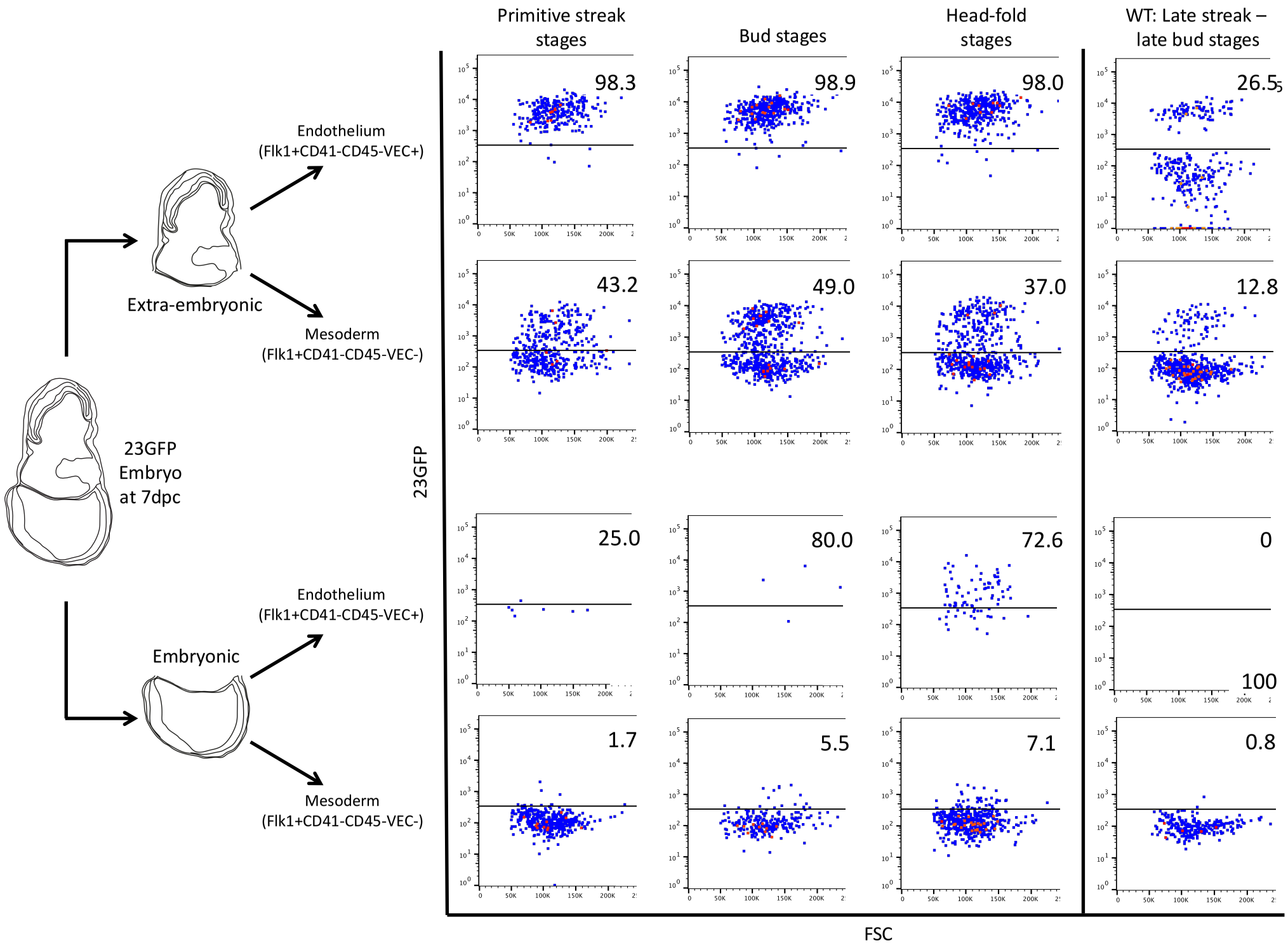


Figure 6.5 23GFP expression analysis in endothelial and mesoderm fractions of 7dpc embryos
Schematic representation of 7dpc embryos where the Flk1+CD41-CD45-VEC+ endothelium and Flk1+CD41-CD45-VEC- mesoderm were analyzed for 23GFP expression within intra- and extra-embryonic portions. Percentages for three developmental stages are shown (n=1). WT embryos are late streak to late bud stages served as GFP control.

23GFP+ (73%), while the intra-embryonic mesoderm showed only little 23GFP expression (increase from 2% to 7% from PS to HF stages). Since in this experiment embryos were ‘genotyped’ based on GFP expression, It is possible that a very early embryo that did not show obvious 23GFP expression yet was included in the WT pool leading to the 23GFP expression observed in the extra-embryonic WT control plot (Figure 6.5). For future experiments the placental cones need to be genotyped by PCR, to avoid contamination.

Collectively, I determined the initiation of 23GFP expression in the mesoderm as well as the endothelial populations, both in sections and in live imaging. My data suggests that at the early embryo stages almost all endothelial cells are 23GFP+, while smaller subsets of the mesoderm were marked by the 23GFP transgene. Future experiments, such as single cell expression profiling will reveal whether this early 23GFP+ endothelium is already primed for a hemogenic fate.

6.2 Establishing and optimizing in vitro cultures of pre-somitic embryos

In order to manipulate or image early stage embryos in culture for lineage tracing purposes, I optimized and established a static in vitro culture system in the lab. The choice of media was critical for embryo survival during culture. CMRL media resulted in the best outcome judging by survival and overall embryo morphology after culture. Depending on which

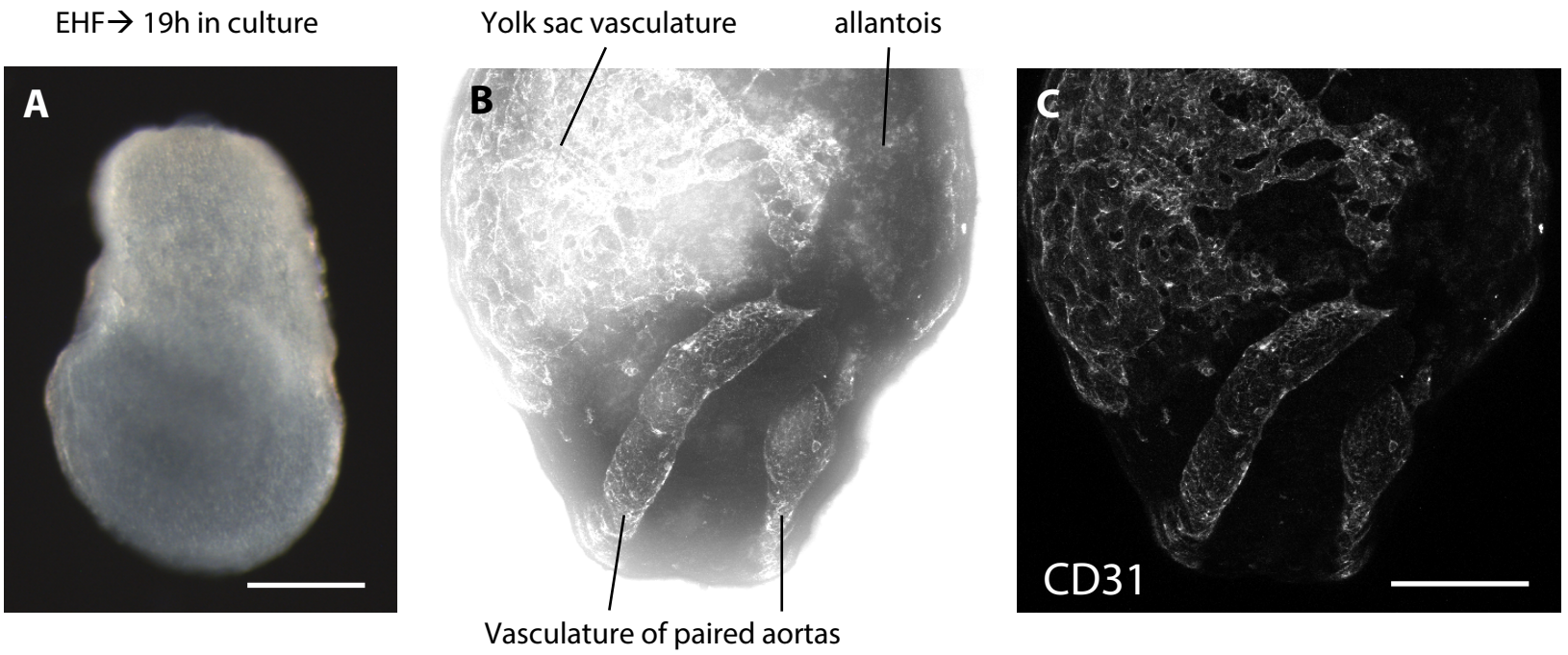
stage of development the embryos were placed into culture, the growth and survival outcome varied. In general, the younger the embryos were (PS stage) the more difficult it was to keep them alive in culture. Slow growth and expansion of epiblasts as well as undefined morphological features were often accompanied with necrotic tissues (opaque-grey in color, not shown). On the other hand, older embryos (bud-HF stages) successfully continued their development in culture. Such embryos grew in size and expanded and retained all gross embryonic structures. Somite pairs formed and it was often (but not always) possible to count these post culture. The majority of embryos exhibited a noticeable heart twitch after 26±2 hours in culture, and in some cases a fully beating heart with visible circulation (Movie 3). However, circulation did not fully establish in all cases (not shown), suggesting that either the heart of cultured embryos was not strong enough to pump blood through the entire conceptus or that not all vasculature had formed allowing a circulatory loop to establish. YS blood islands formed successfully in cultured embryos, judging by strong 23GFP expression in transgenic embryos, as previously documented. The most striking morphology was the largely extended exocoelom of all cultured embryos. This phenomenon seems to be a common occurrence in early stage, ex utero cultured embryos (Kinder et al., 1999). It may be due to absence of uterine muscle tension ‘keeping’ the epiblast compact or the build-up of additional fluid in the exocoelom due to osmolarity differences between the embryonic fluids and the culture medium.

To assess if the embryonic vasculature had formed correctly during

culture, I analyzed the CD31 expression in EHF-stage embryos cultured for 19h (Figure 6.6 A). CD31 expression was clearly present in cultured embryos and defined two distinct vessels of the paired aortas as well as the yolk sac vascular network and blood islands (Figure 6.6 B & C). An overall increase in the diameter of the paired aortae (not formally measured) was also observed. The reason for this is not known, but it could also result from osmolarity issues or absence of uterine muscle tension.

Next, I determined whether cultured embryos exhibited similar phenotypic and functional characteristics to uncultured stage-matched embryos. Late bud (LB) and HF embryos were culture for 23h, until they developed 4-6sp and 6-9sp, respectively. These were then compared with uncultured embryos staged at 8sp and 10-13sp, based on VEC and CD41 expression. Broadly comparable percentages of VEC and/or CD41 positive cells were seen in cultured and uncultured 8sp embryos (Figure 6.6 D). Cultured embryos showed endothelial expression (VEC+CD41-/lo) as well as a small subset of hematopoietic cells (CD41+), likely derived from the YS component. The cultured HF embryos that developed to 6-9sp showed particular similarity to the 8sp uncultured embryos.

I also subjected cultured and uncultured embryos to colony-forming assays (CFU-Cs). Cell suspensions of HF-stage embryos cultured to 8-9sp, PS-stage embryos cultured to LHF and uncultured E8 (6-10sp) embryos were plated into methylcellulose medium supplemented with



E

	CFU-C_{d7}/10000 cells	CFU-C frequency
Uncultured E8: 6-10sp	11±2 *	1:916
Cultured 7dpc: HF → 8/9sp	26 **	1:378
Cultured 6dpc: PS → LHF	16 ***	1:724

Figure 6.6 Phenotypic and functional validation of pre-somitic embryos cultured in static conditions

A) Brightfield image of an EHF embryo after dissection and prior to 19-hour culture. **B,C)** Same embryo after 19h in static culture. Brightfield image overlain with CD31 (white) expression (**B**). The yolk sac vasculature, allantois and paired aortae are shown. CD31 expression only (**C**). Scale bars at 250um. **D)** Flow cytometry expression analysis of Ter119-CD45- gated VEC and CD41 expression in embryos cultured from 2 different developmental stages (LB and HF) for 23h compared to uncultured, freshly harvested E8 embryos (8sp and 10-13sp) n=1. **E)** Table summary of CFU-C/10000 cells plated and CFU-C frequency of uncultured and cultured embryos. *CFU-C number ± S.D (n=3); **CFU-C number (n=1); ***average CFU-C number (n=2).

hematopoietic growth factors and colonies counted after 7 days. Importantly, all embryos tested harbored colony-forming cells (CFU-C) (Figure 6.6 E). Analysis of additional embryos will reveal if the small differences in frequencies observed are meaningful.

6.3 Tracing the origin of hemogenic endothelium

Set up of fate mapping experiments using DiI labeling

Having determined the exact expression pattern of the early 23GFP transgenic embryo and having established an in vitro culture system of pre-somitic embryos gave me the opportunity to initiate fate mapping experiments of specific segments of the primitive streak. The ultimate goal in this was to determine which primitive streak segments give rise to HE. I therefore set up PS-labeling experiments, similar to those performed by Kinder and Lawson (Kinder et al., 1999; Lawson et al., 1991). Here, however, I specifically focused on the PS origin of the HE subsets, marked by the 23GFP transgene. To that end, 23GFP transgenic embryos were harvested at 6-7 dpc, carefully dissected and staged. Further, transgenic embryos were injected with CM-DiIC18(3), from here on referred to as DiI, into specific segments of the primitive streak. DiI is a carbocyanine dye and highly lipophilic. It is incorporated in cell membranes, has a strong red fluorescence signal and was previously used in similar cell tracing and fate mapping studies (Bildsoe et al., 2007). Immediately after injection, each embryo was briefly imaged, to record the exact site of DiI injection, and

then cultured in individual wells for 24-50h (see schematic in Figure 6.7). After culture, gross morphology and expression of 23GFP and DiI fluorescence were recorded and embryos fixed for cryosectioning or whole mount imaging protocols. Embryos that showed both 23GFP and visible DiI expression were then analyzed by confocal microscopy to determine the exact tissue marked by the dye (Figure 6.7).

Distinct PS segments contribute to YS and intra-embryonic 23GFP+ HE

Previous experiments using either cell-labeling techniques or autologous graft transplants have established a mesoderm fate map of the mouse primitive streak, but HE was not examined directly (Kinder et al., 1999, 2001; Lawson et al., 1991; Parameswaran and Tam, 1995; Tam and Beddington, 1987; Tam et al., 1997). An adaptation of the mesoderm fate map is depicted in Figure 6.8. The first cells to go through the primitive streak of early- to mid-streak embryos give rise to mostly erythrocytes and YS ECs (dark blue and medium blue in Figure 6.8). The mid- to late-streak (bud stage) PS continues to generate mesoderm progenitors of YS endothelium (light blue) but more distal segments of the ingressing PS also contribute to first the heart and cranial mesoderm (bright pink) and slightly later to the lateral plate (light pink) and paraxial mesoderm (yellow). By the late-streak or headfold stage the PS extends from the extra-/intra-embryonic boundary to the distal tip of the embryo. At this stage, it continues to generate mesoderm destined for YS endothelium, but also the bulk of lateral plate and paraxial mesoderm (Figure 6.8).

I was able to revisit parts of the fate mapping in preliminary experiments.

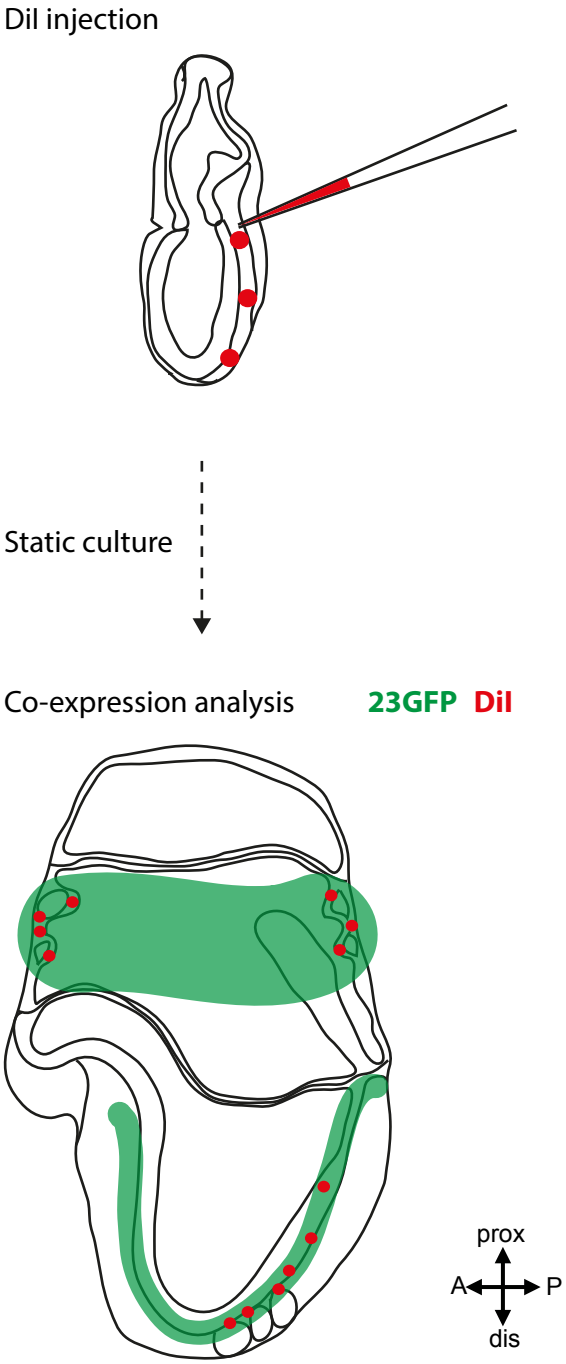


Figure 6.7 Schematic of the experimental set up for dye-labeling fate mapping experiments
Carefully staged 6-7dpc embryos are injected with DiI in different primitive streak positions (red). The position is visually recorded immediately after injection. Embryos are allowed to develop in static culture and expression of 23GFP and DiI visually recorded prior to embryo fixation for further analysis. Co-expressing embryos were either sectioned or processed for wholemount imaging. Embryo orientation is indicated.

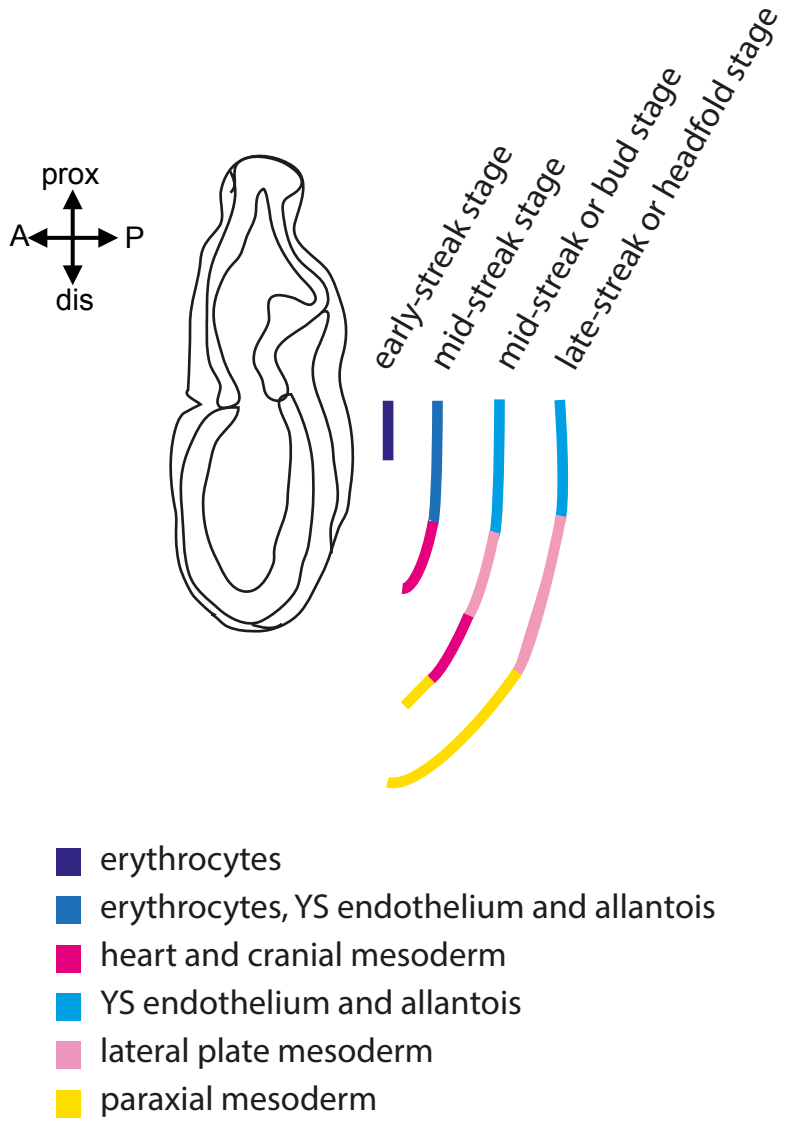


Figure 6.8 The primitive streak fate map
Schematic representation of the primitive streak extension and proposed mesoderm allocation in relation to embryonic development (early-streak to late-streak/headfold stage, 6-7dpc). Embryo orientation is indicated. Adapted from Kinder et al, 2001.

When the most posterior segment of the PS at the mid-streak stage was injected with DiI (red), it resulted in the DiI-labeling of YS erythroid progenitor cells and endothelial cells after 50h in culture (arrow heads in Figure 6.9, n=6). In addition, I observed co-expression of DiI with 23GFP in individual endothelial cells (Figure 6.9 B). Superimposing the proposed fate map of the primitive streak at this stage of development indicates that the dye injections targeted the right PS segment (Figure 6.9 A). Of note DiI did not interfere with the initiation of 23GFP expression within YS HCs and ECs. As static cultures are not optimal for embryo development, the intra-embryonic portion of the conceptus lacked clear morphological landmarks, while it was still possible to clearly distinguish the extra-embryonic YS (cf. Appendix 6.2 A). However, no GFP expression was observed within the embryo proper (Appendix 6.2 A). Obviously, for future studies a more reliable culture system (e.g. roller cultures) for the earliest embryonic time points needs to be established and optimized (Tam, 1998). In comparison to static cultures, roller cultures have been shown to better support embryonic growth ex utero. It is thoughts that the rolling motion is mimicking the movement of the mother mouse as it develops (Tam, 1998).

This was different at 7dpc; the middle PS segment of LB/EHF embryos were injected with DiI and embryos cultured for 28h (Figure 6.10 A). This time, DiI expression localized to intra-embryonic areas (n=3). In one such embryo, which was sectioned and stained for CD31 expression, the vasculature of the paired aortae showed DiI labeling (arrow head in Figure 6.10 B). Furthermore, 23GFP+ HE was labeled in these embryos.

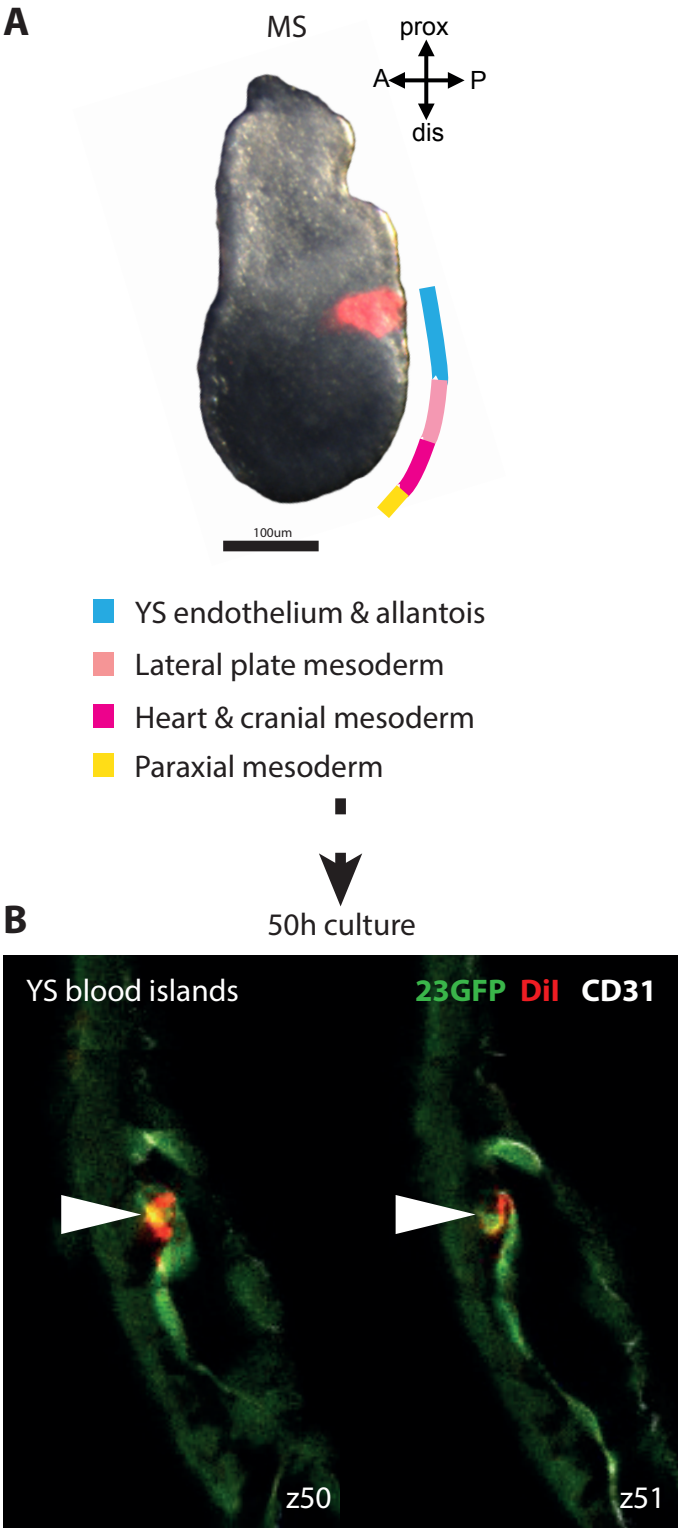


Figure 6.9 Fate mapping the extra-embryonic hemogenic endothelium
A) Brightfield image of a 23GFP transgenic embryo at mid-streak stage. DiI (red) was injected into the posterior most portion of the primitive streak. The proposed mesoderm allocations of the primitive streak are indicated. Embryo orientation is indicated. Images were taken on the Leica MZFLIII brightfield microscope with a 1X planapo objective. Scale bar at 100um. **B)** After 50h in static culture DiI co-expressed with 23GFP+ hemogenic endothelium (arrow heads) in the yolk sac CD31+ vasculature as observed in consecutive z-slices (z50, z51). Images were taken on the Zeiss 780 upright confocal microscope with a 25X oil-immersion objective. The embryo projection was reconstructed from tiled images and 2um optical slices. Optical zooms were generated in the IMARIS software.

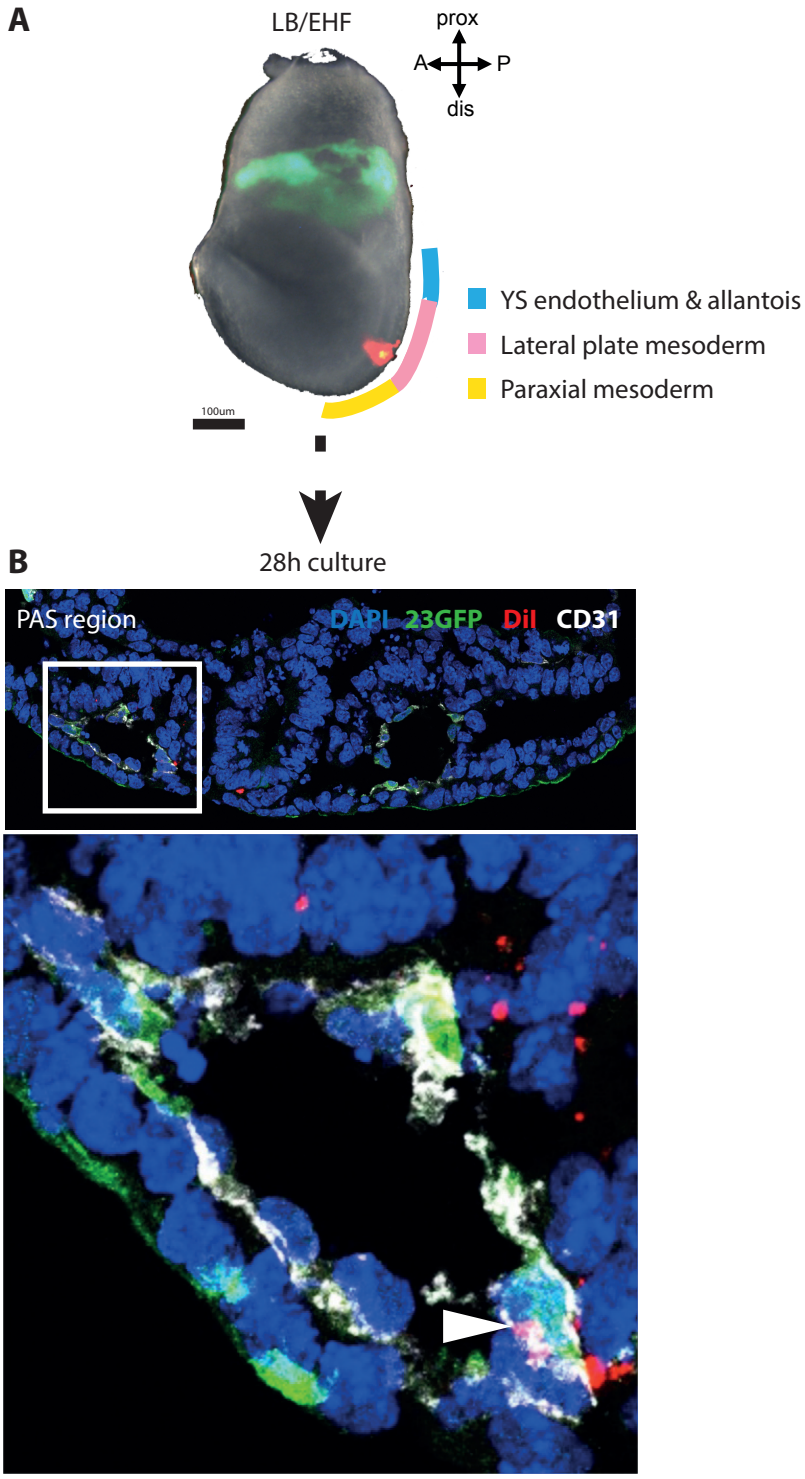


Figure 6.10 Fate mapping intra-embryonic hemogenic endothelium
A) Brightfield image of a 23GFP transgenic embryo at late bud/early headfold stage. DiI (red) was injected into the middle of the primitive streak. The proposed mesoderm allocations of the primitive streak are indicated. 23GFP expression was already present in the YS blood islands. Embryo orientation is indicated. Images were taken on the Leica MZFLIII brightfield microscope with a 1X planapo objective. Scale bar at 100um. **B)** After 28h in static culture DiI was observed in the PAS region. DiI was co-expressed with 23GFP+ hemogenic endothelium (arrow head) in the CD31+ vasculature of the paired aortas (zoomed in imaged of boxed area). Nuclei were stained with DAPI (blue). Images were taken on the Zeiss 780 inverted confocal microscope with a 40X and 63X oil-immersion objective. The PAS image was reconstructed from tiled images.

Consulting the fate map, the area of labeling corresponded to the lateral plate mesoderm, an area directly linked to the HSC lineage (Pardanaud et al., 1996; Wasteson et al., 2008; Zovein et al., 2010). In addition, the specific PS segment injected here, did not result in DiI-labeling of the YS endothelium and was only restricted to the PAS region (Appendix 6.2 B). This further strengthens the PS fate map at the late streak/HF stages, since only posterior-most parts of the PS contribute to the YS endothelium.

In conclusion, I have successfully labeled specific mesoderm precursors of extra- and intra-embryonic HE, marked by the 23GFP transgene. Evidently, this data is preliminary and more embryos need to be injected (potentially with a different labeling agent) and analyzed in detail. Further, more elegant studies need be performed, since the DiI labeling system has its disadvantages such as the unreliable distribution of DiI to daughter cells and the difficulty handling the dye crystals, which do not readily dissolve. However, results presented here are a promising start in order to map the exact origin(s) of the YS and AGM HE.

6.4 Conclusions and discussion

In this chapter I revisited early fate mapping studies and performed preliminary dye labeling experiments marking specific subset of the PS. I observed dye labeling in the 23GFP+ HE in the YS and separately in the PAS endothelium. These data are in line with previous fate mapping studies of the PS mesoderm and provide a basis for further experiments.

As a next step, roller cultures (Tam, 1998) will be set up and optimized for the fate mapping experiments, as those are known to better support embryo development.

When does hemogenic endothelium become hemogenic?

Here I have established a detailed description of the 23GFP expression pattern in the early mouse embryo. Such analysis revealed the location of the earliest 23GFP-marked angioblasts, and therefore putative HE. Interestingly several studies have suggested that all nascent ECs have the potential to respond to blood-inducing signals and are therefore hemogenic (Richard et al., 2013; Swiers et al., 2013). The observation that virtually all YS HE and around 70% of intra-embryonic endothelium at the headfold stage express the 23GFP transgene (Figure 5.6), suggests that at this early stage virtually all endothelial-like cells (Flk1+VEC+CD31+) may have hemogenic potential. By E8.5 the 23GFP transgene only labels 30% of the PAS endothelium (Swiers et al., 2013), suggesting that only a subset of ECs are HE. Indeed, functional and molecular analysis of the E8.5 HE indicated that these cells are competent to respond to blood inducing factors. To test if also earlier 23GFP+ endothelium has (latent) hemogenic potential, functional studies on the early 23GFP+ endothelial subset could be performed, to assess the hemogenic potential of this nascent endothelium. Since the OP9 co-cultures are already technically challenging at E8.5 (Chapter 4; Swiers et al., 2013), those assays may prove difficult to perform on the 7dpc endothelium. Instead, the molecular signature of 23GFP+ ECs could be analyzed and compared to the 23GFP-

EC subset of the 7dpc embryo, in order to identify potential hemogenic signatures of the former. Recently, two studies have analyzed single cell gene expression patterns at various stages of mouse gastrulation (Moignard et al., 2015; Scialdone et al., 2016). The main findings revealed that cells mature at different speeds and many express both *Kdr* and *Runx1* (the expression of the latter was used to segregate ECs from blood), indicative of hematopoietic specification and/or commitment (Moignard et al., 2015). As the 23GFP transgene expresses prior to Runx1 expression in the embryo proper (Swiers et al., 2013), it would be of interest to perform similar transcriptome analysis on specifically 23GFP+ ECs. In addition, previous studies never dissected the intra- and extra-embryonic parts prior to analysis. Doing so may provide further insights into the molecular signature of the YS and AGM HE.

Tracing the origin of HE

While most endothelial cells at 7dpc are 23GFP+, they later get 'diluted' by non-23GFP-expressing ECs, which potentially originate from different segments of the primitive streak. This may point toward an early segregation of the hemogenic and vascular endothelial lineages similar to the one described in the *in vitro* ES cell differentiation system (Ditadi et al., 2015) (Chapter 1, section 1.10). In order to assess such theory, lineage tracing studies using an inducible 23-Cre mouse line are required. The +23-mediated Cre activity could then be induced at specific timepoints early in development and asses their contribution to HE, EC and HC.

Further, in order to trace the origin of HE, PS grafting experiments can be

performed, whereby specific segments of the 23GFP transgenic PS could be grafted into the PS of WT embryos and 23GFP expression observed after appropriate culture. This would establish which PS segments are able to induce 23GFP expression when grafted into the right permissive PS environment.

Additionally, in order to trace the origin of HE on a clonal level, low-frequency inducible Cre expriments can be performed, utilizing an endothelial marker (e.g. Etv2, Tie2). This would allow the labeling of distinct cells of the PS, which could then be followed to the 23GFP+ HE. This is a similar experimental approach as the one used by Padron-Barthe and colleagues who showed that YS blood and endothelium of the blood islands are already segregated at the epiblast stage (Padron-Barthe et al., 2014), Chapter 1, Section 1.5).

Overall I have initiated studies into the origin of HE, utilizing the 23GFP mouse line to label HE. Preliminary dye labeling experiments established that it is possible to label 23GFP-marked YS HE or AGM HE, depending on the stage and location of the dye injection. In order to address the question of single or dual origin of HE, further lineage tracing and/or cell grafting approaches will be undertaken in the lab.

Chapter 7

General discussion

7.1 Summary of results

The work described in this thesis aimed to contribute to our knowledge of HE by identifying more specific markers to purify this population for functional and molecular studies. I utilized the cell type-specific activity of different *Runx1* enhancers to isolate specific subsets of the developing endothelium. I have generated a novel 204GFP mouse line and have shown that it marks all sites of developmental hematopoiesis and recapitulates parts of endogenous *Runx1* expression (**Chapter 3**). In contrast to the +23 enhancer (which marked all stages of EHT), the +204 enhancer marked all functional HE and part of the LT-HSCs, but did not label clonogenic blood progenitors (**Chapter 4**). This provided a basis to study specifically HE on a molecular level by analyzing expression patterns of several genes associated with hematopoietic development. Based on the molecular signature in a subset of cells, I have identified that expression of the 204GFP transgene enriches for HE. Co-expression analysis of the 204GFP and another novel reporter line generated here (23Cherry), established that when used in combination, both transgenes label a small percentage of the endothelium which comprises the functional HE. In support of this, I also detected an upregulation of hematopoietic genes in the double-positive HE cells of compound transgenic embryos (**Chapter 5**). Apart from being tools to isolate and study HE, the *Runx1* enhancer-reporter transgenes can be used to trace back the developmental site of origin of HE. In **Chapter 6**, I initiated studies to revisit early fate mapping experiments, utilizing the 23GFP reporter mouse line to mark all HE. Previous studies never directly

addressed the HE origin due to lack of suitable markers available. Here, my preliminary experiments show that using a dye labeling approach in 23GFP transgenic embryos, it is possible to trace the 23GFP+ HE in the YS and PAS region to specific segments of the PS (**Chapter 6**).

7.2 Hemogenic endothelial subsets or maturation stages?

One of the aims of this thesis was to identify new tools in order to further purify or sub-dissect the HE population. Interestingly, contrary to the latter speculation, the 204GFP was not labeling a particular subset of HE (as shown functionally), but rather allowed a further purification of HEs: I have shown that isolation of ECs based on co-expression of the 204GFP and 23Cherry transgenes allowed for further enrichment of the HE population (Figure 7.1 A). This is an important finding as previous analysis of HE was hampered by the lack of specific HE markers. I have also initiated studies into the molecular signature of this enriched HE population. Such gene expression analysis confirmed that the 204GFP+23Cherry+ endothelial subset exhibits clear signs of a HE signature, so these enhancer-reporter tools will facilitate further molecular profiling studies. To add, some 204GFP and 23Cherry single-positive ECs showed elevated expression levels of hematopoiesis-associated genes. However, the number of cells analyzed is too small to exclude a stochastic effect. In addition, I already discussed the possibility of contamination from neighboring populations at the time of the sort and future experiments will take these technicalities into account. Despite these considerations, it would also be interesting to

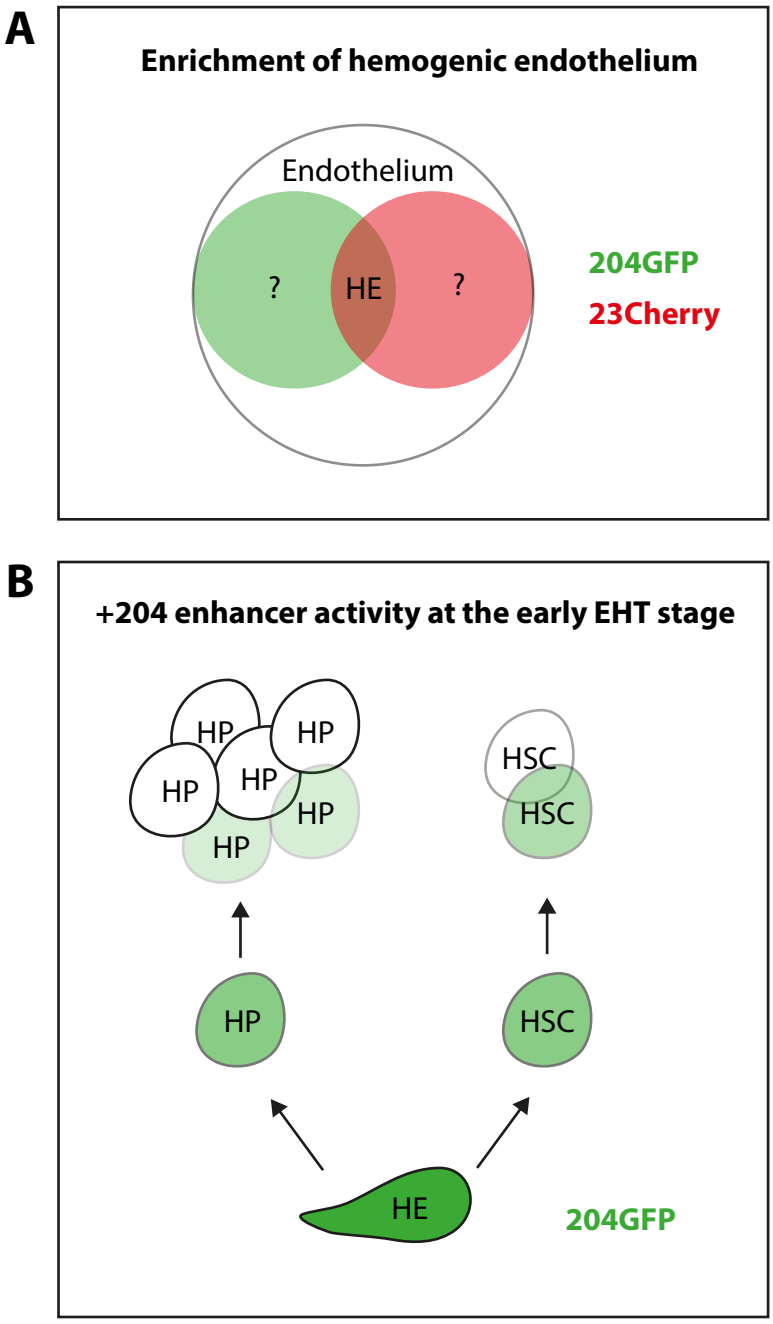


Figure 7.1 Cell type-specific *Runx1*-enhancer activities to study hemogenic endothelium
A) The combined activity of the +23 and +204 Runx1 enhancers allows the isolation of an endothelial population that is enriched for hemogenic endothelium, providing a valuable tool for further analysis. **B)** A model to depict the cell type specific activity of the +204 enhancer, which specifically marks the early EHT cellular intermediates (HE and early precursors) but not mature blood cell cell types. Proliferation levels in hematopoietic progenitors (HP) are higher than in HSCs, likely contributing to the dilution of any residual GFP in those EHT popualtions.

understand the difference(s) between the 'purely structural' ECs (204GFP-23Cherry-) and ECs that express either 204GFP or 23Cherry. It is possible that ECs marked by either 204GFP or 23Cherry represent different stages of HE maturation and only show discreet gene expression changes on a molecular level.

Data presented here already suggest that the +204 enhancer is active at an early stage of EHT only, since 204GFP expression readily observed in ECs but rarely in hematopoietic cluster cells. Interestingly, my transplant data suggests that LT-HSC potential lies within both 204GFP+ and 204GFP- populations. This may be due to carryover of GFP from the HE stage, rather than from active transcription of the transgene within the HSC itself. Further, the reason for only limited blood progenitor potential within the 204GFP+ population may be due to the active proliferation of progenitors, which would dilute any carryover GFP much quicker than in HSCs, which were reported to cycle less (Taoudi et al., 2008) (Figure 7.1 B).

7.3 Transcription factor binding and enhancer activity

In Chapter 1 I have already discussed four *Runx1* enhancers and their accessibility to upstream TFs regulating Runx1 expression and function. Specifically, the +204 enhancer had an open chromatin conformation in ES cell-derived HE, but not in hematopoietic progenitor cells (HPCs) (Figure 1.7; Goode et al., 2016). Analysis of the +204 enhancer activity in different cellular intermediates of the EHT, performed here, also suggests

an early activity of the +204 enhancer in specifically the HE fraction. While recent TFBS and mutagenesis analysis revealed clear differences in motifs present and their requirement for enhancer activity, that analysis was not extensive for the +204 enhancer region: Schütte et al., analyzed a shorter fragment of the +204 sequence than the one used here to generate the 204GFP reporter mouse line (Schütte et al., 2016). It might be interesting to extend previous findings and analyze the larger sequence for TFBS analysis.

Recent years have seen an increase in research on gene regulatory networks underlying developmental hematopoiesis, and the complexity of this system is enormous. The techniques required for such analysis, to date, require large numbers of cells and are therefore often performed in hematopoietic cell lines or in ES cell-derived differentiated cell subsets. However, in order to fully comprehend the regulatory control underlying EHT processes, such analysis needs to be performed in primary tissues, thus in embryonic hematopoietic tissues. Novel techniques such as ATAC-Seq have been developed that reduce the number of cells required to as low as 500 cells while still reliably assessing chromatin accessibility (Buenrostro et al., 2013; Lara-Astiaso et al., 2014). Such assays are currently being optimized in out lab for embryo-derived cells.

7.4 Endoderm and developmental hematopoiesis

When analyzing the expression patterns of 204GFP transgenic or 204lacZ transient transgenic embryos, the earliest expression was observed in the

endoderm from as early as the zero bud stage (7dpc; cf. Figure 3.9). In addition, endogenous *Runx1* expression was observed in the endoderm of headfold stage embryos (North et al., 1999). It would be interesting to identify if the +204 enhancer activity overlaps with endogenous Runx1 expression within this endoderm population, since the endoderm has been previously linked to hematopoietic specification of early mesoderm. A role for Runx1 in the induction of the mesoderm, however, has never been formally addressed.

Early studies of developmental hematopoiesis established that, depending on the anatomical association with either endoderm or ectoderm, the primitive streak mesoderm follows a different fate (Miura and Wilt, 1969; Moore and Metcalf, 1970; Pardanaud and Dieterlen-Lièvre, 1993; Wilt, 1965). Specifically, mesoderm, giving rise to the hemato-endothelial lineages was found to be splanchnopleural mesoderm and of close association with the endoderm (Moore and Metcalf, 1970; Pardanaud and Dieterlen-Lièvre, 1993). In contrast, somatopleural mesoderm rarely, if at all, produced blood and endothelium and was associated with the ectoderm (Pardanaud and Dieterlen-Lièvre, 1993). Moreover, it was established that the earliest fate decisions were guided by the visceral endoderm at pre-streak stages (Belaoussoff et al., 1998). The endoderm was able to re-specify the anterior ectoderm to a hematopoietic fate and it was determined that no cell contact was required for this, suggesting the secretion of a soluble factor from the endoderm (Belaoussoff et al., 1998). In a follow-up study, it was established that Indian Hedgehog (Ihh) was required for the hematopoietic induction of the epiblast and that it was

likely secreted by the endoderm (Dyer et al., 2001). It was proposed that Ihh acts on BMP signaling, which in turn induces hematopoiesis (Baron, 2005, 2001; Dyer et al., 2001). Interestingly, around mid-gastrulation, at the beginning of the headfold stages, the inductive effect of the endoderm was no longer required for hematopoiesis (Palis et al., 1995).

Another consideration is if and where the +204-marked endoderm cells are in close association with the emerging angioblast cells. If they are, it raises the question whether Runx1 also has a non-cell autonomous role. To address this question, future experiments could explore the effects on hematopoieic development when *Runx1* is deleted specifically in the endoderm. Alternatively, if +204 enhancer-reporter expression does not overlap endogenous *Runx1* expression, it would still be of interest to investigate the role of these +204-marked endoderm cells in ex vivo assays testing their capacity to support hematopoietic specification, along with examining their expression profiles for genes involved in e.g. Hh and BMP signaling.

Concluding remarks

Overall, I have demonstrated how the use of novel *Runx1* enhancer-reporter mouse lines provides a multi-functional tool to study different aspects of developmental hematopoiesis. By combining enhancer-mediated reporter expression with commonly used antibodies, it is possible to isolate populations specifically enriched for HE (and in future other EHT subsets). Such findings provide a platform for more advanced molecular studies, furthering our understanding of the elusive HE.

References

Abedin, M.J., Nguyen, A., Jiang, N., Perry, C.E., Shelton, J.M., Watson, D.K., and Ferdous, A. (2014). Fli1 acts downstream of Etv2 to govern cell survival and vascular homeostasis via positive autoregulation. Circ. Res. *114*, 1690–1699.

Adamo, L., Naveiras, O., Wenzel, P.L., McKinney-Freeman, S., Mack, P.J., Gracia-Sancho, J., Suchy-Dicey, A., Yoshimoto, M., Lensch, M.W., Yoder, M.C., et al. (2009). Biomechanical forces promote embryonic haematopoiesis. Nature *459*, 1131–1135.

Alva, J.A., Zovein, A.C., Monvoisin, A., Murphy, T., Salazar, A., Harvey, N.L., Carmeliet, P., and Iruela-Arispe, M.L. (2006). VE-Cadherin-Cre-recombinase transgenic mouse: A tool for lineage analysis and gene deletion in endothelial cells. Dev. Dyn. *235*, 759–767.

Alvarez-Silva, M., Belo-Diabangouaya, P., Salaün, J., and Dieterlen-Lièvre, F. (2003). Mouse placenta is a major hematopoietic organ. Development *130*, 5437–5444.

Ayllón, V., Bueno, C., Ramos-Mejía, V., Navarro-Montero, O., Prieto, C., Real, P.J., Romero, T., García-León, M.J., Toribio, M.L., Bigas, A., et al. (2015). The Notch ligand DLL4 specifically marks human hematoendothelial progenitors and regulates their hematopoietic fate. Leukemia *29*, 1741–1753.

Azcoitia, V., Aracil, M., Martínez-A, C., and Torres, M. (2005). The homeodomain protein Meis1 is essential for definitive hematopoiesis and vascular patterning in the mouse embryo. Dev. Biol. *280*, 307–320.

Azzoni, E., Conti, V., Campana, L., Dellavalle, A., Adams, R.H., Cossu, G., and Brunelli, S. (2014). Hemogenic endothelium generates mesoangioblasts that contribute to several mesodermal lineages in vivo. Development *141*, 1821–1834.

Baldwin, H.., Shen, H.M., Yan, H.-C., DeLisser, H., Chung, A., Mickanin, C., Trask, T., Kirschbaum, N.E., Newman, P.J., Albelda, S.M., et al. (1994). Platelet endothelial cell adhesion molecule-1 (PECAM-1 / CD31): alternatively spliced, functionally distinct isoforms expressed during mammalian cardiovascular development. Development *120*, 2539–2553.

Ballen, K.K., King, R.J., Chitphakdithai, P., Bolan, C.D., Agura, E., Hartzman, R.J., and Kernan, N.A. (2008). The National Marrow Donor Program 20 Years of Unrelated Donor Hematopoietic Cell Transplantation. Biol. Blood Marrow Transplant. *14*, 2–7.

Baron, M. (2005). Early patterning of the mouse embryo: Implications for hematopoietic commitment and differentiation. Exp. Hematol. *33*, 1015–1020.

Baron, M.H. (2001). Induction of embryonic hematopoietic and endothelial stem/progenitor cells by hedgehog-mediated signals. Differentiation *68*, 175–185.

Beard, C., Hochedlinger, K., Plath, K., Wutz, A., and Jaenisch, R. (2006). Efficient method to generate single-copy transgenic mice by site-specific integration in embryonic stem cells. Genesis *44*, 23–28.

Bee, T., Liddiard, K., Swiers, G., Bickley, S.R.B., Vink, C.S., Jarratt, A., Hughes, J.R., Medvinsky, A., and de Bruijn, M.F.T.R. (2009a). Alternative Runx1 promoter usage in mouse developmental hematopoiesis. Blood Cells. Mol. Dis. *43*, 35–42.

Bee, T., Ashley, E.L.K., Bickley, S.R.B., Jarratt, A., Li, P.-S., Sloane-Stanley, J., Gottgens, B., and de Bruijn, M.F.T.R. (2009b). The mouse Runx1 +23 hematopoietic stem cell enhancer confers hematopoietic specificity to both Runx1 promoters. Blood *113*, 5121–5124.

Bee, T., Swiers, G., Muroi, S., Pozner, A., Nottingham, W., Santos, A.C., Li, P.S., Taniuchi, I., and de Bruijn, M.F.T.R. (2010). Nonredundant roles for Runx1 alternative promoters reflect their activity at discrete stages of developmental hematopoiesis. Blood *115*, 3042–3050.

Belaoussoff, M., Farrington, S.M., and Baron, M.H. (1998). Hematopoietic induction and respecification of A-P identity by visceral endoderm signaling in the mouse embryo. Dev. Camb. Engl. *125*, 5009–5018.

Bernex, F., De Sepulveda, P., Kress, C., Elbaz, C., Delouis, c, and Panthier, J.-J. (1996). Spatial and temporal patterns of c-kit-expressing cells in WlacZ/+ and WlacZ/WlacZ mouse embryos. Development *122*, 3023–3033.

Bertrand, J.Y., Giroux, S., Golub, R., Klaine, M., Jalil, A., Boucontet, L., Godin, I., and Cumano, A. (2005). Characterization of purified intraembryonic hematopoietic stem cells as a tool to define their site of origin. Proc. Natl. Acad. Sci. U. S. A. *102*, 134–139.

Bertrand, J.Y., Chi, N.C., Santoso, B., Teng, S., Stainier, D.Y.R., and Traver, D. (2010). Haematopoietic stem cells derive directly from aortic endothelium during development. Nature *464*, 108–111.

Bildsoe, H., Franklin, V., and Tam, P.P.L. (2007). Fate-Mapping Technique: Using Carbocyanine Dyes for Vital Labeling of Cells in Gastrula-Stage Mouse Embryos Cultured In Vitro. Cold Spring Harb. Protoc. *2007*, pdb.prot4915.

Böiers, C., Carrelha, J., Lutteropp, M., Luc, S., Green, J.C.A., Azzoni, E., Woll, P.S., Mead, A.J., Hultquist, A., Swiers, G., et al. (2013). Lymphomyeloid Contribution of an Immune-Restricted Progenitor Emerging Prior to Definitive Hematopoietic Stem Cells. Cell Stem Cell *13*, 535–548.

Boisset, J.-C., van Cappellen, W., Andrieu-Soler, C., Galjart, N., Dzierzak, E., and Robin, C. (2010). In vivo imaging of haematopoietic cells emerging from the mouse aortic endothelium. Nature *464*, 116–120.

Bos, F.L., Hawkins, J.S., and Zovein, A.C. (2015). Single-cell resolution of morphological changes in hemogenic endothelium. Development *142*, 2719–2724.

Bresciani, E., Carrington, B., Wincovitch, S., Jones, M., Gore, A.V., Weinstein, B.M., Sood, R., and Liu, P.P. (2014). CBF and RUNX1 are required at 2 different steps during the development of hematopoietic stem cells in zebrafish. Blood *124*, 70–78.

de Bruijn, M.F., Ploemacher, R.E., Mayen, A.E., Voerman, J.S., Slieker, W.A., van Ewijk, W., and Leenen, P.J. (1996). High-level expression of the ER-MP58 antigen on mouse bone marrow hematopoietic progenitor cells marks commitment to the myeloid lineage. Eur. J. Immunol. *26*, 2850–2858.

de Bruijn, M.F., van Vianen, W., Ploemacher, R.E., Bakker-Woudenberg, I.A., Campbell, P.A., van Ewijk, W., and Leenen, P.J. (1998). Bone marrow cellular composition in Listeria monocytogenes infected mice detected using ER-MP12 and ER-MP20 antibodies: a flow cytometric alternative to differential counting. J. Immunol. Methods *217*, 27–39.

de Bruijn, M.F.T.R., Speck, N.A., Peeters, M.C.E., and Dzierzak, E. (2000). Definitive hematopoietic stem cells first develop within the major arterial regions of the mouse embryo. EMBO J. *19*, 2465–2474.

de Bruijn, M.F.T.R., Ma, X., Robin, C., Ottersbach, K., Sanchez, M.-J., and Dzierzak, E. (2002). Hematopoietic Stem Cells Localize to the Endothelial Cell Layer in the Midgestation Mouse Aorta. Immunity *16*, 673–683.

Buenrostro, J.D., Giresi, P.G., Zaba, L.C., Chang, H.Y., and Greenleaf, W.J. (2013). Transposition of native chromatin for fast and sensitive epigenomic profiling of open chromatin, DNA-binding proteins and nucleosome position. Nat. Methods *10*, 1213–1218.

Burns, C.E., Traver, D., Mayhall, E., Shepard, J.L., and Zon, L.I. (2005). Hematopoietic stem cell fate is established by the Notch–Runx pathway. Genes Dev. *19*, 2331–2342.

Butko, E., Distel, M., Pouget, C., Weijts, B., Kobayashi, I., Ng, K., Mosimann, C., Poulain, F.E., McPherson, A., Ni, C.-W., et al. (2015). Gata2b is a restricted early regulator of hemogenic endothelium in the zebrafish embryo. Development *142*, 1050–1061.

Cai, Z., de Bruijn, M., Ma, X., Dortland, B., Luteijn, T., Downing, R.J., and Dzierzak, E. (2000). Haploinsufficiency of AML1 affects the temporal and spatial generation of hematopoietic stem cells in the mouse embryo. Immunity *13*, 423–431.

Carpenter, L., Malladi, R., Yang, C.-T., French, A., Pilkington, K.J., Forsey, R.W., Sloane-Stanley, J., Silk, K.M., Davies, T.J., Fairchild, P.J., et al. (2011). Human induced pluripotent stem cells are capable of B-cell lymphopoiesis. Blood *117*, 4008–4011.

Chen, M.J., Yokomizo, T., Zeigler, B.M., Dzierzak, E., and Speck, N.A. (2009). Runx1 is required for the endothelial to haematopoietic cell transition but not thereafter. Nature *457*, 887–891.

Chen, M.J., Li, Y., De Obaldia, M.E., Yang, Q., Yzaguirre, A.D., Yamada-Inagawa, T., Vink, C.S., Bhandoola, A., Dzierzak, E., and Speck, N.A. (2011). Erythroid/Myeloid Progenitors and Hematopoietic Stem Cells Originate from Distinct Populations of Endothelial Cells. Cell Stem Cell *9*, 541–552.

Cheshier, S.H., Morrison, S.J., Liao, X., and Weissman, I.. (1999). In vivo proliferation and cell cycle kinetics of long-term self-renewing hematopoietic stem cells. Proc. Natl. Acad. Sci. *96*, 3120–3125.

Choi, K., Kennedy, M., Kazarov, A., Papadimitriou, J.C., and Keller, G. (1998). A common precursor for hematopoietic and endothelial cells. Development *125*, 725–732.

Chong, D.C., Koo, Y., Xu, K., Fu, S., and Cleaver, O. (2011). Stepwise arteriovenous fate acquisition during mammalian vasculogenesis. Dev. Dyn. *240*, 2153–2165.

Ciau-Uitz, A., Walmsley, M., and Patient, R. (2000). Distinct Origins of Adult and Embryonic Blood in Xenopus. Cell *102*, 787–796.

Clements, W.K., Kim, A.D., Ong, K.G., Moore, J.C., Lawson, N.D., and Traver, D. (2011). A somitic Wnt16/Notch pathway specifies haematopoietic stem cells. Nature *474*, 220–224.

Cole, L.J., Fishler, M.C., Ellis, M.E., and Bond, V.P. (1952). Protection of Mice Against X-Irradiation by Spleen Homogenates Administered After Exposure. Proc. Soc. Exp. Biol. Med. *80*, 112–117.

Craft, A.M., Rockel, J.S., Nartiss, Y., Kandel, R.A., Alman, B.A., and Keller, G.M. (2015). Generation of articular chondrocytes from human pluripotent stem cells. Nat. Biotechnol. *33*, 638–645.

Crisan, M., Kartalaei, P.S., Vink, C., Yamada-Inagawa, T., Bollerot, K., van IJcken, W., van der Linden, R., de Sousa Lopes, S.M.C., Monteiro, R., Mummery, C., et al. (2015). BMP signalling differentially regulates distinct haematopoietic stem cell types. Nat. Commun. *6*, 8040.

Crisan, M., Solaimani Kartalaei, P., Neagu, A., Karkanpouna, S., Yamada-Inagawa, T., Purini, C., Vink, C.S., van der Linden, R., van Ijcken, W., Chuva de Sousa Lopes, S.M., et

al. (2016). BMP and Hedgehog Regulate Distinct AGM Hematopoietic Stem Cells Ex Vivo. Stem Cell Rep. *6*, 383–395.

Cumano, A., Dieterlen-Lièvre, F., and Godin, I.E. (1996). Lymphoid Potential, Probed before Circulation in Mouse, Is Restricted to Caudal Intraembryonic Splanchnopleura. Cell *86*, 907–916.

Cumano, A., Ferraz, J.C., Klaine, M., Di Santo, J., and Godin, I. (2001). Intraembryonic, but Not Yolk Sac Hematopoietic Precursors, Isolated before Circulation, Provide Long-Term Multilineage Reconstitution. Immunity *15*, 477–485.

Cvejic, A., Serbanovic-Canic, J., Stemple, D.L., and Ouwehand, W.H. (2011). The role of meis1 in primitive and definitive hematopoiesis during zebrafish development. Haematologica *96*, 190–198.

Daane, J.M., and Downs, K.M. (2011). Hedgehog signaling in the posterior region of the mouse gastrula suggests manifold roles in the fetal-umbilical connection and posterior morphogenesis. Dev. Dyn. *240*, 2175–2193.

Dancis, J., Jansen, V., Gorstein, F., and Douglas, G.W. (1968). Hematopoietic cells in mouse placenta. Am. J. Obstretics Gynecol. *100*, 1110–1121.

Dieterlen-Lievre, F. (1975). On the origin of haemopoietic stem cells in the avian embryo: an experimental approach. Development *33*, 607–619.

Ditadi, A., Sturgeon, C.M., Tober, J., Awong, G., Kennedy, M., Yzaguirre, A.D., Azzola, L., Ng, E.S., Stanley, E.G., French, D.L., et al. (2015). Human definitive haemogenic endothelium and arterial vascular endothelium represent distinct lineages. Nat. Cell Biol. *17*, 580–591.

Douagi, I., Vieira, P., and Cumano, A. (2002). Lymphocyte commitment during embryonic development, in the mouse. Semin. Immunol. *14*, 361–369.

Downs, K.M., and Davies, T. (1993). Staging of gastrulating mouse embryos by morphological landmarks in the dissecting microscope. Development *118*, 1255–1266.

Drake, C.J., and Fleming, P.A. (2000). Vasculogenesis in the day 6.5 to 9.5 mouse embryo. Blood *95*, 1671–1679.

Drissen, R., Buza-Vidas, N., Woll, P., Thongjuea, S., Gambardella, A., Giustacchini, A., Mancini, E., Zriwil, A., Lutteropp, M., Grover, A., et al. (2016). Distinct myeloid progenitor–differentiation pathways identified through single-cell RNA sequencing. Nat. Immunol. *17*, 666–676.

Dumont, D.J., Fong, G.H., Puri, M.C., Gradwohl, G., Alitalo, K., and Breitman, M.L. (1995). Vascularization of the mouse embryo: a study of flk-1, tek, tie, and vascular endothelial growth factor expression during development. Dev. Dyn. Off. Publ. Am. Assoc. Anat. *203*, 80–92.

Durand, C., Robin, C., and Dzierzak, E. (2006). Mesenchymal lineage potentials of aorta-gonad-mesonephros stromal clones. Haematologica *91*, 1172–1179.

Durand, C., Robin, C., Bollerot, K., Baron, M.H., Ottersbach, K., and Dzierzak, E. (2007). Embryonic stromal clones reveal developmental regulators of definitive hematopoietic stem cells. Proc. Natl. Acad. Sci. U. S. A. *104*, 20838–20843.

Dyer, M.A., Farrington, S.M., Mohn, D., Munday, J.R., and Baron, M.H. (2001). Indian hedgehog activates hematopoiesis and vasculogenesis and can respecify prospective neurectodermal cell fate in the mouse embryo. Dev. Camb. Engl. *128*, 1717–1730.

Eaves, C.J. (2015). Hematopoietic stem cells: concepts, definitions, and the new reality. Blood *125*, 2605–2613.

Echelard, Y., Epstein, D.J., St-Jacques, B., Shen, L., Mohler, J., McMahon, J.A., and McMahon, A.P. (1993). Sonic hedgehog, a member of a family of putative signaling molecules, is implicated in the regulation of CNS polarity. Cell *75*, 1417–1430.

Eilken, H.M., Nishikawa, S.-I., and Schroeder, T. (2009). Continuous single-cell imaging of blood generation from haemogenic endothelium. Nature *457*, 896–900.

Elcheva, I., Brok-Volchanskaya, V., Kumar, A., Liu, P., Lee, J.-H., Tong, L., Vodyanik, M., Swanson, S., Stewart, R., Kyba, M., et al. (2014). Direct induction of haematoendothelial programs in human pluripotent stem cells by transcriptional regulators. Nat. Commun. *5*.

Elefanty, A.G., Begley, C.G., Hartley, L., Papaevangeliou, B., and Robb, L. (1999). SCL expression in the mouse embryo detected with a targeted lacZ reporter gene demonstrates its localization to hematopoietic, vascular, and neural tissues. Blood *94*, 3754–3763.

Eliades, A., Wareing, S., Marinopoulou, E., Fadlullah, M.Z.H., Patel, R., Grabarek, J.B., Plusa, B., Lacaud, G., and Kouskoff, V. (2016). The Hemogenic Competence of Endothelial Progenitors Is Restricted by Runx1 Silencing during Embryonic Development. Cell Rep. *15*, 2185–2199.

Ema, M., Yokomizo, T., Wakamatsu, A., Terunuma, T., Yamamoto, M., and Takahashi, S. (2006). Primitive erythropoiesis from mesodermal precursors expressing VE-cadherin, PECAM-1, Tie2, endoglin, and CD34 in the mouse embryo. Blood *108*, 4018–4024.

Ferdous, A., Caprioli, A., Iacovino, M., Martin, C.M., Morris, J., Richardson, J.A., Latif, S., Hammer, R.E., Harvey, R.P., Olson, E.N., et al. (2009). Nkx2–5 transactivates the Ets-related protein 71 gene and specifies an endothelial/endocardial fate in the developing embryo. Proc. Natl. Acad. Sci. *106*, 814–819.

Ferkowicz, M.J., Starr, M., Xie, X., Li, W., Johnson, S.A., Shelley, W.C., Morrison, P.R., and Yoder, M.C. (2003). CD41 expression defines the onset of primitive and definitive hematopoiesis in the murine embryo. Development *130*, 4393–4403.

Frame, J.M., Fegan, K.H., Conway, S.J., McGrath, K.E., and Palis, J. (2016). Definitive Hematopoiesis in the Yolk Sac Emerges from Wnt-Responsive Hemogenic Endothelium Independently of Circulation and Arterial Identity: EMPs Arise from Arteriovenous Hemogenic Endothelia. STEM CELLS *34*, 431–444.

Galić, Z., Kitchen, S.G., Kacena, A., Subramanian, A., Burke, B., Cortado, R., and Zack, J.A. (2006). T lineage differentiation from human embryonic stem cells. Proc. Natl. Acad. Sci. *103*, 11742–11747.

Gama-Norton, L., Ferrando, E., Ruiz-Herguido, C., Liu, Z., Guiu, J., Islam, A.B.M.M.K., Lee, S.-U., Yan, M., Guidos, C.J., López-Bigas, N., et al. (2015). Notch signal strength controls cell fate in the haemogenic endothelium. Nat. Commun. *6*, 8510.

Gao, X., Johnson, K.D., Chang, Y.-I., Boyer, M.E., Dewey, C.N., Zhang, J., and Bresnick, E.H. (2013). *Gata2* cis-element is required for hematopoietic stem cell generation in the mammalian embryo. J. Exp. Med. *210*, 2833–2842.

Garcia-Porrero, J.A., Godin, I.E., and Dieterlen-Lièvre, F. (1995). Potential intraembryonic hemogenic sites at pre-liver stages in the mouse. Anat. Embryol. (Berl.) *192*, 425–435.

Gekas, C., Dieterlen-Lièvre, F., Orkin, S.H., and Mikkola, H.K.A. (2005). The Placenta Is a Niche for Hematopoietic Stem Cells. Dev. Cell *8*, 365–375.

Gering, M., and Patient, R. (2005). Hedgehog Signaling Is Required for Adult Blood Stem Cell Formation in Zebrafish Embryos. Dev. Cell *8*, 389–400.

Gering, M., Rodaway, A.R., Göttgens, B., Patient, R.K., and Green, A.R. (1998). The SCL gene specifies haemangioblast development from early mesoderm. EMBO J. *17*, 4029–4045.

Gering, M., Yamada, Y., Rabbitts, T.H., and Patient, R.K. (2003). Lmo2 and Scl/Tal1 convert non-axial mesoderm into haemangioblasts which differentiate into endothelial cells in the absence of Gata1. Development *130*, 6187–6199.

Geyer, G., and Linss, W. (1978). Toluidine blue staining of cartilage proteoglycan subunits. Acta Histochem. *61*, 127–134.

Godin, I.E., Garcia-Porrero, J.A., Coutinho, A., Dieterlen-Lièvre, F., and Marcos, M.A. (1993). Para-aortic splanchnopleura from early mouse embryos contains B1a cell progenitors. Nature *364*, 67–70.

Godin, I.E., Dieterlen-Lièvre, F., and Cumano, A. (1995). Emergence of multipotent hemopoietic cells in the yolk sac and paraaortic splanchnopleura in mouse embryos, beginning at 8.5 days postcoitus. Proc. Natl. Acad. Sci. *92*, 773–777.

Goldman, D.C., Bailey, A.S., Pfaffle, D.L., Al Masri, A., Christian, J.L., and Fleming, W.H. (2009). BMP4 regulates the hematopoietic stem cell niche. Blood *114*, 4393–4401.

Gomez Perdiguero, E., Klapproth, K., Schulz, C., Busch, K., Azzoni, E., Crozet, L., Garner, H., Trouillet, C., de Bruijn, M.F., Geissmann, F., et al. (2014). Tissue-resident macrophages originate from yolk-sac-derived erythro-myeloid progenitors. Nature *518*, 547–551.

Goode, D.K., Obier, N., Vijayabaskar, M.S., Lie-A-Ling, M., Lilly, A.J., Hannah, R., Lichtinger, M., Batta, K., Florkowska, M., Patel, R., et al. (2016). Dynamic Gene Regulatory Networks Drive Hematopoietic Specification and Differentiation. Dev. Cell *36*, 572–587.

Gordon-Keylock, S., Sobiesiak, M., Rybtsov, S., Moore, K., and Medvinsky, A. (2013). Mouse extraembryonic arterial vessels harbor precursors capable of maturing into definitive HSCs. Blood *122*, 2338–2345.

Guiu, J., Shimizu, R., D'Altri, T., Fraser, S.T., Hatakeyama, J., Bresnick, E.H., Kageyama, R., Dzierzak, E., Yamamoto, M., Espinosa, L., et al. (2013). Hes repressors are essential regulators of hematopoietic stem cell development downstream of Notch signaling. J. Exp. Med. *210*, 71–84.

Hamaguchi, I., Huang, X.L., Takakura, N., Tada, J., Yamaguchi, Y., Kodama, H., and Suda, T. (1999). In vitro hematopoietic and endothelial cell development from cells expressing TEK receptor in murine aorta-gonad-mesonephros region. Blood *93*, 1549–1556.

Hanna, J., Wernig, M., Markoulaki, S., Sun, C., Meissner, A., Cassady, J.P., Beard, C., Brambrink, T., Wu, L., Townes, T., et al. (2007). Treatment of Sickle Cell Anemia Mouse Model with iPS Cells Generated from Autologous Skin. Science *318*, 1920–1923.

Hock, H., Hamblen, M.J., Rooke, H.M., Schindler, J.W., Saleque, S., Fujiwara, Y., and Orkin, S.H. (2004). Gfi-1 restricts proliferation and preserves functional integrity of haematopoietic stem cells. Nature *431*, 1002–1007.

Hoogenkamp, M., Krysinska, H., Ingram, R., Huang, G., Barlow, R., Clarke, D., Ebralidze, A., Zhang, P., Tagoh, H., Cockerill, P.N., et al. (2007). The Pu.1 Locus Is Differentially Regulated at the Level of Chromatin Structure and Noncoding Transcription by Alternate

Mechanisms at Distinct Developmental Stages of Hematopoiesis. Mol. Cell. Biol. *27*, 7425–7438.

Huang, G., Zhang, P., Hirai, H., Elf, S., Yan, X., Chen, Z., Koschmieder, S., Okuno, Y., Dayaram, T., Growney, J.D., et al. (2008). PU.1 is a major downstream target of AML1 (RUNX1) in adult mouse hematopoiesis. Nat. Genet. *40*, 51–60.

Huber, T.L., Kouskoff, V., Joerg Fehling, H., Palis, J., and Keller, G. (2004). Haemangioblast commitment is initiated in the primitive streak of the mouse embryo. Nature *432*, 625–630.

Iizuka, K., Yokomizo, T., Watanabe, N., Tanaka, Y., Osato, M., Takaku, T., and Komatsu, N. (2016). Lack of Phenotypical and Morphological Evidences of Endothelial to Hematopoietic Transition in the Murine Embryonic Head during Hematopoietic Stem Cell Emergence. PLOS ONE *11*, e0156427.

Inlay, M.A., Serwold, T., Mosley, A., Fathman, J.W., Dimov, I.K., Seita, J., and Weissman, I.L. (2014). Identification of Multipotent Progenitors that Emerge Prior to Hematopoietic Stem Cells in Embryonic Development. Stem Cell Rep. *2*, 457–472.

Jacobson, L.O., Simmons, E.L., Marks, E.K., and Eldredge, J.H. (1951). Recovery from Radiation Injury. Science *113*, 510–511.

Jaffredo, T., Gautier, R., Eichmann, A., and Dieterlen-Lièvre, F. (1998). Intraaortic hemopoietic cells are derived from endothelial cells during ontogeny. Development *125*, 4575–4583.

Johnson, G.R., and Moore, M. a. S. (1975). Role of stem cell migration in initiation of mouse foetal liver haemopoiesis. Nature *258*, 726–728.

Kaimakis, P., de Pater, E., Eich, C., Solaimani Kartalaei, P., Kauts, M.-L., Vink, C.S., van der Linden, R., Jaegle, M., Yokomizo, T., Meijer, D., et al. (2016). Functional and molecular characterization of mouse Gata2-independent hematopoietic progenitors. Blood *127*, 1426–1437.

Kalev-Zylinska, M.L., Horsfield, J.A., Flores, M.V.C., Postlethwait, J.H., Vitas, M.R., Baas, A.M., Crosier, P.S., and Crosier, K.E. (2002). Runx1 is required for zebrafish blood and vessel development and expression of a human RUNX1-CBF2T1 transgene advances a model for studies of leukemogenesis. Dev. Camb. Engl. *129*, 2015–2030.

Kataoka, H., Hayashi, M., Kobayashi, K., Ding, G., Tanaka, Y., and Nishikawa, S.-I. (2013). Region-specific Etv2 ablation revealed the critical origin of hemogenic capacity from Hox6-positive caudal-lateral primitive mesoderm. Exp. Hematol. *41*, 567–581.e9.

Kennedy, M., D'Souza, S.L., Lynch-Kattman, M., Schwantz, S., and Keller, G. (2007). Development of the hemangioblast defines the onset of hematopoiesis in human ES cell differentiation cultures. Blood *109*, 2679–2687.

Kim, P.G., Albacker, C.E., Lu, Y. -f., Jang, I. -h., Lim, Y., Heffner, G.C., Arora, N., Bowman, T.V., Lin, M.I., Lensch, M.W., et al. (2013). Signaling axis involving Hedgehog, Notch, and Scl promotes the embryonic endothelial-to-hematopoietic transition. Proc. Natl. Acad. Sci. *110*, E141–E150.

Kim, P.G., Nakano, H., Das, P.P., Chen, M.J., Rowe, R.G., Chou, S.S., Ross, S.J., Sakamoto, K.M., Zon, L.I., Schlaeger, T.M., et al. (2015). Flow-induced protein kinase A–CREB pathway acts via BMP signaling to promote HSC emergence. J. Exp. Med. *212*, 633–648.

Kinder, S.J., Tsang, T.E., Quinlan, G.A., Hadjantonakis, A.K., Nagy, A., and Tam, P.P. (1999). The orderly allocation of mesodermal cells to the extraembryonic structures and

the anteroposterior axis during gastrulation of the mouse embryo. Dev. Camb. Engl. *126*, 4691–4701.

Kinder, S.J., Loebel, D.A.F., and Tam, P.P.L. (2001). Allocation and Early Differentiation of Cardiovascular Progenitors in the Mouse Embryo. Trends Cardiovasc. Med. *11*, 177–184.

Kingsley, P.D., Malik, J., Fantauzzo, K.A., and Palis, J. (2004). Yolk sac–derived primitive erythroblasts enucleate during mammalian embryogenesis. Blood *104*, 19–25.

Kissa, K., and Herbomel, P. (2010). Blood stem cells emerge from aortic endothelium by a novel type of cell transition. Nature *464*, 112–115.

Knorr, D.A., Ni, Z., Hermanson, D., Hexum, M.K., Bendzick, L., Cooper, L.J.N., Lee, D.A., and Kaufman, D.S. (2013). Clinical-Scale Derivation of Natural Killer Cells From Human Pluripotent Stem Cells for Cancer Therapy. Stem Cells Transl. Med. *2*, 274–283.

Kobayashi-Osaki, M., Ohneda, O., Suzuki, N., Minegishi, N., Yokomizo, T., Takahashi, S., Lim, K.-C., Engel, J.D., and Yamamoto, M. (2005). GATA Motifs Regulate Early Hematopoietic Lineage-Specific Expression of the Gata2 Gene. Mol. Cell. Biol. *25*, 7005–7020.

Kocabas, F., Zheng, J., Thet, S., Copeland, N.G., Jenkins, N.A., DeBerardinis, R.J., Zhang, C., and Sadek, H.A. (2012). Meis1 regulates the metabolic phenotype and oxidant defense of hematopoietic stem cells. Blood *120*, 4963–4972.

Kothary, R., Clapoff, S., Darling, S., Perry, M.D., Moran, L.A., and Rossant, J. (1989). Inducible expression of an hsp68-lacZ hybrid gene in transgenic mice. Dev. Camb. Engl. *105*, 707–714.

Kretzschmar, K., and Watt, F.M. (2012). Lineage Tracing. Cell *148*, 33–45.

Kumaravelu, P., Hook, L., Morrison, A.M., Ure, J., Zhao, S., Zuyev, S., Ansell, J., and Medvinsky, A. (2002). Quantitative developmental anatomy of definitive haematopoietic stem cells/ long-term repopulating units (HSC/RUs): role of the aorta-gonad-mesonephros (AGM) region and the yolk sac in colonisation of the mouse embryonic liver. Development *129*, 4891–4899.

Lacaud, G., Gore, L., Kennedy, M., Kouskoff, V., Kingsley, P., Hogan, C., Carlsson, L., Speck, N., Palis, J., and Keller, G. (2002). Runx1 is essential for hematopoietic commitment at the hemangioblast stage of development in vitro. Blood *100*, 458–466.

Lam, E.Y.N., Hall, C.J., Crosier, P.S., Crosier, K.E., and Flores, M.V. (2010). Live imaging of Runx1 expression in the dorsal aorta tracks the emergence of blood progenitors from endothelial cells. Blood *116*, 909–914.

Lancrin, C., Sroczynska, P., Stephenson, C., Allen, T., Kouskoff, V., and Lacaud, G. (2009). The haemangioblast generates haematopoietic cells through a haemogenic endothelium stage. Nature *457*, 892–895.

Lancrin, C., Mazan, M., Stefanska, M., Patel, R., Lichtinger, M., Costa, G., Vargel, O., Wilson, N.K., Moroy, T., Bonifer, C., et al. (2012). GFI1 and GFI1B control the loss of endothelial identity of hemogenic endothelium during hematopoietic commitment. Blood *120*, 314–322.

Lara-Astiaso, D., Weiner, A., Lorenzo-Vivas, E., Zaretsky, I., Jaitin, D.A., David, E., Keren-Shaul, H., Mildner, A., Winter, D., Jung, S., et al. (2014). Chromatin state dynamics during blood formation. Science *345*, 943–949.

Lawson, K.A., Meneses, J.J., and Pedersen, R.A. (1991). Clonal analysis of epiblast fate during germ layer formation in the mouse embryo. Dev. Camb. Engl. *113*, 891–911.

Lee, D., Park, C., Lee, H., Lugus, J.J., Kim, S.H., Arentson, E., Chung, Y.S., Gomez, G., Kyba, M., Lin, S., et al. (2008). ER71 Acts Downstream of BMP, Notch, and Wnt Signaling in Blood and Vessel Progenitor Specification. Cell Stem Cell *2*, 497–507.

Lee, D., Kim, T., and Lim, D.-S. (2011). The Er71 Is an Important Regulator of Hematopoietic Stem Cells in Adult Mice. STEM CELLS *29*, 539–548.

Lee, L.K., Ueno, M., Van Handel, B., and Mikkola, H.K.A. (2010). Placenta as a newly identified source of hematopoietic stem cells. Curr. Opin. Hematol. *17*, 313–318.

Lee, Y., Manegold, J.E., Kim, A.D., Pouget, C., Stachura, D.L., Clements, W.K., and Traver, D. (2014). FGF signalling specifies haematopoietic stem cells through its regulation of somitic Notch signalling. Nat. Commun. *5*, 5583.

Levanon, D., Glusman, G., Bangsow, T., Ben-Asher, E., Male, D.A., Avidan, N., Bangsow, C., Hattori, M., Taylor, T.D., Taudien, S., et al. (2001). Architecture and anatomy of the genomic locus encoding the human leukemia-associated transcription factor RUNX1/AML1. Gene *262*, 23–33.

Li, W., Ferkowicz, M.J., Johnson, S.A., Shelley, W.C., and Yoder, M.C. (2005). Endothelial cells in the early murine yolk sac give rise to CD41-expressing hematopoietic cells. Stem Cells Dev. *14*, 44–54.

Li, Z., Chen, M.J., Stacy, T., and Speck, N.A. (2006). Runx1 function in hematopoiesis is required in cells that express Tek. Blood *107*, 106–110.

Li, Z., Lan, Y., He, W., Chen, D., Wang, J., Zhou, F., Wang, Y., Sun, H., Chen, X., Xu, C., et al. (2012). Mouse Embryonic Head as a Site for Hematopoietic Stem Cell Development. Cell Stem Cell *11*, 663–675.

Li, Z., Vink, C.S., Mariani, S.A., and Dzierzak, E. (2016). Subregional localization and characterization of Ly6aGFP-expressing hematopoietic cells in the mouse embryonic head. Dev. Biol. *416*, 34–41.

Liakhovitskaia, A., Gribi, R., Stamateris, E., Villain, G., Jaffredo, T., Wilkie, R., Gilchrist, D., Yang, J., Ure, J., and Medvinsky, A. (2009). Restoration of Runx1 Expression in the Tie2 Cell Compartment Rescues Definitive Hematopoietic Stem Cells and Extends Life of Runx1 Knockout Animals Until Birth. Stem Cells *27*, 1616–1624.

Liakhovitskaia, A., Lana-Elola, E., Stamateris, E., Rice, D.P., van 't Hof, R.J., and Medvinsky, A. (2010). The essential requirement for Runx1 in the development of the sternum. Dev. Biol. *340*, 539–546.

Liakhovitskaia, A., Rybtsov, S., Smith, T., Batsivari, A., Rybtsova, N., Rode, C., de Bruijn, M., Buchholz, F., Gordon-Keylock, S., Zhao, S., et al. (2014). Runx1 is required for progression of CD41+ embryonic precursors into HSCs but not prior to this. Development *141*, 3319–3323.

Lichtinger, M., Ingram, R., Hannah, R., Müller, D., Clarke, D., Assi, S.A., Lie-A-Ling, M., Noailles, L., Vijayabaskar, M.S., Wu, M., et al. (2012). RUNX1 reshapes the epigenetic landscape at the onset of haematopoiesis: RUNX1 shifts transcription factor binding patterns. EMBO J. *31*, 4318–4333.

Ling, K.-W., Ottersbach, K., van Hamburg, J.P., Oziemlak, A., Tsai, F.-Y., Orkin, S.H., Ploemacher, R., Hendriks, R.W., and Dzierzak, E. (2004). GATA-2 Plays Two Functionally Distinct Roles during the Ontogeny of Hematopoietic Stem Cells. J. Exp. Med. *200*, 871–882.

Liu, F., Li, D., Yu, Y.Y.L., Kang, I., Cha, M.-J., Kim, J.Y., Park, C., Watson, D.K., Wang, T., and Choi, K. (2015). Induction of hematopoietic and endothelial cell program orchestrated by ETS transcription factor ER71/ETV2. EMBO Rep. *16*, 654–669.

Lizama, C.O., Hawkins, J.S., Schmitt, C.E., Bos, F.L., Zape, J.P., Cautivo, K.M., Borges Pinto, H., Rhyner, A.M., Yu, H., Donohoe, M.E., et al. (2015). Repression of arterial genes in hemogenic endothelium is sufficient for haematopoietic fate acquisition. Nat. Commun. *6*, 7739.

Longenecker, G., and Kulkarni, A.B. (2009). Generation of Gene Knockout Mice by ES Cell Microinjection. In Current Protocols in Cell Biology, J.S. Bonifacino, M. Dasso, J.B. Harford, J. Lippincott-Schwartz, and K.M. Yamada, eds. (Hoboken, NJ, USA: John Wiley & Sons, Inc.), p.

Longo, L., Bygrave, A., Grosveld, F.G., and Pandolfi, P.P. (1997). The chromosome make-up of mouse embryonic stem cells is predictive of somatic and germ cell chimaerism. Transgenic Res. *6*, 321–328.

Lorenz, E., Congdon, C., and Uphoff, D. (1952). Modification of Acute Irradiation Injury in Mice and Guinea-Pigs by Bone Marrow Injections. Radiology *58*, 863–877.

Lorsbach, R.B., Moore, J., Ang, S.O., Sun, W., Lenny, N., and Downing, J.R. (2004). Role of RUNX1 in adult hematopoiesis: analysis of RUNX1-IRES-GFP knock-in mice reveals differential lineage expression. Blood *103*, 2522–2529.

Lu, S., Li, F., Yin, H., Feng, Q., Kimbrel, E.., Hahm, E., Thon, J.N., Wang, W., Italiano, J.E., and Lanza, R. (2011). Platelets generated from human embryonic stem cells are functional in vitro and in the microcirculation of living mice. Cell Res. *21*, 530–545.

Lugus, J.J., Chung, Y.S., Mills, J.C., Kim, S.-I., Grass, J.A., Kyba, M., Doherty, J.M., Bresnick, E.H., and Choi, K. (2007). GATA2 functions at multiple steps in hemangioblast development and differentiation. Development *134*, 393–405.

Lux, C.T., Yoshimoto, M., McGrath, K., Conway, S.J., Palis, J., and Yoder, M.C. (2008). All primitive and definitive hematopoietic progenitor cells emerging before E10 in the mouse embryo are products of the yolk sac. Blood *111*, 3435–3438.

Manaia, A., Lemarchandel, V., Klaine, M., Max-Audit, I., Romeo, P., Dieterlen-Lièvre, F., and Godin, I. (2000). Lmo2 and GATA-3 associated expression in intraembryonic hemogenic sites. Dev. Camb. Engl. *127*, 643–653.

Marshall, C.J., Kinnon, C., and Thrasher, A.J. (2000). Polarized expression of bone morphogenetic protein-4 in the human aorta-gonad-mesonephros region. Blood *96*, 1591–1593.

Martin, D.I.K., and Whitelaw, E. (1996). The vagaries of variegating transgenes. BioEssays *18*, 919–923.

McGrath, K., Frame, J.M., Fromm, G.J., Koniski, A.D., Kingsley, P.D., Little, J., Bulger, M., and Palis, J. (2011). A transient definitive erythroid lineage with unique regulation of the -globin locus in the mammalian embryo. Blood *117*, 4600–4608.

McGrath, K.E., Koniski, A.D., Malik, J., and Palis, J. (2003). Circulation is established in a stepwise pattern in the mammalian embryo. Blood *101*, 1669–1675.

McGrath, K.E., Frame, J.M., Fegan, K.H., Bowen, J.R., Conway, S.J., Catherman, S.C., Kingsley, P.D., Koniski, A.D., and Palis, J. (2015). Distinct Sources of Hematopoietic Progenitors Emerge before HSCs and Provide Functional Blood Cells in the Mammalian Embryo. Cell Rep. *11*, 1892–1904.

Medvinsky, A., and Dzierzak, E. (1996). Definitive Hematopoiesis Is Autonomously Initiated by the AGM Region. Cell *86*, 897–906.

Medvinsky, A., Samoylina, N.L., Muller, A.M., and Dzierzak, E. (1993). An early pre-liver intra-embryonic source of CFU-S in the developing mouse. Nature *364*, 64–67.

Medvinsky, A., Glan, O.., Semenova, M.L., and Samoylina, N.L. (1996). Development of Day-8 Colony-Forming Unit-Spleen Hematopoietic Progenitors During Early Murine Embryogenesis: Spatial and Temporal Mapping. Blood *87*, 557–566.

Medvinsky, A., Rybtsov, S., and Taoudi, S. (2011). Embryonic origin of the adult hematopoietic system: advances and questions. Development *138*, 1017–1031.

van der Meer, L.T., Jansen, J.H., and van der Reijden, B.A. (2010). Gfi1 and Gfi1b: key regulators of hematopoiesis. Leukemia *24*, 1834–1843.

Mendes, S.C., Robin, C., and Dzierzak, E. (2005). Mesenchymal progenitor cells localize within hematopoietic sites throughout ontogeny. Development *132*, 1127–1136.

Miller, J., Horner, A., Stacy, T., Lowrey, C., Lian, J.B., Stein, G., Nuckolls, G.H., and Speck, N.A. (2002). The core-binding factor β subunit is required for bone formation and hematopoietic maturation. Nat. Genet. *32*, 645–649.

Miller, M.E., Rosten, P., Lemieux, M.E., Lai, C., and Humphries, R.K. (2016). Meis1 Is Required for Adult Mouse Erythropoiesis, Megakaryopoiesis and Hematopoietic Stem Cell Expansion. PLOS ONE *11*, e0151584.

Minasi, M.G., Riminucci, M., De Angelis, L., Borello, U., Berarducci, B., Innocenzi, A., Caprioli, A., Sirabella, D., Baiocchi, M., De Maria, R., et al. (2002). The meso-angioblast: a multipotent, self-renewing cell that originates from the dorsal aorta and differentiates into most mesodermal tissues. Dev. Camb. Engl. *129*, 2773–2783.

Minegishi, N., Ohta, J., Yamagiwa, H., Suzuki, N., Kawauchi, S., Zhou, Y., Takahashi, S., Hayashi, N., Engel, J.D., and Yamamoto, M. (1999). The mouse GATA-2 gene is expressed in the para-aortic splanchnopleura and aorta-gonads and mesonephros region. Blood *93*, 4196–4207.

Minegishi, N., Suzuki, N., Yokomizo, T., Pan, X., Fujimoto, T., Takahashi, S., Hara, T., Miyajima, A., Nishikawa, S., and Yamamoto, M. (2003). Expression and domain-specific function of GATA-2 during differentiation of the hematopoietic precursor cells in midgestation mouse embryos. Blood *102*, 896–905.

Mirshekar-Syahkal, B., Haak, E., Kimber, G.M., van Leusden, K., Harvey, K., O'Rourke, J., Laborda, J., Bauer, S.R., de Bruijn, M.F.T.R., Ferguson-Smith, A.C., et al. (2013). Dlk1 is a negative regulator of emerging hematopoietic stem and progenitor cells. Haematologica *98*, 163–171.

Miura, Y., and Wilt, F.H. (1969). Tissue interaction and the formation of the first erythroblasts of the chick embryo. Dev. Biol. *19*, 201–211.

Moignard, V., Woodhouse, S., Haghverdi, L., Lilly, A.J., Tanaka, Y., Wilkinson, A.C., Buettner, F., Macaulay, I.C., Jawaid, W., Diamanti, E., et al. (2015). Decoding the regulatory network of early blood development from single-cell gene expression measurements. Nat. Biotechnol. *33*, 269–276.

Monteiro, R., Pinheiro, P., Joseph, N., Peterkin, T., Koth, J., Repapi, E., Bonkhofer, F., Kirmizitas, A., and Patient, R. (2016). Transforming Growth Factor β Drives Hemogenic Endothelium Programming and the Transition to Hematopoietic Stem Cells. Dev. Cell *38*, 358–370.

Moore, M.A.S., and Metcalf, D. (1970). Ontogent of the haematopoietic system: yolk sac origin of in vivo and in vitro colony forming cells in the developing mouse embryo. Blood *18*, 279–296.

Mucenski, M.L., McLain, K., Kier, A.B., Swerdlow, S.H., Schreiner, C.M., Miller, T.A., Pietryga, D.W., Scott, W.J., and Potter, S.S. (1991). A functional c-myb gene is required for normal murine fetal hepatic hematopoiesis. Cell *65*, 677–689.

Mukouyama, Y., Chiba, N., Hara, T., Okada, H., Ito, Y., Kanamaru, R., Miyajima, A., Satake, M., and Watanabe, T. (2000). The AML1 Transcription Factor Functions to Develop and Maintain Hematogenic Precursor Cells in the Embryonic Aorta–Gonad–Mesonephros Region. Dev. Biol. *220*, 27–36.

Mukouyama, Y. s, Chiba, N., Mucenski, M.L., Satake, M., Miyajima, A., Hara, T., and Watanabe, T. (1999). Hematopoietic cells in cultures of the murine embryonic aorta-gonad-mesonephros region are induced by c-Myb. Curr. Biol. CB *9*, 833–836.

Müller, A.M., Medvinsky, A., Strouboulis, J., Grosveld, F., and Dzierzakt, E. (1994). Development of hematopoietic stem cell activity in the mouse embryo. Immunity *1*, 291–301.

Müller, A.M., Huppertz, S., and Henschler, R. (2016). Hematopoietic Stem Cells in Regenerative Medicine: Astray or on the Path? Transfus. Med. Hemotherapy *43*, 247–254.

Murray, P.D.F. (1932). The development in vitro of blood of the early chick embryo. Proc. R. Soc. Lond. *111*, 497–521.

Nakagawa, M., Ichikawa, M., Kumano, K., Goyama, S., Kawazu, M., Asai, T., Ogawa, S., Kurokawa, M., and Chiba, S. (2006). AML1/Runx1 rescues Notch1-null mutation-induced deficiency of para-aortic splanchnopleural hematopoiesis. Blood *108*, 3329–3334.

Nakano, H., Liu, X., Arshi, A., Nakashima, Y., van Handel, B., Sasidharan, R., Harmon, A.W., Shin, J.-H., Schwartz, R.J., Conway, S.J., et al. (2013). Haemogenic endocardium contributes to transient definitive haematopoiesis. Nat. Commun. *4*, 1564.

Nakayama, N., Duryea, D., Manoukian, R., Chow, G., and Han, C.-Y.E. (2003). Macroscopic cartilage formation with embryonic stem-cell-derived mesodermal progenitor cells. J. Cell Sci. *116*, 2015–2028.

Ng, C.E.L., Yokomizo, T., Yamashita, N., Cirovic, B., Jin, H., Wen, Z., Ito, Y., and Osato, M. (2010). A Runx1 Intronic Enhancer Marks Hemogenic Endothelial Cells and Hematopoietic Stem Cells. STEM CELLS *28*, 1869–1881.

Nishikawa, S.-I., Nishikawa, S., kawamoto, H., Yoshida, H., Kizumoto, M., Kataoka, H., and katsura, Y. (1998a). In Vitro Generation of Lymphohematopoietic Cells from Endothelial Cells Purified from Murine Embryos. Immunity *8*, 761–769.

Nishikawa, S.-I., Nishikawa, S., Hirashima, M., matsuyoshi, n, and Kodama, H. (1998b). Progressive lineage analysis by cell sorting and culture identifies FLK1+VE- cadherin+ cells at a diverging point of endothelial and hemopoietic lineages. Development *125*, 1747–1757.

North, T.E., Gu, T.-L.G., Stacy, T., Wang, Q., Howard, L., Binder, M., Marin-Padilla, M., and Speck, N.A. (1999). Cbfa2 is required for the formation of intra-aortic hematopoietic clusters. Development *126*, 2563–2575.

North, T.E., De Bruijn, M., Stacy, T., Talebian, L., Lind, E., Robin, C., Binder, M., Dzierzak, E., and Speck, N.A. (2002). Runx1 Expression Marks Long-Term Repopulating Hematopoietic Stem Cells in the Midgestation Mouse Embryo. Immunity *16*, 661–672.

North, T.E., Stacy, T., Matheny, C.J., Speck, N.A., and de Bruijn, M.F.T.R. (2004). Runx1 is expressed in adult mouse hematopoietic stem cells and differentiating myeloid and lymphoid cells, but not in maturing erythroid cells. Stem Cells Dayt. Ohio *22*, 158–168.

North, T.E., Goessling, W., Peeters, M., Li, P., Ceol, C., Lord, A.M., Weber, G.J., Harris, J., Cutting, C.C., Huang, P., et al. (2009). Hematopoietic Stem Cell Development Is Dependent on Blood Flow. Cell *137*, 736–748.

Nottingham, W.T., Jarratt, A., Burgess, M., Speck, C.L., Cheng, J.-F., Prabhakar, S., Rubin, E.M., Li, P.-S., Sloane-Stanley, J., Kong-a-San, J., et al. (2007). Runx1-mediated hematopoietic stem-cell emergence is controlled by a Gata/Ets/SCL-regulated enhancer. Blood *110*, 4188–4197.

Oberlin, E., El Hafny, B., Petit-Cocault, L., and Souyri, M. (2010). Definitive human and mouse hematopoiesis originates from the embryonic endothelium: a new class of HSCs based on VE-cadherin expression. Int. J. Dev. Biol. *54*, 1165–1173.

Okuda, T., van Deursen, J., Hiebert, S.W., Grosveld, G., and Downing, J.R. (1996). AML1, the target of multiple chromosomal translocations in human leukemia, is essential for normal fetal liver hematopoiesis. Cell *84*, 321–330.

Oostendorp, R.A.J., Harvey, K.N., Kusadasi, N., de Bruijn, M.F.T.R., Saris, C., Ploemacher, R.E., Medvinsky, A.L., and Dzierzak, E.A. (2002). Stromal cell lines from mouse aorta-gonads-mesonephros subregions are potent supporters of hematopoietic stem cell activity. Blood *99*, 1183–1189.

Oran, B., and Shpall, E. (2012). Umbilical cord blood transplantation: a maturing technology. Am. Soc. Hematol. 215–222.

Osborne, G.W. (2011). Chapter 21 - Recent Advances in Flow Cytometric Cell Sorting. In Methods in Cell Biology, E.H. Zbigniew Darzynkiewicz Alberto Orfao, William Telford and Donald Wlodkowic, ed. (Academic Press), pp. 533–556.

Ottersbach, K., and Dzierzak, E. (2005). The Murine Placenta Contains Hematopoietic Stem Cells within the Vascular Labyrinth Region. Dev. Cell *8*, 377–387.

Padron-Barthe, L., Temino, S., Villa del Campo, C., Carramolino, L., Isern, J., and Torres, M. (2014). Clonal analysis identifies hemogenic endothelium as the source of the blood-endothelial common lineage in the mouse embryo. Blood *124*, 2523–2532.

Palis, J., McGrath, K.E., and Kingsley, P.D. (1995). Initiation of hematopoiesis and vasculogenesis in murine yolk sac explants. Blood *86*, 156–163.

Palis, J., Robertson, S., Kennedy, M., Wall, C., and Keller, G. (1999). Development of erythroid and myeloid progenitors in the yolk sac and embryo proper of the mouse. Development *126*, 5073–5084.

Parameswaran, M., and Tam, P.P. (1995). Regionalisation of cell fate and morphogenetic movement of the mesoderm during mouse gastrulation. Dev. Genet. *17*, 16–28.

Pardanaud, L., and Dieterlen-Lièvre, F. (1993). Emergence of endothelial and hemopoietic cells in the avian embryo. Anat. Embryol. (Berl.) *187*, 107–114.

Pardanaud, L., Luton, D., Prigent, M., Bourcheix, L.M., Catala, M., and Dieterlen-Lievre, F. (1996). Two distinct endothelial lineages in ontogeny, one of them related to hemopoiesis. Development *122*, 1363–1371.

de Pater, E., Kaimakis, P., Vink, C.S., Yokomizo, T., Yamada-Inagawa, T., van der Linden, R., Kartalaei, P.S., Camper, S.A., Speck, N., and Dzierzak, E. (2013). *Gata2* is required for HSC generation and survival. J. Exp. Med. *210*, 2843–2850.

Patterson, L.J., Gering, M., and Patient, R. (2005). Scl is required for dorsal aorta as well as blood formation in zebrafish embryos. Blood *105*, 3502–3511.

Patterson, L.J., Gering, M., Eckfeldt, C.E., Green, A.R., Verfaillie, C.M., Ekker, S.C., and Patient, R. (2007). The transcription factors Scl and Lmo2 act together during development of the hemangioblast in zebrafish. Blood *109*, 2389–2398.

Peacock, J.D., Lu, Y., Koch, M., Kadler, K.E., and Lincoln, J. (2008). Temporal and spatial expression of collagens during murine atrioventricular heart valve development and maintenance. Dev. Dyn. *237*, 3051–3058.

Peeters, M., Ottersbach, K., Bollerot, K., Orelio, C., de Bruijn, M., Wijgerde, M., and Dzierzak, E. (2009). Ventral embryonic tissues and Hedgehog proteins induce early AGM hematopoietic stem cell development. Development *136*, 2613–2621.

Pennacchio, L.A., Bickmore, W., Dean, A., Nobrega, M.A., and Bejerano, G. (2013). Enhancers: five essential questions. Nat. Rev. Genet. *14*, 288–295.

Pimanda, J.E., Ottersbach, K., Knezevic, K., Kinston, S., Chan, W.Y.I., Wilson, N.K., Landry, J.-R., Wood, A.D., Kolb-Kokocinski, A., Green, A.R., et al. (2007). Gata2, Fli1, and Scl form a recursively wired gene-regulatory circuit during early hematopoietic development. Proc. Natl. Acad. Sci. U. S. A. *104*, 17692–17697.

Porcher, C., Swat, W., Rockwell, K., Fujiwara, Y., Alt, F.W., and Orkin, S.H. (1996). The T cell leukemia oncoprotein SCL/tal-1 is essential for development of all hematopoietic lineages. Cell *86*, 47–57.

Qiu, J., Fan, X., Wang, Y., Jin, H., Song, Y., Han, Y., Huang, S., Meng, Y., Tang, F., and Meng, A. (2016). Embryonic hematopoiesis in vertebrate somites gives rise to definitive hematopoietic stem cells. J. Mol. Cell Biol. *8*, 288–301.

Rasmussen, T.L., Kweon, J., Diekmann, M.A., Belema-Bedada, F., Song, Q., Bowlin, K., Shi, X., Ferdous, A., Li, T., Kyba, M., et al. (2011). ER71 directs mesodermal fate decisions during embryogenesis. Development *138*, 4801–4812.

Rasmussen, T.L., Shi, X., Wallis, A., Kweon, J., Zirbes, K.M., Koyano-Nakagawa, N., and Garry, D.J. (2012). VEGF/Flk1 Signaling Cascade Transactivates Etv2 Gene Expression. PLoS ONE *7*, e50103.

Richard, C., Drevon, C., Canto, P.-Y., Villain, G., Bollérot, K., Lempereur, A., Teillet, M.-A., Vincent, C., Rosselló Castillo, C., Torres, M., et al. (2013). Endothelio-Mesenchymal Interaction Controls runx1 Expression and Modulates the notch Pathway to Initiate Aortic Hematopoiesis. Dev. Cell *24*, 600–611.

Riddell, J., Gazit, R., Garrison, B.S., Guo, G., Saadatpour, A., Mandal, P.K., Ebina, W., Volchkov, P., Yuan, G.-C., Orkin, S.H., et al. (2014). Reprogramming Committed Murine Blood Cells to Induced Hematopoietic Stem Cells with Defined Factors. Cell *157*, 549–564.

Robb, L., Lyons, I., Li, R., Hartley, L., Köntgen, F., Harvey, R.P., Metcalf, D., and Begley, C.G. (1995). Absence of yolk sac hematopoiesis from mice with a targeted disruption of the scl gene. Proc. Natl. Acad. Sci. U. S. A. *92*, 7075–7079.

Robert-Moreno, À., Espinosa, L., Pompa, J.L. de la, and Bigas, A. (2005). RBPjκ-dependent Notch function regulates Gata2 and is essential for the formation of intra-embryonic hematopoietic cells. Development *132*, 1117–1126.

Robert-Moreno, A., Guiu, J., Ruiz-Herguido, C., López, M.E., Inglés-Esteve, J., Riera, L., Tipping, A., Enver, T., Dzierzak, E., Gridley, T., et al. (2008). Impaired embryonic

haematopoiesis yet normal arterial development in the absence of the Notch ligand Jagged1. EMBO J. *27*, 1886–1895.

Rybtsov, S., Sobiesiak, M., Taoudi, S., Souilhol, C., Senserrich, J., Liakhovitskaia, A., Ivanovs, A., Frampton, J., Zhao, S., and Medvinsky, A. (2011). Hierarchical organization and early hematopoietic specification of the developing HSC lineage in the AGM region. J. Exp. Med. *208*, 1305–1315.

Rybtsov, S., Batsivari, A., Bilotkach, K., Paruzina, D., Senserrich, J., Nerushev, O., and Medvinsky, A. (2014). Tracing the Origin of the HSC Hierarchy Reveals an SCF-Dependent, IL-3-Independent CD43− Embryonic Precursor. Stem Cell Rep. *3*, 489–501.

Rybtsov, S., Ivanovs, A., Zhao, S., and Medvinsky, A. (2016). Concealed expansion of immature precursors underpins acute burst of adult HSC activity in foetal liver. Development *143*, 1284–1289.

Sabin, F. (1921). THE VITALLY STAINABLE GRANULES AS A SPECIFIC CRITERION FOR ERYTHRO- BLASTS AND THE DIFFERENTIATION OF ,THE THREE STRAINS OF THE WHITE BLOOD-CELLS AS SEEN IN THE LIVING CHICK'S YOLK-SAC. John Hopkins Hosp. Bull. *368*, 314–321.

Samokhvalov, I.M., Samokhvalova, N.I., and Nishikawa, S. (2007). Cell tracing shows the contribution of the yolk sac to adult haematopoiesis. Nature *446*, 1056–1061.

Sánchez, M.J., Holmes, A., Miles, C., and Dzierzak, E. (1996). Characterization of the first definitive hematopoietic stem cells in the AGM and liver of the mouse embryo. Immunity *5*, 513–525.

Sanchez, M.-J., Gottgens, B., Sinclair, A.M., Stanley, M., Begley, C.G., Hunter, S., and Green, A.R. (1999). An SCL 3′ enhancer targets developing endothelium together with embryonic and adult haematopoietic progenitors. Development *126*, 3891–3904.

Sasaki, K., Yagi, H., Bronson, R.T., Tominaga, K., Matsunashi, T., Deguchi, K., Tani, Y., Kishimoto, T., and Komori, T. (1996). Absence of fetal liver hematopoiesis in mice deficient in transcriptional coactivator core binding factor beta. Proc. Natl. Acad. Sci. U. S. A. *93*, 12359–12363.

Sato, T.N., Qin, Y., Kozak, C.A., and Audus, K.L. (1993). Tie-1 and tie-2 define another class of putative receptor tyrosine kinase genes expressed in early embryonic vascular system. Proc. Natl. Acad. Sci. U. S. A. *90*, 9355–9358.

Schulz, C., Perdiguero, E.G., Chorro, L., Szabo-Rogers, H., Cagnard, N., Kierdorf, K., Prinz, M., Wu, B., Jacobsen, S.E.W., Pollard, J.W., et al. (2012). A Lineage of Myeloid Cells Independent of Myb and Hematopoietic Stem Cells. Science *336*, 86–90.

Schütte, J., Wang, H., Antoniou, S., Jarratt, A., Wilson, N.K., Riepsaame, J., Calero-Nieto, F.J., Moignard, V., Basilico, S., Kinston, S.J., et al. (2016a). An experimentally validated network of nine haematopoietic transcription factors reveals mechanisms of cell state stability. eLife *5*.

Schütte, J., Wang, H., Antoniou, S., Jarratt, A., Wilson, N.K., Riepsaame, J., Calero-Nieto, F.J., Moignard, V., Basilico, S., Kinston, S.J., et al. (2016b). An experimentally validated network of nine haematopoietic transcription factors reveals mechanisms of cell state stability. eLife *5*, e11469.

Scialdone, A., Tanaka, Y., Jawaid, W., Moignard, V., Wilson, N.K., Macaulay, I.C., Marioni, J.C., and Göttgens, B. (2016). Resolving early mesoderm diversification through single-cell expression profiling. Nature *535*, 289–293.

Scott, E.W., Simon, M.C., Anastasi, J., and Singh, H. (1994). Requirement of transcription factor PU.1 in the development of multiple hematopoietic lineages. Science *265*, 1573–1577.

Shalaby, F., Rossant, J., Yamaguchi, T.P., Gertsenstein, M., Wu, X.-F., Breitman, M.L., and Schuh, A.C. (1995). Failure of blood-island formation and vasculogenesis in Flk-1-deficient mice. Nature *376*, 62–66.

Shalaby, F., Ho, J., Stanford, W.L., Fischer, K.D., Schuh, A.C., Schwartz, L., Bernstein, A., and Rossant, J. (1997). A requirement for Flk1 in primitive and definitive hematopoiesis and vasculogenesis. Cell *89*, 981–990.

Sheridan, J.M., Taoudi, S., Medvinsky, A., and Blackburn, C.C. (2009). A novel method for the generation of reaggregated organotypic cultures that permits juxtaposition of defined cell populations. Genesis *47*, 346–351.

Shi, X., Richard, J., Zirbes, K.M., Gong, W., Lin, G., Kyba, M., Thomson, J.A., Koyano-Nakagawa, N., and Garry, D.J. (2014). Cooperative interaction of Etv2 and Gata2 regulates the development of endothelial and hematopoietic lineages. Dev. Biol. *389*, 208–218.

Shivdasani, R.A., Mayer, E.L., and Orkin, S.H. (1995). Absence of blood formation in mice lacking the T-cell leukaemia oncoprotein tal-1/SCL. Nature *373*, 432–434.

Siminovitch, L., Till, J.E., and McCulloch, E.A. (1964). Decline in colony-forming ability of marrow cells subjected to serial transplantation into irradiated mice. J. Cell. Comp. Physiol. *64*, 23–31.

Slukvin, I.I. (2016). Generating human hematopoietic stem cells *in vitro* -exploring endothelial to hematopoietic transition as a portal for stemness acquisition. FEBS Lett.

Smith, R.A., and Glomski, C.A. (1982). HEMOGENIC ENDOTHELIUM" OF THE EMBRYONICAORTA: DOESITEXIST? Dev. Comp. Immunol. *6*, 359–368.

Song, W.J., Sullivan, M.G., Legare, R.D., Hutchings, S., Tan, X., Kufrin, D., Ratajczak, J., Resende, I.C., Haworth, C., Hock, R., et al. (1999). Haploinsufficiency of CBFA2 causes familial thrombocytopenia with propensity to develop acute myelogenous leukaemia. Nat. Genet. *23*, 166–175.

Souilhol, C., Gonneau, C., Lendinez, J.G., Batsivari, A., Rybtsov, S., Wilson, H., Morgado-Palacin, L., Hills, D., Taoudi, S., Antonchuk, J., et al. (2016a). Inductive interactions mediated by interplay of asymmetric signalling underlie development of adult haematopoietic stem cells. Nat. Commun. *7*, 10784.

Souilhol, C., Lendinez, J.G., Rybtsov, S., Murphy, F., Wilson, H., Hills, D., Batsivari, A., Binagui-Casas, A., McGarvey, A.C., MacDonald, H.R., et al. (2016b). Developing HSCs become Notch independent by the end of maturation in the AGM region. Blood *128*, 1567–1577.

Spyropoulos, D.D., Pharr, P.N., Lavenburg, K.R., Jackers, P., Papas, T.S., Ogawa, M., and Watson, D.K. (2000). Hemorrhage, impaired hematopoiesis, and lethality in mouse embryos carrying a targeted disruption of the Fli1 transcription factor. Mol. Cell. Biol. *20*, 5643–5652.

Sroczynska, P., Lancrin, C., Kouskoff, V., and Lacaud, G. (2009). The differential activities of Runx1 promoters define milestones during embryonic hematopoiesis. Blood *114*, 5279–5289.

Staber, P.B., Zhang, P., Ye, M., Welner, R.S., Nombela-Arrieta, C., Bach, C., Kerenyi, M., Bartholdy, B.A., Zhang, H., Alberich-Jordà, M., et al. (2013). Sustained PU.1 Levels

Balance Cell-Cycle Regulators to Prevent Exhaustion of Adult Hematopoietic Stem Cells. Mol. Cell *49*, 934–946.

Sugiyama, D., Ogawa, M., Hirose, I., Jaffredo, T., Arai, K., and Tsuji, K. (2003). Erythropoiesis from acetyl LDL incorporating endothelial cells at the preliver stage. Blood *101*, 4733–4738.

Sugiyama, D., Arai, K., and Tsuji, K. (2005). Definitive Hematopoiesis from Acetyl LDL Incorporating Endothelial Cells in the Mouse Embryo. Stem Cells Dev. *14*, 687–696.

Swiers, G., Baumann, C., O'Rourke, J., Giannoulatou, E., Taylor, S., Joshi, A., Moignard, V., Pina, C., Bee, T., Kokkaliaris, K.D., et al. (2013). Early dynamic fate changes in haemogenic endothelium characterized at the single-cell level. Nat. Commun. *4*.

Szabo, E., Rampalli, S., Risueño, R.M., Schnerch, A., Mitchell, R., Fiebig-Comyn, A., Levadoux-Martin, M., and Bhatia, M. (2010). Direct conversion of human fibroblasts to multilineage blood progenitors. Nature *468*, 521–526.

Takahashi, K., and Yamanaka, S. (2006). Induction of Pluripotent Stem Cells from Mouse Embryonic and Adult Fibroblast Cultures by Defined Factors. Cell *126*, 663–676.

Takakura, N., Watanabe, T., Suenobu, S., Yamada, Y., Noda, T., Ito, Y., Satake, M., and Suda, T. (2000). A role for hematopoietic stem cells in promoting angiogenesis. Cell *102*, 199–209.

Tam, P.P. (1998). Postimplantation mouse development: whole embryo culture and micro-manipulation. Int. J. Dev. Biol. *42*, 895–902.

Tam, P.P., and Beddington, R.S. (1987). The formation of mesodermal tissues in the mouse embryo during gastrulation and early organogenesis. Dev. Camb. Engl. *99*, 109–126.

Tam, P.P., Parameswaran, M., Kinder, S.J., and Weinberger, R.P. (1997). The allocation of epiblast cells to the embryonic heart and other mesodermal lineages: the role of ingression and tissue movement during gastrulation. Dev. Camb. Engl. *124*, 1631–1642.

Taoudi, S. (2005). Progressive divergence of definitive haematopoietic stem cells from the endothelial compartment does not depend on contact with the foetal liver. Development *132*, 4179–4191.

Taoudi, S., and Medvinsky, A. (2007). Functional identification of the hematopoietic stem cell niche in the ventral domain of the embryonic dorsal aorta. Proc. Natl. Acad. Sci. U. S. A. *104*, 9399–9403.

Taoudi, S., Gonneau, C., Moore, K., Sheridan, J.M., Blackburn, C.C., Taylor, E., and Medvinsky, A. (2008). Extensive Hematopoietic Stem Cell Generation in the AGM Region via Maturation of VE-Cadherin+CD45+ Pre-Definitive HSCs. Cell Stem Cell *3*, 99–108.

Tavian, M., Coulombel, L., Luton, D., Clemente, H.S., Dieterlen-Lièvre, F., and Peault, B. (1996). Aorta-associated CD34+ hematopoietic cells in the early human embryo. Blood *87*, 67–72.

Tavian, M., Robin, C., Coulombel, L., and Peault, B. (2001). The Human Embryo, but Not Its Yolk Sac, Generates Lympho-Myeloid Stem Cells: Mapping Multipotent Hematopoietic Cell Fate in Intraembryonic Mesoderm. Immunity *15*, 487–495.

Taylor, E., Taoudi, S., and Medvinsky, A. (2010). Hematopoietic stem cell activity in the aorta-gonad-mesonephros region enhances after mid-day 11 of mouse development. Int. J. Dev. Biol. *54*, 1055–1060.

Thambyrajah, R., Mazan, M., Patel, R., Moignard, V., Stefanska, M., Marinopoulou, E., Li, Y., Lancrin, C., Clapes, T., Möröy, T., et al. (2015). GFI1 proteins orchestrate the emergence of haematopoietic stem cells through recruitment of LSD1. Nat. Cell Biol. *18*, 21–32.

Thambyrajah, R., Ucanok, D., Jalali, M., Hough, Y., Wilkinson, R.N., McMahon, K., Moore, C., and Gering, M. (2016). A gene trap transposon eliminates haematopoietic expression of zebrafish Gfi1aa, but does not interfere with haematopoiesis. Dev. Biol. *417*, 25–39.

Thomas, E.D., Lochte, H.L.J., Lu, W.C., and Ferrebee, J.W. (1957). Intravenous Infusion of Bone Marrow in Patients Receiving Radiation and Chemotherapy. N. Engl. J. Med. *257*, 491–496.

Thomas, E.D., Lochte, H.L., Cannon, J.H., Sahler, O.D., and Ferrebee, J.W. (1959). SUPRALETHAL WHOLE BODY IRRADIATION AND ISOLOGOUS MARROW TRANSPLANTATION IN MAN*. J. Clin. Invest. *38*, 1709–1716.

Thompson, M.A., Ransom, D.G., Pratt, S.J., MacLennan, H., Kieran, M.W., Detrich, H.W., Vail, B., Huber, T.L., Paw, B., Brownlie, A.J., et al. (1998). The cloche and spadetail genes differentially affect hematopoiesis and vasculogenesis. Dev. Biol. *197*, 248–269.

Tober, J., Koniski, A., McGrath, K.E., Vemishetti, R., Emerson, R., de Mesy-Bentley, K.K.L., Waugh, R., and Palis, J. (2007). The megakaryocyte lineage originates from hemangioblast precursors and is an integral component both of primitive and of definitive hematopoiesis. Blood *109*, 1433–1441.

Tober, J., Yzaguirre, A.D., Piwarzyk, E., and Speck, N.A. (2013). Distinct temporal requirements for Runx1 in hematopoietic progenitors and stem cells. Dev. Camb. Engl. *140*, 3765–3776.

Tsai, F.Y., Keller, G., Kuo, F.C., Weiss, M., Chen, J., Rosenblatt, M., Alt, F.W., and Orkin, S.H. (1994). An early haematopoietic defect in mice lacking the transcription factor GATA-2. Nature *371*, 221–226.

Ueno, H., and Weissman, I.L. (2006). Clonal Analysis of Mouse Development Reveals a Polyclonal Origin for Yolk Sac Blood Islands. Dev. Cell *11*, 519–533.

Ueno, H., and Weissman, I.L. (2010). The origin and fate of yolk sac hematopoiesis: application of chimera analyses to developmental studies. Int. J. Dev. Biol. *54*, 1019–1031.

Unnisa, Z., Clark, J.P., Roychoudhury, J., Thomas, E., Tessarollo, L., Copeland, N.G., Jenkins, N.A., Grimes, H.L., and Kumar, A.R. (2012). Meis1 preserves hematopoietic stem cells in mice by limiting oxidative stress. Blood *120*, 4973–4981.

Vargel, Ö., Zhang, Y., Kosim, K., Ganter, K., Foehr, S., Mardenborough, Y., Shvartsman, M., Enright, A.J., Krijgsveld, J., and Lancrin, C. (2016). Activation of the TGFβ pathway impairs endothelial to haematopoietic transition. Sci. Rep. *6*, 21518.

Vierstra, J., Rynes, E., Sandstrom, R., Zhang, M., Canfield, T., Hansen, R.S., Stehling-Sun, S., Sabo, P.J., Byron, R., Humbert, R., et al. (2014). Mouse regulatory DNA landscapes reveal global principles of cis-regulatory evolution. Science *346*, 1007–1012.

Vodyanik, M.A., Yu, J., Zhang, X., Tian, S., Stewart, R., Thomson, J.A., and Slukvin, I.I. (2010). A Mesoderm-Derived Precursor for Mesenchymal Stem and Endothelial Cells. Cell Stem Cell *7*, 718–729.

Vogeli, K.M., Jin, S.-W., Martin, G.R., and Stainier, D.Y.R. (2006). A common progenitor for haematopoietic and endothelial lineages in the zebrafish gastrula. Nature *443*, 337–339.

Voyta, J.C., Via, D.P., Butterfield, C.E., and Zetter, B.R. (1984). Identification and isolation of endothelial cells based on their increased uptake of acetylated-low density lipoprotein. J. Cell Biol. *99*, 2034–2040.

Wang, H.U., Chen, Z.F., and Anderson, D.J. (1998). Molecular distinction and angiogenic interaction between embryonic arteries and veins revealed by ephrin-B2 and its receptor Eph-B4. Cell *93*, 741–753.

Wang, Q., Stacy, T., Binder, M., Marin-Padilla, M., Sharpe, A.H., and Speck, N.A. (1996a). Disruption of the Cbfa2 gene causes necrosis and hemorrhaging in the central nervous system and blocks definitive hematopoiesis. Proc. Natl. Acad. Sci. U. S. A. *93*, 3444–3449.

Wang, Q., Stacy, T., Miller, J.D., Lewis, A.F., Gu, T.L., Huang, X., Bushweller, J.H., Bories, J.C., Alt, F.W., Ryan, G., et al. (1996b). The CBFbeta subunit is essential for CBFalpha2 (AML1) function in vivo. Cell *87*, 697–708.

Wang, X.-Y., Lan, Y., He, W.-Y., Zhang, L., Yao, H.-Y., Hou, C.-M., Tong, Y., Liu, Y.-L., Yang, G., Liu, X.-D., et al. (2008). Identification of mesenchymal stem cells in aorta-gonad-mesonephros and yolk sac of human embryos. Blood *111*, 2436–2443.

Wang, Y., Belflower, R.M., Dong, Y.-F., Schwarz, E.M., O'Keefe, R.J., and Drissi, H. (2005). Runx1/AML1/Cbfa2 Mediates Onset of Mesenchymal Cell Differentiation Toward Chondrogenesis. J. Bone Miner. Res. *20*, 1624–1636.

Wareing, S., Mazan, A., Pearson, S., Göttgens, B., Lacaud, G., and Kouskoff, V. (2012). The Flk1-Cre-Mediated Deletion of ETV2 Defines Its Narrow Temporal Requirement During Embryonic Hematopoietic Development. STEM CELLS *30*, 1521–1531.

Wasteson, P., Johansson, B.R., Jukkola, T., Breuer, S., Akyurek, L.M., Partanen, J., and Lindahl, P. (2008). Developmental origin of smooth muscle cells in the descending aorta in mice. Development *135*, 1823–1832.

Wilkinson, A.C., Kawata, V.K.S., Schutte, J., Gao, X., Antoniou, S., Baumann, C., Woodhouse, S., Hannah, R., Tanaka, Y., Swiers, G., et al. (2014). Single-cell analyses of regulatory network perturbations using enhancer-targeting TALEs suggest novel roles for PU.1 during haematopoietic specification. Development *141*, 4018–4030.

Wilkinson, R.N., Pouget, C., Gering, M., Russell, A.J., Davies, S.G., Kimelman, D., and Patient, R. (2009). Hedgehog and Bmp Polarize Hematopoietic Stem Cell Emergence in the Zebrafish Dorsal Aorta. Dev. Cell *16*, 909–916.

Wilson, N.K., Timms, R.T., Kinston, S.J., Cheng, Y.-H., Oram, S.H., Landry, J.-R., Mullender, J., Ottersbach, K., and Gottgens, B. (2010). Gfi1 Expression Is Controlled by Five Distinct Regulatory Regions Spread over 100 Kilobases, with Scl/Tal1, Gata2, PU.1, Erg, Meis1, and Runx1 Acting as Upstream Regulators in Early Hematopoietic Cells. Mol. Cell. Biol. *30*, 3853–3863.

Wilson, N.K., Schoenfelder, S., Hannah, R., Sánchez Castillo, M., Schütte, J., Ladopoulos, V., Mitchelmore, J., Goode, D.K., Calero-Nieto, F.J., Moignard, V., et al. (2016). Integrated genome-scale analysis of the transcriptional regulatory landscape in a blood stem/progenitor cell model. Blood *127*, e12-23.

Wilt, F.H. (1965). Erythropoiesis in the Chick Embryo: The Role of Endoderm. Science *147*, 1588–1590.

Woll, P.S., Grzywacz, B., Tian, X., Marcus, R.K., Knorr, D.A., Verneris, M.R., and Kaufman, D.S. (2009). Human embryonic stem cells differentiate into a homogeneous population of natural killer cells with potent in vivo antitumor activity. Blood *113*, 6094–6101.

Wood, H.B., May, G., Healy, L., Enver, T., and Morriss-Kay, G.. (1997). CD34 Expression Patterns During Early Mouse Development Are Related to Modes of Blood Vessel Formation and Reveal Additional Sites of Hematopoiesis. Blood *90*, 2300–2311.

Yamaguchi, T.P., Dumont, D.J., Conlon, R.A., Breitman, M.L., and Rossant, J. (1993). flk-1, an flt-related receptor tyrosine kinase is an early marker for endothelial cell precursors. Dev. Camb. Engl. *118*, 489–498.

Yamashiro, T., Wang, X.-P., Li, Z., Oya, S., Åberg, T., Fukunaga, T., Kamioka, H., Speck, N.A., Takano-Yamamoto, T., and Thesleff, I. (2004). Possible Roles of Runx1 and Sox9 in Incipient Intramembranous Ossification. J. Bone Miner. Res. *19*, 1671–1677.

Yoder, M.C., and Hiatt, K. (1997). Engraftment of Embryonic Hematopoietic Cells in Conditioned Newborn Recipients. Blood *89*, 2176–2183.

Yoder, M.C., Hiatt, K., Dutt, P., Mukherjee, P., Bodine, D.M., and Orlic, D. (1997). Characterization of Definitive Lymphohematopoietic Stem Cells in the Day 9 Murine Yolk Sac. Immunity *7*, 335–344.

Yokomizo, T., and Dzierzak, E. (2010). Three-dimensional cartography of hematopoietic clusters in the vasculature of whole mouse embryos. Development *137*, 3651–3661.

Yokomizo, T., Ogawa, M., Osato, M., Kanno, T., Yoshida, H., Fujimoto, T., Fraser, S., Nishikawa, S., Okada, H., Satake, M., et al. (2001). Requirement of Runx1/AML1/PEBP2αB for the generation of haematopoietic cells from endothelial cells. Genes Cells *6*, 13–23.

Yokomizo, T., Hasegawa, K., Ishitobi, H., Osato, M., Ema, M., Ito, Y., Yamamoto, M., and Takahashi, S. (2008). Runx1 is involved in primitive erythropoiesis in the mouse. Blood *111*, 4075–4080.

Yoshimoto, M., Montecino-Rodriguez, E., Ferkowicz, M.J., Porayette, P., Shelley, W.C., Conway, S.J., Dorshkind, K., and Yoder, M.C. (2011). Embryonic day 9 yolk sac and intra-embryonic hemogenic endothelium independently generate a B-1 and marginal zone progenitor lacking B-2 potential. Proc. Natl. Acad. Sci. *108*, 1468–1473.

Yoshimoto, M., Porayette, P., Glosson, N.L., Conway, S.J., Carlesso, N., Cardoso, A.A., Kaplan, M.H., and Yoder, M.C. (2012). Autonomous murine T-cell progenitor production in the extra-embryonic yolk sac before HSC emergence. Blood *119*, 5706–5714.

Yzaguirre, A.D., and Speck, N.A. (2016). Insights into blood cell formation from hemogenic endothelium in lesser-known anatomic sites: 3D Analysis of Embryonic Hematopoiesis. Dev. Dyn. *245*, 1011–1028.

Zeigler, B.M., Sugiyama, D., Chen, M., Guo, Y., Downs, K.M., and Speck, N.A. (2006). The allantois and chorion, when isolated before circulation or chorio-allantoic fusion, have hematopoietic potential. Development *133*, 4183–4192.

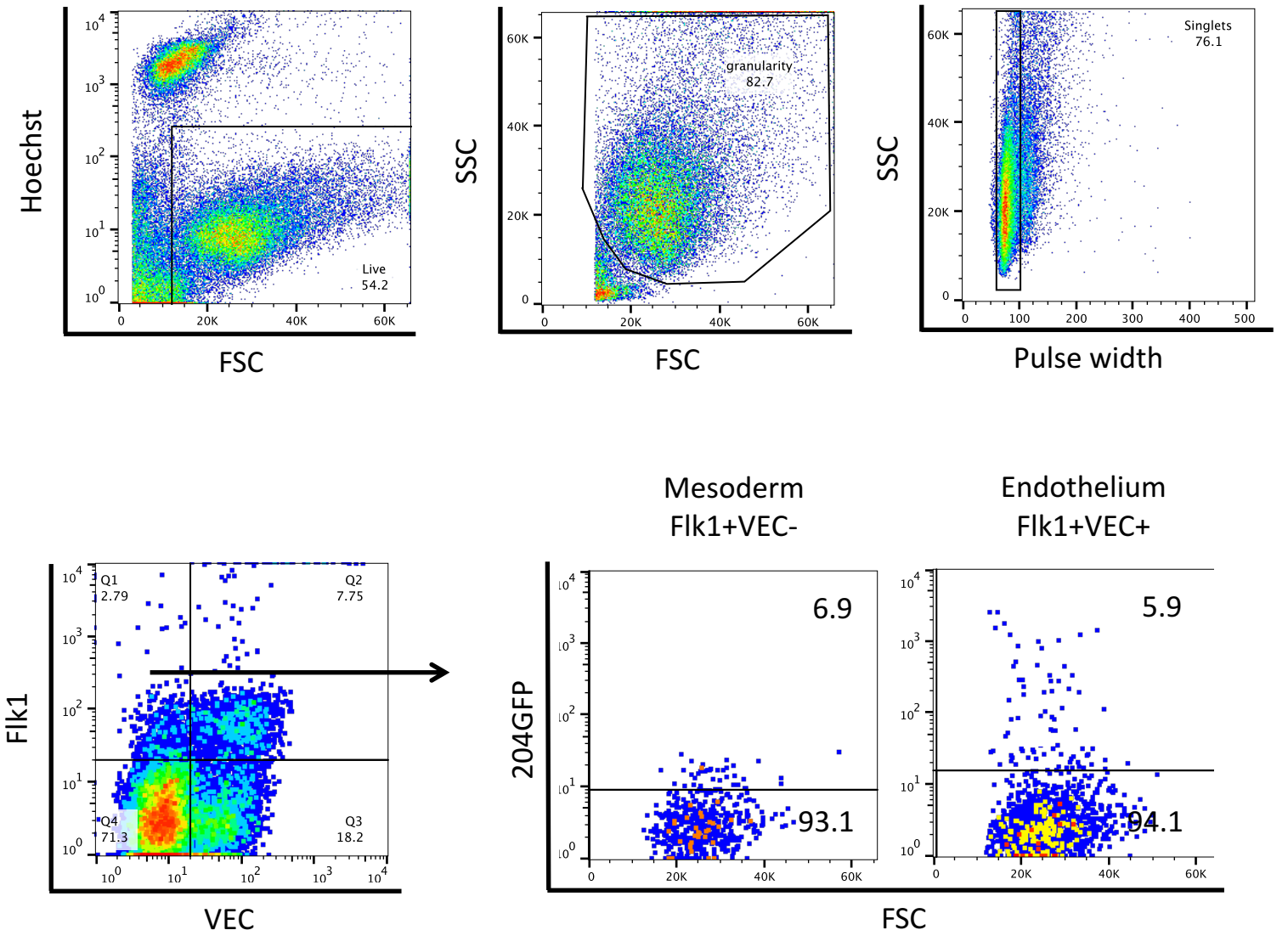
Zeng, H., Yücel, R., Kosan, C., Klein-Hitpass, L., and Möröy, T. (2004). Transcription factor Gfi1 regulates self-renewal and engraftment of hematopoietic stem cells. EMBO J. *23*, 4116–4125.

Zhou, F., Li, X., Wang, W., Zhu, P., Zhou, J., He, W., Ding, M., Xiong, F., Zheng, X., Li, Z., et al. (2016). Tracing haematopoietic stem cell formation at single-cell resolution. Nature *533*, 487–492.

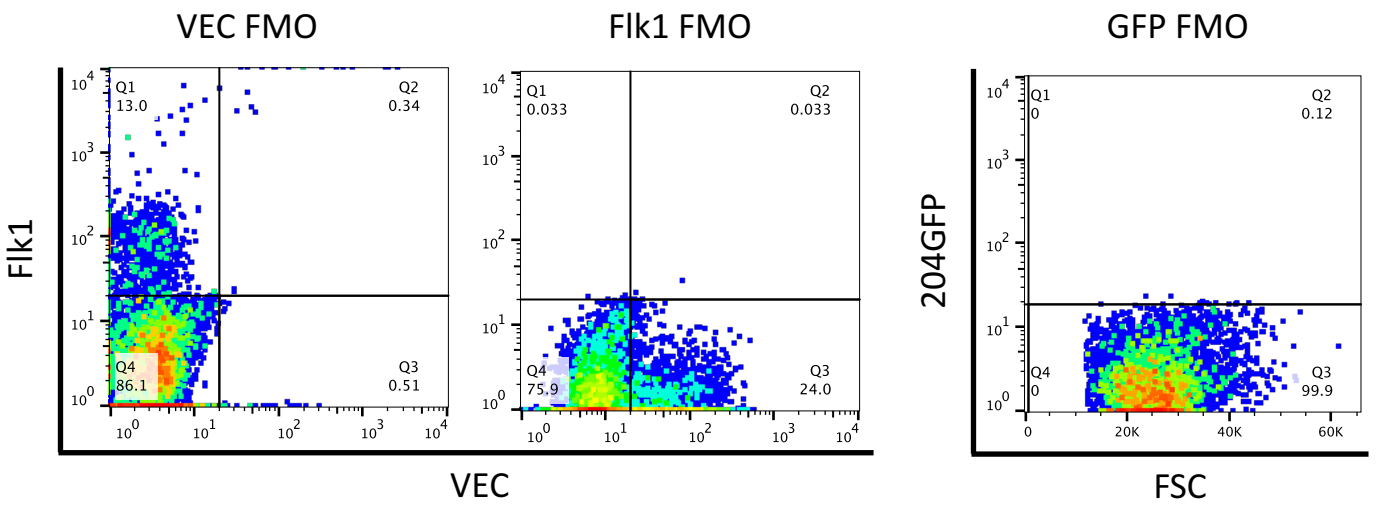
Zorn (2008). Liver Development. StemBook.

Zovein, A.C., Hofmann, J.J., Lynch, M., French, W.J., Turlo, K.A., Yang, Y., Becker, M.S., Zanetta, L., Dejana, E., Gasson, J.C., et al. (2008). Fate Tracing Reveals the Endothelial Origin of Hematopoietic Stem Cells. Cell Stem Cell *3*, 625–636.

Zovein, A.C., Turlo, K.A., Ponec, R.M., Lynch, M.R., Chen, K.C., Hofmann, J.J., Cox, T.C., Gasson, J.C., and Iruela-Arispe, M.L. (2010). Vascular remodeling of the vitelline artery initiates extravascular emergence of hematopoietic clusters. Blood *116*, 3435–3444.

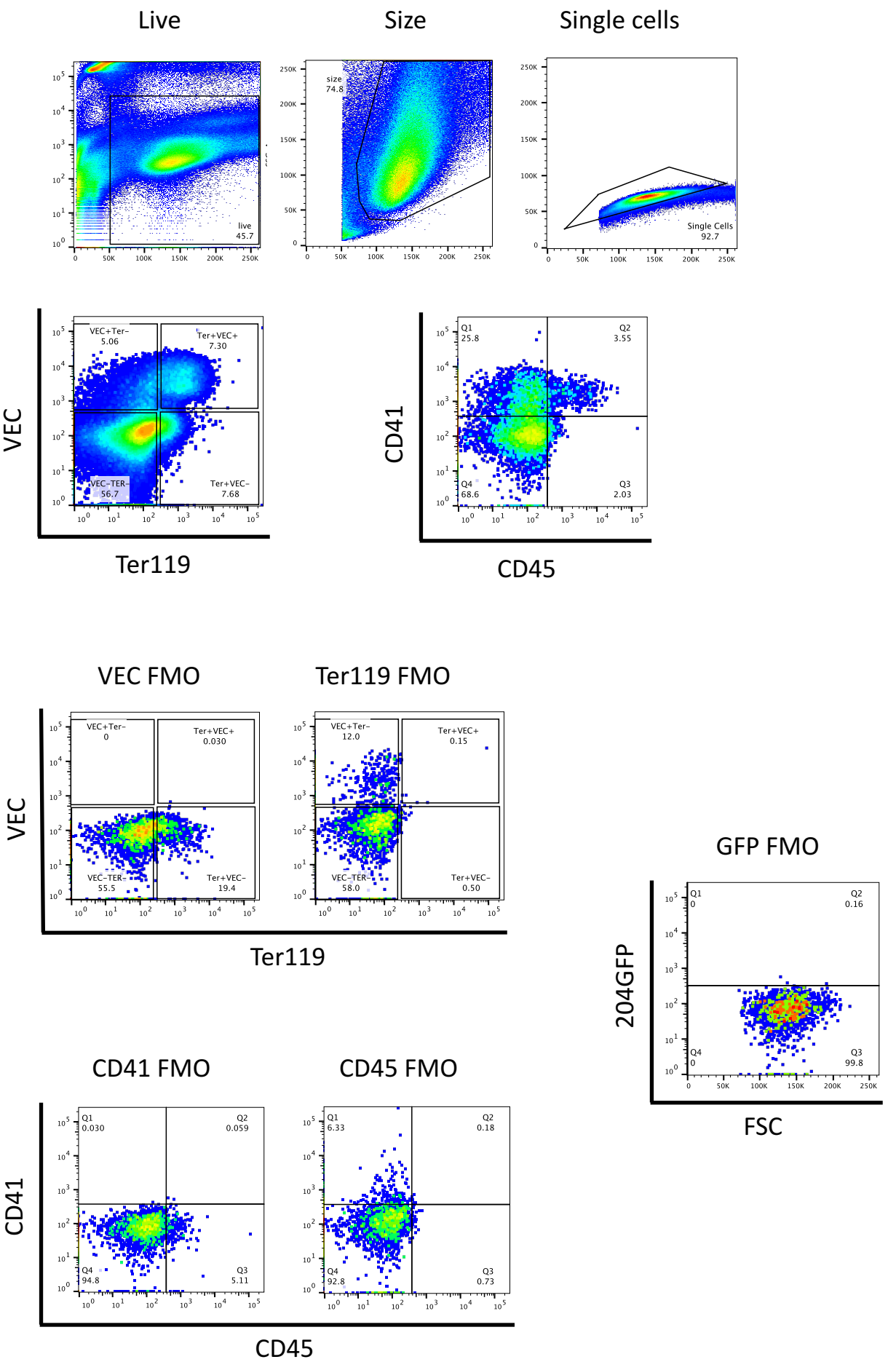


E7.5 controls

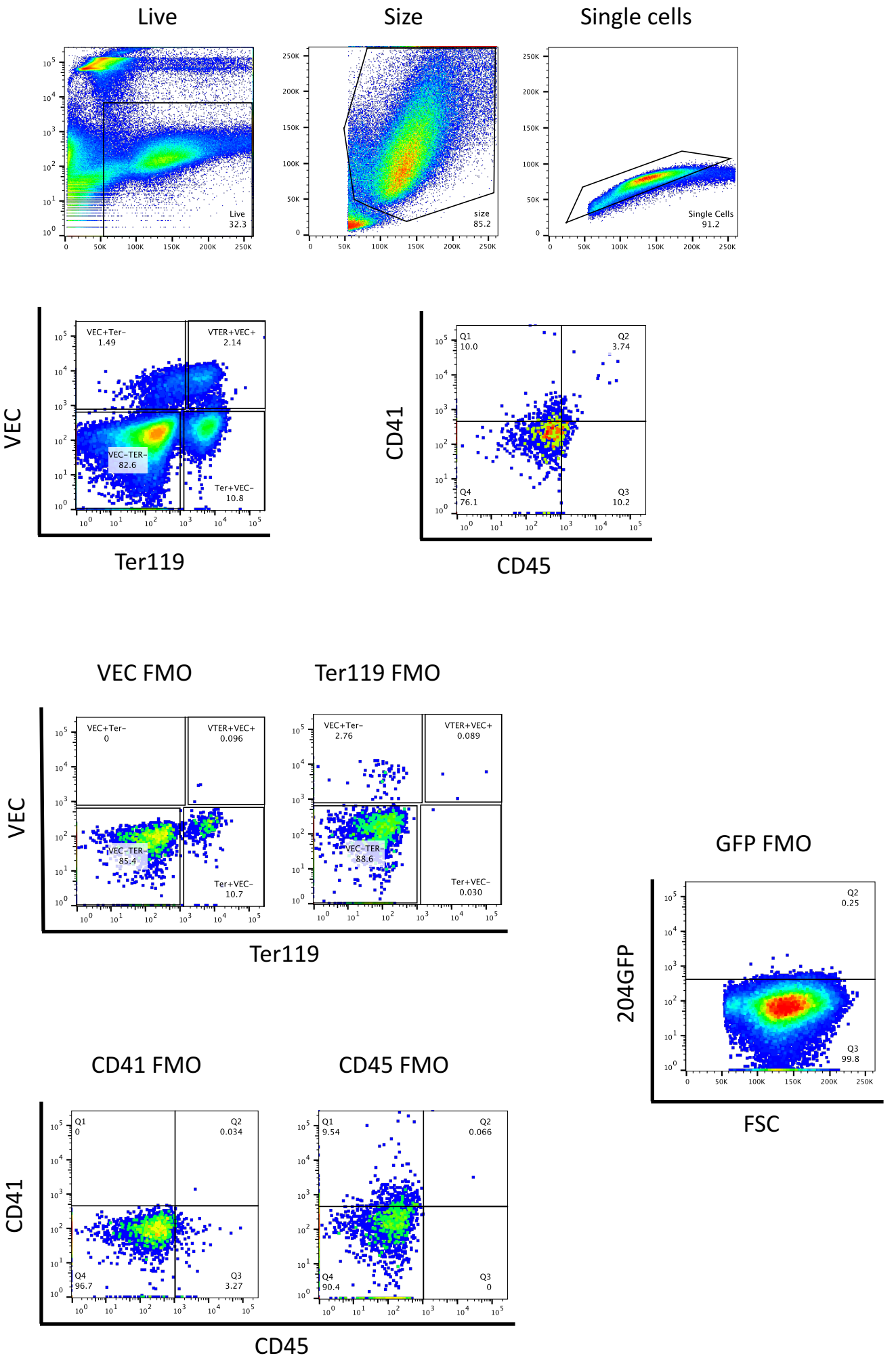


Appendix 3.1 The earliest 204GFP expression in the endothelium starts at the headfold stage

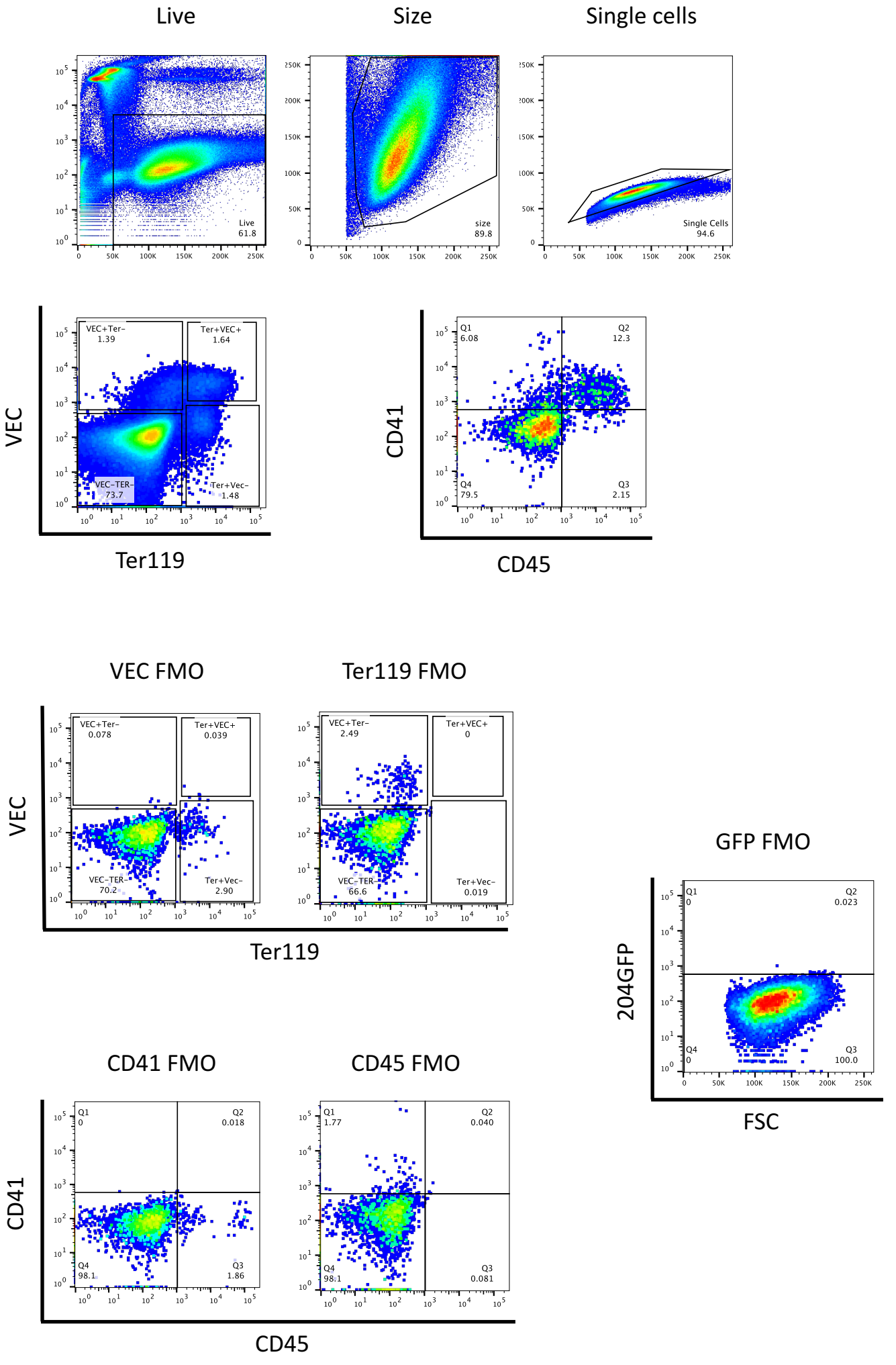
Flow cytometry analysis of headfold stage (7dpc) 204GFP transgenic embryos. Live (Hoechst-), single cells were gated based on Flk1 and VEC expression. 204GFP expression was then analyzed in mesoderm (Flk1+VEC-) and endothelial (Flk1+VEC+) cells. Percentages of one experiment are given. 204GFP expression is so low at 7dpc that we are not able to observe it in fresh and GFP-stained wholemount embryos (cf. Figure 3.9). Bottom panel shows the FMO controls.



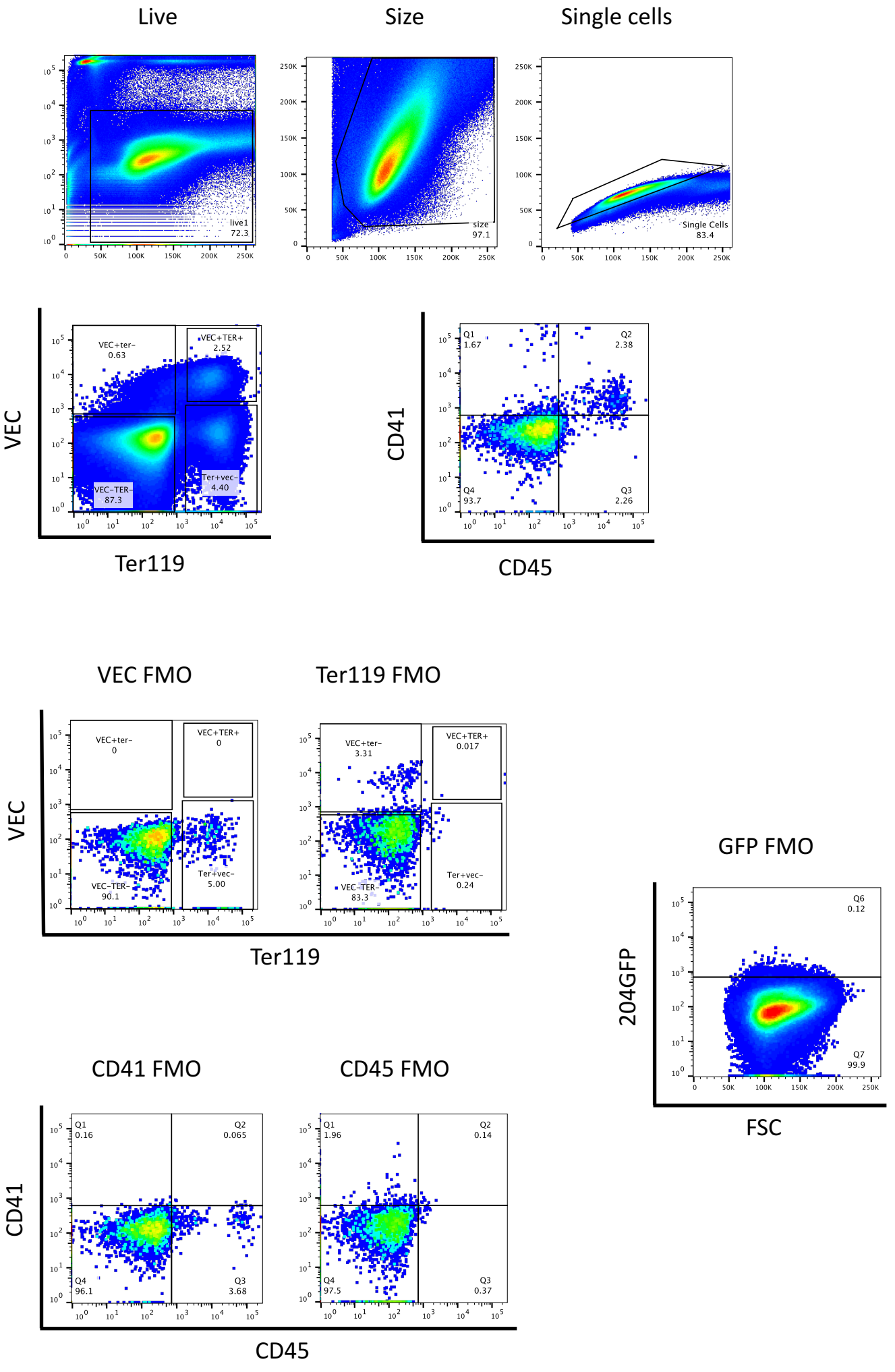
Appendix 3.2 Control plots for 204GFP expression at E8.5
Representative gates for live, single, VEC/Ter119 and CD41/CD45 plots for E8.5 experiments are given. Gates were drawn based on fluorescence minus one (FMO) control for all 5 fluorochromes. Controls are directly linked to E8.5 data in Figure 3.14 and Figure 3.15.



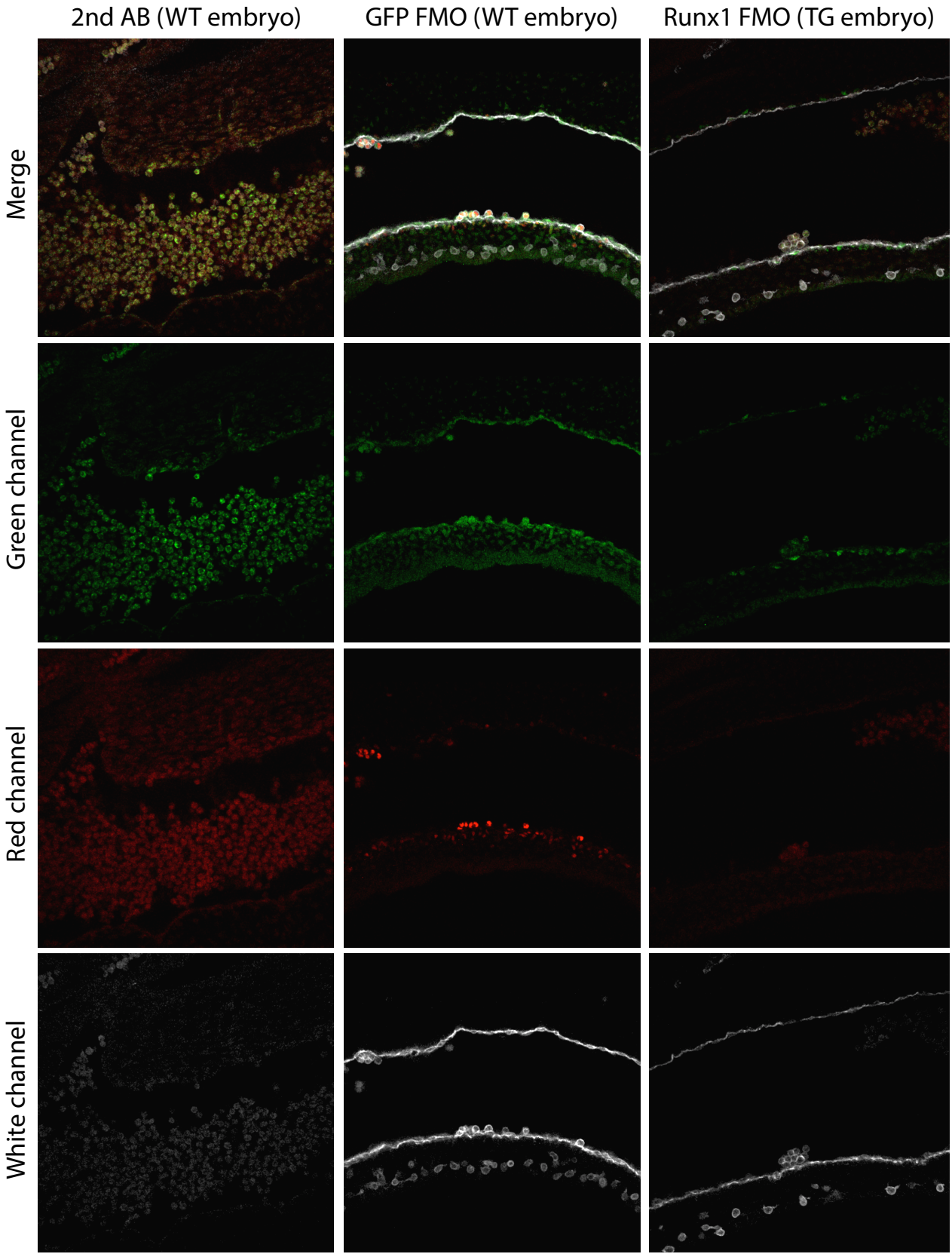
Appendix 3.3 Control plots for 204GFP expression at E9.5
Representative gates for live, single, VEC/Ter119 and CD41/CD45 plots for E9.5 experiments are given. Gates were drawn based on fluorescence minus one (FMO) control for all 5 fluorochromes. Controls are directly linked to E9.5 data in Figure 3.14 and Figure 3.15.



Appendix 3.4 Control plots for 204GFP expression at E10.5
Representative gates for live, single, VEC/Ter119 and CD41/CD45 plots for E10.5 experiments are given. Gates were drawn based on fluorescence minus one (FMO) control for all 5 fluorochromes. Controls are directly linked to E10.5 data in Figure 3.14 and Figure 3.15.



Appendix 3.5 Control plots for 204GFP expression at E11.5
Representative gates for live, single, VEC/Ter119 and CD41/CD45 plots for E11.5 experiments are given. Gates were drawn based on fluorescence minus one (FMO) control for all 5 fluorochromes. Controls are directly linked to E11.5 data in Figure 3.14 and Figure 3.15.



Appendix 3.6 Staining controls for E10.5 wholemount co-expression analysis
Staining controls for E10.5 wholemount co-expression analysis are shown. Secondary antibody control, GFP FMO control and Runx1 FMO contols are shown with expression in individual channels. Controls correspond to Figure 3.17.

OP90018: E10.5 AGM+VU (31-34sp)

	No cell control	EC 205GFP-		EC 205GFP+		EC whole	VEC+41+
Cells plated	0	200	500	200	96	200	50
Blood-like cells (confirmed by CD45 flow)				yes			Yes
CD31 endothelial colonies	0	9	20	5	0	9	0
CD31-stained blood colonies				2			2
Frequency of EC colonies/cells		1:22	1:25	1:40	>1:96	1:22	

WT EC purity: 100%

OP90022: E10.5 AGM+VU (32-39sp)

	No cell control	EC 205GFP-		EC 205GFP+		EC whole		VEC+41+
Cells plated	0	200	300	200	209	200	300	40
Blood-like cells (confirmed by CD45 flow)					yes			yes
CD31 endothelial colonies	0	8	8	1	4	6	10	ND
CD31-stained blood colonies					1			
Frequency of EC colonies/cells		1:25	1:38	1:200	1:52	1:33	1:30	

WT EC purity: 89.1%

OP90024: E10.5 AGM+VU (31-36sp)

	No cell control	EC 205GFP-			EC 205GFP+			EC whole		VEC+41 +
Cells plated	0	100	200	500	100	200	500	500	1000	100
Blood-like cells (confirmed by CD45 flow)						yes				Yes
CD31 endothelial colonies	0	3	4	21	2	5	8	16	22	0
CD31-stained blood colonies						1				2
Frequency of EC colonies/cells		1:33	1:50	1:24	1:50	1:40	1:63	1:31	1:46	

WT EC purity: 96.5%; 204GFP+ EC purity: 87.5%; 204GFP- EC purity: 100%;

Appendix 4.1 E10.5 OP9 co-culture data

Table of raw data from E10.5 OP9 co-culture assays. Number of cells plated, whether blood-like colonies were detected after 8 days in culture, number of CD31+ endothelial network detected, number of CD31+ blood colonies detected and the rough frequency of endothelial networks per cells plated are given for 3 experiments. No cell control - no cells were plated onto OP9 stromal layer; VEC+CD41+ control - blood output assay control, referred to as CD41+ blood or cluster cells in the text.

OP90019: E8.5 (5-13sp) whole conceptus

	No cell control	EC 205GFP-	EC 205GFP+	EC whole	VEC+41+
Cells plated	0	1200	863	1200	200
Blood-like cells					Yes
CD31 endothelial colonies		~22	~17	~33	0
Freq. EC/cells		1:55	1:51	1:36	

WT EC purity: 95.9%

OP90020: E8.5 (6-12sp) whole conceptus

	No cell control	EC 205GFP-	EC 205GFP+	EC whole	VEC+41+
Cells plated	0	2000	569	2000	510
Blood-like cells					Yes
CD31 endothelial colonies		~14	~2	~22	1
Freq. EC/cells		1:143	1:285	1:91	1:510

WT EC purity: 95.7%

OP90021: E8.5 (3-13sp) whole conceptus

	No cell control	EC 205GFP-	EC 205GFP+	EC whole	VEC+41+
Cells plated	0	500	2941	2000	500
Blood-like cells					Yes
CD31 endothelial colonies		~11+	~16++	~18+	1
Freq. EC/cells		1:45	1:184	1:111	1:500

WT EC purity: 97.4%

Appendix 4.2 E8.5 OP9 co-culture data

Table of raw data from E8.5 OP9 co-culture assays. Number of cells plated, whether blood-like colonies were detected after 8 days in culture, number of CD31+ endothelial network detected, number of CD31+ blood colonies detected and the rough frequency of endothelial networks per cells plated are given for 3 experiments. No cell control - no cells were plated onto OP9 stromal layer; VEC+CD41+ control - blood output assay control, referred to as CD41+ blood or cluster cells in the text.

A

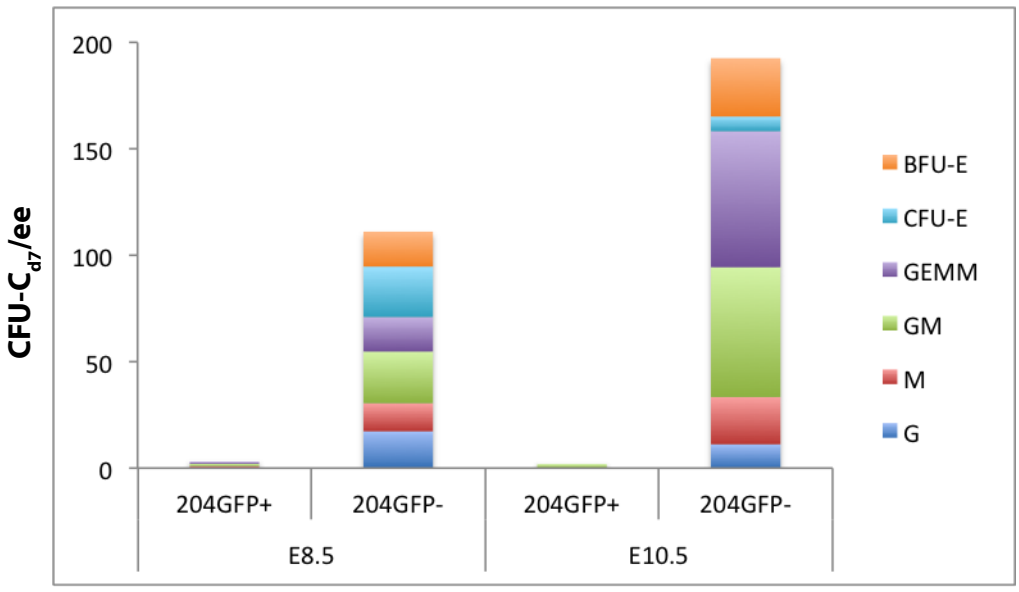
Embryo stage	Experiment no.	Tissue	Purities	Cells plated/ dish	No. of CFU-C	CFU-C/10000 cells	CFU-C/ee	CFU-C distribution
E8.5 (5-8sp)	FACS025	204GFP+	95.7%	573	1.5	26.2	3.2	2.8
		204GFP-	100%	20880	47	22.5	113	97.2
		WT unsorted	NA	30000	42.5	14.2	75.9	NA
E8.5 (5-9sp)	FACS026	204GFP+	88.6%	1534	0.5	3.3	0.5	0.7
		204GFP-	99.5%	33213	78	23.5	80.5	99.3
		WT unsorted	NA	30000	35	11.7	88.7	NA
E8.5 (6-8sp)	FACS027	204GFP+	49.5%	1413	3.5	24.8	5.8	4.0
		204GFP-	99.3%	29520	78	26.4	139.9	96.0
		WT unsorted	NA	30000	30.5	10.2	62.6	NA

B

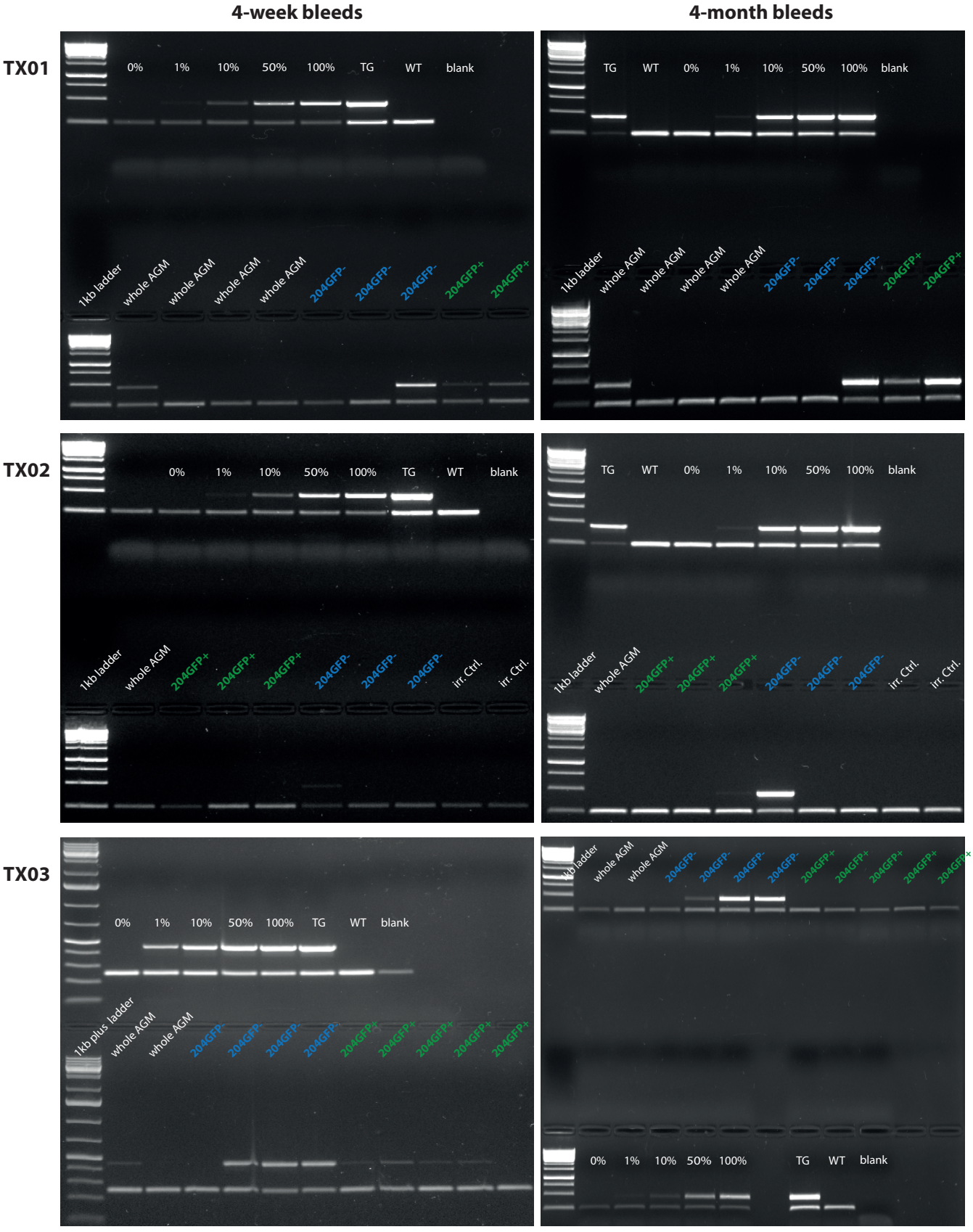
Embryo stage	Experiment no.	Tissue	Purities	Cells plated/ dish	No. of CFU-C	CFU-C/10000 cells	CFU-C/ee	CFU-C distribution
E10.5 (27-33sp)	FACS021	204GFP+	62.7%	2840	1	3.52	7.9	2.9
		204GFP-	95.8%	46894	32.5	6.93	261	97.1
E10.5 (39-35sp)	FACS024	204GFP+	79%	3384	1	2.9	1.8	1
		204GFP-	99%	48960	49.5	10.1	170	99
		WT unsorted	NA	33333	33	9.9	178	NA
E10.5 (27-34sp)	FACS028	204GFP+	85.4%	1571	1.5	9.6	2	1
		204GFP-	99.5%	30000	45	15	208	99
		WT unsorted	NA	30000	27.5	9.2	149	NA

Appendix 4.3 Raw data of CFU-C assays on E8.5 and E10.5 embryos

Summary tables of raw data for CFU-C experiment is shown for E8.5 (**A**) and E10.5 (**B**). the number of cells plated per dish, the number of CFU-Cs counted at day 7 (average of 2 duplicate dishes), the calculated number of CFU-Cs per 10000 cells plated, the number of CFU-Cs per ee and the CFU-C distribution between 204GFP+ and 204GFP- populations is shown



Appendix 4.4 Blood progenitor lineage output from CFU-C cultures
Graph representation of CFU-C colonies counted per embryo equivalent (ee) with the distribution of blood progenitor lineages indicated. BFU-E — blast-forming-unit erythroid; CFU-E — culture-forming-unit erythroid; GEMM — multi potent myeloid progenitor giving rise to granulocyte, erythrocyte, monocyte and megakaryocytic progenitors; GM- bi-potential myeloid progenitors giving rise to granulocyte and monocyte progenitors; M — megakaryocyte progenitor; G — granulocyte progenitor. Colonies were counted on day 7 of culture (n=3).

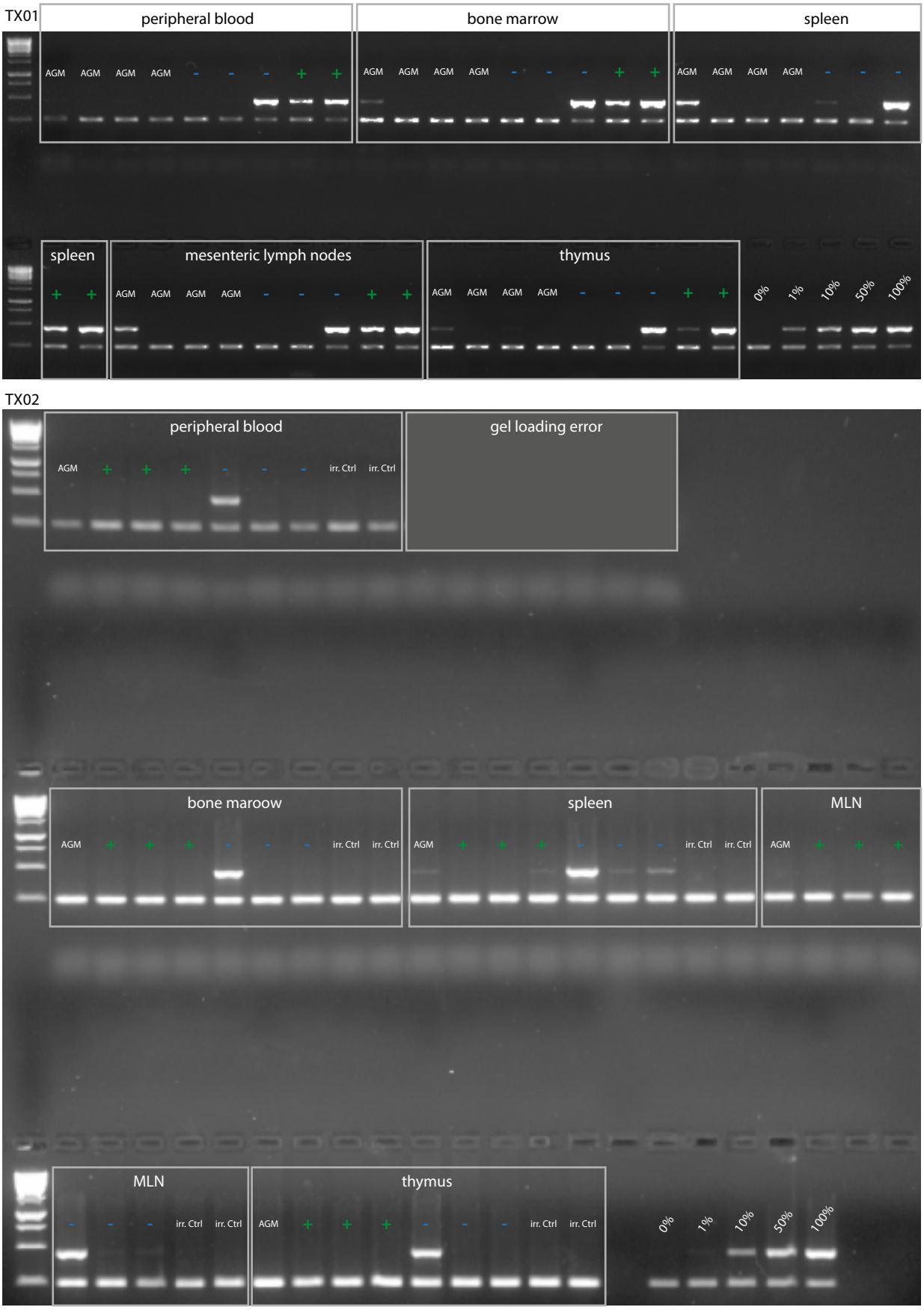


Appendix 4.5 Raw transplant data from 4 weeks and 4 months analysis
Raw gel images of DNA from the blood of translated recipient mice at 4 weeks and 4 months post-transplantation. DNA standards with known concentration of *Gfp* DNA was run alongside individual experiments. Reconstitution percentages were calculated based on the ratio of band intensity between WT and GFP bands. DNA ladders used are show (n=3).

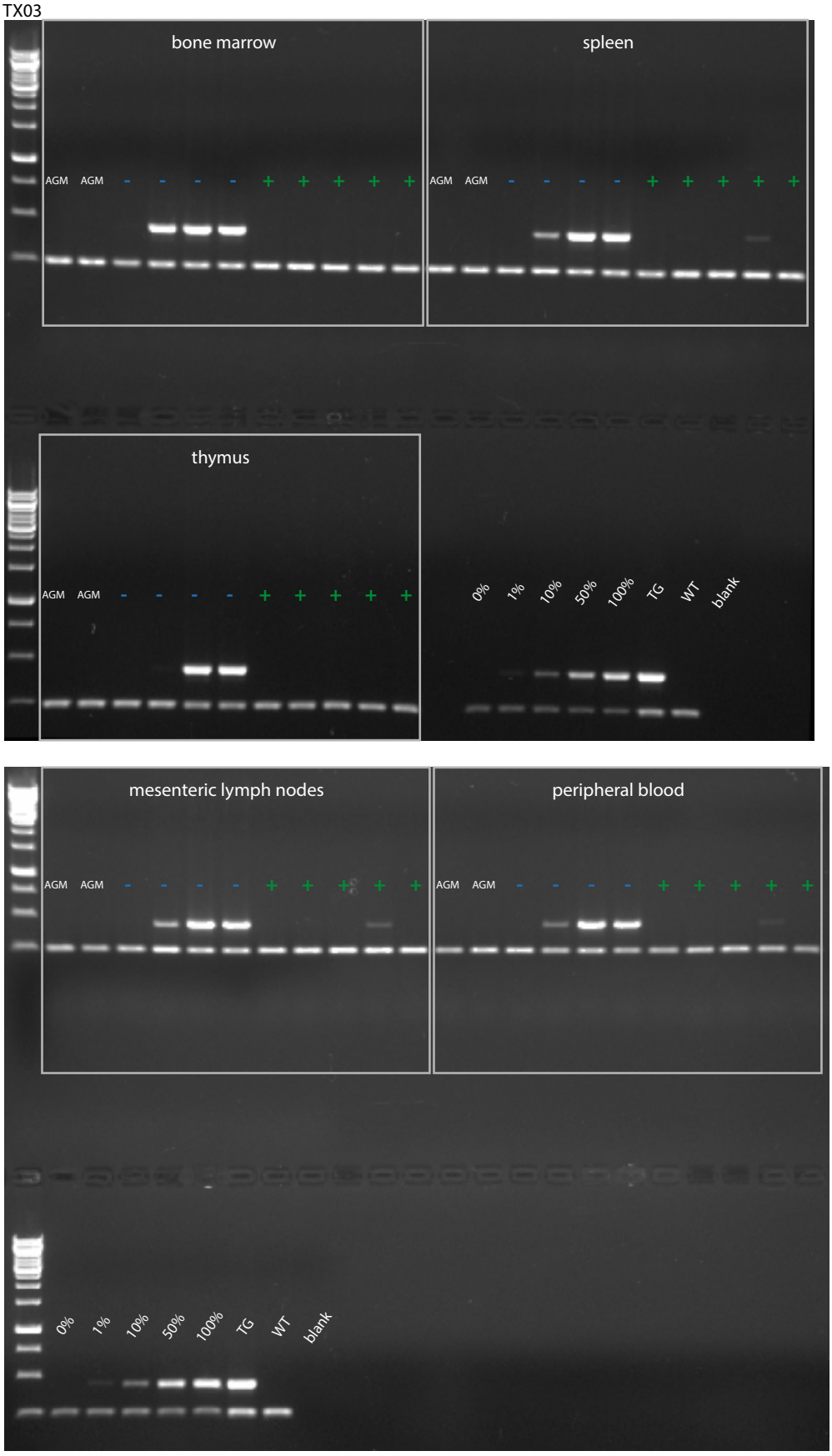
			4 weeks	4 months	4 months										
			tail vein bleeds		whole tissues					sorted BM			sorted spleen		
Experiment no.	individual mou transplant ID	test group	blood	blood	blood	BM	spleen	MNL	thymus	Erythroid	Myeloid	Lymphoid	Erythroid	Myeloid	Lymphoid
TX01	1_1	**AGM**	**10%**	8%	<1%	<1%	7%	7%	<1%	0%	<1%	0%	0%	0%	2-3%
	1_2	**AGM**	0%	0%	0%	0%	0%	0%	0%	ND	ND	ND	ND	ND	ND
	1_3	**AGM**	0%	0%	0%	0%	0%	0%	0%	ND	ND	ND	ND	ND	ND
	1_4	**AGM**	0%	0%	0%	0%	0%	0%	0%	ND	ND	ND	ND	ND	ND
	1_5	**204GFP-**	0%	0%	0%	0%	<1%	0%	0%	ND	ND	ND	ND	ND	ND
	1_6	**204GFP-**	0%	0%	0%	0%	0%	0%	0%	0%	0%	0%	0%	0%	0%
	1_7	**204GFP-**	**40%**	**100%**	**100%**	**55%**	**50%**	**85%**	**100%**	**40%**	**40%**	**100%**	**100%**	**100%**	**40%**
	1_8	**204GFP+**	5%	9%	**15%**	9%	**20%**	**25%**	<1%	3-4%	4%	**11%**	5%	8%	9%
	1_9	**204GFP+**	7%	**100%**	**100%**	**40%**	**70%**	**60%**	**60%**	**100%**	**100%**	**100%**	**100%**	**100%**	**100%**
TX02	2_1	**AGM**	0%	0%	0%	0%	2-3%	0%	0%	0%	0%	0%	x	0%	2-3%
	2_2	**204GFP+**	0%	0%	0%	0%	0%	0%	0%	ND	ND	ND	ND	ND	ND
	2_3	**204GFP+**	0%	0%	0%	0%	0%	0%	0%	ND	ND	ND	ND	ND	ND
	2_4	**204GFP+**	0%	<1%	0%	0%	2-3%	0%	0%	0%	0%	0%	x	0%	<1%
	2_5	**204GFP-**	5%	**100%**	**60%**	**35%**	**40%**	**37%**	8%	**90%**	**45%**	**60%**	x	**100%**	**60%**
	2_6	**204GFP-**	0%	0%	0%	0%	2-3%	<1%	0%	0%	0%	0%	x	0%	2-3%
	2_7	**204GFP-**	0%	0%	0%	0%	5%	1%	0%	ND	ND	ND	ND	ND	ND
	2_8	**spleen**	0%	0%	0%	0%	0%	0%	0%	ND	ND	ND	ND	ND	ND
	2_9	**spleen**	0%	0%	0%	0%	0%	0%	0%	ND	ND	ND	ND	ND	ND
TX03	3_1	**AGM**	<1%	0%	0%	0%	0%	0%	0%	ND	ND	ND	ND	ND	ND
	3_2	**AGM**	0%	0%	0%	0%	0%	0%	0%	ND	ND	ND	ND	ND	ND
	3_3	**204GFP-**	0%	0%	0%	0%	0%	0%	0%	0%	0%	0%	0%	0%	0%
	3_4	**204GFP-**	9%	2%	5%	**25%**	4-5%	9%	0%	**100%**	**40%**	**100%**	0%	<1%	**15%**
	3_5	**204GFP-**	**55%**	**50%**	**47%**	**35%**	**30%**	**45%**	**38%**	**100%**	**40%**	**100%**	0%	**100%**	**100%**
	3_6	**204GFP-**	**40%**	**50%**	**49%**	**30%**	**28%**	**40%**	**29%**	**100%**	**100%**	**100%**	0%	**100%**	**100%**
	3_7	**204GFP+**	<1%	0%	0%	0%	0%	0%	0%	ND	ND	ND	ND	ND	ND
	3_8	**204GFP+**	<1%	0%	0%	0%	0%	0%	0%	ND	ND	ND	ND	ND	ND
	3_9	**204GFP+**	<1%	0%	0%	0%	0%	0%	0%	ND	ND	ND	ND	ND	ND
	3_10	**204GFP+**	<1%	0%	<1%	0%	<1%	1%	0%	ND	ND	ND	ND	ND	ND
	3_11	**204GFP+**	0%	0%	0%	0%	0%	0%	0%	ND	ND	ND	ND	ND	ND

Appendix 4.6 Summary table of transplant data for individual recipient mice

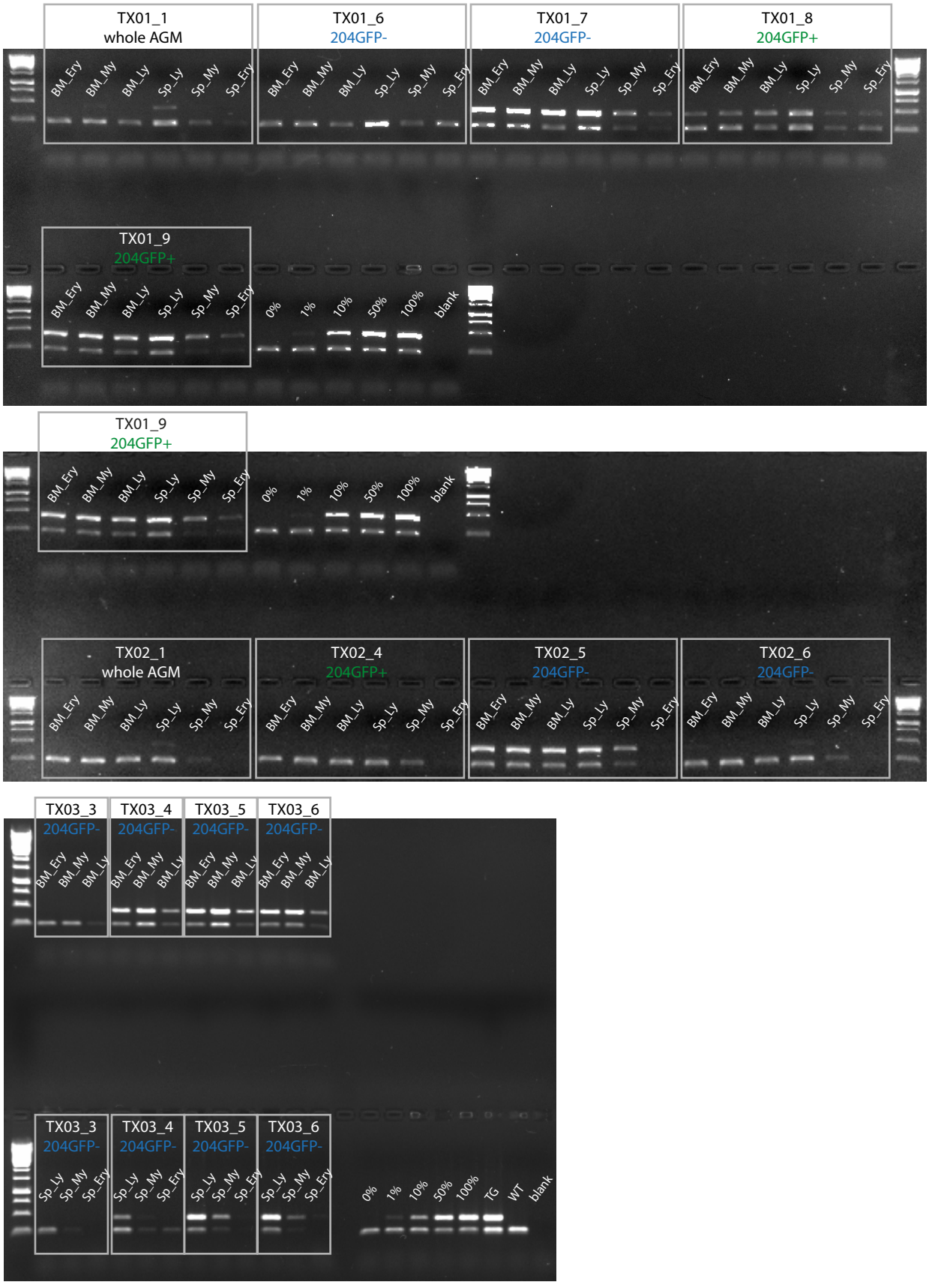
Table summary of the reconstitution percentages of individual recipient mice in different tissues at different timepoints of analysis. The BM and spleen of selected mice (grey tabs) were sorted for different blood lineages and analysed. X= no WT or GFP bands detected.



Appendix 4.7A Raw transplant data from tissue samples of TX01 and TX02
Raw gel images of DNA from tissues of translated recipient mice harvested at 4 months. DNA standards with known concentration of *Gfp* DNA was run alongside individual experiments. Reconstitution percentages were calculated based on the ratio of band intensity between WT and GFP bands. Data from transplant experiments TX01 and TX02 are shown.



Appendix 4.7B Raw transplant data from tissue samples of TX03
Raw gel images of DNA from tissues of translated recipient mice harvested at 4 months. DNA standards with known concentration of *Gfp* DNA was run alongside individual experiments. Reconstitution percentages were calculated based on the ratio of band intensity between WT and GFP bands. Data from transplant experiment TX03 is shown.

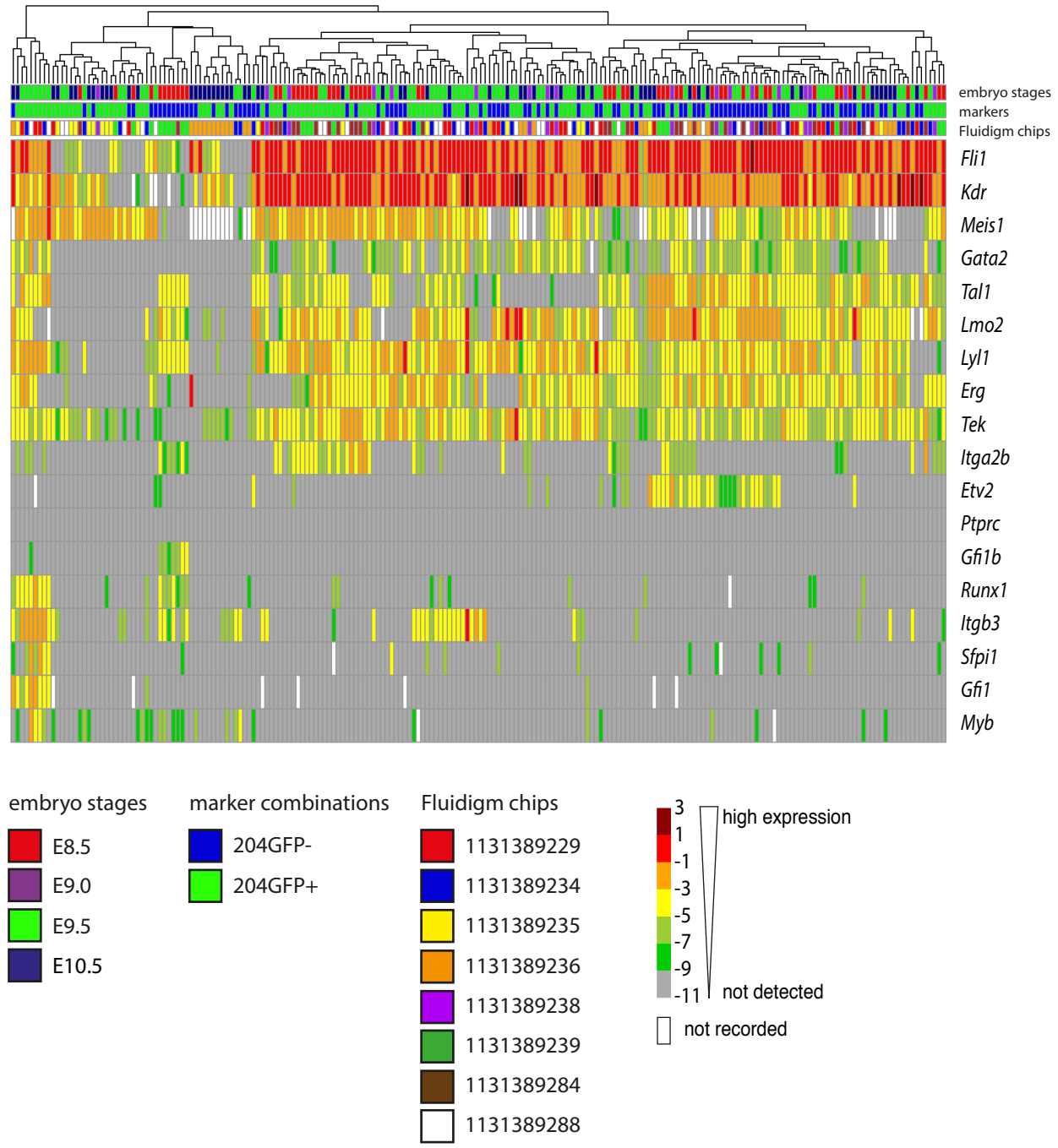


Appendix 4.8 Raw transplant data from sorted bone marrow and spleen cells

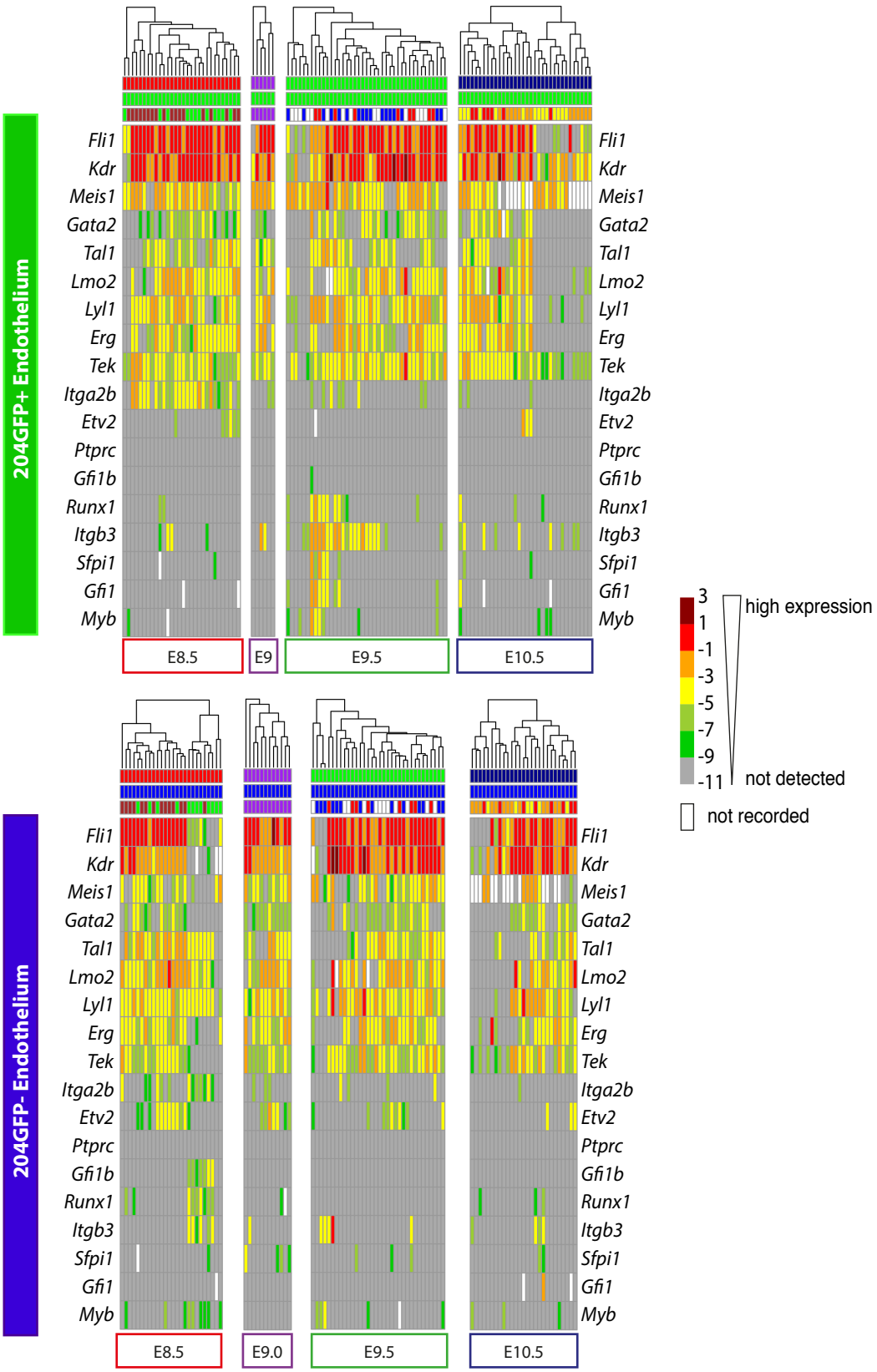
Raw gel images of DNA from sorted erythroid (Ery), myeloid (My) and lymphoid (Ly) cells. Bone marrow (BM) and spleens (Sp) were sorted. DNA standards with known concentration of *Gfp* DNA was run alongside individual experiments. Reconstitution percentages were calculated based on the ratio of band intensity between WT and GFP bands. Data from selected reconstituted and control recipients are shown for each transplant experiment (grey tabs in Appendix 4.6).

		Endotheli um	E8.5	E9.0	E9.5	E10.5	Total
204GFP	unfiltered	204GFP+	30	6	42	35	113
		204GFP-	26	12	36	29	103
	filtered for EC only	204GFP+	27	5	33	19	84
		204GFP-	17	12	29	19	77
204GFP::23Cherry	unfiltered	G-C-	14	ND	8	30	52
		G+C-	14	ND	8	38	60
		G+C+	13	ND	9	82	104
		G-C+	23	ND	10	38	71
		CD41+	ND	ND	ND	11	11
		CD45+	ND	ND	ND	10	10
	filtered for EC only	G-C-	7	ND	7	21	35
		G+C-	14	ND	8	18	40
		G+C+	8	ND	7	43	58
		G-C+	4	ND	6	26	36

Appendix 5.1 Number of single cells used for Fluidigm qRT-PCR analysis



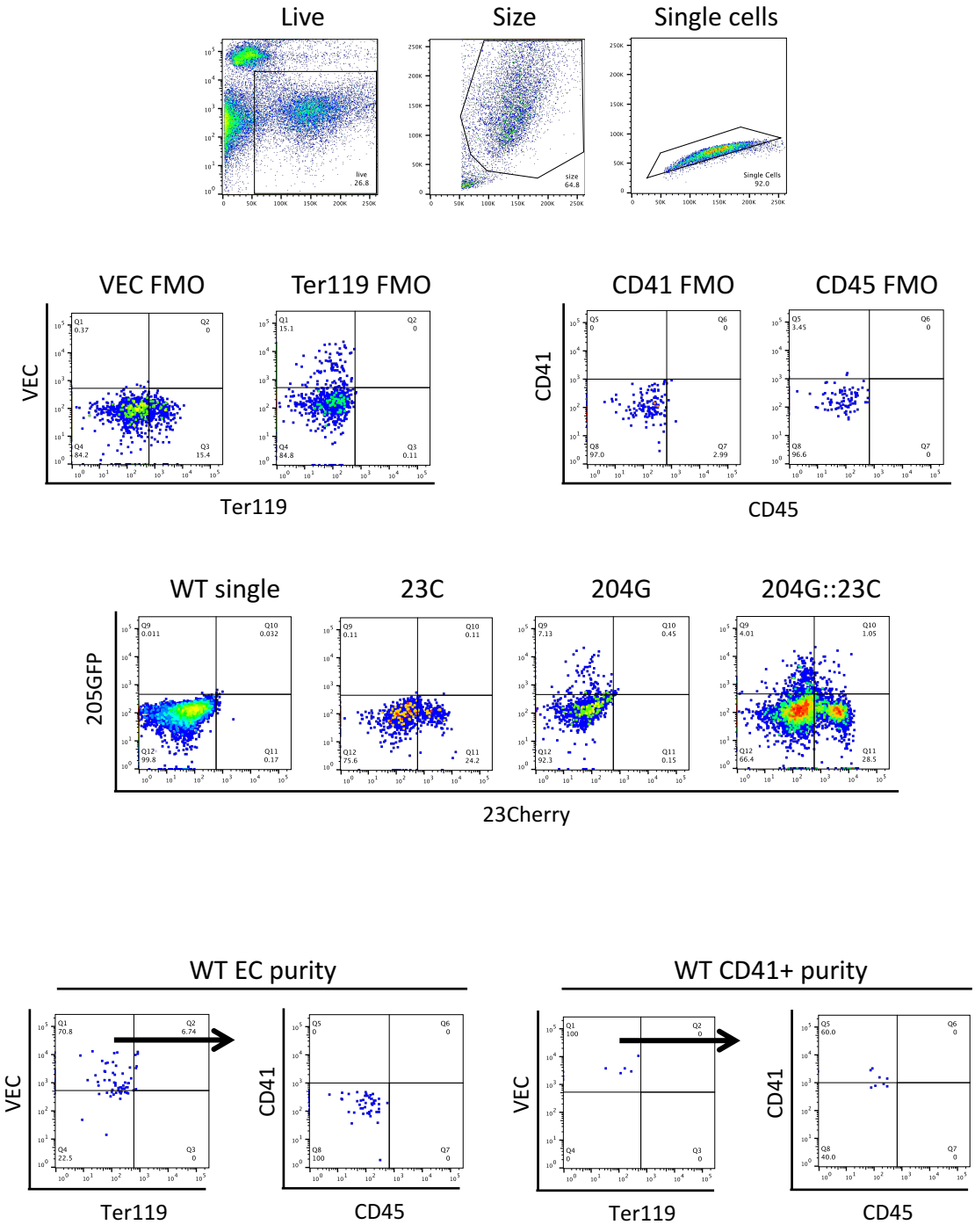
Appendix 5.2 Raw single cell expression data for 204GFP+/- endothelium
Hierarchical clustering of all single cells used for the gene expression analysis of 204GF-P+/- endothelial subsets. The left arm of the hierarchy likely represents the erythroid progenitor and mesenchyme contamination based on gene expresssion signature. Such cells were filtered out for Figure 5.2.



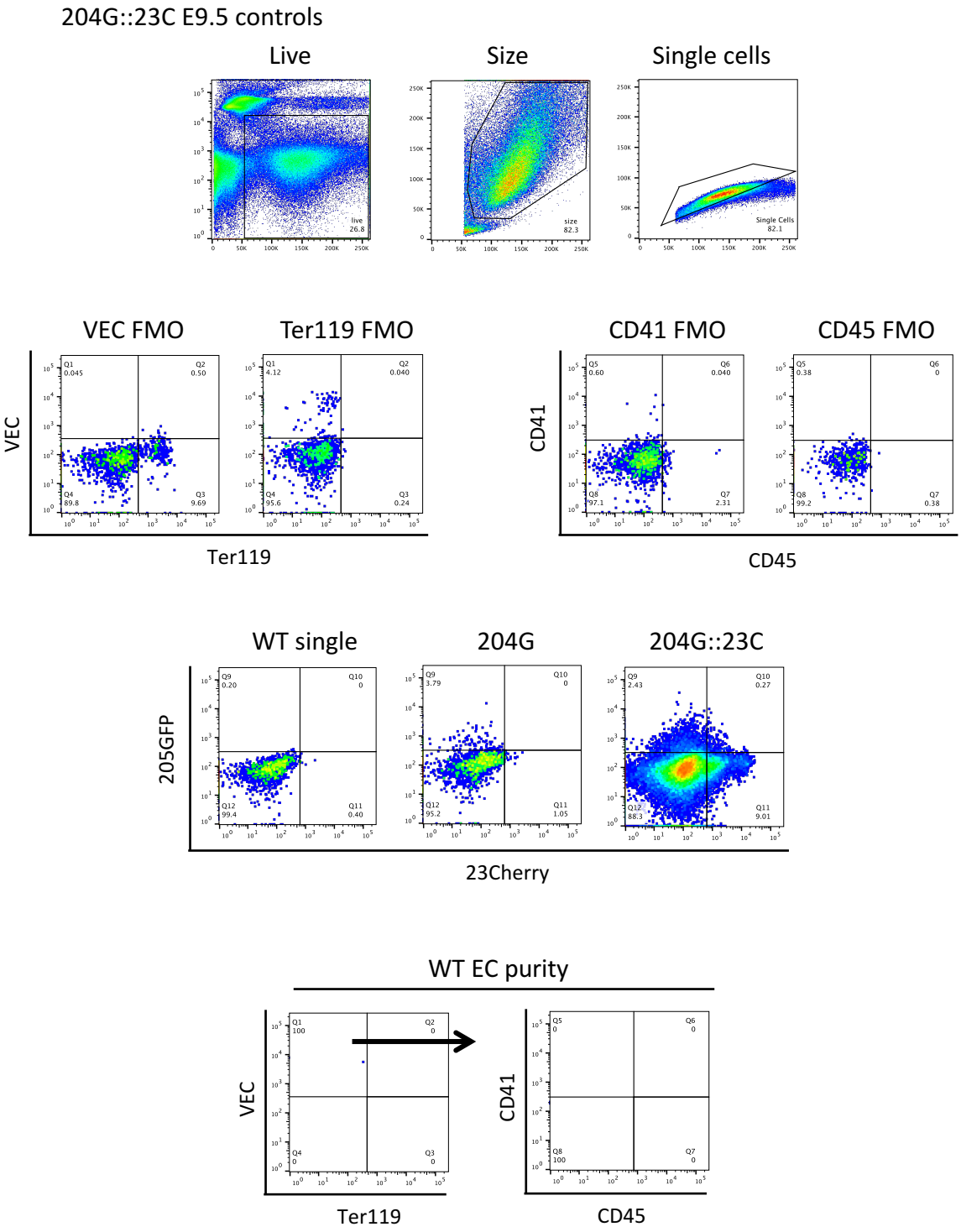
Appendix 5.3 Raw single cell expression data for 204GFP+/- endothelium segregated based on developmental time

Hierarchical clustering of all single cells used for the gene expression analysis of 204GFP+/- endothelial subsets. Data is segregated in 4 developmetal timepoints. In contrast to Figure 5.2, this data is unfiltered and shows all cells analysed.

204G::23C E8.5 controls

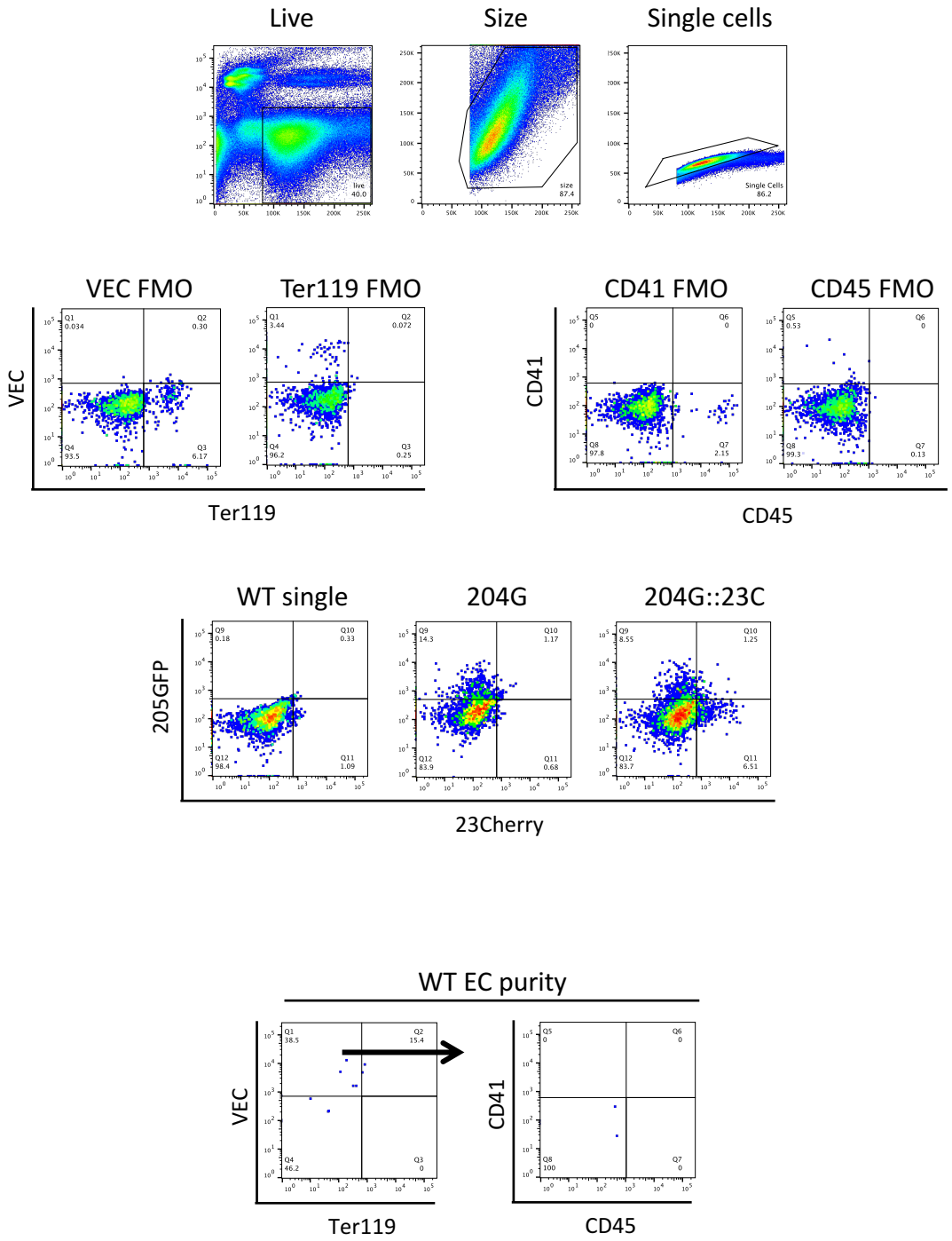


Appendix 5.4 Control plots for 204GFP and 23Cherry co-expression at E8.5
Flow cytometry gates for live, single, VEC/Ter119 and CD41/CD45 plots for E8.5 experiments are given. Gates were drawn based on fluorescence minus one (FMO) control for all 6 fluorochromes. Controls are directly linked to E8.5 data in Figure 5.8 and Figure 5.9. n=1

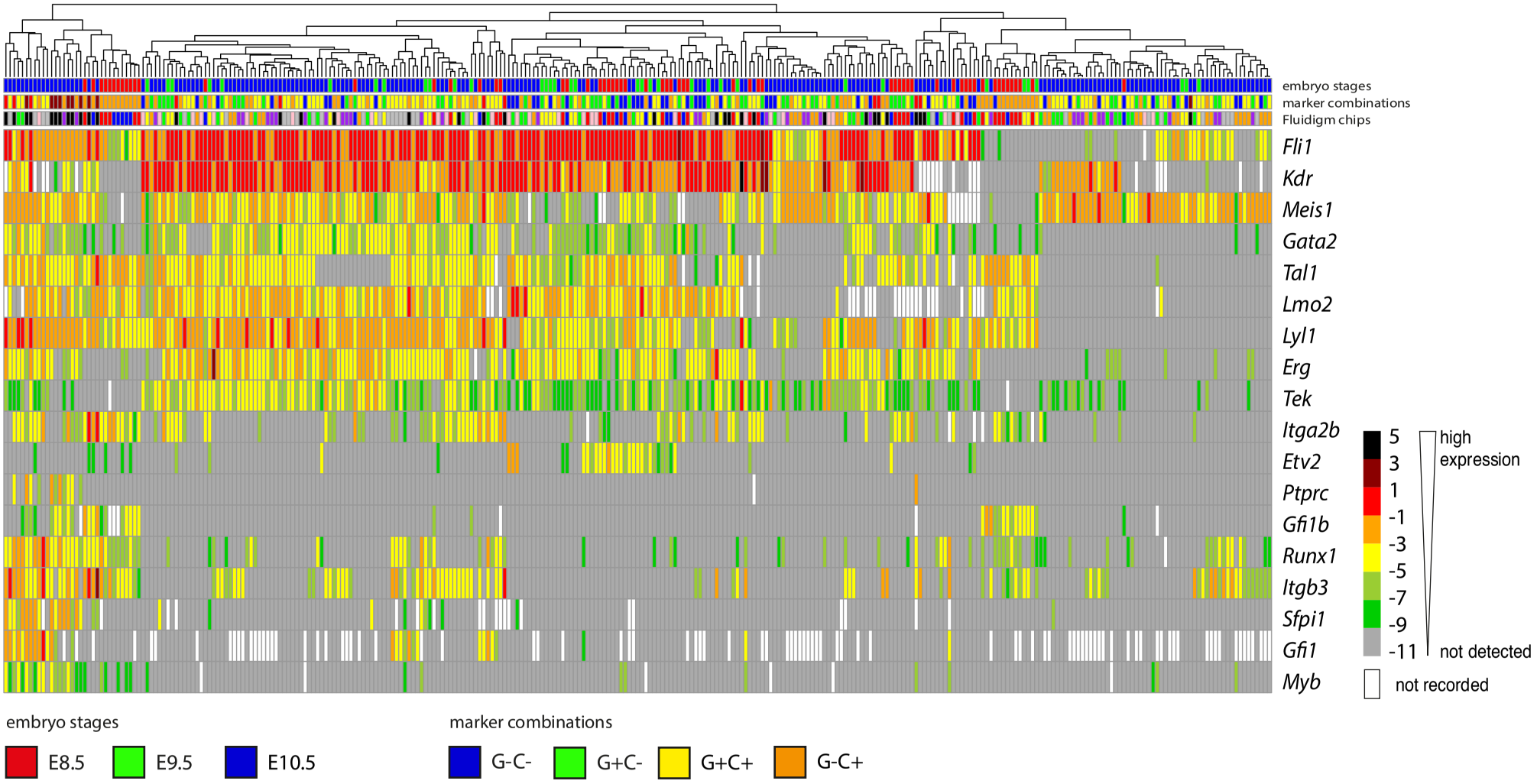


Appendix 5.5 Control plots for 204GFP and 23Cherry co-expression at E9.5
Flow cytometry gates for live, single, VEC/Ter119 and CD41/CD45 plots for E8.5 experiments are given. Gates were drawn based on fluorescence minus one (FMO) control for all 6 fluorochromes. Controls are directly linked to E8.5 data in Figure 5.8 and Figure 5.9. n=1

204G::23C E10.5 controls

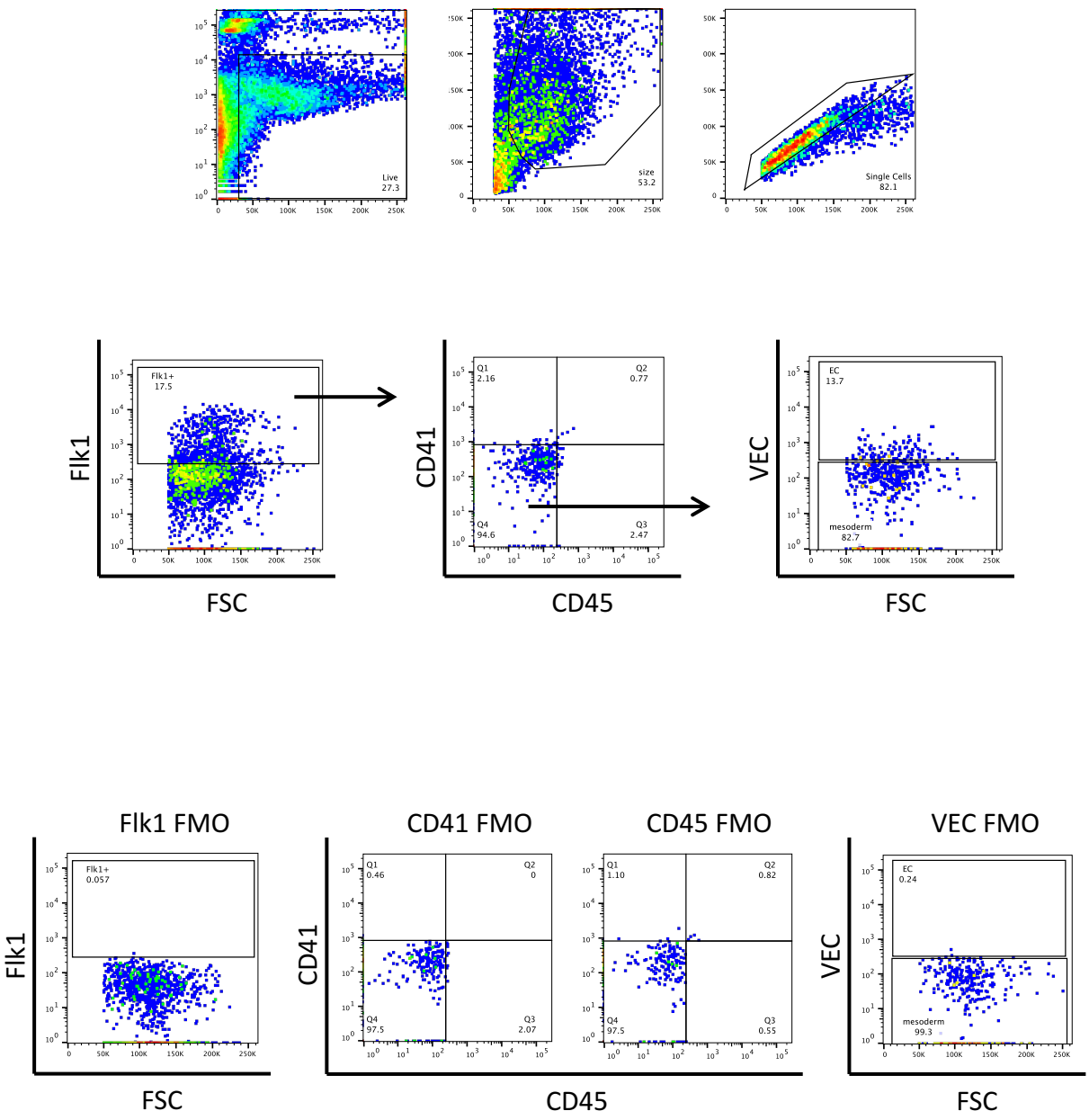


Appendix 5.6 Control plots for 204GFP and 23Cherry co-expression at E10.5
Flow cytometry gates for live, single, VEC/Ter119 and CD41/CD45 plots for E8.5 experiments are given. Gates were drawn based on fluorescence minus one (FMO) control for all 6 fluorochromes. Controls are directly linked to E8.5 data in Figure 5.8 and Figure 5.9. n=1



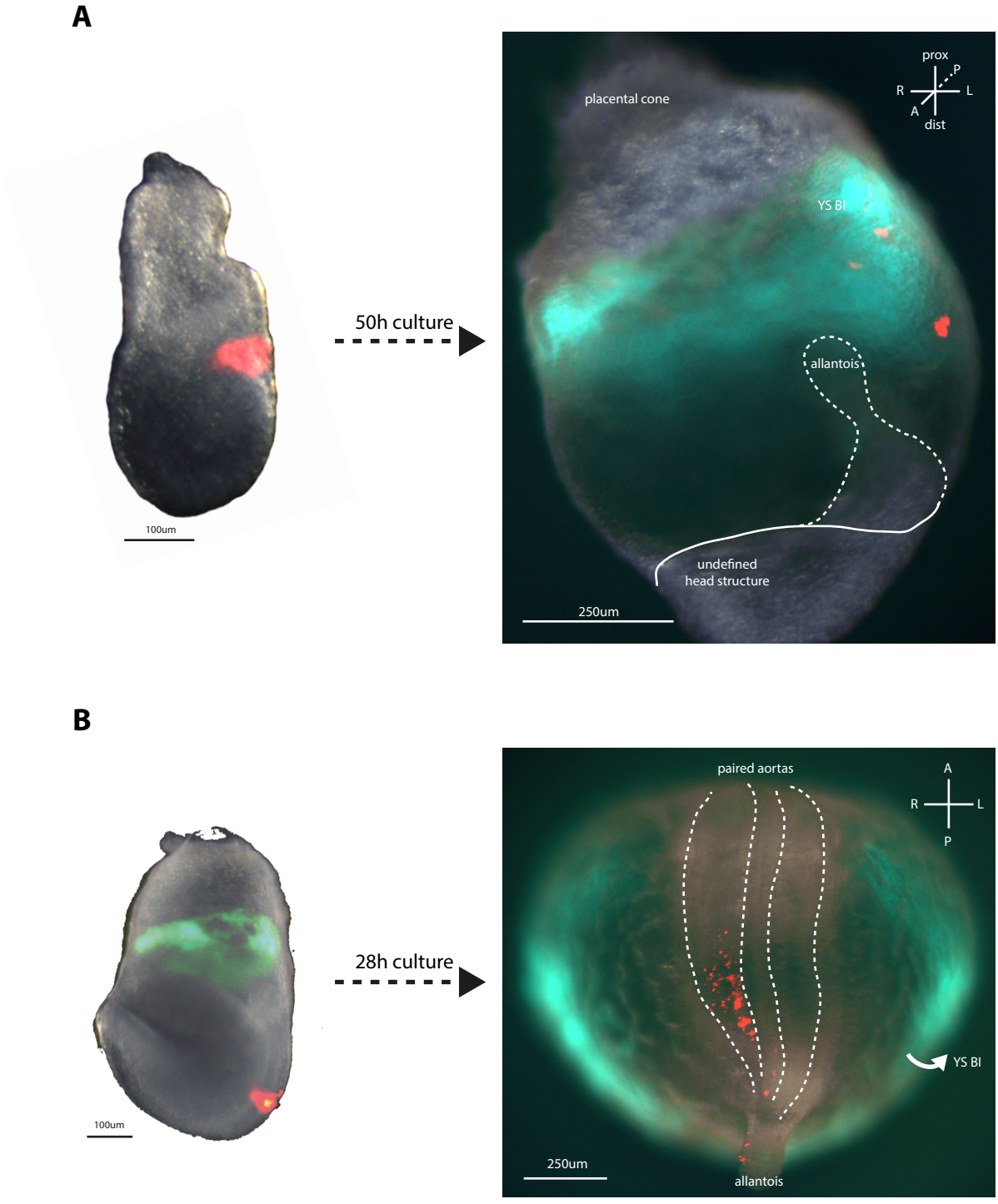
Appendix 5.7 Raw single cell expression data for 4 endothelial subsets (unfiltered)

Hierarchical clustering of all single cells used for the gene expression analysis of 4 endothelial subsets, segregated based on 204GFP and 23Cherry transgene expressions.



Appendix 6.1 Gating strategy and controls for E7 flow cytometry analysis of 23GFP transgenic embryos

Single, live cells were gated on Flk1 expression. CD41 an CD45 double negative cells were analyzed for VEC expression. FMO controls for four fluorophores are shown. Controls were performed on headfold stage embryos (n=1)



Appendix 6.2 Raw images of fate mapping experiments
A) MS embryo injected with DiI and cultured for 50h only showed DiI expression within the yolk sac blood islands and vasculature, not within the embryo body. The raw image record of the cultured embryo prior to fixation is shown. Anatomical hallmarks and the embryo orientation are indicated. The head structure was not defined after 50h-long cultures. The posterior position of the allantois is indicated (dashed line). **B)** LB/EHF embryo injected with DiI and cultured for 28h only showed expression within PAS (and allantois), not YS vasculature. The raw image record of the cultured embryo prior to fixation is shown. Anatomical hallmarks and the embryo orientation are indicated. 23GFP expression within the paired aortas is not visible due to the weak sensitivity of the microscope. Images were taken on the Leica MZFLIII brightfield microscope with a 1X planapo objective. Scale bars as indicated.

Movie 1 and 2: Dynamic upregulation of 23GFP expression in the developing intra-aortic vasculature at E7.5
Full movie from still images in Figure 6.3.

Movie 3. Beating heart of cultured embryo
LHF stage embryos cultured for 24h (till early sp) often exhibited a beating heart. Movie shows the heart contractions of one cultured embryo.